Deformation Capacity and Cracks of Reinforced Concrete Beams

Henriksen, Michael Strandskov

Publication date:
1999

Document Version
Publisher's PDF, also known as Version of record

Scale Effects and Transitional Failure Phenomena of
Reinforced Concrete Beams in Flexure

DEFORMATION CAPACITY AND CRACKS OF REINFORCED CONCRETE BEAMS

By

Michael Strandskov Henriksen

Ph.D. Thesis

Department of Building Technology and Structural Engineering
Aalborg University, Aalborg, Denmark

May 1999

Deformation Capacity and Cracks of Reinforced Concrete Beams

By

Michael Strandskov Henriksen, Building Engineer, M. Sc., Ph. D. Student

The Department of Building Technology and Structural Engineering
Aalborg University
Sohngaardsholmsvej 57
9000 Aalborg
Denmark

May 1999

Contents

	Preface	vii
	Acknowledgement	viii
1.	Introduction	1-1
	1.1 Backgrounds and Motivation	1-1
	1.2 Scope of Work	1-2
	1.3 Readers Guide	1-3
2.	Model for Rotational Capacity of Lightly Reinforced Concrete Beams	2-1
	2.1 Introduction	2-1
	2.2 Flexural Behaviour of Lightly Reinforced Concrete Beams Assuming Rebar Tension Failure	2-4
	2.2.1 Modelling the Load-Deflection Curve	2-4
	2.2.2 Modelling the Rotational Capacity	2-14
	2.3 Basic Properties of the Model	2-15
	2.3.1 Material Parameters of the Concrete and Reinforcement	2-16
	2.3.2 Model Results	2-19
	2.3.3 Size Effects on the Rotational Capacity	2-24
	2.4 Concluding Remarks	2-28
3.	Model for Rotational Capacity of Heavily Reinforced Concrete Beams	3-1
	3.1 Introduction	3-1
	3.2 Basic Assumptions of the State of Compression Failure	3-5
	3.3 Flexural Behaviour of Heavily Reinforced Concrete Beams Assuming Compression Failure	3-6
	3.3.1 Modelling the Cross-Sectional Moment Curvature Relation	3-7
	3.3.2 Modelling the Load-Displacement Curve	3-18
	3.3.3 Modelling the Rotational Capacity	3-25
4.	Experimental Study on the Scale and Strength Dependency on the Ductility of Reinforced Concrete Beams	4-1
	4.1 Test Programme	4-2
	4.2 Materials	4-4
	4.2.1 Concrete	4-4
	4.2.2 Reinforcement	4-7
	4.3 Testing Equiptment and Procedure	4-10
	4.3.1 Boundary Conditions	4-10
	4.3.2 Measurements	4-10
	4.3.3 Data Acquistion	4-11

4.3.4 Testing Procedure 4.11
4.4 Results and Discussion 4-14
4.4.1 Load-Deflection Responses 4-14
4.4.2 Rotational Capacity 4-21
4.4.3 Discussion 4-26

5. Experimental Study on Rotational Capacity of Lightly and Heavily Reinforced Concrete Beams 5-1
5.1 Introduction 5-1
5.2 Test Programme 5-2
5.2.1 The Test Programme for Heavily Reinforced Beams 5-2
5.2.2 The Test Programme for Lightly Reinforced Beams 5-4
5.2.3 Identification of Beams 5-5
5.3 Materials 5-5
5.3.1 Concrete 5-5
5.3.2 Reinforcement 5-9
5.3.3 Bond-Slip Between Reinforcement and Concrete 5-13
5.4 Experiments 5-17
5.4.1 Preparation and Test Series 5-17
5.4.2 Test Set-up for Heavily Reinforced Beams 5-17
5.4.3 Test Set-up for Lightly Reinforced Beams 5-19
5.4.4 Testing Procedure 5-20
5.5 Experimental Results 5-27
5.5.1 Load-Displacement Responses for the Test Beams 5-27
5.5.2 Results for Heavily Reinforced Beams 5-33
5.5.3 Results for Lightly Reinforced Beams 5-33
5.5.4 Measured Rotations of the Test Beams 5-34
5.6 Rotational Capacity of the Test Beams 5-36
5.6.1 Basic Assumption on Rotational Capacity 5-36
5.6.2 Rotational Capacity according to Plasticity Theory 5-37
5.6.3 Rotational Capacity according to Rotations of the Beam Supports 5-38
5.6.4 Rotational Capacity according to Rotations of the Midspan 5-38
5.6.5 Plastic Rotational Capacity of the Test Beams 5-39

6. Comparison of Analytical and Experimental Methods 6-1
6.1 Modelling of Heavily Reinforced Beams 6-1
6.1.1 Model Results of Plastic Rotational Capacity 6-2
6.2 Modelling of Lightly Reinforced Beams 6-7

7. Conclusion and Summary 7-1

8. References 8-1

9. Summary in Danish 9-1

A Test Results for Reinforced Concrete Beams of Different Scale and Strength A-1
A1 Flexural Response Curves and Curvature Distribution for Test Beams in ESIS 1 A-1
A1.1 Test Results for Normal Strength Concrete Beams A, D and G with Reinforcement Ratio 0.78 % and Slenderness Number 6 A-2
A1.2 Test Results for Normal Strength Concrete Beams B, E and H with Reinforcement Ratio 0.78 % and Slenderness Number 12 A-4
A1.3 Test Results for Normal Strength Concrete Beams C, F and I with Reinforcement Ratio 0.78 % and Slenderness Number 18 A-6
A1.4 Test Results for Normal Strength Concrete Beams A, D and G with Reinforcement Ratio 1.57 % and Slenderness Number 6 A-8
A1.5 Test Results for Normal Strength Concrete Beams B, E and H with Reinforcement Ratio 1.57 % and Slenderness Number 12 A-10
A1.6 Test Results for Normal Strength Concrete Beams C, F and I with Reinforcement Ratio 1.57 % and Slenderness Number 18 A-12
A1.7 Test Results for Normal Strength Concrete Beams B, E and H with Reinforcement Ratio 0.14 % and Slenderness Number 12 A-14
A1.8 Test Results for Normal Strength Concrete Beams B, E and H with Reinforcement Ratio 0.25 % and Slenderness Number 12 A-16
A1.9 Test Results for Normal Strength Concrete Beams B, E and H with Reinforcement Ratio 0.39 % and Slenderness Number 12 A-18
A1.10 Test Results for High Strength Concrete Beams B, E and H with Reinforcement Ratio 0.14 % and Slenderness Number 12 A-20
A1.11 Test Results for High Strength Concrete Beams B, E and H with Reinforcement Ratio 0.25 % and Slenderness Number 12 A-22
A1.12 Test Results for High Strength Concrete Beams B, E and H with Reinforcement Ratio 0.39 % and Slenderness Number 12 A-24
A2 Rotational Capacity of Reinforced Normal Strength and High Strength Concrete Beams A-26

Preface

The present thesis *Deformation Capacity and Cracks of Reinforced Concrete Beams* has been made as a part of my Ph.D. - study programme carried out in the period June 1995 - May 1999 at the Department of Building Technology and Structural Engineering, Aalborg University, Denmark. The Ph.D. work has been a part of the research programme on *Scale Effects and Transitional Failure Phenomena of Reinforced Concrete Beams in Flexure* sponsored by the Danish Technical Research Council.

This thesis summarizes experimental investigations on reinforced concrete beams subjected to three point bending. One of the main purposes of the experiments has been to investigate the plastic rotational capacity of very lightly reinforced beams and very high reinforced beams. The beam tests have been performed at the Structural Research Laboratory at the Department of Building Technology and Structural Engineering, Aalborg University under the period of February 1994 to June 1998.

From the period of February 1994 to October 1995 several beam tests were performed at the Structural Research Laboratory with the purpose to investigate scale effects and transitional failure phenomena of reinforced concrete beams in flexure. This study was done in cooperation with the European Structural Integrity Society under Technical Commitee 9 on concrete. From the knowledge of these tests and results another research project was established in order to more investigate the lightly reinforced regime and the heavily reinforced regime.

This thesis consists of a main report and one appendix. In the main report the experimental and analytical investigations are outlined, and in the appendix most of the result can be found.

May 1999

Michael S. Henriksen

Acknowledgement

The financial support from the Danish Technical Research Council (STVF) is grateful acknowledged.

The excellent work performed by the staff at the Concrete Technology Laboratory and Structural Research Laboratory are very grateful appreciated. In planning of the project a lot of thanks goes to Jens Kristian Jehrbo Jensen and Lars Pilegaard Hansen for their kindness and support.

The work performed by Henning Andersen and Morten Olsen in preparing test set-ups for beam tests and carring out fracture energy tests and bond-slip tests are very acknowledged. The help and understanding from Henning Andersen and Morten Olsen is very appreciated and valuable.

I would also like to thank Professor Kent Gylltoft from the Division of Concrete Structures at Chalmers University of Technology, Göteborg, Sweden for making my visit at his Department in the period 4/7 1998 - 5/10 1998 possible and enjoyable.

Finally, special thanks to my supervisors Associate Professor Rune Brincker and Assosiate Professor Gert Heshe, Department of Building Technology and Structural Engineering, Aalborg University for sharing their ideas and experience in failure of concrete. Also, a lot of thanks to Jens Peder Ulfkjær for enjoyable discussions on testing and modelling of concrete.

I would also like to thank my colleagues at the Department, and especially my colleagues in the concrete group Frede Christensen and John Simonsen for valuable discussions and helping out with computer programming.

Finally, my wife Vannisa and my children have never complained, that I have spent a lot of time here at the Department, so I owe them a huge amount of thanks and love.

Chapter 1

Introduction

This thesis contains investigations of methods to predict plastic rotational capacities for reinforced concrete beams subjected to three-point bending.

The plastic rotational capacity of a reinforced concrete beam is defined as the non-elastic mutual rotation of the beam, i.e. the capability to obtain plastic deformations. Using reinforcement with a large ultimate steel strength and a normal strength concrete will in most cases be sufficient to preserve a high rotational capacity, when the structure is normal reinforced, i.e. the steel strain is higher than the yield strength but lower than the ultimate steel strain and the concrete is at the compression failure state corresponding to a strain of 0.35 %. According to the Danish Code a reinforced structure must be reinforced equal to the normal reinforced state in order to obtain sufficient ductility and resistance against sudden failure.

In this thesis several parameters are varied and their influence on the rotational capacity is analyzed both analytically and experimentally. Efforts are made to investigate the size dependency on the ductility of a plastic hinge in a reinforced structure, which is actually a very popular subject among concrete researchers nowadays. From an overview of the huge amount of research on this topic and by comparison with experimental results and simple modelling some basic design rules are established, and a parametric study is performed.

1.1 Backgrounds and Motivation

In December 1993 the Department of Building Technology and Structural Engineering at Aalborg University joined an international research project on scale effects and transitional failure phenomena of reinforced concrete beams in flexure under the guideness of the European Structural Integrity Society Technical Commitee 9 on concrete also refered to as ESIS-TC9.

The co-operators consisted of nine European and one Australian laboratory, and the chairman of the Round Robin was Professor Alberto Carpinteri from the Politecnico di Torino in Italy. The

purpose of the investigations was to verify the scale dependency of plastic rotational capacity and minimum reinforcement and the existance of transitional phenomena of failure. At the Structural Laboratory, Aalborg University a test-setup was established in which it was possible to examine reinforced concrete beams with variable parameters such as scale, percentage of reinforcement and slenderness.

A test programme was then initiated and consisted of a total of 117 beams, where beams with six different reinforcement ratios, two compressive strengths, three different sizes and three slenderness ratios were investigated. Additional reinforcement such as compressive reinforcement and stirrups were left out of the investigations. As the test were performed in three-point bending, stirrups were only placed in the beams to prevent anchorage failure and shear failure at the same time as they were placed in such a way that the stirrups had no influence on development of the plastic hinge. This project is also refered to as the first part, *ESIS 1*.

On the basis of the results of these tests, a new project was initiated to perform further investigations on the lightly reinforced regime and the heavily reinforced regime. This project deals with rotational capacity of lightly and heavily reinforced concrete beams and are refered to as the second part, *ESIS 2*.

One of the reasons to investigate these two regimes are that for both lightly and heavily reinforced concrete beams there seems to be a lack of deformation capacity due to that only a few cracks will develop in the lightly area giving tensile failure of the reinforcement and that crushing of the concrete for the heavily area is the most important factor. Thus, in the lightly area parameters such as choice of reinforcement type, concrete type and bond-slip behaviour are the most important factors on the the failure mode. For the heavily area, additional reinforcement such as compressive reinforcement, stirrups spacing, steel fibers and type of main reinforcement are very important for the ductility of the plastic hinge in a beam and therefore also very significant for the failure mode.

1.2 Scope of Work

This thesis is limited to experimental and theoretical investigations of plastic rotational capacity of normal strength concrete of grade C50 and high strength concrete of grade C90.

In the*ESIS 1* research project various parameters have been investigated such as five different reinforcement ratios, two compressive strengths, three different sizes and three different slenderness numbers.

The *ESIS 2* research project deals with lightly reinforced beams of the dimension: 100 x 200 x 2400 *mm* using two different types of reinforcement and heavily reinforced beams with the dimension: 200 x 400 x 7200 mm with three types of confinement of the compression zone. The reinforcement types in the lightly reinforced regime have been chosen as ribbed and smooth plain rebars with no significant yield capacity and ribbed and smooth plain rebars showing strain hardening effects.

The main purpose of chosing different kind of steel types is that it is possible to investigate both very brittle reinforced and very ductile reinforced beams and thereby estimate different rotational capacities. The results are also compared with lightly reinforced beams from the *ESIS 1* project. In the heavily reinforced regime beams of different reinforcement ratios are tested to ultimate failure in order to investigate the plastic rotational capacity. Beams with plain concrete confinement as the beams tested in the *ESIS 1* project, steel-fiber confinement and stirrup confinement of the compression zone are investigated.

The experiments are compared with a model for rebar tensile failure and a model for compression failure. The purpose of the models are to estimate the plastic rotational capacity using different methods based on the measurements of the beams. The models are based on a semi-classical approach for the lightly reinforced regime taking into account the multiple cracking and the debonding between the reinforcement and the concrete, and on a fracture mechanical concept for the heavily reinforced regime, where the softening in compression are assumed to be dependent on the size of the structure.

Analytical parametric studies of the two regimes are performed for a variation of the key parameters, and comparisons with different calculations models for plastic rotational capacity are carried out.

1.3 Readers Guide

In the two first chapters 2 and 3, some basic models of reinforced concrete beams under three-point bending is defined. The models are based on classical principles using semi-classical fracture mechanical concepts for prediction of cracking response and bond-slip behaviour for the lightly reinforced state. The model predicts number of cracks, load-deflection response and an estimate of the plastic rotational capacity.

In chapter 3 a model for the normal and over-reinforced state is defined using basic constitutive relations and equivalence conditions for the cross-section. The softening of the concrete in compression is modelled using simple softening relations and methods taken from the literature.

In chapter 4 experimental results for a huge test programme are summarized. The test programme have consisted of beam of different sizes and different strengths.

In chapter 5 investigations of the limits of the reinforcement ratio are performed as beams at very low and very high reinfiorcement ratios are tested to ultimate failure.

Finally, a comparison of the analytical methods and the experiments are performed in chapter 6. The estimated key parameters found herein are compared with literary studies.

In chapter 7 a summary of the investigations are made, and some suggestitions to further research on the topic are discussed and proposed.

Chapter 2

Model for Rotational Capacity of Lightly Reinforced Concrete Beams

The main focus of this chapter is to obtain a tool for modelling the flexural behaviour of simply supported lightly reinforced concrete beams subjected to ultimate failure. Knowing the flexural behaviour it is possible to gain a measure for the ductility of a beam given by the rotational capacity. Here, the rotational capacity will be defined as the total plastic work obtained from the area under the load-deflection curve divided by the yielding moment of the beam taking into account also the tensile fracture energy dissipation from the multiple cracking along the beam-axis. Features of the model tool will be shown for beams of different size and different reinforcement in order to observe size effects and influence of debonding on the crack spacing. The model tool is suitable for modelling RC beams in a load control system showing only re-bar tension failure.

2.1 Introduction

The purpose of this chapter is to formulate a model for the rotational capacity of reinforced concrete beams assuming re-bar tension failure. The model is based on a classical approach and establishes the load-deflection curve of a reinforced concrete beam. The rotational capacity is then obtained as the area under the load-deflection curve divided by the yield moment of the beam. In calculating the load-deflection curve, the cracking process of the concrete is ignored. By assuming that all cracks are fully opened, the energy dissipated during cracking of the concrete is taken into account by simply adding the total tensile fracture energy to the total plastic work obtained by the classical analysis.

The considered problem is the bending behaviour of simply supported beams, Figure 2.1. The basic variables are the beam geometry given by the width b, the depth h and the span l, the concentrated load F acting at the middle of the beam and the corresponding displacement u.

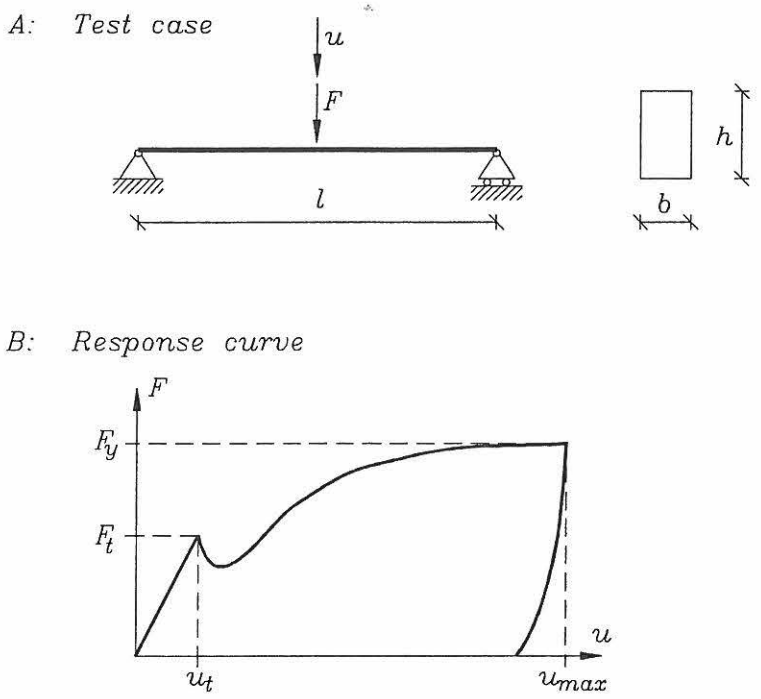

Figure 2.1: *Fundamental problem of the investigation. A: The test case, B: Response curve.*

The bending response of the beam is described by the load-deflection curve, Figure 2.1, depicting the loading force F as a function of the displacement u.

It is assumed, that the parameters influencing the bending response of the beam, apart from the basic parameters mentioned above, are the concrete type described by Young's Modulus E_{co}, the tensile and compressive strength f_t and f_c, the reinforcement type given by the stress-strain relation for the steel and the shear friction friction stress τ_f for the debonding, the reinforcement ratio $\rho = (A_s / b\, h_{ef})$, where A_s is the reinforcement area, the number of re-bars n_{ref} and the placement of the re-bars as given by the distance h_{ef} from the top of the beam. It should be noted, that no softening relation of the concrete and reinforcement is considered. Thus, in this analysis, the contribution from necking of the re-bars and cracking of the concrete are neglected.

At early stages of the failure process, the response is governed by the tensile properties of the concrete, the elastic properties of the reinforcement steel and the debonding process between concrete and steel. Typically, the response will show a local force maximum F_t where the concrete starts cracking, a decrease afterwards, and the a slowly increasing response as the reinforcement starts debonding taking over the stresses relieved by concrete tensile fracture. Later, when the tensile stresses in the concrete have decreased to zero, and yielding of the reinforcement bars is fully developed, the response curve reaches a nearly constant value F_y. For convience, here F_y is just defined as the maximum value of the response in the "yielding regime".

Since concrete tension failure is highly size dependent, the first part of the response curve will show strong size effects. For large beams, the concrete contribution will be small and brittle compared to smaller beams, meaning that the ratio F_t / F_y will be size dependent. Thus, the ratio F_t / F_y is a central parameter for description of the size effects at early stages of the failure process. It describes, one can say, the size effect on the load scale. In most standards, the minimum reinforcement requirements aim at keeping this ratio below a certain value, securing a ductile behaviour of the beam in load control. Therefore, size effects at early stages of the failure process are closely associated with the minimum reinforcement issue.

When studying size effects on the late stages of the failure process, it is necessary to focus on the deformation scale. Thus, it might seem natural to choose a corresponding set of displacement parameters u_t and u_{max}, see Figure 2.1, and then define the corresponding ratio as the key parameter. However, since both displacements are inluenced by the elastic response of the beam, in this chapter a non-dimensional parameter θ describing size effects on the displacement scale is defined by the work equation

$$\theta M_y = \int_0^\infty F \, du \tag{2.1}$$

where M_y is the yield moment corresponding to the yield force F_y.

Now, using the simple relationship $M_y = \frac{1}{4} F_y l$, the parameter θ is given by

$$\theta = \frac{4}{l} \int_0^\infty \frac{F}{F_y} \, du \tag{2.2}$$

As it appears, the integral has the dimension of length, describing the total plastic deformation of the beam. This measure is not influenced by the elastic contributions and is non-sensitive to the tension failure behaviour of the concrete as long as the contribution to the area under the response curve is small.

The geometric interpretation of the parameter θ is the total concentrated rotation at the yielding section under the loading force. Thus, it is a measure of the rotational capacity of the beam.

In the next sections a semi-classical model for the flexural behaviour of a lightly reinforced concrete beam is presented. Knowing the load-deflection response of a lightly reinforced concrete beam, it is possible to calculate the plastic rotational capacity using Equation (2.2). Finally, size effects on the rotational capacity of concrete beams are studied using the semi-classical approach for the lightly reinforced case, where the the rotational capacity is controlled by the number of cracks in the tension side of the beam.

2.2 Flexural Behaviour of Lightly Reinforced Concrete Beams assuming Rebar Tension Failure

In this section modelling of the load-deflection curve of a lightly reinforced concrete beam is presented taking into account multiple cracking and bond-slip between reinforcement and concrete.

In the analysis it is assumed, that the beam is simply supported, and that the main reinforcement is placed in one layer as shown in Figure 2.2. Besides, no stirrups and compressive reinforcement have been considered, and contributions to the ductility of the beam from the shear forces are not taken account. In order to simplify the analysis it is assumed that plane sections remain plane.

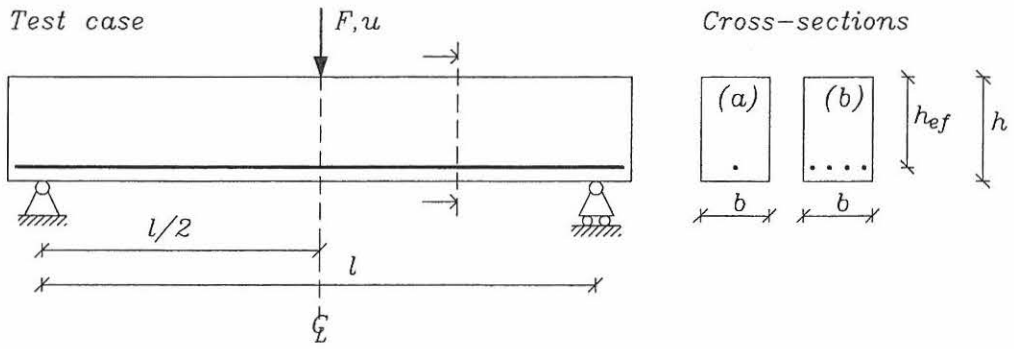

Figure 2.2: *A simply supported lightly reinforced concrete beam used in the analysis showing two choices of cross-section (a) and (b).*

The stress-strain relation of the concrete and reinforcement used in the analysis are given in Figure 2.3 as (*A*), symbolizes the stresses in the critical cross-section before cracking, and (*B*) immediatly after cracking of the concrete. It is possible to define the reinforcement either as a high ductile (steel type A) or a brittle steel (steel type B), see Figure 2.3, assuming that the reinforcement stress σ_s increases for increasing reinforcement strain ε_s, because within this analysis, it is not possible to model a softening load-deflection curve. The ultimate failure picture of the beam is here defined as re-bar tension failure occuring when the ultimate reinforcement strain ε_{su} is reached, allowing the compressive concrete strain ε_c to be of a higher value than the ultimate concrete strain ε_{cu}, which will occur in the normal reinforced regime.

2.2.1 Modelling the Load-Deflection Curve

In etablishing the load-deflection curve until ultimate failure it has been conviened to describe the flexural behaviour in three states by a load factor $\psi = M_{cr} / M$, where M_{cr} is the cracking moment and M the bending moment subjected to the beam at the midspan.

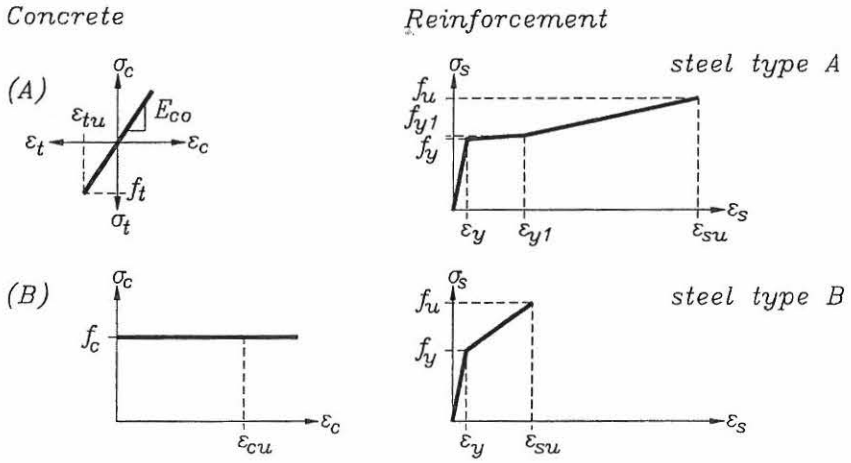

Figure 2.3: *Simplified stress-strain relation for the concrete (left) before (A) and after (B) cracking of the concrete, and choice of steel type (right): steel type A (high yield capacity) and steel type B (low yield capacity).*

The states are defined as: a *continuum state*, where the concrete and reinforcement behave in an elastically manner ($\psi < 1$), a *cracking state* defining the cracking moment of the beam, as the 1. crack develops ($\psi = 1$), a *discrete/multiple cracking state* allowing the 1. crack or even more cracks to develop, until tensile failure of the reinforcement occurs ($\psi > 1$), and finally a *deloading state* simply given by redrawing the elastic deflection at the maximum load.

An example of the full range behaviour of a bent beam with a discrete and multiple cracking picture is illustrated in Figure 2.4, where the different states are marked only for the beam showing discrete cracking.

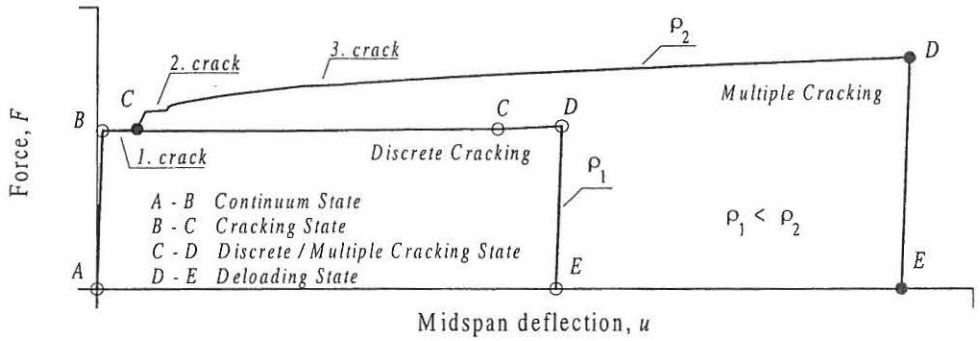

Figure 2.4: *Types of load-deflection curves for lightly reinforced concrete beams showing both discrete cracking and multiple cracking while running through the four different states for the critical cross-section (A→E) of the beam.*

Typical stress and strain distributions for the critical cross-section and each of the fracture states are shown in Figure 2.5.

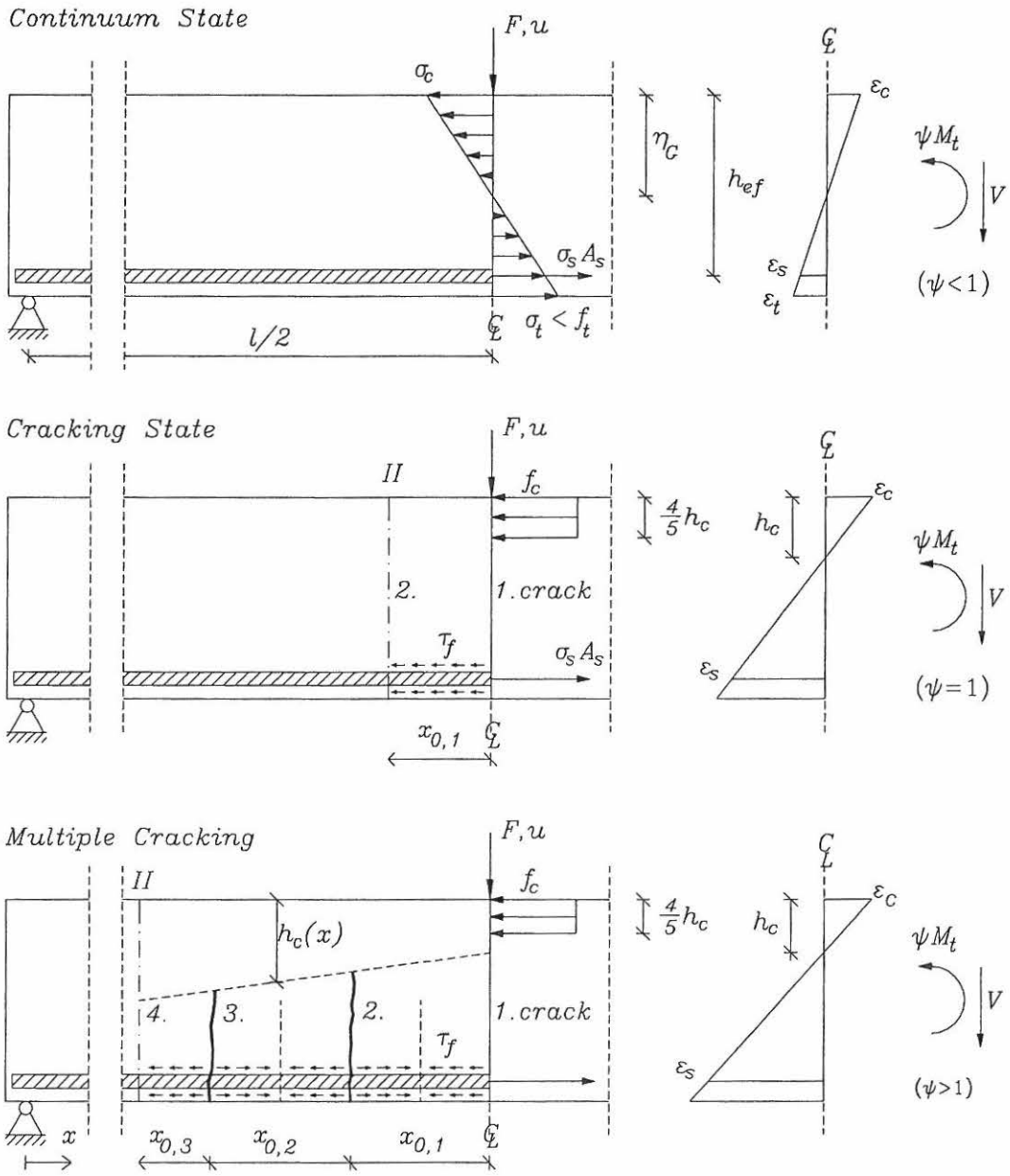

Figure 2.5: *Stress and strain distribution for the critical cross-section of a lightly reinforced concrete beam in the three different states.*

The Continuum State

For the continuum state it is assumed, that before cracking of the concrete, both the concrete and the reinforcement are assumed to behave elastically, and no slip is assumed between concrete and reinforcement. Assuming a linear variation of the normal beam strain over the cross-section, the stress distribution is obtained by classical beam theory.

As the bending moment is given by $M = \psi M_{cr}$, $\psi < 1$, the stresses and strains for the concrete at the bottom of the critical cross-section, σ_c and ε_c and for the reinforcement, σ_s and ε_s are therefore

$$\sigma_t = \frac{\psi M_{cr}}{I_{zt,r}}(h - \eta_G) \quad \text{and} \quad \varepsilon_t = \frac{\sigma_t}{E_{co}} \quad \text{for} \quad \psi < 1$$
$$\sigma_s = \alpha \frac{\psi M_{cr}}{I_{zt,r}}(h_{ef} - \eta_G) \quad \text{and} \quad \varepsilon_s = \frac{\sigma_s}{E_s} \quad \text{for} \quad \psi < 1 \tag{2.3}$$

where α is the ratio of the E-modulus E_s / E_{co}, $I_{zt,r}$ the transformed moment of inertia, and η_G the distance from the top of the beam to the centre of gravity of the cross-section.

The flexural behaviour for the continuum state is described as non-dimensional load - deflection curves with respect to the yielding load F_y and the span of the beam l simply by

$$\frac{F}{F_y} = \psi \frac{M_{cr}}{M_y} \quad \Rightarrow \quad F = \frac{4}{l} \psi M_{cr} \quad \text{for} \quad \psi < 1$$
$$\frac{u}{l} = \frac{1}{48} \frac{F l^2}{E_{co} I_{zt,r}} \quad \Rightarrow \quad u = \frac{1}{48} \frac{F l^3}{E_{co} I_{zt,r}} \quad \text{for} \quad \psi < 1 \tag{2.4}$$

defining a linear function, $F(u)$ until the point (F_t, u_t).

The Cracking State

The cracking state is defined as the state, where the tensile strength is reached at the tensile side of the beam, and the concrete is assumed to crack. Further, cracks are assumed to be formed during constant bending moment (no decrease of the bending moment) and are allowed to extend until the level of the neutral axis.

When the concrete tensile strength is reached, the constitutive relations for the concrete and reinforcement are given as

$$\sigma_t = f_t \qquad \text{and} \qquad \varepsilon_t = \varepsilon_{tu} \qquad \text{for} \qquad \psi = 1$$

$$\sigma_s = \alpha \frac{M_{cr}}{I_{zt,r}} (h_{ef} - \eta_G) \qquad \text{and} \qquad \varepsilon_s = \frac{\sigma_s}{E_s} \qquad \text{for} \qquad \psi = 1 \tag{2.5}$$

and the cracking moment and the cracking point (F_t, u_t) are hereby expressed by

$$M_{cr} = \frac{f_t \, I_{zt,r}}{h - \eta_G} \qquad \text{for} \qquad \psi = 1$$

$$\frac{F_t}{F_y} = \frac{M_{cr}}{M_y} \qquad \text{and} \qquad \frac{u_t}{l} = \frac{1}{48} \frac{F_t l^2}{E_{co} I_{zt,r}} \qquad \text{for} \qquad \psi = 1 \tag{2.6}$$

At the time of cracking, the moment of the compressive and tensile forces in the cracked cross-section is eqvivalent with the cracking moment. The tension force N_s from the reinforcement is balanced by compression stresses N_c in the concrete. The size of the compression zone h_c is obtained by assuming a uniform distribution of the compression stresses and using an equilibrium equation.

The consitutive relations are now expressed as

$$\sigma_c = f_c \qquad \text{and} \qquad \varepsilon_c = \frac{1}{\xi - 1} \varepsilon_s \qquad \text{for} \qquad \psi = 1$$

$$\sigma_s = \frac{M_t}{A_s h_{int}} \qquad \text{and} \qquad \varepsilon_s = \varepsilon_s (\sigma_s) \qquad \text{for} \qquad \psi = 1 \tag{2.7}$$

where ξ is the normalized size of the compression zone h_c / h_{ef} and h_{int} the inner moment arm $h_{ef} - \frac{2}{5} h_c$.

The size of the compression zone $h_c = \xi h_{ef}$ is calculated using the equivalence of the moment

$$M_t = \frac{4}{5} h_c b f_c (h_{ef} - \frac{2}{5} h_c) \quad \Rightarrow \quad \xi = \frac{5}{4} \pm \frac{5}{4} \sqrt{1 - 2 \frac{M_t}{b f_c h_{ef}^2}} \qquad \text{for} \qquad \psi = 1 \tag{2.8}$$

At the cracked section the tensile force N_s in the reinforcement is transferred to the surrounding

concrete by assuming a formation of two debonded zones around the crack with constant shear friction stress τ_f, see Figure 2.5. Assuming a pure friction model, the size of the debonding zone x_0 is given as

$$A_s(\sigma_s - E_s \varepsilon_{tu}) = \tau_f p x_0 \quad \Rightarrow \quad x_0 = (\sigma_s - \frac{E_s}{E_{co}} f_t) \frac{d}{4 \tau_f} \quad \text{for} \quad \psi = 1 \tag{2.9}$$

where p is the perimeter of the re-bar πd.

The crack width (total bond slip from both crack surfaces) is the sum of the strains distributed along the debonding length, x_0 expressed by

$$w_c = 2 \int_0^{x_0} \varepsilon_s(\sigma_s)\, dx - 2 \int_0^{x_0} \varepsilon_c(x)\, dx \qquad \text{for} \qquad \psi = 1 \tag{2.10}$$

The crack angle (the angle between two crack surfaces on one crack) and the curvature for the critical cross-section is assumed to be equal to the rotation of the beam over the debonding length and is then determined according to

$$\varphi = \frac{w_c}{h_{ef} - h_c} \qquad \text{and} \qquad \varkappa = \frac{\varphi}{x_0} = \frac{\varepsilon_s}{h_{ef} - h_c} \qquad \text{for} \qquad \psi = 1 \tag{2.11}$$

Assuming that the beam deforms like a rigid body, the total vertical deflection of the midspan for the 1. crack u is given by

$$u_\varphi = \frac{\varphi l}{4} \quad \Rightarrow \quad u = u_t + u_\varphi \qquad \text{for} \qquad \psi = 1 \tag{2.12}$$

and while the bending moment M_t is constant during formation of the 1. crack, until the level of the neutal axis, the load-deflection curve is now given by

$$\frac{F}{F_y} = \frac{F_t}{F_y} = \frac{M_t}{M_y} \qquad \text{and} \qquad \frac{u}{l} = \frac{u_t}{l} + \frac{u_\varphi}{l} = \frac{1}{48} \frac{F_t l^2}{E_{co} I_{z,t}} + \frac{\varphi}{4} \qquad \text{for} \quad \psi = 1 \tag{2.13}$$

defining a horizontal part on the load-deflection curve until the point (F_t, u).

The Discrete / Multiple Cracking State

In the discrete/multiple cracking state the bending moment is increased beyond the cracking moment allowing either a discrete cracking (1 crack develops) or a multiple cracking (several cracks develop) picture at the ultimate state.

The crack development is initated, when the tensile strength is reached at the tensile side of the beam in the cross-section with maximum bending moment. This corresponds to the situation in the cracking state, see also Figure 2.4 and 2.5. As the load increases, that is $\psi > 1$, cracks might form in neighbour sections. If the bending moment is equal to the cracking moment at section II, see Figure 2.5, a new crack will be formed at section II using the principles of the cracking state. If the bending moment is less than the cracking moment, the load is increased causing the debonded zones to extend, and section II will be in the continuum state. By repeating this procedure cracks are formed one by one, until tensile failure of the reinforcement bar. At the time a new crack is formed, it is assumed, that the strain at section II is the same in the concrete and in the reinforcement, and that the strain is equal to the tensile fracture strain of the concrete, and thus given by $\varepsilon_{tu} = f_t / E_{co}$.

The constitutive relation for the critical cross-section is simply given by

$$\begin{aligned} \sigma_c &= f_c \quad \text{and} \quad \varepsilon_c = \frac{1}{\xi - 1}\varepsilon_s \quad \text{for} \quad \psi > 1 \\ \sigma_s &= \frac{\psi M}{A_s h_{int}} \quad \text{and} \quad \varepsilon_s = \varepsilon_s(\sigma_s) \quad \text{for} \quad \psi > 1 \end{aligned} \tag{2.14}$$

The load-deflection curve is found by integrating the curvature over the length of the beam. The curvature is determined as the ratio between the reinforcement strain and the distance from the to the neutral axis at the cracked sections. Actually, the load-deflection curve is estimated using a summation of the total beam rotation given by the total sum of crack angles distributed over the length of the beam, and the deflection u could be expressed as

$$\begin{aligned} &\text{Discrete cracking:} \quad u = u_t + \frac{1}{4}\varphi_1 l \quad \psi > 1 \\ &\text{Multiple cracking:} \quad u = u_t + \frac{1}{2}(\varphi_1 + \varphi_2 + \ldots + \varphi_m) l \quad \psi > 1 \end{aligned} \tag{2.15}$$

where φ_m is the crack angle of the m. crack on the half of the beam given by

$$\varphi_1 = \frac{w_{c,1}}{h_{ef} - h_{c,1}} \quad \text{and} \quad w_{c,1} = 2\int_0^{x_{0,1}} \varepsilon_1(x)\,dx$$

$$\varphi_m = \frac{w_{c,m}}{h_{ef} - h_{c,m}} \quad \text{and} \quad w_{c,m} = \int_0^{\frac{1}{2}x_{0,m}} \varepsilon_m(x)\,dx + \int_0^{\frac{1}{2}x_{0,m+1}} \varepsilon_m(x)\,dx \tag{2.16}$$

where $\varepsilon_m(x) = \varepsilon_{s,m}(x) - \varepsilon_c(x)$.

As the bending moment increases for $\psi > 1$, the load-deflection curve is now expressed by

$$\frac{F}{F_y} = \psi \frac{M_t}{M_y} \qquad \text{for} \qquad \psi > 1$$

$$\frac{u}{l} = \frac{u_t}{l} + \frac{1}{2}(\varphi_1 + \varphi_1 + \ldots + \varphi_m) \qquad \text{for} \qquad \psi > 1 \tag{2.17}$$

which defines a increasing function, until a new crack develops giving a horizontal part, and then again an increasing part and so on.

Typical load-deflection curves for a normal strength concrete beam of different sizes and two different reinforcement ratios $\rho = 0.11$ % and $\rho = 0.21$ % are shown in Figure 2.6 and Figure 2.7 using a shear friction stress τ_f = 5 N/mm^2 and a concrete strength f_c = 60 N/mm^2. The reinforcement is chosen as a high yield capacity steel bar (steel type A).

For the beams of the reinforcement ratio equal to $\rho = 0.11$ %, is it observed, that only a few cracks will develop in the beam before ultimate failure, whereas for the beams of reinforcement ratio $\rho = 0.21$ % more cracks will develop, and the cracks will occur at the same force ratio F / F_y of each beam.

By this rebar tensile failure analysis, no size effects on the load-deflection response are observed, when the same type of concrete and reinforcement and bond slip behaviour are used in scaling of the beams. When all cracks are fully developed, the load-deflection response is only influenced by the reinforcement properties.

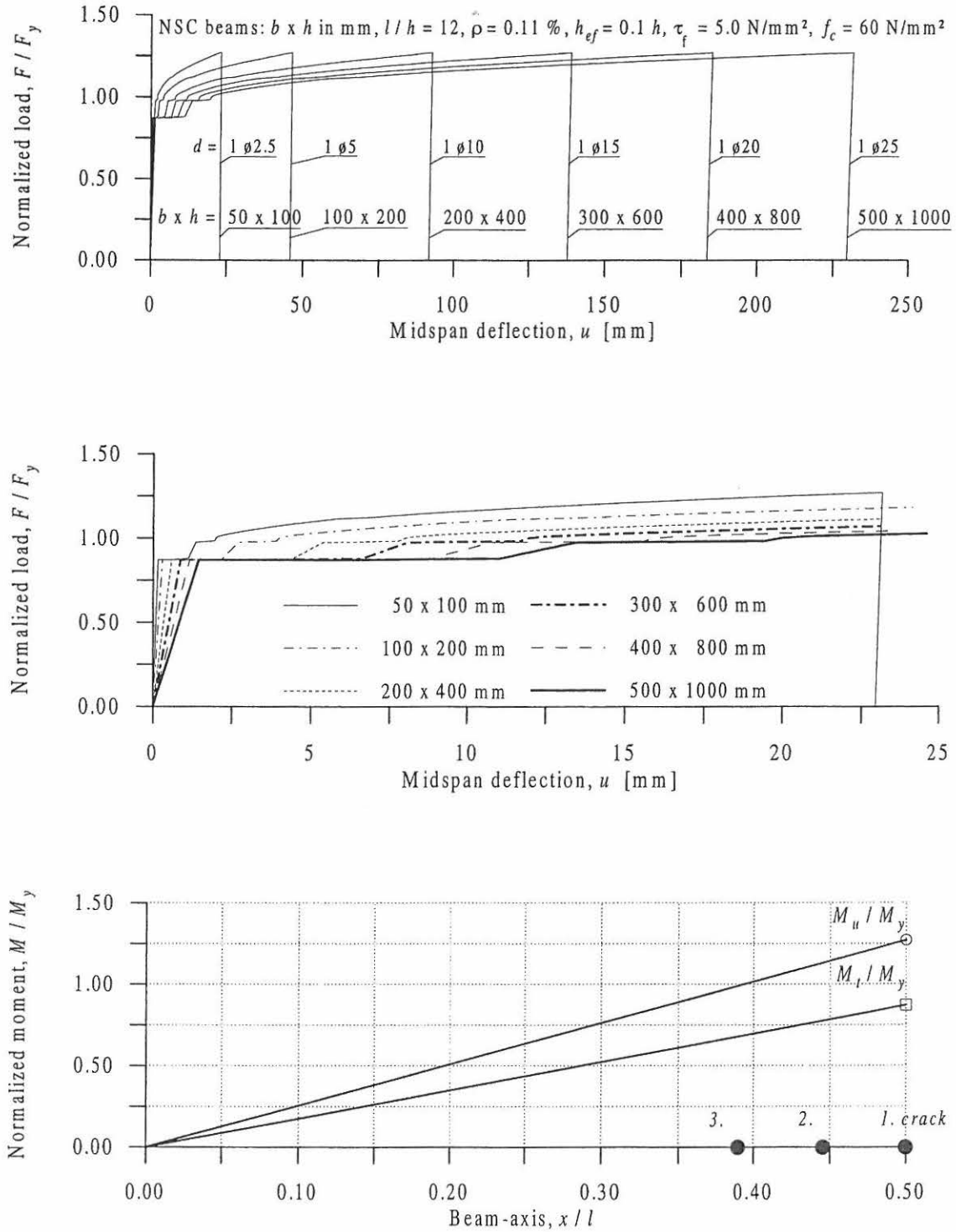

Figure 2.6: *Load-deflection curves for a normal strength concrete beam of different sizes (b x h). The slenderness number is l / h = 12, the reinforcement ratio ρ = 0.11 % and the shear friction stress τ_f = 5 N/mm². (Top) Full range behaviour, (middle) the multiple cracking of the concrete and (bottom) normalized tensile and ultimate moment distributed along the beam axis.*

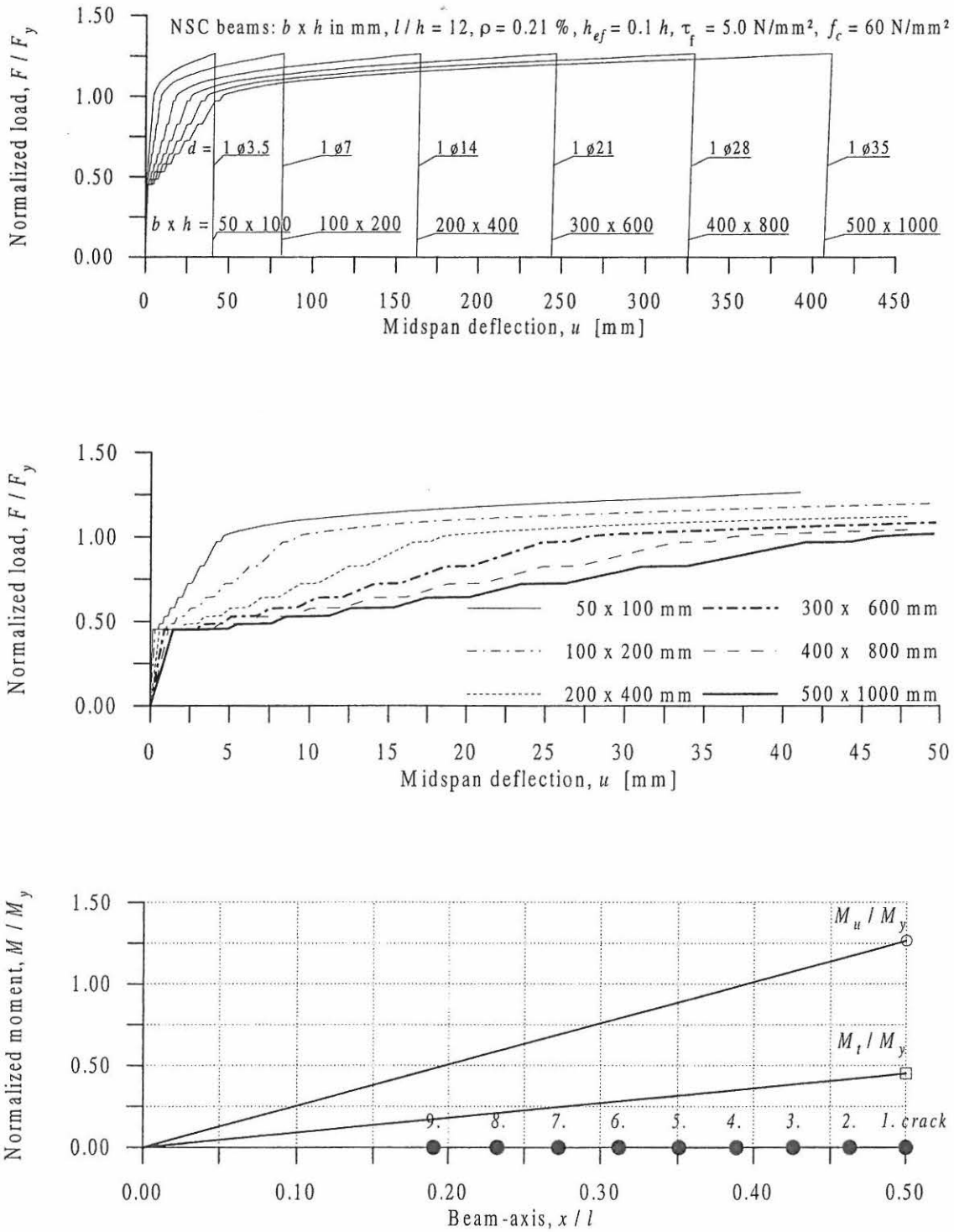

Figure 2.7: *Load-deflection curves for a normal strength concrete beam of different sizes (b x h). The slenderness number is l / h = 12, the reinforcement ratio ρ = 0.21 % and the shear friction stress τ_f = 5 N/mm². (Top) Full range behaviour, (middle) the multiple cracking of the concrete and (bottom) normalized tensile and ultimate moment distributed along the beam axis.*

2.2.2 Modelling the Rotational Capacity

The rotational capacity is calculated by integrating the load-deflection curve according to Equation (2.1) and adding the energy dissipated in the crack formation process estimated as nA_cG_F, where n is the number of cracks given as $2m$ - 1, A_c is the cross-sectional area of the beam b x h, and G_F is the tensile fracture energy of the concrete.

The rotational capacity θ could then be expressed, as the total work under the load-deflection curve deducting the elastic part from the deloading state, and thus the rotational capacity θ is

$$\theta = \theta_{work} + \theta_{cracks} \quad \Rightarrow$$

$$\theta_{work} = \frac{1}{M_y}\int_0^{u_{max}} F\,du - \frac{1}{2}\frac{1}{M_y}u_{el,u}F_u \tag{2.18}$$

$$\theta_{cracks} = \frac{n A_c G_F}{M_y} \qquad \text{where} \qquad n = 2m - 1$$

where $u_{el,u}$ is the deflection from the deloading at the force F and M is the yield moment according to DS411 (1997).

The yield moment of the cross-section is given by

$$M_y = A_s f_y (h_{ef} - \frac{2}{5}h_c) \qquad \text{where} \qquad h_c = \frac{5 A_s f_y}{4 b f_c} \tag{2.19}$$

In Figure 2.8 the rotational capacities calculated by Equation (3.18) of the normal strength concrete beams presented in Figure 2.6 for $\rho = 0.11$ % and in Figure 2.7 for $\rho = 0.21$ % are shown as a function of the beam depth.

It is observed, that the rotational capacity is highest for the smallest beam types, but the function is actually almost constant. The contribution to the rotational capacity from the crack distribution is low, but it seems to be highest also for the smaller beams. Besides, the difference in doubling the reinforcement ratio are higher for θ_{work} than for θ_{cracks}, because of the increasing ultimate deflection and multiple cracking.

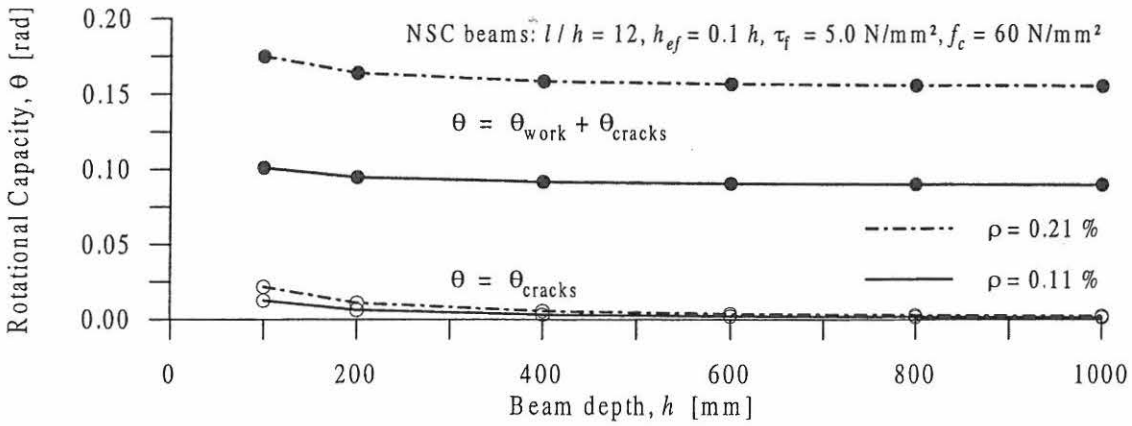

Figure 2.8: *Rotational capacity as a function of the beam depth for a normal reinforced concrete beam of different sizes. The slenderness number is l/h = 12, and the reinforcement ratio is ρ = 0.11 % and 0.21 %.*

2.3 Basic Properties of the Model

In the past section it has been able to produce a tool for modelling the load-deflection curve and thereby a calculation model for the rotational capacity valid for three point bending statically systems. It has been observed, that increasing the reinforcement ratio under a constant shear friction stress will result in an increasing amount of cracks along the beam-axis and a higher ductility of the plastic hinge at the center of a beam, when the ultimate failure is dependent only on the deformation capacity of the steel.

In the next subsections some properties of the model are presented mainly concerning the variation of the shear friction stress describing the bond slip behaviour, the reinforcement strength parameters and the concrete strength parameters.

The main topics are

- The influence of shear friction stress
- The influence of reinforcement strain hardening and ultimate steel strain
- The influence of concrete strength parameters

on the rotational capacity of a lightly reinforced concrete beam.

The properties of the model are investigated for a lightly reinforced concrete beam of dimension: width b = 100 mm, depth h = 200 mm and span l = 2400 mm, and in order to investigate any size effects b, h and l/h are varied. The main reinforcement are placed in the cross-section of the beam as one single bar at an effective depth of $h_{ef} = \zeta\, h$, where ζ is chosen as 0.90, from the top of the beam giving a concrete thickness layer of 0.1 h.

2.3.1 Material Parameters of the Concrete and Reinforcement

The material parameters of the concrete and reinforcement are chosen to comply with the modelled constitutive relations presented in Figure 2.3.

Reinforcement

Investigating the model properties, results have been derived using the values of the material parameters as shown for the reinforcement steel types in Figure 2.9.

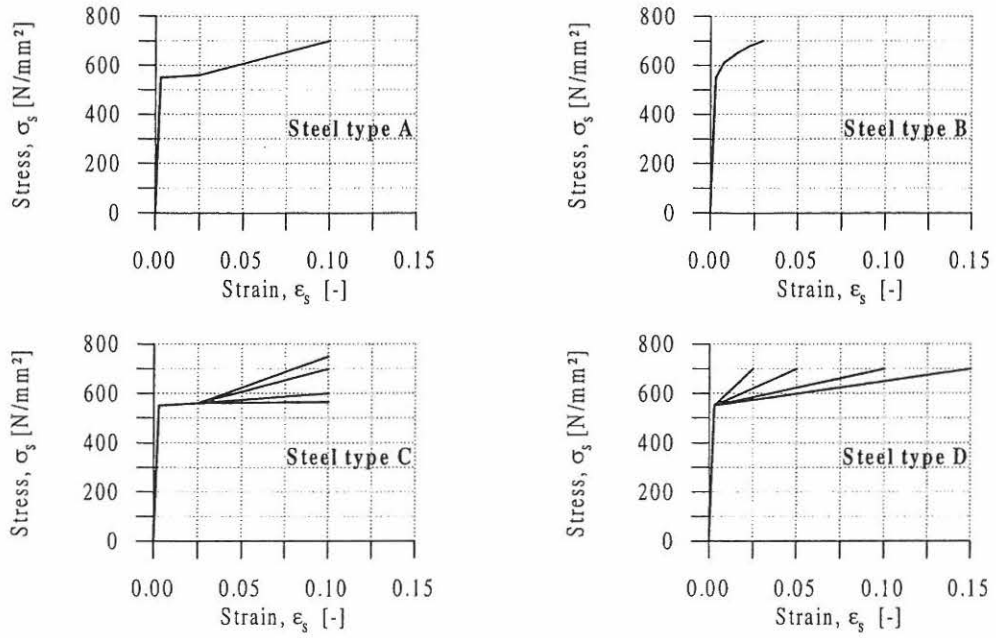

Figure 2.9: *Chosen stress-strain relations (top) and values of the strain hardening parameter and the ultimate strain (bottom) for the reinforcement steel type A and B used in modelling the failure reponse of lightly reinforced concrete beams.*

The reinforcement is chosen as rebars with a high yield capacity, (steel type A) and with a low yield capacity (steel type B), e.g. hotrolled ribbed bars and cold deformed ribbed bars. The values of strain hardening parameters and ultimate steel strains used in the modelling are characterized by steel type C and steel type D. In Table 2.1 the characteristics of the steel types are given. The reinforcement ratio ρ is varied from 0.08 % (1 ø 4.2 mm) and 0.11 % (1 ø 5 mm) to 0.63 % (1 ø 12 mm) increasing the diameter by 1 mm.

The bond between the reinforcement and concrete are assumed to be linear distributed with a constant shear friction stress τ_f in the range of 1.0 N/mm^2 to 20 N/mm^2, e.g. low values for plain reinforcing bars and higher values for ribbed, ductile bars with a large rib area.

Steel	E_s	ε_{yl}	ε_{su}	f_y	f_{yl}	f_{su}
	[N/mm^2]	[%]	[%]	[N/mm^2]	[N/mm^2]	[N/mm^2]
A	2.0E5	2.5	10	550	560	700
B	2.0E5	-	3.0	550	-	700
C	2.0E5	2.5	10	550	560	565, 600, 700, 750
D	2.0E5	-	2.5, 5.0, 10, 15	550	-	700

Table 2.1: *Material parameters for the chosen reinforcement types A, B, C and D. The symbols for the material parameters are shown in Figure 2.3. The yield strain of the reinforcement is defined as* $\varepsilon_y = f_y / E_s$.

Concrete

The material parameters used for the constitutive relation of the concrete are the compressive strength, the tensile strength and the modulus of elasticity, see Figure 2.3. Besides, also the fracture energy and the shear friction stress are influenced by the concrete strength parameters.

The material properties of the normal strength and high strength concrete are determined according to the Danish Code, DS 411 (1997), which is valid for a maximum concrete grade of C50. Here, it is assumed, that the rules also are valid for grades beyond C50. Secondly, to investigate also high strength concrete, the parameters are also described according to the Comité Euro-International du Béton, CEB-FIP Model Code 1990 (1991), which is valid up to C80, and according to CEB Bulletin 228 (1995), which describes recommendations for concrete grades beyond C80.

Thus for case 1, the tensile strength $f_t = f_{ctk}$ and the modulus of elasticity $E_{oc} = E_{ok}$ are determined according to DS 411 (1997) as

$$f_{ctk} = \sqrt{0.1 f_{ck}} \qquad \text{and} \qquad E_{ok} = 51{,}000 \frac{f_{ck}}{13 + f_{ck}} \tag{2.20}$$

where $f_c = f_{ck}$ is the characteristic compressive strength.

The fracture energy is here assumed to be $G_F(f_c) = 0.120$ Nmm/mm^2, and the shear friction stress is assumed to be $\tau_f(f_c) = 5.0$ N/mm^2.

For case 2, it is assumed, that the concrete properties are given as a function of the compressive strength according to the CEB Bulletins. Thus, the tensile strength $f_t = f_{ctm}$ and modulus of

elasticity $E_{co} = E_{ci}$ are calculated from CEB Bulletin 228 (1995) as

$$f_{ctm} = f_{ctko,m}\left(\frac{f_{ck} + \Delta f}{f_{cko} + \Delta f}\right)^{0.6} \quad \text{and} \quad E_{ci} = E_{co}\left(\frac{f_{ck} + \Delta f}{f_{cmo}}\right)^{0.3} \tag{2.21}$$

and the fracture energy is expressed according to CEB-FIP Model Code 1990 (1991)

$$G_F = \alpha_F\left(\frac{f_{cm}}{f_{cmo}}\right)^{0.7} \quad \text{where} \quad \begin{cases} \alpha_F = 0.02\ \text{Nmm/mm}^2 & \text{for } d_{max} = 8\ \text{mm} \\ \alpha_F = 0.03\ \text{Nmm/mm}^2 & \text{for } d_{max} = 16\ \text{mm} \\ \alpha_F = 0.05\ \text{Nmm/mm}^2 & \text{for } d_{max} = 32\ \text{mm} \end{cases} \tag{2.22}$$

where $\Delta f = 8$ N/mm^2, $E_{co} = 22{,}000$ N/mm^2, $f_{cko}, f_{cmo} = 10$ N/mm^2, $f_{cm} = f_{ck} + \Delta f$ and $f_{ctko,m} = 1.80$ N/mm^2.

The coefficient α_F depends on the maximum aggregate size d_{max}. It should be noted, that the fracture energy is kept constant for all sizes of the structural member.

For simple reasons the friction energy of the debonding zone very close to the crack is neglected in modelling the bond-slip behaviour, and thereby the uniformly distributed shear friction stress according to CEB-FIP Model Code 1990 (1991) for confined concrete, good bond conditions, slip higher than clear rib spacing and ribbed reinforcing steel are assumed to be

$$\tau_f = 0.4\ \tau_{max} \quad \text{where} \quad \tau_{max} = 2.5\sqrt{f_{ck}} \quad \Rightarrow \quad \tau_f = \sqrt{f_{ck}} \tag{2.23}$$

where τ_{max} is the maximum bond strength of the debonding zone very close to the crack assuming a bond-slip equal to a slip value $s_1 = 1.0$ mm.

The material parameters used for the concrete are shown for the 2 cases in Figure 2.10.

In the investigation of the model properties it should be noted, that the normal strength concrete type are chosen according to the case 1 properties, that is the compressive strength, fracture energy and shear bond stress are equal to 60 N/mm^2, 0.120 Nmm/mm^2 and 5.0 N/mm^2, unless no other values are mentioned.

The maximum aggregate size d_{max} is assumed to be 8 mm.

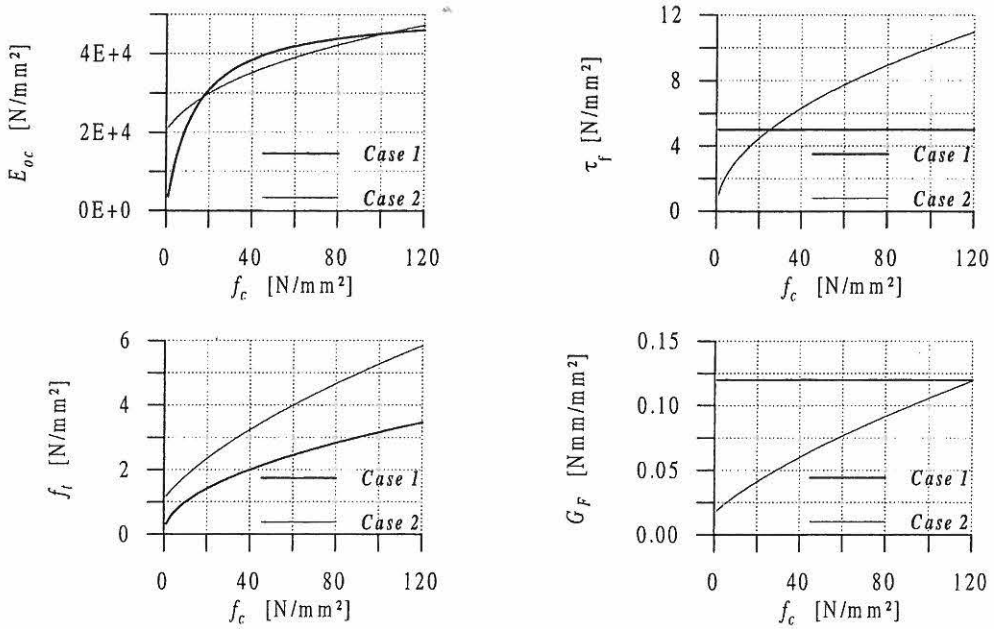

Figure 2.10: *Chosen values of the concrete strength parameters f_t, E_{co} and G_F and the shear friction stress τ_f as a function of f_c according to DS 411 (1997) (case 1), CEB-FIP Model Code 1990 (1991) (case 2) and CEB Bulletin 228 (1995) (case 2).*

2.3.2 Model Results

In the lightly reinforced regime, the rotational capacity is controlled by the number of cracks and the local debonding and yielding of the reinforcement around each crack. If no debonding takes place (case of infinite shear friction stress τ_f), the length over which yielding takes place tends to zero, and thus, the contribution from yielding of the reinforcement tends to zero. In this case however, the number of cracks becomes large and thus, so does the contribution to the total work from the cracking of the concrete. In the extreme case of a very small friction stress, only one crack develops, and thus, yielding of the reinforcement is mainly responsible for maintaining the rotational capacity.

All Figures 2.11 to 2.21 show how the rotational capacity is influenced by the reinforcement ratio. When reinforcement tensile failure controls the failure of the beam the rotational capacity is increasing with increasing reinforcement ratio.

Variation of Shear Friction Stress

One would expect the results of the model to be rather sensitive to the value of the shear friction stress τ_f. However, this is not the case, see Figure 2.11 and 2.12. In Figure 2.11 the load-deflection curves for the model beam (100 x 200 x 2400 mm) for ρ = 0.08 % to 0.63 % and τ_f =

1.0 N/mm^2 and 5.0 N/mm^2 are shown, and it is clearly seen, that by increasing the shear friction stress also will increase the amount of cracks and the yielding zone, thus the ultimate deflection decreases. For τ_f = 1.0 N/mm^2 there is a discrete cracking pattern until ρ = 0.35 %, whereas no discrete cracking occurs for τ_f = 5.0 N/mm^2. Equation (2.9) for the debonding length in pure friction $x_0 = \Delta\sigma\,(\,d\,/\,4\,\tau_f\,)$, where the resulting stress $\Delta\sigma = \sigma_{s,m} - \sigma_{s,m+1}$, shows directly the influence of τ_f on x_0. Also, the bending moment $M(x)_m$ and thereby $\sigma_{s,m}$ has a influence on the debonding length, i.e. effect of the chosen statical system. The rotational capacities of the different beams in Figure 2.11 are presented in Figure 2.12.

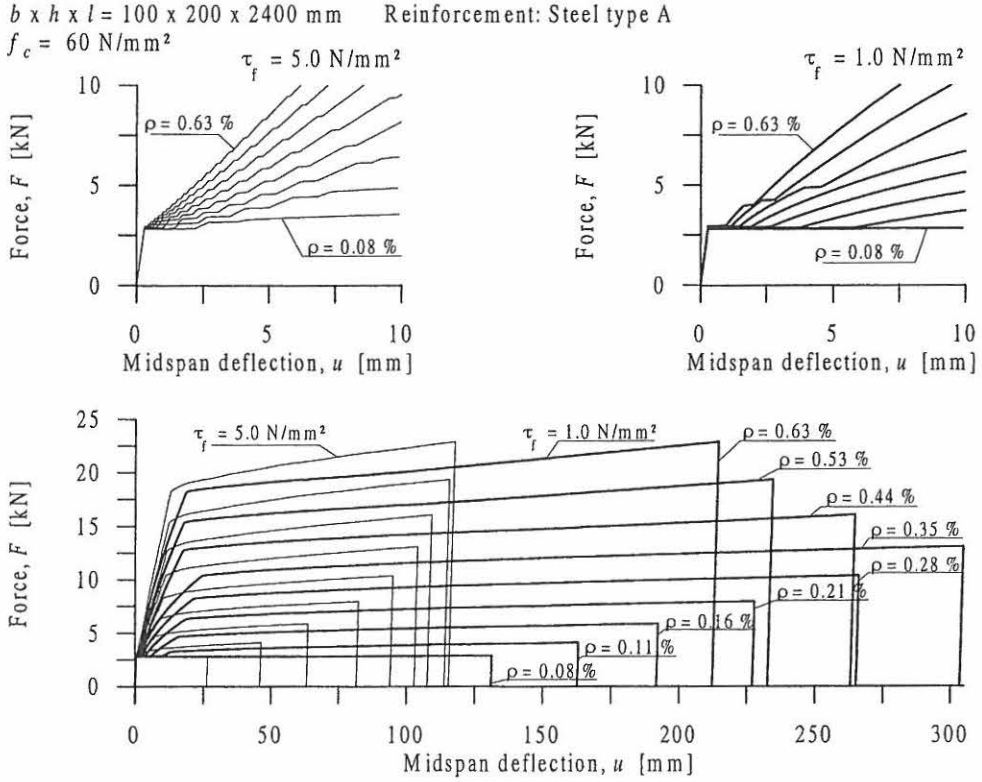

Figure 2.11: *Model results for load-deflection curves for a normal strength concrete beam (100 x 200 x 2400 mm) using shear friction stresses τ_f = 1.0 N/mm^2 and 5.0 N/mm^2 and steel type A. Top: Prepeak behaviour for τ_f = 5.0 N/mm^2 (left) and τ_f = 1.0 N/mm^2 (right). Bottom: Full range behaviour.*

Generally it can be stated, that the rotational capacity decreases with increasing friction stress, although the influence is small for values of τ_f > 1.0 N/mm^2, see Figure 2.12. The energy dissipation due to yielding and debonding decreases with increasing values of the shear friction stress, but at the same time the number of cracks increases, see Figure 2.13, and thus, the contribution from dissipation of energy in the concrete tensile cracks increases.

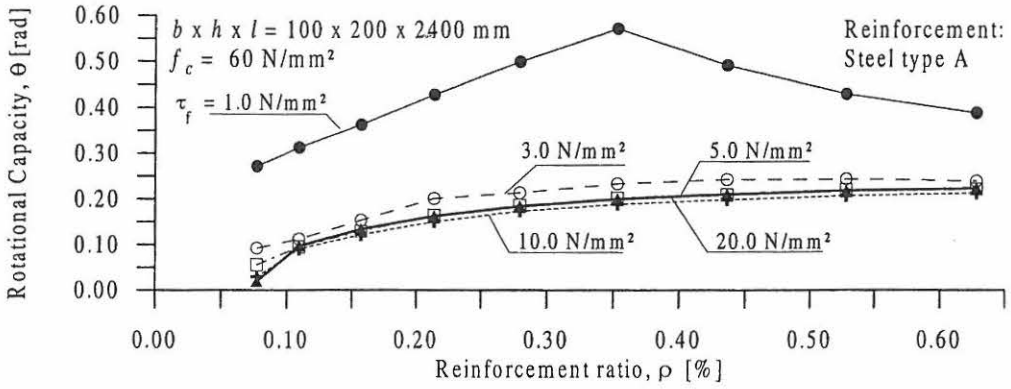

Figure 2.12: *Model results for the rotational capacity versus the reinforcement ratio for different values of the shear friction stress for a normal strength concrete beam (100 x 200 x 2400 mm).*

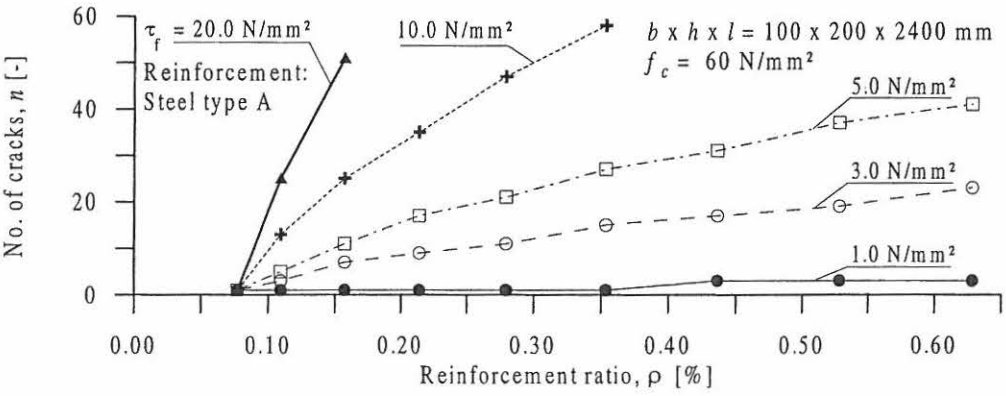

Figure 2.13: *Total number of cracks n distributed along the beam-axis for different reinforcement ratios and shear friction stresses for a normal strength concrete beam (100 x 200 x 2400 mm).*

Variation of Reinforcement Parameters

For this kind of model, one of the most important parameters is the amount of reinforcement strain hardening described by the ratio f_u / f_y. If no strain hardening is present for the steel, i.e. if the ratio $f_u / f_y = 1$, at each crack, only one point (the point situated just between the concrete tensile failure crack faces) can be in the state of yielding. Thus, since the length of the zone over which yielding takes place tends to zero when the ratio tends to 1, the rotational capacity tends to zero. Furthermore, in this case only one crack will be formed reducing the possibilities of energy dissipation even further. The results clearly support these considerations. Figure 2.14 (top) and 2.15 show, that the rotational capacity is highly dependent upon the ratio f_u / f_y. Influence of the size of the ultimate steel strain ε_{su} for a fixed f_u / f_y on the rotational capacity is clearly seen in Figure 2.14 (bottom).

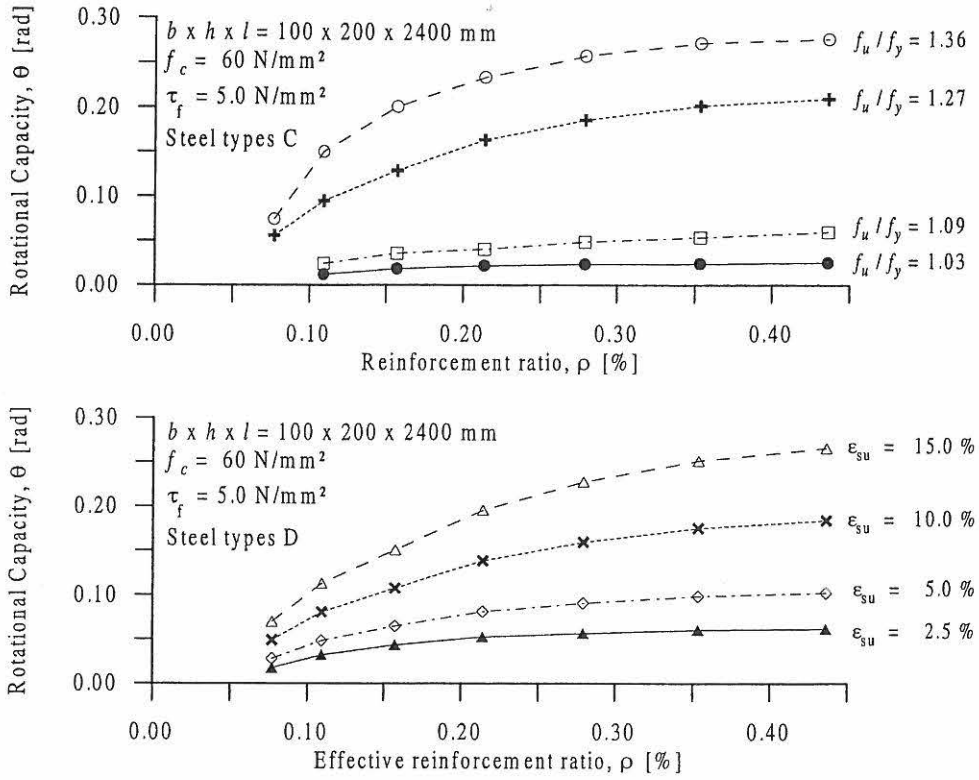

Figure 2.14: *Rotational capacity of a normal strength concrete beam (100 x 200 x 2400 mm) using different reinforcement parameters. (Top) Strain hardening properties, steel type C and (bottom) ultimate reinforcement strains, steel type D.*

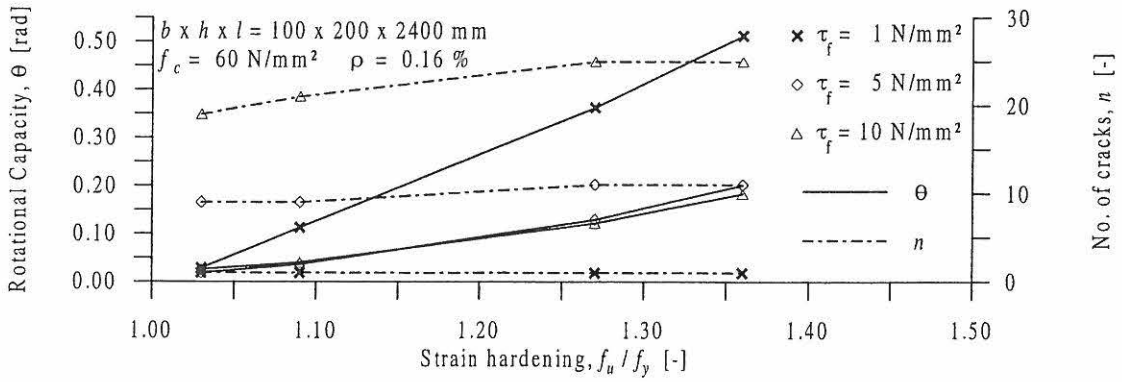

Figure 2.15: *Rotational capacity and total amount of cracks versus the strain hardening factor f_u / f_y using shear friction stresses τ_f= 1.0 N/mm², 5.0 N/mm² and 10.0 N/mm² for a normal strength concrete beam (100 x 200 x 2400 mm) with a reinforcement ratio ρ = 0.16 %.*

Variation of Concrete Strength Parameters

Figure 2.16 shows, that the load-deflection response for a beam of different strengths using the material parameters from Figure 2.10, is highly dependent on the strength of the concrete. The effect of changing the strength parameters, which is performed for case 2, is that the deflections will descrease compared with choosing fixed parameters in case 1.

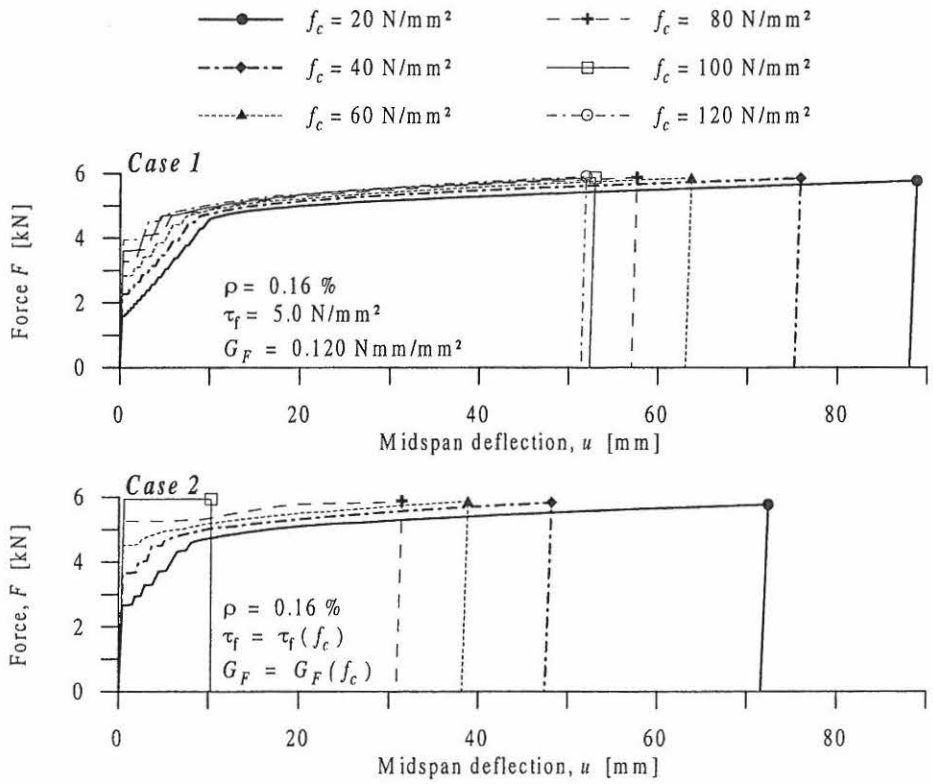

Figure 2.16: *Model results for load-deflection responses of a RC beam (100 x 200 x 2400 mm) of different concrete strengths using the concrete material properties for case 1 (top) and case 2 (bottom), and using the reinforcement steel type A.*

As it appears from Figure 2.17, increasing the concrete strength, decreases the rotational capacity for all values of the reinforcement ratio, and it is also clear, that assuming a constant shear friction stress and a tensile fracture energy for all concrete compressive strengths will result in higher rotational capacities than assuming a variation of the concrete parameters.

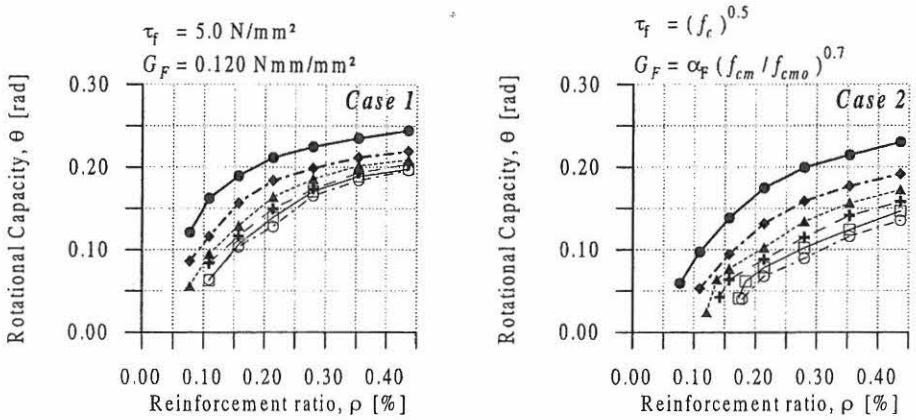

Figure 2.17: *Rotational capacity versus the reinforcement ratio for a RC beam (100 x 200 x 2400 mm) for different concrete strengths using the material properties for case 1 (left) and case 2 (right) and reinforcement steel type A. Symbols refer to Figure 2.16.*

2.3.3 Size Effects on the Rotational Capacity

Results for the rotational capacity for different beam types using steel type A and B are shown in Figure 2.18. The results clearly show, that the rotational capacity is non-sensitive to the size, but highly sensitive to the deformation capacity of the steel. For the low deformation capacity steel type B the value of the ultimate strain has been reduced $\varepsilon_{su} = 3.0$ %, whereas $\varepsilon_{su} = 10$ % for steel type A.

Figure 2.18 shows the size effects for two different values of the shear friction stress τ_f. If the shear friction stress has a small or moderate value (left part of Figure 2.18) then the number of cracks is moderate too, and the influence from the tensile failure on the rotational capacity is small. In this case, the rotational capacity is dominated by the classical contributions from yielding and frictional debonding which does not show size effects, and thus, the size effect is small. However, if the shear friction stress becomes large (right part of Figure 2.18), the number of cracks increases, and so does the contribution to the rotational capacity from dissipation of energy in the tensile cracks. Thus, since this contribution is size dependent, the total rotational capacity becomes size dependent. As it appears from the results, the shear friction stress has to be very large in order to enforce a size effect of importance, and even in that case, the size effects are still moderate.

In Figure 2.19 results of changing the beam depth of the cross-section for a constant beam width assumed to be 200 mm and a constant slenderness number assumed to be 12 are shown. It is clearly seen, that the rotational capacity depends highly on the depth. The maximal rotational capacity is obtained for low beam depths.

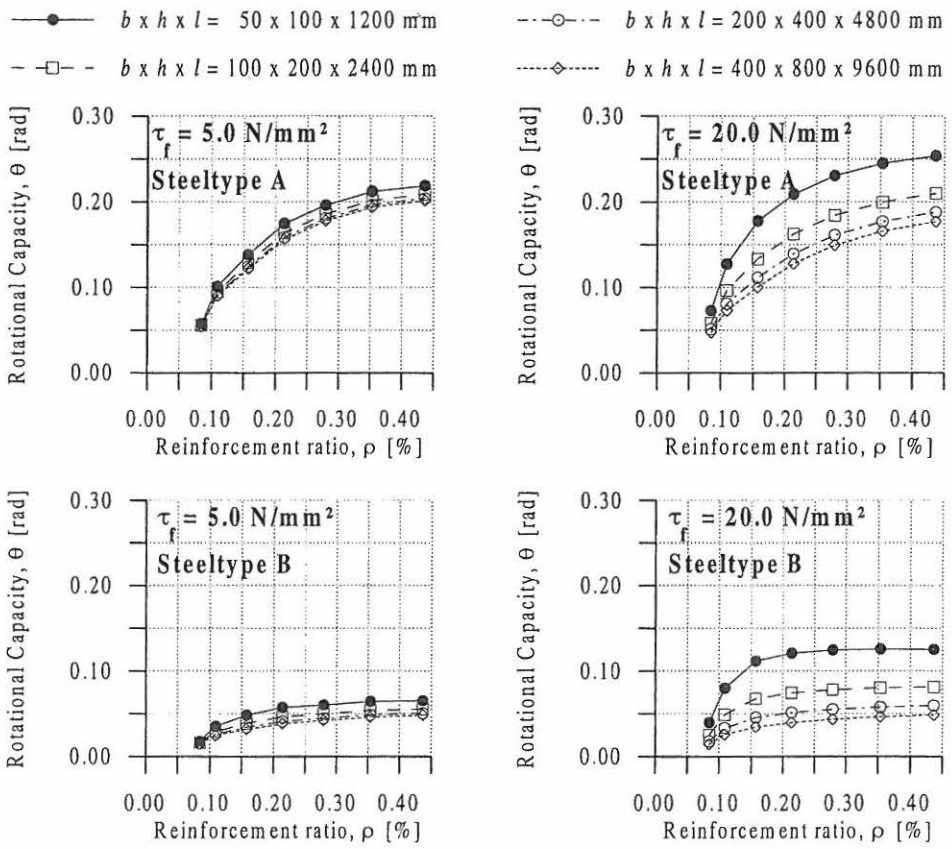

Figure 2.18: *Size effects on the rotational capacity as a function of the reinforcement ratio for different beam sizes and different values of the shear friction stress. (Top) Results for steel type A and (bottom) results for steel type B.*

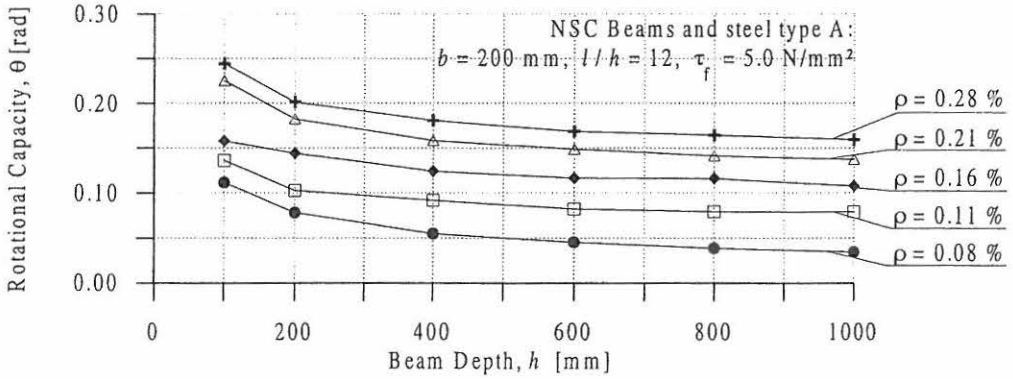

Figure 2.19: *The rotational capacity versus the beam depth for a normal strength concrete beam (b = 200 mm, l/h = 12) for different reinforcement ratios.*

Another important result of changing the size of the structure is found by assuming, that the cross-section is constant e.g. 100 x 200 mm, thus it is observed, that the rotational capacity as a function of the reinforcement ratio is dependent on the length of the beam in three-point bending for different values of the shear friction stress. From the results in Figure 2.12 and 2.20 the rotational capacity is given for increasing slenderness numbers for a fixed beam geometry. This indicates, that while the slope of the bending moment curve along the beam axis decreases for increasing slenderness number, the rotational capacity and the total amount of cracks for different reinforcement ratios are also increasing. Thus, it seems as if the differences in the values of the rotational capacity for the different shear friction stresses become more or less the same.

In Figure 2.21 some results of changing the diameter and the amount of rebars from 1 up to 4 rebars in one layer for the same reinforcement area are given for a normal strength concrete beam (200 x 400 x 4800 mm) reinforced with steel type A and a shear friction stress equal to $\tau_f = 5.0$ N/mm^2. As already mentioned, the debonding length is proportional to the diameter, so using lower values of the diameter, will result in descreasing debonding lengths and more cracks will develop. The ultimate deflections will be lower for beams with several rebars resulting in a lower rotational capacity.

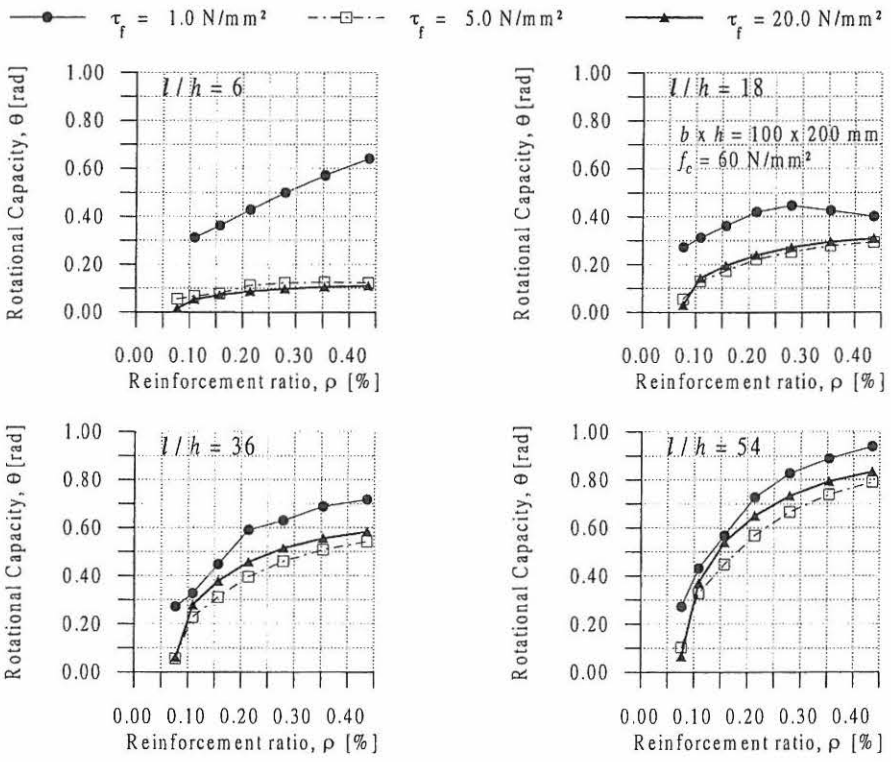

Figure 2.20: *Rotational capacity versus the reinforcement ratios for a normal strength concrete beam (b x h = 100 x 200 mm) for different slenderness numbers and shear friction stresses. The reinforcement is chosen as steel type A.*

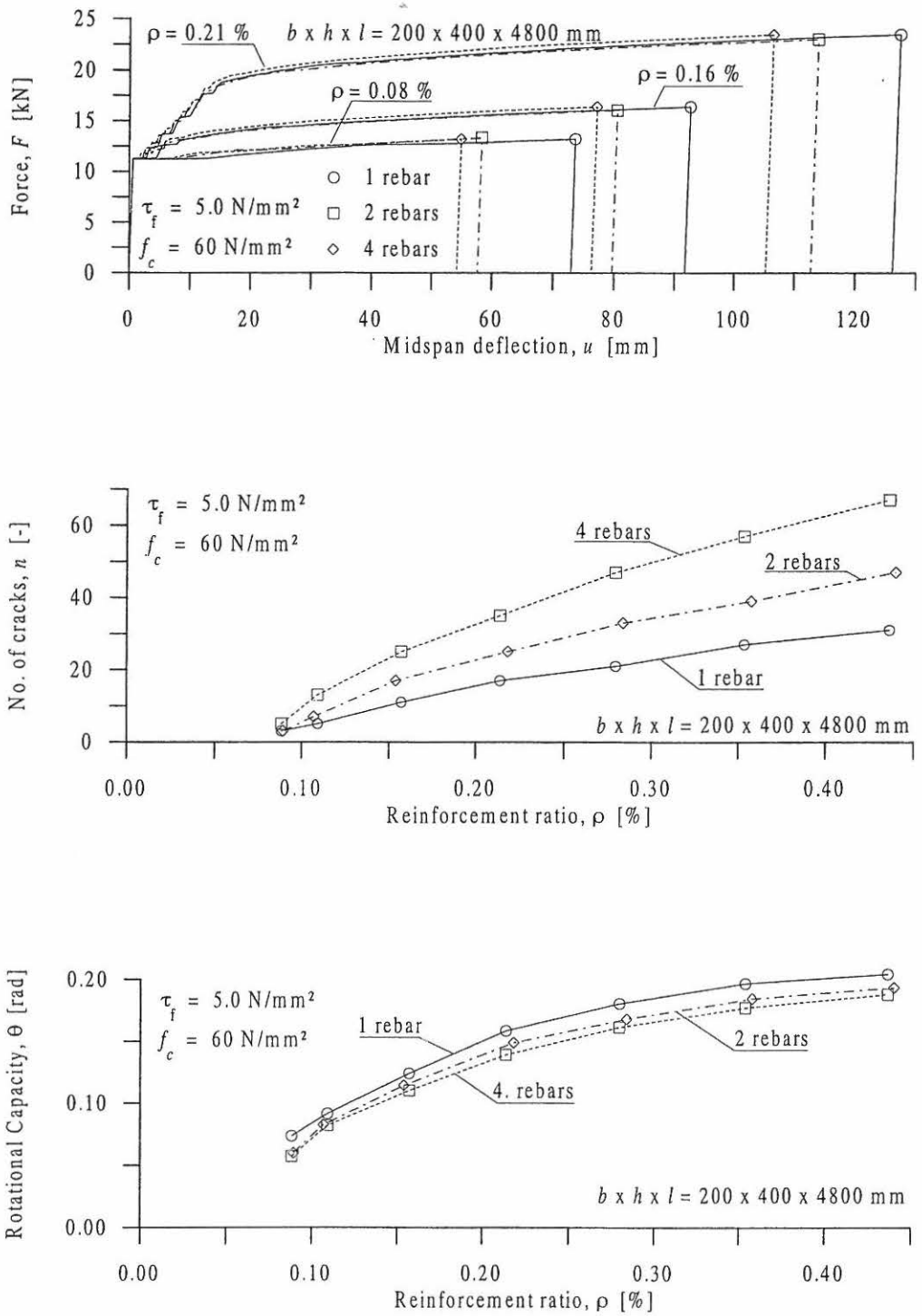

Figure 2.21: *Model results for a normal strength concrete beam (200 x 400 x 4800 mm) using different amount of rebars (steel type A, 1 layer) and different diameter for a fixed reinforcement area. The shear friction stress is* $\tau_f = 5.0\ N/mm^2$. *Top: Failure responses. Middle: Total amount of cracks along the beam axis. Bottom: Rotational capacity for different reinforcement ratios.*

2.4 Concluding Remarks

Using a model like this, the rotational capacity is strongly dependent on the strain hardening of the reinforcement. If the strain hardening is small, yielding takes place only over a small length of the re-bars around each crack, and the only way of extending the yield length of the re-bars, is to increase the strain hardening of the steel.

Another important main result is that the model does not show a so strong dependency on the shear friction stress as one would expect. This is due to the semi-fracture mechanical approach where the increasing values of the shear friction stress reduce the contribution from yielding of the reinforcement, but at the same time increase the contribution from the energy dissipation in the tensile cracks.

Chapter 3

Model for Rotational Capacity of Heavily Reinforced Concrete Beams

In this chapter the flexural behaviour of reinforced concrete beams subjected to three-point bending is investigated by analytical methods originally introduced by Professor Arne Hillerborg, in order to obtain a tool for modelling the ultimate failure response of reinforced concrete beams in the heavily reinforced regime, i.e. where the ultimate failure is controlled by the crushing of the concrete in the compression zone in the top of the beam.

A simple analytically model is presented, which describes the bending moment-curvature relation for normal and over-reinforced concrete beams taking into account the strain localization within the compression zone of the concrete. The strain softening part of the stress-strain curve for the concrete is described as a stress-deformation relation, which is dependent on the length over which the compression failure extends along the beam-axis.

On the basis of the moment-curvature relation estimated by the model, the load-deflection curve is calculated, and three calculations models for the rotational capacity are hereby proposed. The ductility of the plastic hinge is obtained as the total plastic work obtained from the area under the load-deflection curve divided by the yield moment, as the total plastic curvature distribution integrated over the total plastic length and as the total plastic mutual rotation of the beam.

Compared with the previous model from Hillerborg (1990), studies of changing the size of the compression softening curve and of establishing the total load-deflection curve are performed. The results of the model are investigated assuming a linear compression softening curve with different values of critical compression deformation and fracture zone length.

3.1 Introduction

In the past decades researchers have taken a lot of interest in investigating the tensile behaviour of concrete by means of fracture mechanics especially after development of different crack

models for the fracture in tension like the Fictious Crack Model by Hillerborg and coworkers, and research on compression failure using fracture mechanics concepts was at a low level.

But, in the past few years, there has seemed to be a lot attention on the compression failure modelling using fracture mechanics and methods of incorporating fracture mechanical principles in the deformation capacity analysis of RC structures. Different kinds of Round Robin projects involving several concrete researchers worldvide were carried out, e.g. on test methods for the strain softening response of concrete and modelling of over-reinforced concrete beams by RILEM TC 148-SSC, see van Mier *et al.* (1997) and Ulfkjaer *et al.* (1997) and on ductility of reinforced concrete structures by CEB Task Group 2.2, see CEB Bulletin 242 (1998). Resent investigations on concrete failure under compression and on compressive failure in over-reinforced concrete beams involving both experimental and analytical studies have been presented at FRAMCOS-2 and 3, see Wittmann (1995) and Mihashi (1998). The RILEM investigations by van Mier *et al.* (1997) show, that measurements of the total stress-strain response in uniaxial compression are highly influenced by the slenderness *h/d* of the prisms and of the choice of boundary conditions, i.e. low (teflon) / high (steel) friction loading systems as can be clearly seen in Figure 3.1.

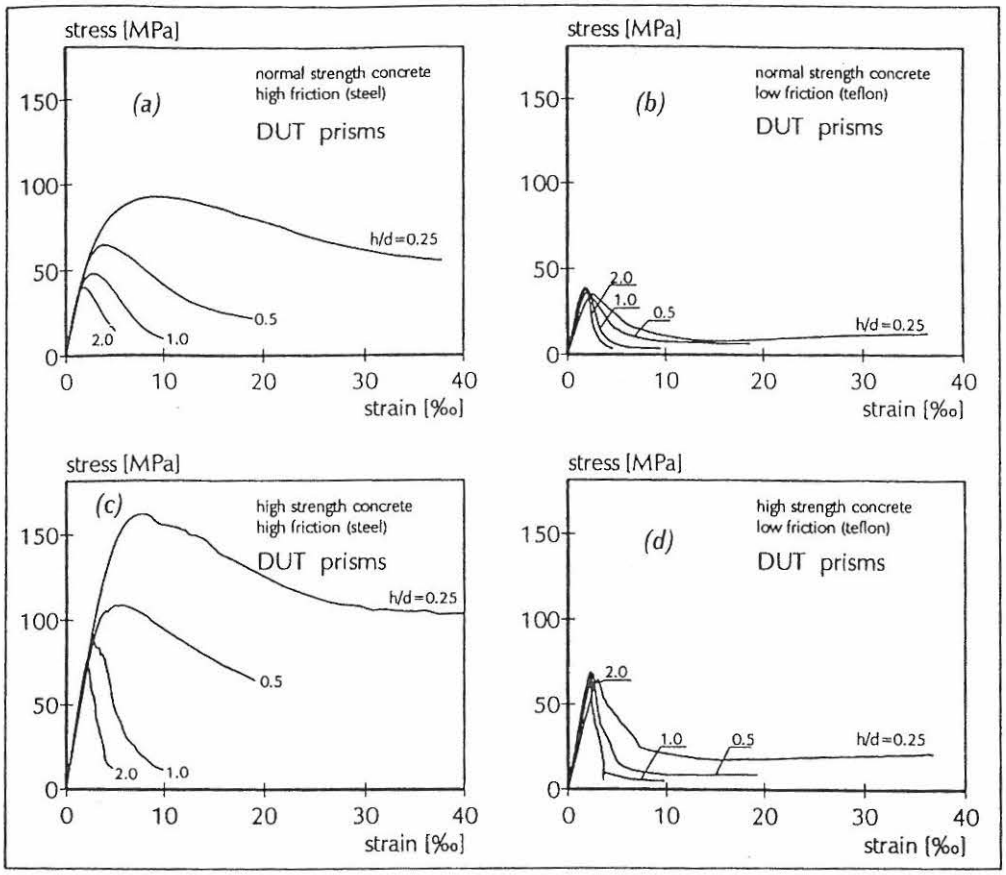

Figure 3.1: *Stress-strain curves from prism tests at the Stevin Laboratory, Delft by van Mier et al (1997). Results for normal strength concrete loaded between steel platens (a), normal strength concrete between teflon platens (b), high strength concrete between steel platens (c) and high strength concrete between teflons platens (d), after van Vliet and van Mier (1995).*

Based on the principles of the FCM model, Hillerborg was one of the researchers, that began to investigate the softening behaviour of the fracture in compression, Hillerborg (1988, 1990, 1991). Hillerborg had already shown, that the softening behaviour in tension was size dependent, and inspired by the work of van Mier (1986), Hillerborg got the idea of using the FCM model for tension softening on compression failure. This led to a simple model describing the uniaxial stress-strain relation for concrete based on fracture mechanical concepts, Figure 3.2. The strain localization within the compression zone was taking into account by defining a characteristic length dependent on the depth of the compression zone.

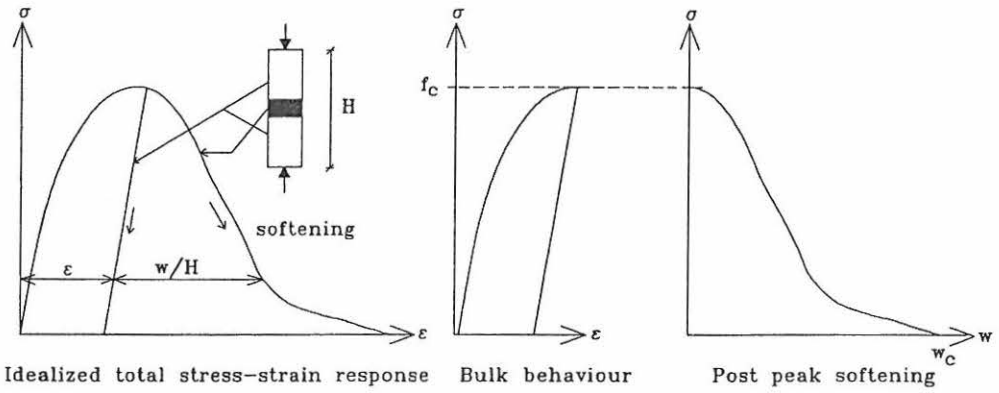

Figure 3.2: *Basic idea of stress-strain relation in compression by Hillerborg (1990).*

Different experimental studies on the full range behaviour in compressive loading of different concrete cubes were carried out by van Mier (1986, 1997) and Vonk (1993) at the Stevin Laboratory as well as performance of micromechanical modelling of compression softening. Recent studies of the behaviour in compression of both normal strength concrete (45 MPa) and high strength concrete (90 MPa) have been presented by Jansen and Shah (1997), who performed experimental investigations on cylinders with constant diameter and different depth's to examine the effect of specimen length on compressive strain softening of concrete, see Figure 3.3. Their results show that the post peak behaviour including the post peak energy dissipation is relatively insensitive to the depth of the cylinder specimen.

Several researchers have examined the influence on compression softening behaviour when changing the depth of test cylinders and when using intermediate layers between the loading plate and the cylinder, but it seems to be a lack of investigations on the influence of changing the diameter. A so-called Compressive Damage Zone (CDZ)-Model has also been established by Markeset (1995) taking into account also localized shear deformation and deformation due to splitting cracks, and incorporating the same principles, a Biegedruckzonen (BDZ)-Model was developed by Meyer (1997) to obtain the total compressive stress-strain curve taking into account the localization of failure in a damage zone and also the effect of tranversal reinforcement on the ductility.

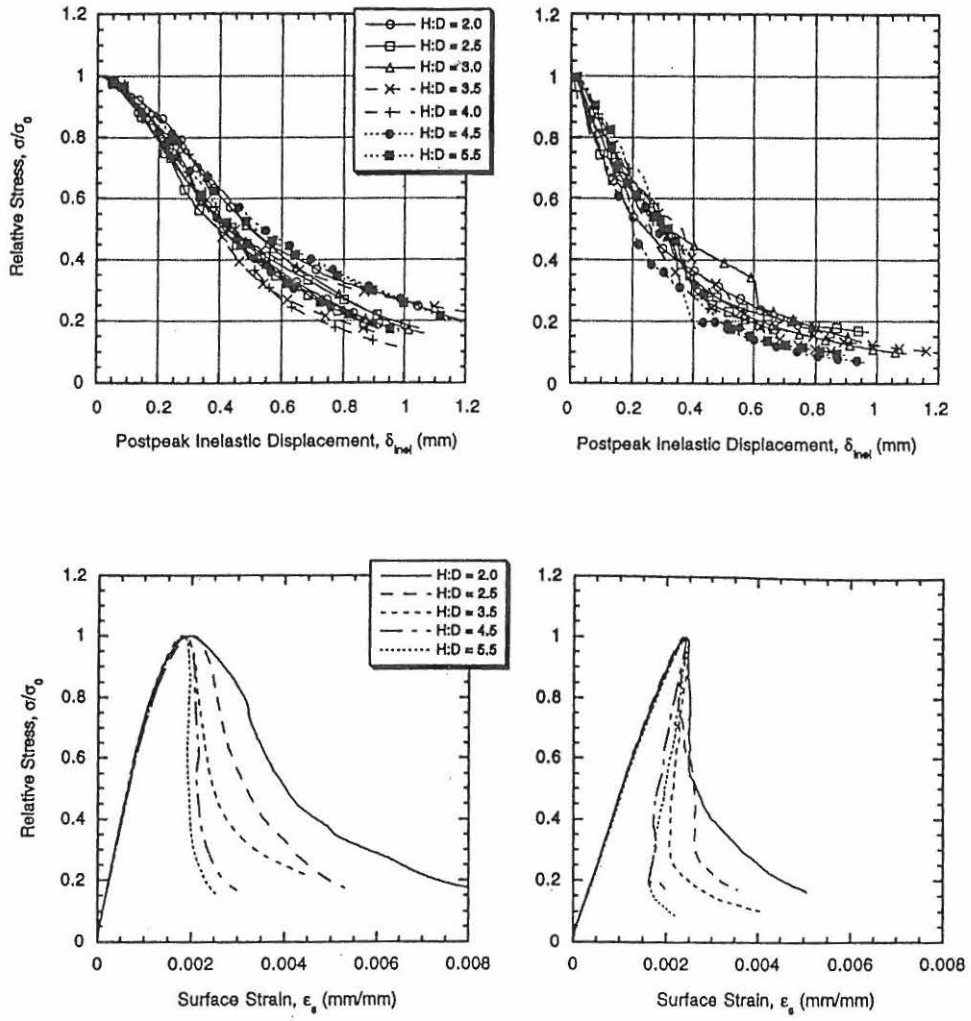

Figure 3.3: *Influence of specimen length on concrete cylinders on the uniaxial compressive stress-strain curve, (diameter 100 mm). Left: Normal strength concrete (45 MPa). Right: High strength concrete (90 MPa). According to Jansen and Shah (1997).*

In this investigation, the length, over which the compression failure extends along the beam axis, is introduced as a characteristic length proportional to the depth of the compression zone $l_{ch} = \beta h_c$ and the softening is assumed to be linear. Thus, the model contains two parameters describing the basic fracture mechanical properties of the model: the characteristic length parameter β and a critical softening deformation w_c. In the following the influence of the parameters β and w_c on the full range behaviour of different model beams is analyzed, and based on the bending moment-curvature relations and the load-deflection curves, the rotational capacity is estimated as the plastic work divided by the yield moment of the beam, as the total plastic curvature distribution multiplied by the total plastic length and as the total mutual rotation of the beam.

3.2 Basic Assumptions of the State of Compression Failure

When a reinforced concrete beam is loaded to ultimate compression failure, and an unloading starts taking place, the critical cross-section is assumed to pass through three different states of failure, see Figure 3.4.

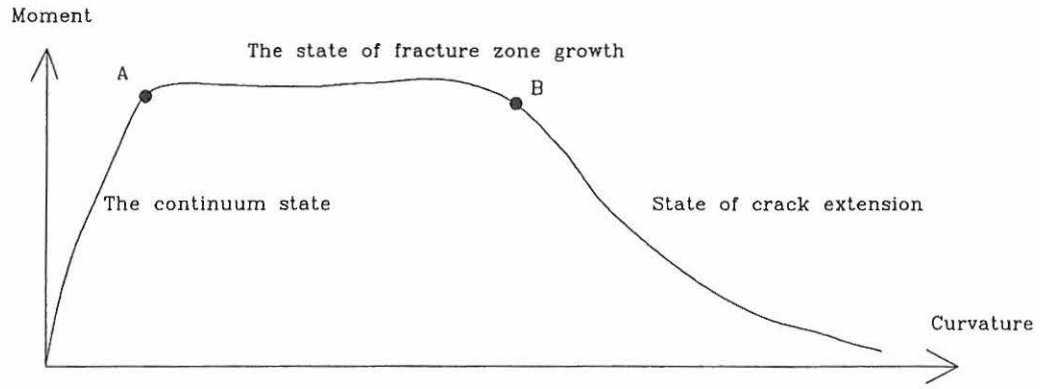

Figure 3.4: *Full range behaviour for a reinforced concrete beam.*

The continuum state for the critical cross-section describes an elastic state for the concrete, where the concrete stresses $\sigma_c < f_c$ for all points in the cross-section. Varying the concrete strain ε_c from zero to the peak strain ε_{co}, the depth of the compression zone h_c will be constant. In this phase the reinforcement is assumed to be in an elastic state corresponding to $\sigma_s < f_y$.

The state of fracture zone growth is reached, when the concrete stress in the compressed edge of the cross-section reaches the concrete compression strength. At this state a fracture zone will start developing. When the fracture zone is fully developed, i.e. when the compression stress at the top of the beam has dropped to zero, the length of the fracture zone along the beam axis is assumed to be l_{ch}, where l_{ch} is defined as a characteristic length. The material within the fracture zone follows a softening branch and outside this zone an unloading takes place. The characteristic length could be assumed to be dependent on either the depth of the compression zone or on the width of the cross-section.

It is well known, that the final compression failure of cylinders is often a so-called "cone-failure", where the concrete fails in a compression-shear mode with the development of slip-planes under an angle γ typically around $\gamma \cong 30°$. Thus, for a cylinder with radius r, the characteristic length might be defined as $l_{ch} \tan(\gamma) = 2r$, and taking the approximation $\tan(\gamma) \cong 0.5$ we get $l_{ch} \cong 4r$, Figure 3.5. Following this idea, the failure mode of the compression zone of a beam is assumed to be a similar compression-shear mode with the development of slip-planes at a certain angle to horizontal. Now, assuming that the slip-planes will start at the point where the strain is zero, the characteristic length becomes proportional to the depth h_c of the compression zone, thus $l_{ch} = \beta h_c$. Assuming that the slip-planes develop at an angle similar to the cylinder failure gives the estimate $\beta \cong 4$, Figure 3.5.

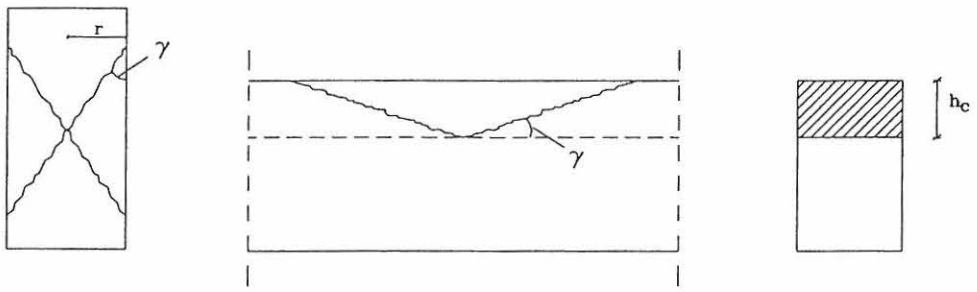

Figure 3.5: *Definition of the parameter β describing the length of the failure zone. Left: Cone failure of a cylinder in compression. Right: Assumed failure mode in the compression zone of a beam in bending.*

However, the relation $l_{ch} = \beta h_c$ is only expected to be valid on the assumption that the depth of the compression zone is small compared to the width b of the beam. If the beam width becomes substantially smaller than the depth of the compression zone, it is more reasonable to assume a failure mode, where vertical slip-planes develop, and thus, for this case it should be assumed, that the characteristic length is proportional to the width b of the beam. In the following however, the relation $l_{ch} = \beta h_c$ will be used.

Using the approach of a characteristic length l_{ch} , the softening deformation can be represented as a strain, and thus, the full range behaviour of both concrete and reinforcement can be represented by a stress-strain relation, see Figure 3.6.

In the state of crack extension a part of the material in the compression zone has totally failed and a " real crack" is formed. The final failure develops as the crack extends downwards through the beam.

3.3 Flexural Behaviour of Heavily Reinforced Concrete Beams assuming Compression Failure

In the modelling of the flexural behaviour of heavily reinforced concrete beams, it is assumed, that the considered beams are subjected to three-point bending, and the critical cross-section is assumed to be reinforced only by main reinforcement. Thus, the influence of compressive reinforcement and stirrups are not taken into account.

The bending tensile strength of the concrete is set equal to zero, which means, that the cross-section is assumed to be cracked from the start. Effects from other cracks along the beam axis as well as bond-slip effects between the concrete and the reinforcement are not considered. For

calculation of the full range behaviour Bernuoilli's assumption (plane sections remain plane) is applied.

The model describing the full range behaviour is based on the simplified linear stress-strain curves for the reinforcement and the concrete, see Figure 3.6. Typical stress and strain distributions for the critical cross-section and each of the fracture states are shown in Figure 3.7.

The full range behaviour is here described by the normalized cross-sectional moment-curvature relation and the load-displacement curve for the midspan of the beam, as the critical cross-section is running through the different fracture states.

3.3.1 Modelling the Cross-sectional Moment Curvature Relation

In this section, the moment-curvature relation for the critical cross-section of a reinforced concrete beam subjected to three-point bending (the cross-section subjected to maximum moment) will be derived for the three fracture states as a function of the normalized depth of the compression zone using the equivalence conditions for the normal force and the bending moment of the cross-section.

The full range flexural behaviour of a beam is determined by varying the concrete compressive strain at the top of the cross-section ε_c in the following interval

$$\begin{array}{lll} \text{Continuum state} & 0 < \varepsilon_c \le \varepsilon_{co} & \sigma_c(\varepsilon_c) \le f_c \\ \text{State of failure zone growth} & \varepsilon_{co} < \varepsilon_c \le \varepsilon_{cu}(h_c(\varepsilon_c)) & \sigma_c(\varepsilon_c) < f_c \\ \text{State of crack extension} & \varepsilon_c > \varepsilon_{cu}(h_c(\varepsilon_c)) & \sigma_c(\varepsilon_c) = 0 \end{array} \qquad (3.1)$$

The bending moment M is normalized with respect to the section modulus W and the compressive strength f_c corresponding to the Bernoullis beam theory and with respect to the yield moment $M_{y,pl}$ corresponding to the plasticity theory in the following way

$$\begin{aligned} \mu_1 &= \frac{M}{W f_c}(\xi,\varepsilon_c) = \frac{6M}{b\,h_{ef}^2 f_c}(\xi,\varepsilon_c) = \frac{3Fl}{2b\,h_{ef}^2 f_c}(\xi,\varepsilon_c) = \frac{3S}{2\zeta^2 f_c}\frac{F}{A_c}(\xi,\varepsilon_c) \\ \mu_2 &= \frac{M}{M_{y,pl}}(\xi,\varepsilon_c) = \frac{M}{A_s f_y h_{ef}}(\xi,\varepsilon_c) = \frac{Fl}{4A_s f_y h_{ef}}(\xi,\varepsilon_c) = \frac{S}{4\zeta^2 A_c f_y}\frac{F}{\rho}(\xi,\varepsilon_c) \end{aligned} \qquad (3.2)$$

where ξ is the normalized depth of the cross-section $h_c(\varepsilon_c) / h$, S is the slenderness number l / h, ζ is the ratio of the effective depth of the cross-section and the beam depth h_{ef} / h , A_c is the cross-sectional area b x h and ρ is the reinforcement ratio $A_s / (b\,h_{ef})$.

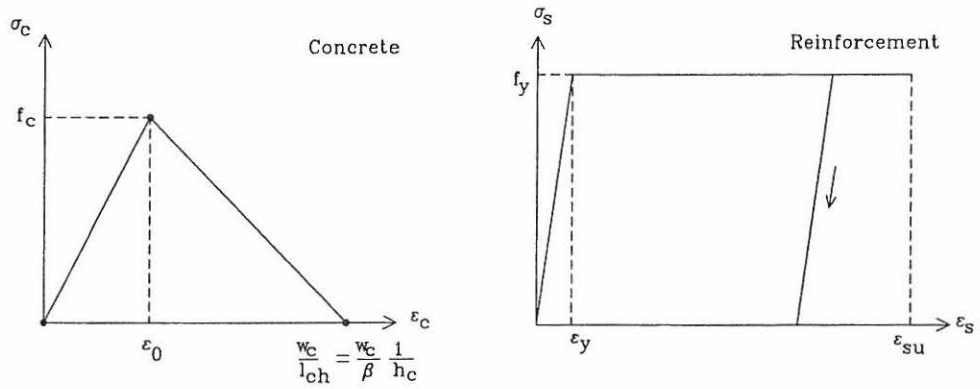

Figure 3.6: *Simplified analytically stress-strain curves for the reinforcement and the concrete.*

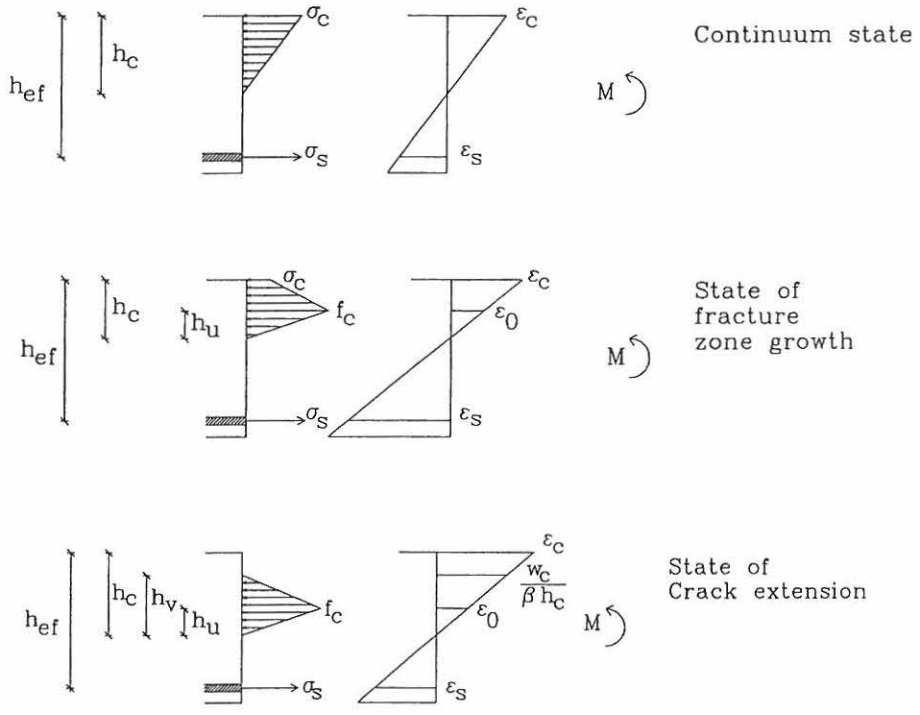

Figure 3.7: *The stress and strain distribution for the critical cross-section.*

The non-dimensional moment μ_1 shows the influence of the size of the structure A_c for geometrically and identically scaled beams, whereas the non-dimensional moment μ_2 shows the influence of changing the reinforcement ratio ρ for a fixed beam geometry.

The curvature of the cross-section is calculated as the ratio of the concrete compressive strain ε_c and the depth of the compression zone h_c, and is normalized with respect to the peak compressive strain ε_{co} and the yield steel strain ε_y. The non-dimensional curvatures are

$$\frac{\kappa}{\kappa_o}(\xi, \varepsilon_c) = \frac{h_{ef}}{\varepsilon_{co}} \frac{\varepsilon_c}{h_c(\varepsilon_c)} = \frac{1}{\varepsilon_{co}} \frac{\varepsilon_c}{\xi} \quad \text{and} \quad \frac{\kappa}{\kappa_{yt}}(\xi, \varepsilon_c) = \frac{h_{ef}}{\varepsilon_y} \frac{\varepsilon_c}{h_c(\varepsilon_c)} = \frac{1}{\varepsilon_y} \frac{\varepsilon_c}{\xi} \tag{3.3}$$

where the curvatures $\kappa_o = \varepsilon_{co} / h_{ef}$ and $\kappa_{yt} = \varepsilon_{co} / h_{ef}$ correspond to a fully compressed and a fully cracked cross-section, respectively.

In the following the constitutive relations for the concrete and the reinforcement are established in order to calculate the depth of the compressive zone, and thereby achieve the normalized moment equations simply by using the equivalence conditions for the critical cross-section in the three failure states. The constituve relations follow the stress-strain curves given by Figure 3.6, and the stress-strain distributions for the critical cross-section are shown in Figure 3.7.

The Continuum State

In the continuum state the reinforcement and the concrete are assumed to behave in an elastic manner for the normal and overreinforced state, and using the principle of plane sections remain plane, the concrete stress and strain at the top of the beam and the reinforcement stress are simply given by

$$\sigma_c(\varepsilon_c) = E_{co}\, \varepsilon_c$$

$$\sigma_s(\varepsilon_c) = E_s\, \varepsilon_s(\varepsilon_c) = E_s\, \varepsilon_c \frac{h_{ef} - h_c(\varepsilon_c)}{h_c(\varepsilon_c)} \quad \text{and} \quad \sigma_s(\varepsilon_s(\varepsilon_c) \geq \varepsilon_y) = f_y \tag{3.4}$$

where the modulus of elasticity for the concrete are given as $E_{co} = f_c / \varepsilon_{co}$ and for the reinforcement $E_s = f_y / \varepsilon_y$. Note, that it is possible to achieve an underreinforced state, as the reinforcement stresses could be beyond the yield strength for concrete stresses below the compressive strength.

From the equivalence condition for the normal force, see Figure 3.7, the depth of the compression zone is expressed by

$$0 = A_s \sigma_s(\varepsilon_c) - \frac{1}{2} b h_c(\varepsilon_c) \sigma_c(\varepsilon) \quad \Rightarrow \quad h_c(\varepsilon_c) = \frac{2A_s}{b} \frac{\sigma_s(\varepsilon_c)}{\sigma_c(\varepsilon_c)} \tag{3.5}$$

Using the constitutive relation, it is possible to express the normalized depth of the compression zone as

$$\xi = \frac{h_c(\varepsilon_c)}{h_{ef}} = -\alpha\rho + \sqrt{(\alpha\rho)^2 + 2\alpha\rho} \tag{3.6}$$

where the ratio of the E-modulus is $\alpha = E_s / E_{co}$ and the reinforcement ratio is $\rho = A_s / (b\, h_{ef})$. Note, that in the continuum state the depth of the compression zone is constant for all ε_c .

The bending moment of the cross-section at the center of the reinforcement using the equivalence conditions is expresssed by

$$M(\varepsilon_c) = \frac{1}{2} b h_c E_{co} \varepsilon_c (h_{ef} - \frac{1}{3} h_c(\varepsilon_c)) \tag{3.7}$$

thus the flexural behaviour for this fracture state is obtained by Equation (4.2) as

$$\begin{aligned} \frac{M}{W f_c}(\xi, \varepsilon_c) &= (3\xi - \xi^2) \frac{\sigma_c(\varepsilon_c)}{f_c} \\ \frac{M}{M_{y,pl}}(\xi, \varepsilon_c) &= \frac{1}{2} \frac{1}{\rho} (\xi - \frac{1}{3} \xi^2) \frac{\sigma_c(\varepsilon_c)}{f_y} \end{aligned} \tag{3.8}$$

It is observed, that in this fracture state, the normalized moments of a beam are linear functions of ε_c, as ξ is constant for the cross-section.

The State of Fracture Zone Growth

In the state of fracture zone growth the concrete strain has reached the compressive peak strain, and the concrete stress is then on the softening branch. The constitutive relations for the concrete and the reinforcement could hereby be expressed as

$$\sigma_c(\varepsilon_c) = \frac{\varepsilon_{cu}(h_c(\varepsilon_c)) - \varepsilon_c}{\varepsilon_{cu}(h_c(\varepsilon_c)) - \varepsilon_{co}} f_c \qquad \text{where} \qquad \varepsilon_{cu}(h_c(\varepsilon_c)) = \frac{w_c}{\beta}\frac{1}{h_c(\varepsilon_c)}$$

$$\sigma_s(\varepsilon_c) = E_s\,\varepsilon_s(\varepsilon_c) = E_s\,\varepsilon_c\,\frac{h_{ef} - h_c(\varepsilon_c)}{h_c(\varepsilon_c)} \qquad \text{and} \qquad \sigma_s(\varepsilon_s(\varepsilon_c) \geq \varepsilon_y) = f_y \tag{3.9}$$

where the ultimate concrete strain ε_{cu} is dependent on the size of the compression zone $h_c(\varepsilon_c)$, the critical softening deformation w_c and the characteristic length parameter β.

Using the equivalence condition for the normal force, see Figure 3.6, the depth of the compression zone is given by

$$0 = A_s\,\sigma_s(\varepsilon_c) - \tfrac{1}{2}h_u(\varepsilon_c)\,b f_c - \tfrac{1}{2}(h_c(\varepsilon_c) - h_u(\varepsilon_c))\,b\,(f_c + \sigma_c(\varepsilon_c))$$

$$\text{where} \quad h_u(\varepsilon_c) = \frac{\varepsilon_{co}}{\varepsilon_c}h_c(\varepsilon_c) \quad \Rightarrow \quad h_c(\varepsilon_c) = \frac{2A_s\,\sigma_s(\varepsilon_c)}{b f_c + (1 - \frac{\varepsilon_{co}}{\varepsilon_c})\,b\,\sigma_c(\varepsilon_c)} \tag{3.10}$$

and the normalized depth of the compression zone is hereby given as

$$\xi = \frac{h_c(\varepsilon_c)}{h_{ef}} = \frac{2\rho\,\sigma_s(\varepsilon_c)}{f_c + (1 - \frac{\varepsilon_{co}}{\varepsilon_c})\,\sigma_c(\varepsilon_c)} \tag{3.11}$$

From the equivalence condition, the bending moment of the cross-section at the center of the reinforcement is expressed as

$$\begin{aligned} M(\varepsilon_c) = {} & \tfrac{1}{2}h_u(\varepsilon_c)\,b f_c\,(h_{ef} - h_c(\varepsilon_c) + \tfrac{2}{3}h_u(\varepsilon_c)) \\ & + (h_c(\varepsilon_c) - h_u(\varepsilon_c))\,b\,\sigma_c(\varepsilon_c)\,(h_{ef} - \tfrac{1}{2}(h_c(\varepsilon_c) - h_u(\varepsilon_c))) \\ & + \tfrac{1}{2}(h_c(\varepsilon_c) - h_u(\varepsilon_c))\,b\,(f_c - \sigma_c(\varepsilon_c))\,(h_{ef} - \tfrac{2}{3}(h_c(\varepsilon_c) - h_u(\varepsilon_c))) \end{aligned} \tag{3.12}$$

Using Equation (3.10) the flexural behaviour is described by the non-dimensional moments as follows

$$\frac{M}{W f_c}(\xi, \varepsilon_c) = 3\xi + (\frac{\varepsilon_{co}}{\varepsilon_c} - 2)\xi^2 + ((3 - 3\frac{\varepsilon_{co}}{\varepsilon_c})\xi - (1 + \frac{\varepsilon_{co}}{\varepsilon_c}(\frac{\varepsilon_{co}}{\varepsilon_c} - 2))\xi^2)\frac{\sigma_c(\varepsilon_c)}{f_c}$$

$$\frac{M}{M_{y,pl}}(\xi, \varepsilon_c) = \frac{1}{6\omega}(3 - (\frac{\varepsilon_{co}}{\varepsilon_c} + 2)\xi)\xi - \frac{1}{6\rho}\frac{\sigma_c(\varepsilon_c)}{f_y}((1 + (2 + \frac{\varepsilon_{co}}{\varepsilon_c})\frac{\varepsilon_{co}}{\varepsilon_c})\xi + 3(1 + \frac{\varepsilon_{co}}{\varepsilon_c}))\xi \qquad (3.13)$$

where the mechanical reinforcement ratio is defined as $\omega = (A_s f_y)/(b h_{ef} f_c)$.

The State of Crack Extension

In the state of crack extension it is assumed, that a real crack is formed running from the upper part of the beam vertical downwards through the cross-section. The constitutive relations for the concrete and the reinforcement are thus

$$\sigma_c(\varepsilon_c) = 0$$

$$\sigma_s(\varepsilon_c) = E_s \varepsilon_s(\varepsilon_c) = E_s \varepsilon_c \frac{h_{ef} - h_c(\varepsilon_c)}{h_c(\varepsilon_c)} \quad \text{and} \quad \sigma_s(\varepsilon_s(\varepsilon_c) \geq \varepsilon_y) = f_y \qquad (3.14)$$

The depth of the compression zone is derived from the equivalence condition, see Figure 3.6 for the normal force as

$$0 = A_s \sigma_s(\varepsilon_c) - \frac{1}{2} b h_u(\varepsilon_c) f_c + \frac{1}{2} b (h_v(\varepsilon_c) - h_u(\varepsilon_c)) f_c$$

$$\text{where} \quad h_u(\varepsilon_c) = \frac{\varepsilon_{co}}{\varepsilon_c} h_c(\varepsilon_c) \quad \text{and} \quad h_v(\varepsilon_c) = \frac{\varepsilon_{cu}(h_c(\varepsilon_c))}{\varepsilon_c} h_c(\varepsilon_c) \qquad (3.15)$$

$$\Rightarrow \quad h_c(\varepsilon_c) = \frac{\varepsilon_c}{\varepsilon_{co} - \frac{1}{2}\varepsilon_{cu}(h_c(\varepsilon_c))} \frac{A_s \sigma_s(\varepsilon_c)}{b f_c}$$

The normalized depth of the cross-section is then obtained as

$$\xi = \frac{\varepsilon_c}{\varepsilon_{co} - \frac{1}{2}\varepsilon_{cu}(h_c(\varepsilon_c))} \frac{\sigma_s(\varepsilon_c)}{f_c} \rho \tag{3.16}$$

The bending moment of the cross-section at the center of the reinforcement is obtained by

$$\begin{aligned} M(\varepsilon_c) &= \frac{1}{2} b\, h_u(\varepsilon_c) f_c (h_{ef} - h_c(\varepsilon_c) + \frac{2}{3} h_u(\varepsilon_c)) \\ &+ \frac{1}{2} b\, (h_v(\varepsilon_c) - h_u(\varepsilon_c)) f_c (h_{ef} - h_c(\varepsilon_c) + h_u(\varepsilon_c) + \frac{1}{3}(h_v(\varepsilon_c) - h_u(\varepsilon_c))) \end{aligned} \tag{3.17}$$

and the non-dimensional moments are hereby

$$\begin{aligned} \frac{M}{W f_c}(\xi, \varepsilon_c) &= (3\frac{w_c}{\beta h_c \varepsilon_c} + \frac{w_c^2}{(\beta h_c)^2 \varepsilon_c^2})\xi + (2\frac{w_c \varepsilon_{co}}{\beta h_c \varepsilon_c^2} - 3\frac{w_c}{\beta h_c \varepsilon_c})\xi^2 \\ \frac{M}{M_{y,pl}}(\xi, \varepsilon_c) &= \frac{1}{6\rho}((\frac{w_c^2}{(\beta h_c)^2 \varepsilon_c^2} - (3 - \frac{\varepsilon_{co}}{\varepsilon_c})\frac{w_c}{\beta h_c \varepsilon_c})\xi^2 + 3\frac{w_c}{\beta h_c \varepsilon_c}\xi) \end{aligned} \tag{3.18}$$

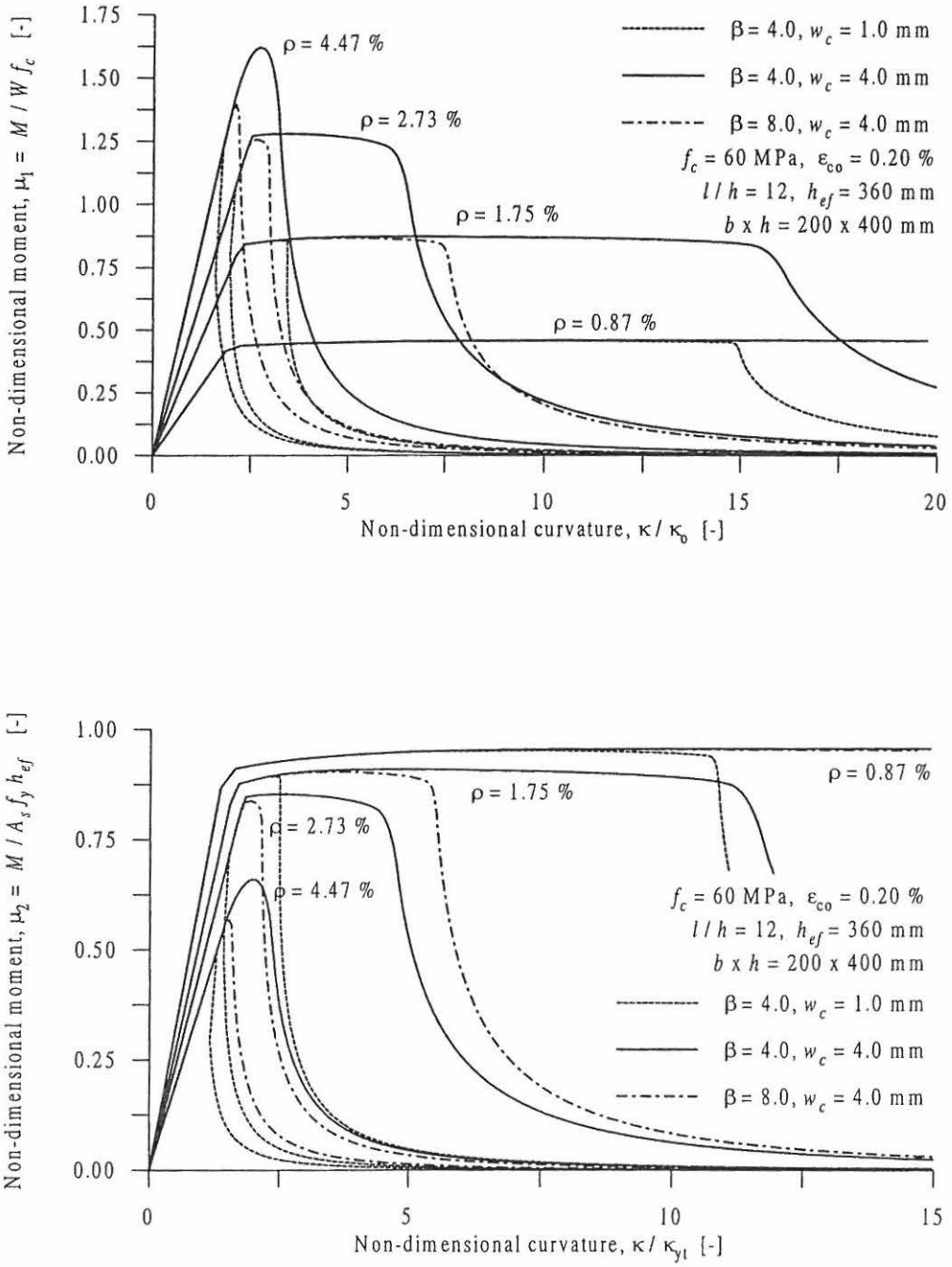

Figure 3.8: *Model results for non-dimensional bending moment - curvature relations for a normal strength concrete beam (200 x 400 x 4800 mm) and different values of w_c and β. (Top) bending moment normalized with regard to compression strength and (bottom) with regard to the yield strength.*

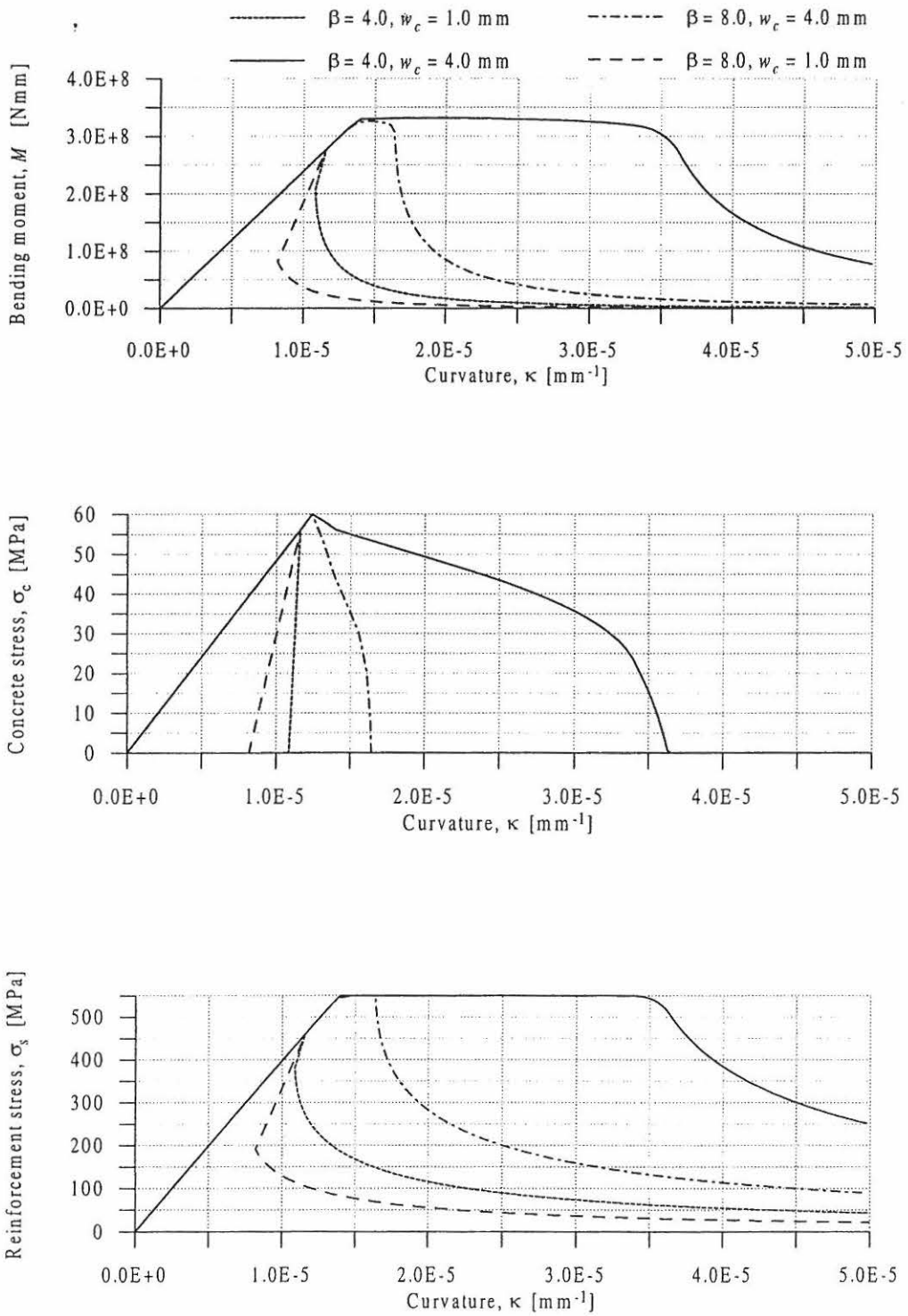

Figure 3.9: *Model results for the bending moment M (top), the concrete stress σ_c at the top of the beam (middle) and the reinforcement stress σ_s (bottom) versus the curvature κ for a normal strength concrete beam (200 x 400 x 4800 mm) with reinfocement ratio ρ = 2.73 % and different values of w_c and β.*

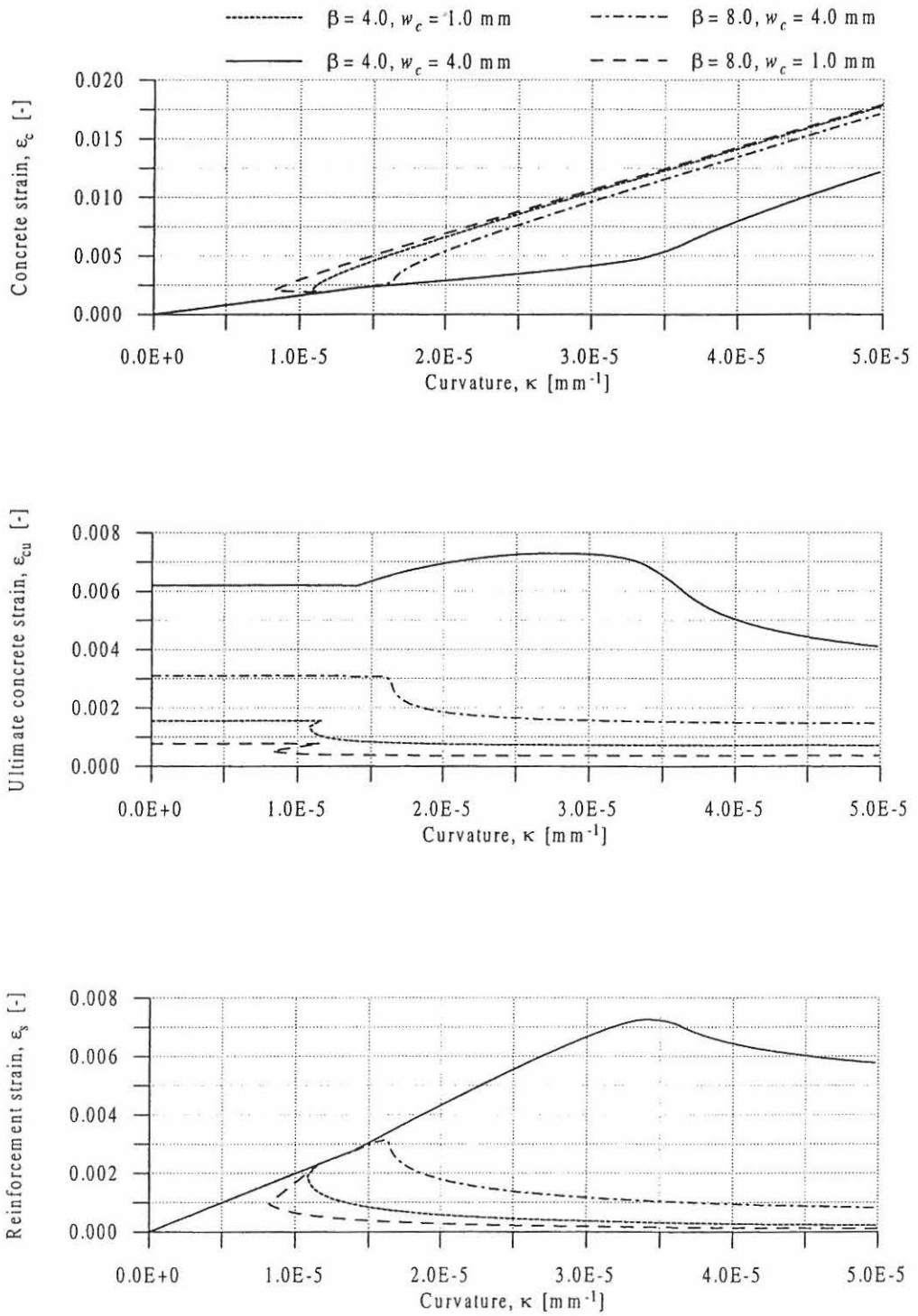

Figure 3.10: *Model results for the varying concrete strain ε_c at the top of the beam (top), the ultimate concrete strain ε_{cu} (middle) and the reinforcement strain ε_s (bottom) versus the curvature κ for a normal strength concrete beam (200 x 400 x 4800 mm) with reinfocement ratio ρ = 2.73 % and different values of w_c and β.*

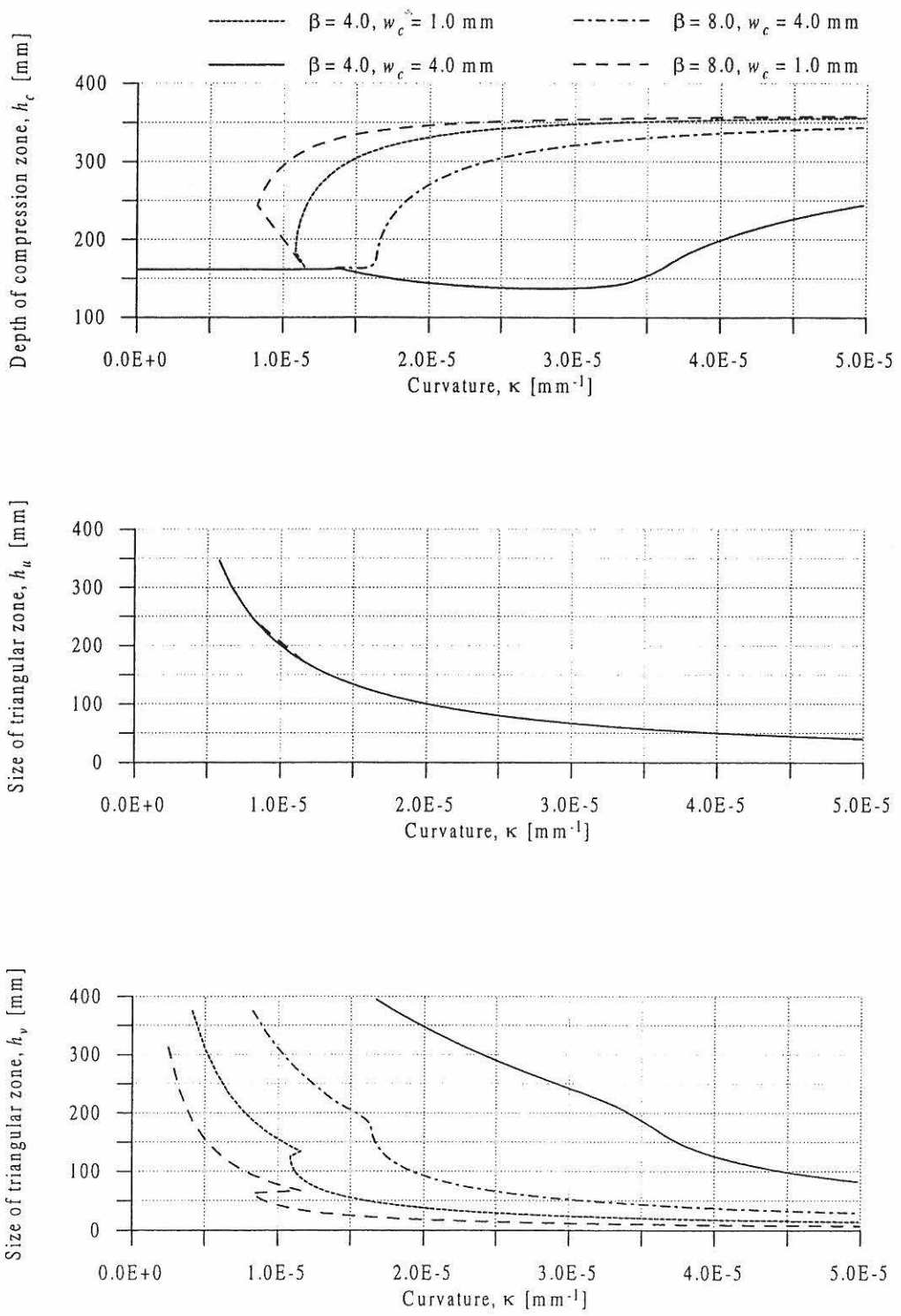

Figure 3.11: *Model results for depth of the compression zone h_c (top) and the two sizes of the tringular compression zones h_u (middle) and h_v (bottom) versus the curvature κ for a normal strength concrete beam (200 x 400 x 4800 mm) with reinfocement ratio ρ = 2.73 % and different values of w_c and β.*

3.3.2 Modelling the Load - Displacement Curve

In this section, the midspan deflection of a reinforced concrete beam is calculated using the principle of virtual work. It is assumed, that the total deflection of the midspan consists of contributions from elastic deformations and deformations due to yielding of the reinforcement and due to localized crushing of the concrete.

Neglecting the contribution to the deflection from shear forces V, load-deflection curves are obtained by integrating the curvature distribution according to the principle of virtual work. When the curvature is integrated, it is kept constant over the characteristic length, see Figure 3.12, where the distribution of curvature along the beam axis is shown in the state of ultimate failure, here defined as the transition between the state of fracture zone growth and the state of crack extension. The softening of the compressive stresses in the concrete is assumed only to happen within the localized fracture zone at the time of ultimate failure. Outside this zone the concrete stress is assumed to follow a linear distribution, whereas the reinforcement stresses dependent on the amount of reinforcement are either less than f_y for $x < x_1$ or equal to f_y for $x > x_1$, where x_1 is the point of onset of yielding along the beam axis, see Figure 3.13.

Assuming three-point bending and a normal reinforced state, see Figure 3.12, the total extent of elastic deformations $2x_1$ and yielding of the reinforcement $2(x_2 - x_1)$ outside the localized fracture zone l_{ch} could be expressed by the ratio of the yield moment $M_{y,x1}(\varepsilon_{c,x1})$ at x_1 and the applied moment $M(\varepsilon_c)$ at the midspan in the following way

$$x_1 = \frac{1}{2}\frac{M_{y,x_1}(\varepsilon_{c,x_1})}{M(\varepsilon_c)}\,l \qquad \text{and} \qquad x_2 = \frac{1}{2}(l - l_{ch}(\varepsilon_c)) \tag{3.19}$$

The critical moment $M_{y,x1}(\varepsilon_{c,x1})$ describing the shift in the reinforcement stresses, i.e. the onset of yielding given by the point x_1 on the beam, could be expressed by equivalence conditions for the cracked cross-section, see Figure 3.13. Assuming the following constitutive relation for the concrete and the reinforcement in the cracked cross-section at x_1

$$\sigma_{c,x_1} = E_{co}\,\varepsilon_{c,x_1} \qquad \text{where} \qquad \varepsilon_{c,x_1} = \varepsilon_y \frac{h_{c,x_1}}{(h_{ef} - h_{c,x_1})}$$
$$\sigma_{s,x_1} = f_y \qquad \text{where} \qquad \varepsilon_{s,x_1} = \varepsilon_y \tag{3.20}$$

the size of the compression zone is calculated as the normal force $N = 0$ according to

$$0 = A_s f_y - \frac{1}{2} h_{c,x_1}\, b\, \sigma_{c,x_1} \quad \Rightarrow \quad h_{c,x_1} = \frac{2A_s}{b}\frac{f_y}{\sigma_{c,x_1}} = \frac{2A_s}{b}\frac{E_s}{E_{co}}\frac{\varepsilon_y}{\varepsilon_{c,x_1}} \tag{3.21}$$

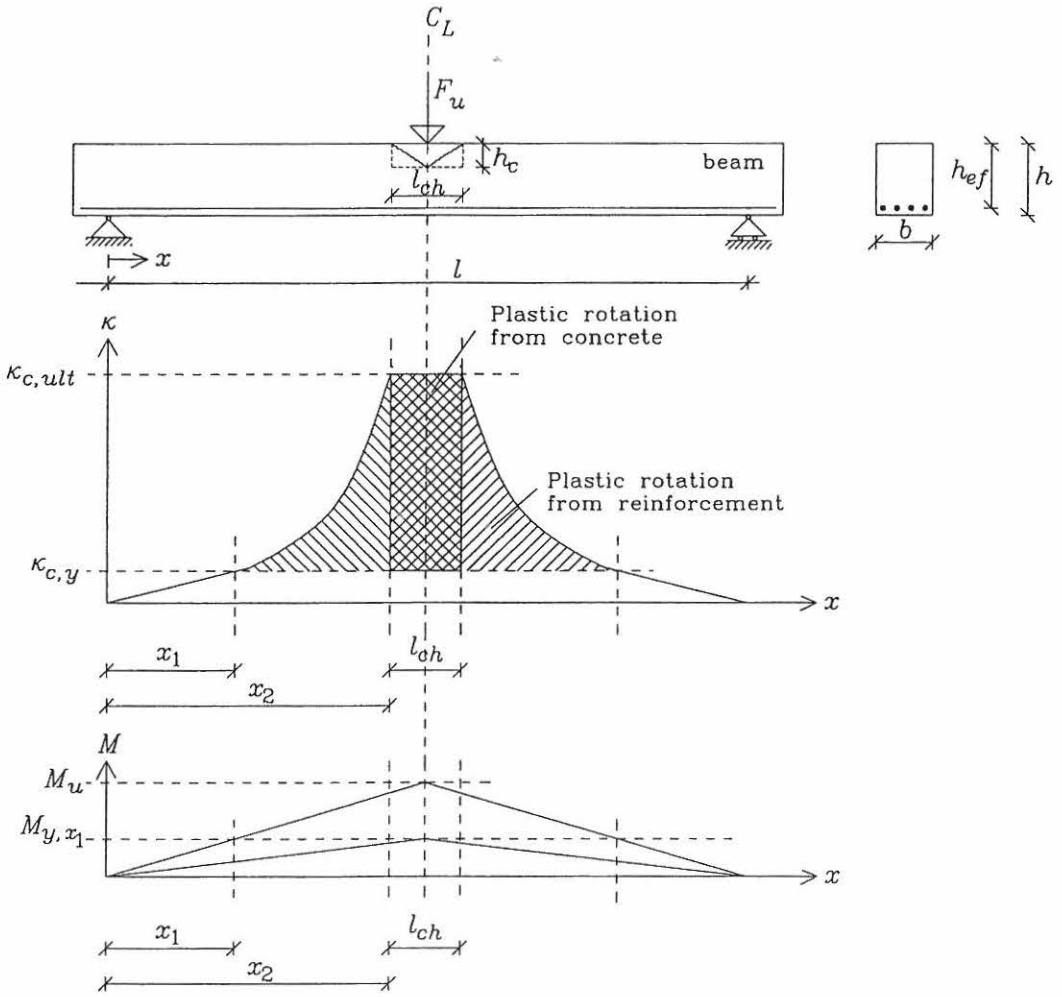

Figure 3.12: *Typical moment and curvature distribution along the beam axis for a beam at ultimate load.*

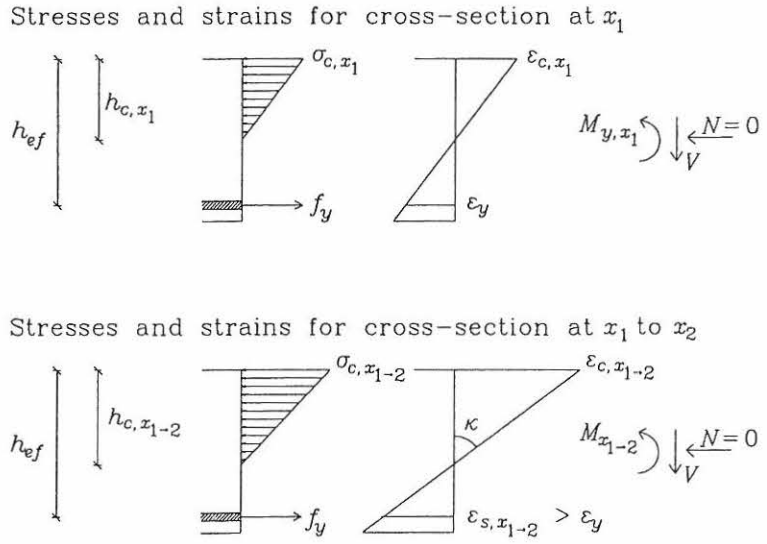

Figure 3.13: *Stress and strain distributions for definition of plastic zone from x_1 to x_2.*

and assuming, that plane sections remain plane and inserting the ratio of the strains, the size of the compression zone is obtained by

$$h_{c,x_1}^2 + \frac{2A_s\alpha}{b} h_{c,x_1} - \frac{2A_s\alpha}{b} h_{ef} = 0 \Rightarrow \frac{h_{c,x_1}}{h_{ef}} = -\alpha\rho + \sqrt{(\alpha\rho)^2 + 2\alpha\rho} \quad (3.22)$$

Now, the critical moment of the onset of yielding at x_1 could be expressed as

$$M_{y,x_1}(\varepsilon_{c,x_1}) = \frac{1}{2} b\, h_{c,x_1}\, \sigma_{c,x_1} (h_{ef} - \frac{1}{3} h_{c,x_1}) \quad (3.23)$$

If no yielding of the reinforcement will occur until the point of ultimate failure, then the beam is in an over-reinforced state. The elastic contribution to the total deflection of the beam is hereby large, as the extent of the elastic deformation along the beam-axis will be equal to $2x_2$ as $x_1 = x_2$.

Identifying the overall behaviour of the beam by dividing the beam into an elastic part from 0 to x_1, a yielding part from x_1 to x_2 and a localized compression failure part from x_2 to $l/2$, the total displacement of the midspan is obtained by the work equation

$$1\, u = \int_0^l M_1(x)\, \kappa(x)\, dx \quad (3.24)$$

where $M_1(x) = \frac{1}{2} x$ is the bending moment from the 1 force system, and $\kappa(x)$ is the cross-sectional curvature along the beam axis.

As mentioned, the midspan deflection is divided into the following parts

$$u = u_{el} + u_{y,ref} + u_{c,loc} \quad (3.25)$$

where u_{el} , $u_{y,ref}$ and $u_{c,loc}$ are displacements due to elastic behaviour of the reinforcement and the concrete, yielding of the reinforcement and localized crushing of the concrete, respectively.

The elastic contribution to the displacement at the midspan is calculated from Equation (3.25) as

$$u_{el} = 2\int_0^{x_1} M_1(x)\, \kappa(x)\, dx = \frac{1}{6} \frac{F(\varepsilon_c)}{E_{co} I_{zt,r}} x_1^3 \quad \text{as} \quad \kappa(x) = \frac{M(x)}{E_{co} I_{zt,r}} = \frac{1}{2} \frac{F(\varepsilon_c)}{E_{co} I_{zt,r}} x \quad (3.26)$$

where $I_{zt,r}$ is the transformed moment of inertia at the onset of yielding corresponding to the point x_1 on the beam axis.

The transformed moment of inertia of the cracked cross-section at x_1 , see Figure 3.13 is given by

$$I_{zt,r} = \frac{1}{3} b\, h_{c,x_1} + (h_{ef} - h_{c,x_1})^2\, \alpha A_s \tag{3.27}$$

The contribution from yielding of the reinforcement in the region from x_1 to x_2 can be expressed by

$$u_{y,ref} = 2 \int_{x_1}^{x_2} M_1(x)\, \kappa(x)\, dx \qquad \text{where} \qquad \kappa(x) = \kappa(M) \tag{3.28}$$

By using equivalence conditions in this region from x_1 to x_2, see Figure 3.13, it is possible to express the curvature as a function of the bending moment $M(x) = M_{x_{1-2}}$.

The constitutive relation for the concrete and the reinforcement are defined as

$$\begin{aligned} \sigma_{c,x_{1-2}} &= E_{co}\, \varepsilon_{c,x_{1-2}} \qquad \text{where} \qquad \varepsilon_{c,x_{1-2}} = \kappa h_{c,x_{1-2}} \\ \sigma_{s,x_{1-2}} &= f_y \qquad\qquad\quad \text{where} \qquad \varepsilon_{s,x_{1-2}} > \varepsilon_y \end{aligned} \tag{3.29}$$

The depth of the compression zone is calculated according to

$$0 = A_s f_y - \frac{1}{2} h_{c,x_{1-2}}\, b\, \sigma_{c,x_{1-2}} \quad \Rightarrow \quad h_{c,x_{1-2}} = \frac{2 A_s f_y}{b\, \sigma_{c,x_{1-2}}} = \sqrt{\frac{2 A_s f_y}{b E_{co}} \frac{1}{\kappa}} \tag{3.30}$$

The moment of the cross-section at the center of the reinforcement is given as

$$M_{x_{1-2}} = \frac{1}{2} b\, h_{c,x_{1-2}}\, \sigma_{c,x_{1-2}} (h_{ef} - \frac{1}{3} h_{c,x_{1-2}}) = A_s f_y (h_{ef} - \frac{1}{3} \sqrt{\frac{2 A_s f_y}{b E_{co}} \frac{1}{\kappa}}) \tag{3.31}$$

From Equation (3.34) the curvature from x_1 to x_2 can then be isolated, and hereby

$$\kappa = \frac{2}{9}\frac{A_s f_y}{b E_{co}}\left(h_{ef} - \frac{M_{x_{1-2}}}{A_s f_y}\right)^{-2} = \frac{2}{9}\frac{A_s f_y}{b E_{co}}\left(h_{ef} - \frac{1}{2}\frac{F(\varepsilon_c)}{A_s f_y}x\right)^{-2} \tag{3.32}$$

Now, the displacement due to yielding of the reinforcement outside the fracture zone is calculated according to Equation (3.30) by inserting Equation (3.35), and thus

$$\begin{aligned} u_{y,ref} &= \frac{2}{9}\frac{A_s f_y}{b E_{co}}\int_{x_1}^{x_2}\frac{x}{(a_1 x + a_0)^2}\,dx \quad \text{where} \quad a_0 = h_{ef} \text{ and } a_1 = -\frac{1}{2}\frac{F(\varepsilon_c)}{A_s f_y} \\ &= \frac{8}{9}\frac{1}{b E_{co}}\left(\frac{A_s f_y}{F(\varepsilon_c)}\right)^2\left[\frac{a_0}{a_1 x + a_0} + \ln(a_1 x + a_0)\right]_{x_1}^{x_2} \end{aligned} \tag{3.33}$$

Finally, the deflection at the midspan due to crushing of the concrete in the compression zone within the localized fracture zone is given by

$$\begin{aligned} u_{c,loc} &= 2\int_{x_2}^{\frac{1}{2}l}\kappa(x = \tfrac{1}{2}l)\,M_1(x = \tfrac{1}{2}l)\,dx \\ &= \int_{\frac{1}{2}(l - l_{ch})}^{\frac{1}{2}l}\frac{1}{2}\kappa(\varepsilon_c)\,l\,dx = \frac{1}{4}\kappa(\varepsilon_c)\,l_{ch}(\varepsilon_c)\,l \qquad \text{where} \qquad \kappa(\varepsilon_c) = \frac{\varepsilon_c}{h_c} \end{aligned} \tag{3.34}$$

where $\kappa(\varepsilon_c)$ is the curvature of the critical section, and l_{ch} is the size of the fracture zone. As the the curvature and hereby the bending moment at $x = l/2$ is assumed to be constant over the length of the fracture zone, it should be noted, that also the moment from the 1 force system is assumed to be constant.

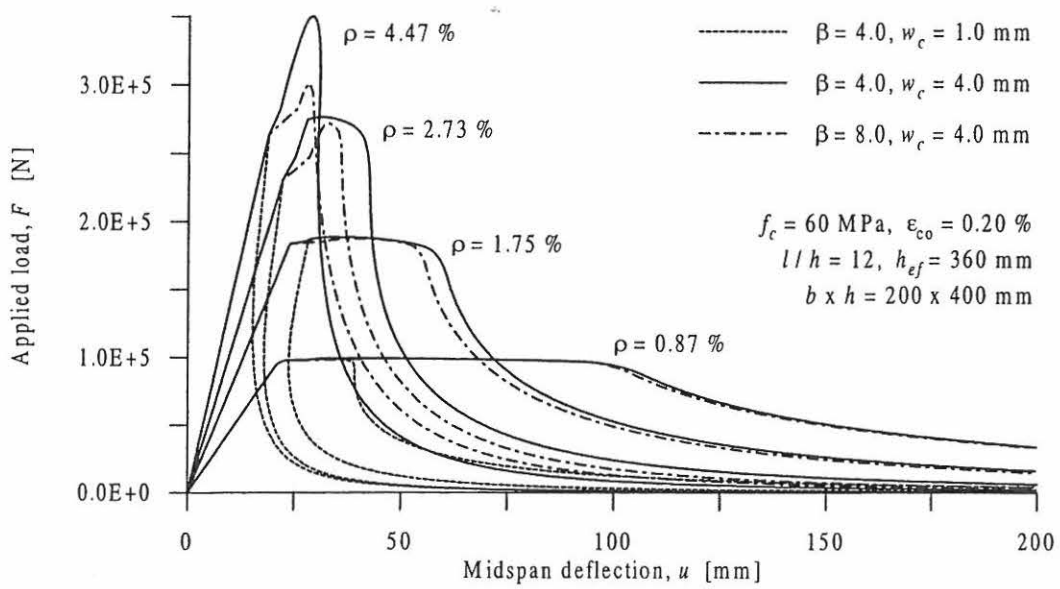

Figure 3.14: *Model results for load-deflection relation for a normal strength concrete beam (200 x 400 x 4800 mm) and different values of w_c and β.*

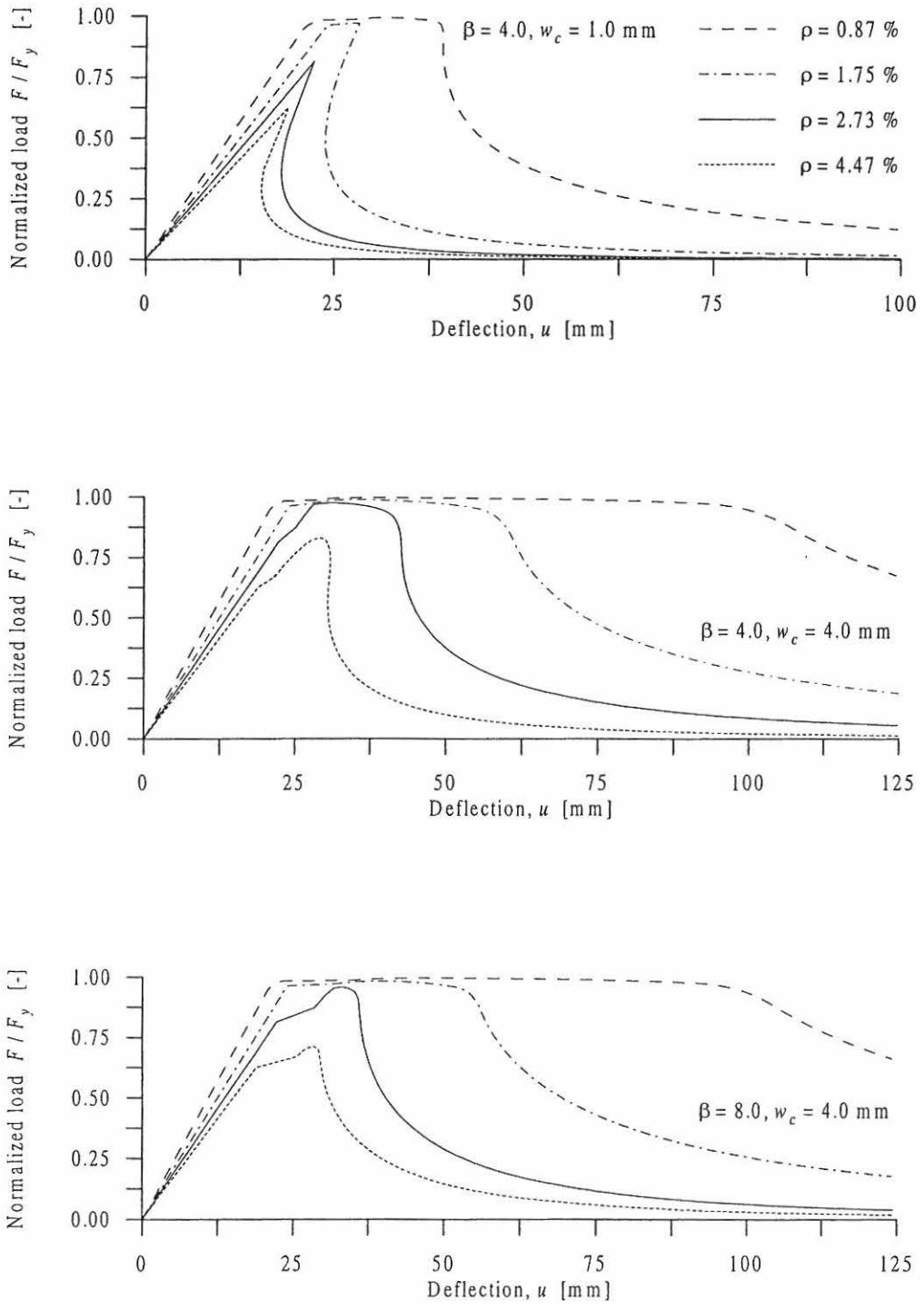

Figur 3.15: *Model results for the applied load F normalized with respect to the yield load F_y versus the deflection u for a normal strength concrete beam (200 x 400 x 4800 mm) and different values of w_c and β.*

3.3.3 Modelling the Rotational Capacity

The main purpose of this section is to model the plastic rotation of a reinforced concrete beam subjected to three-point bending, and thereby obtain a measure for the ductility of the plastic hinge, which will develop in the midspan of the beam, also called the rotational capacity of the beam. It is assumed, that the critical section of the beam is reinforced only by main reinforcement, and that the beam-parts are reinforced with stirrups in order to avoid shear failure. Effects from shear forces in the failure zone and additional reinforcement as stirrups and compressive reinforcement outside the localized compressive failure zone of the beam on the ductility of the plastic hinge are not taken into account.

In the following, three models for the rotational capacity are presented, which are based on a measure of the total plastic curvature along the beam axis, a measure of the total plastic work of the beam by integrating the load-deflection curve and a measure of the mutual plastic rotation of the beam.

Model 1 describes a method of to determine the plastic rotational capacity from the curvature distribution along the beam axis. Considering a beam loaded in three point bending, the hinge will develop in the center of the beam. At ultimate limit state, here defined as the transition between the state of fracture zone growth and the state of crack extension, compression failure of the concrete and yielding of reinforcement develop in the fracture zone l_{ch} and only yielding of the reinforcement in the zone $2(x_2 - x_1)$ under the assumption of a normal reinforced state. To achive the plastic curvature distribution the curvature at the onset of yielding given by x_1 has to be redrawn. Integrating the plastic curvature distribution $\kappa_{pl}(x)$, a measure of the plasticity of the beam is obtained. Thus, the plasticity of the beam is the rotational capacity expressed by

$$\theta_1 = \theta_{1,pl,con} + \theta_{1,pl,ref} = 2 \int_{x_1}^{l/2} \kappa_{pl}(x)\, dx \tag{3.35}$$

where $\theta_{1,pl,con}$ and $\theta_{1,pl,ref}$ is the rotational capacity due to compression failure and yielding of reinforcement in the failure zone and due to yielding of the reinforcement outside the fracture zone, respectively. The plastic rotational capacities for the two zones are obtained by

$$\begin{aligned} \theta_{1,pl,con} &= \theta_{1,tot,con} - \theta_{1,el,con} \\ \theta_{1,pl,ref} &= \theta_{1,tot,ref} - \theta_{1,el,ref} \end{aligned} \tag{3.36}$$

where $\theta_{1,tot,con}$ and $\theta_{1,tot,ref}$ is the total rotational capacities and $\theta_{1,el,con}$ and $\theta_{1,el,ref}$ is the elastic rotational capacities due to the concrete compression failure and reinforcement yielding, respectively.

The plastic rotational capacities from the crushing of concrete and yielding of the reinforcement are derived from the plastic curvatures.

For a normal reinforced state, the distribution of the plastic curvatures in the two zones l_{ch} and $2(x_2 - x_1)$ for half a beam are calculated as the total ultimate curvature redrawing the elastic part in the following way

$$\kappa_{pl}(x) = \frac{2}{9}\frac{A_s f_y}{b E_{co}}\left(h_{ef} - \frac{M(x)}{A_s f_y}\right)^{-2} - \frac{M(x)}{E_{co} I_{zt,r}} \qquad \text{for} \qquad x_1 \le x \le x_2$$

$$\kappa_{pl}(x) = \frac{1}{4}\frac{w_c}{\beta}\left(\frac{b f_c}{A_s f_y}\right)^2 - \frac{M(x = l/2)}{E_{co} I_{zt,r}} \qquad \text{for} \qquad x_2 \le x \le l/2 \tag{3.37}$$

where $M(x)$ is the bending moment, $I_{zt,r}$ is the transformed moment of inertia at x_1, w_c and β the key parameters.

In the following, the above total ultimate curvature of the localized failure zone at the transition between the state of fracture zone growth and the crack extension is derived using the angle of the strain distribution

$$\kappa_{c,ult} = \frac{\varepsilon_{cu}}{h_{c,ult}} = \frac{\varepsilon_{co}}{h_u} \quad \Rightarrow \quad h_u = \frac{\varepsilon_{co}}{\varepsilon_{cu}} h_{c,ult} \quad \text{where} \quad \varepsilon_{cu} = \frac{w_c}{l_{ch}} = \frac{w_c}{\beta}\frac{1}{h_{c,ult}} \tag{3.38}$$

where the depth of the compression zone and the bending moment at the ultimate state is calculated according to

$$0 = A_s f_y - \left(\frac{1}{2} h_u b f_c + \frac{1}{2}(h_{c,ult} - h_u) b f_c\right) \quad \Rightarrow \quad h_{c,ult} = \frac{2 A_s f_y}{b f_c}$$

$$M(x = l/2) = M_u = \frac{1}{3}\left(\frac{1}{2}\frac{\varepsilon_{co}}{\varepsilon_{cu}} - 1\right) b f_c h_{c,ult}^2 + \frac{1}{2} h_{ef} b f_c h_{c,ult} \tag{3.39}$$

Thus, the ultimate and elastic curvature can be expressed as

$$\kappa_{c,ult} = \frac{1}{4}\frac{w_c}{\beta}\left(\frac{b f_c}{A_s f_y}\right)^2 \qquad \text{and} \qquad \kappa_{c,y} = \frac{M_u}{E_{co} I_{zt,r}} \tag{3.40}$$

The contributions to the total plastic rotational capacity $\theta_1(\varepsilon_c)$ as a function of the varying parameter ε_c are then obtained by integrating the curvatures over the plastic lengths in Equation (3.40)

$$\theta_1(\varepsilon_c) = \theta_{1,pl,con}(\varepsilon_c) + \theta_{1,pl,ref}(\varepsilon_c) \qquad \text{where}$$

$$\theta_{1,pl,ref}(\varepsilon_c) = \frac{16}{9}\frac{(A_s f_y)^3}{b E_{co} F(\varepsilon_c)}\left[\frac{1}{2A_s f_y h_{ef} - F(\varepsilon_c) x}\right]_{x_1}^{x_2} - \frac{F(\varepsilon_c)}{2 E_{co} I_{zt,r}}(x_2^2 - x_1^2) \tag{3.41}$$

$$\theta_{1,pl,con}(\varepsilon_c) = \frac{b G_c}{A_s f_y} - \frac{F(\varepsilon_c) l}{4 E_{co} I_{zt,r}} \qquad \text{where} \qquad G_c = \frac{1}{2} f_c w_c$$

where G_c is the compressive fracture energy.

Model 2 is based on the load-deflection curve for the midspan of the beam. The ritational capacity is estimated by integrating the load-deflection curves to obtaion the total plastic work, and then dividing by the yield moment to obtain a non-dimensional parameter θ_2. The parameter θ_2 is a direct measure of the rotational capacity of the beam. Thus, the rotational capacity can be expressed by

$$\theta_2(\varepsilon_c) = \frac{1}{M_{y,2}} \int_0^\infty F(\varepsilon)\, du \tag{3.42}$$

where $M_{y,2}$ is the yield moment of a normal reinforced cross-section according to Method A, DS 411(1997)

$$M_{y,2} = \frac{4}{5} b h_{c,2} f_c (h_{ef} - \frac{2}{5} h_{c,2}) \qquad \text{where} \qquad h_{c,2} = \frac{5 A_s f_y}{4 b f_c} \tag{3.43}$$

Model 3 is based on the rotation of the beam assuming rigid body rotations of the beam parts. The rotational capacity could then be expressed as the plastic mutual rotation

$$\theta_3(\varepsilon_c) = \frac{4(u(\varepsilon_c) - u_{el}(\varepsilon_c))}{l} \tag{3.44}$$

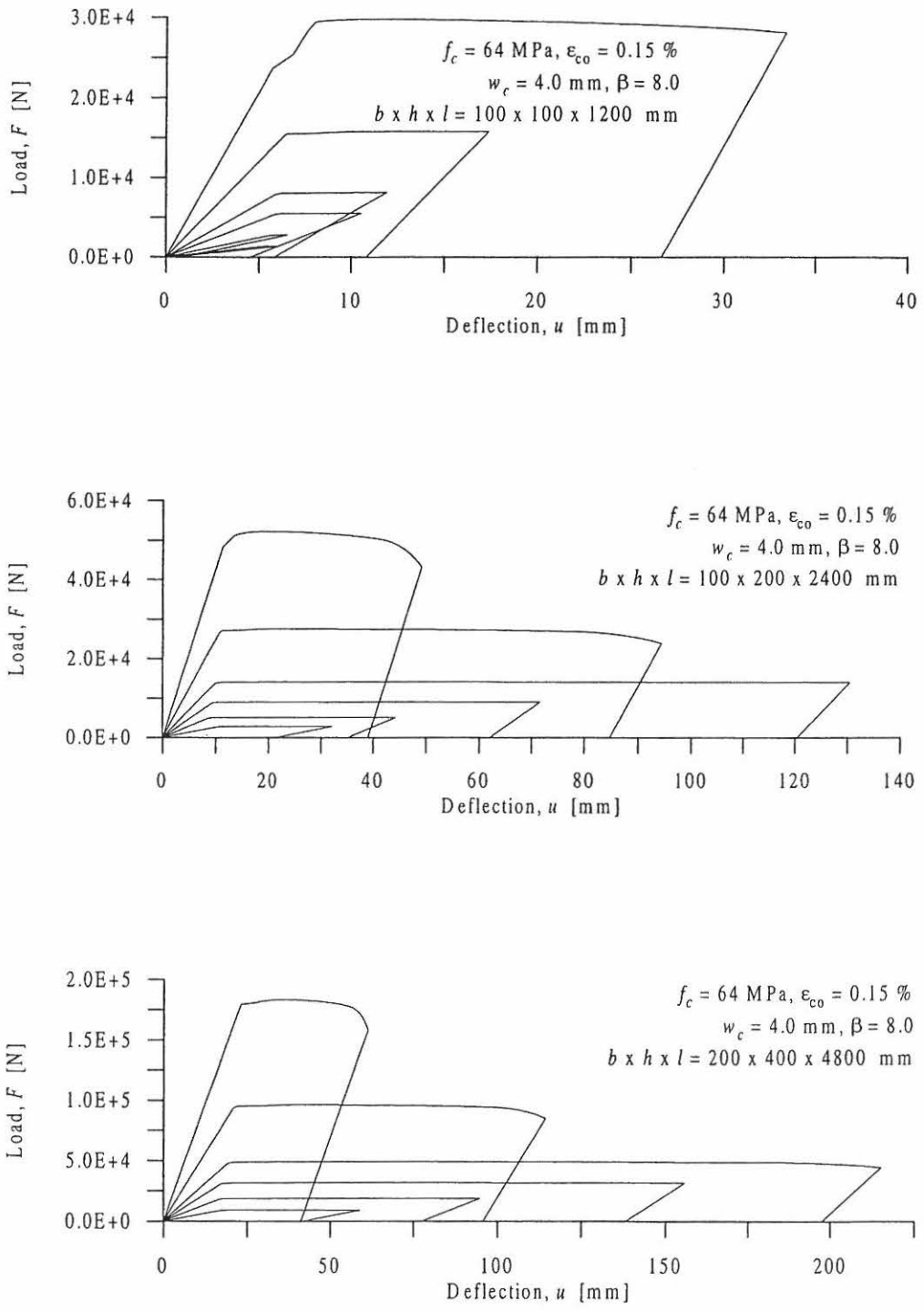

Figure 3.16: *Model results for load-deflection curves for normal strength concrete beams of cross-section 100 x 100 mm (top), 100 x 200 mm (middle) and 200 x 400 mm (bottom), slenderness number 12 and w_c = 4.0 mm and β = 8.0. The total reinforcement ratios starting from the lowest ultimate load are 0.06 %, 0.14 %, 0.25 %, 0.39 %, 0.78 % and 1.57 %.*

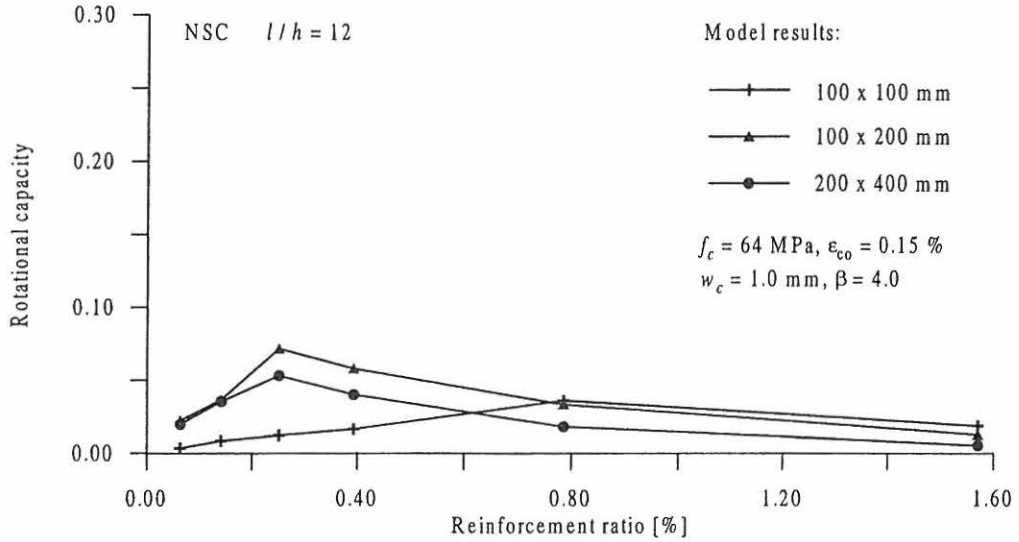

Figure 3.17: *Model results for normal strength concrete beams with w_c = 1.0 mm and β = 4.0.*

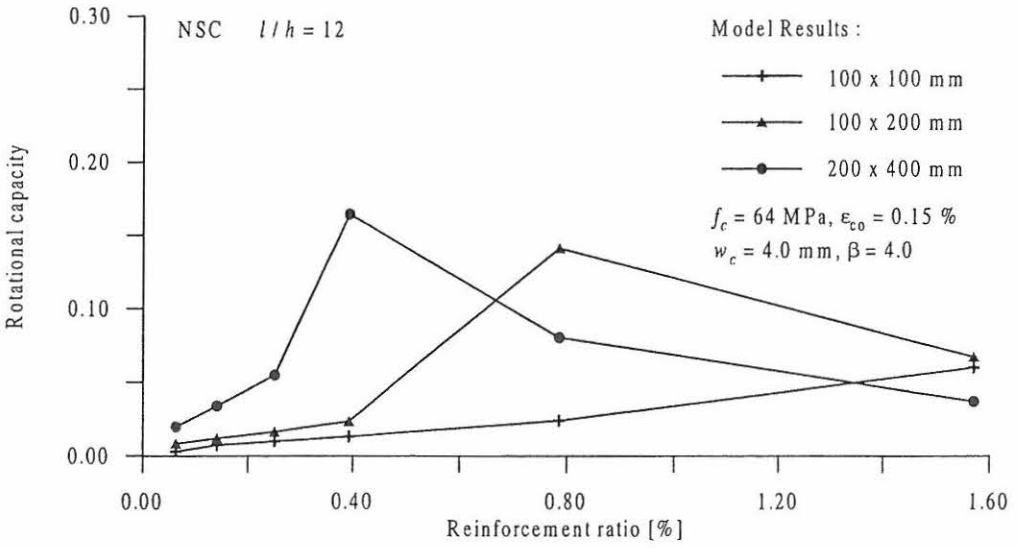

Figure 3.18: *Model results for normal strength concrete beams with w_c = 4.0 mm and β = 4.0.*

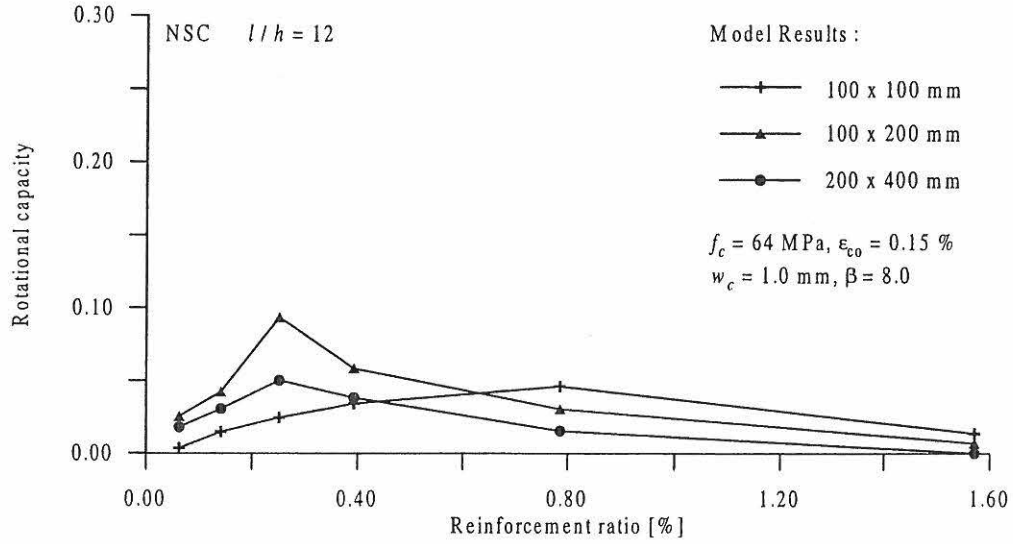

Figure 3.19: *Model results for normal strength concrete beams with w_c = 1.0 mm and β = 8.0.*

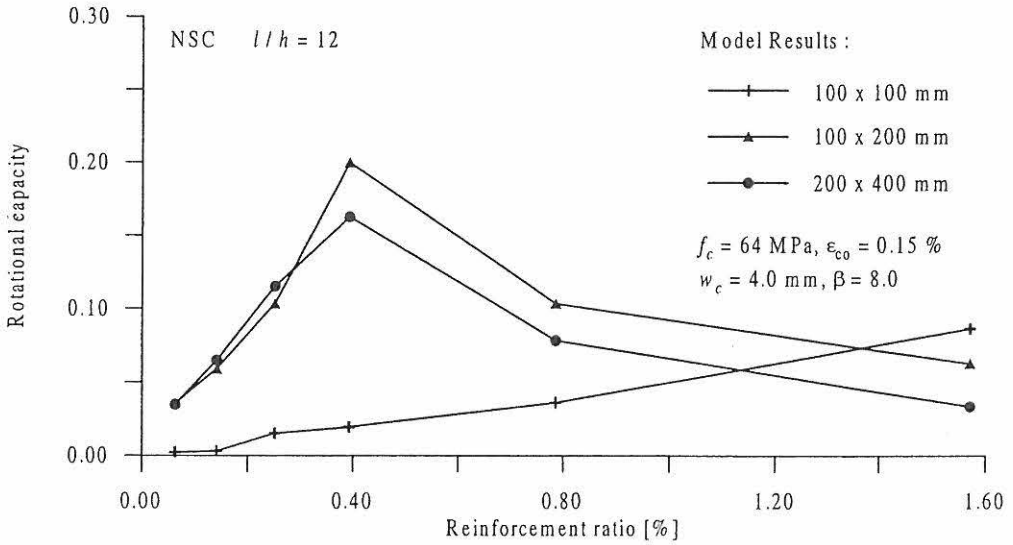

Figure 3.20: *Model results for normal strength concrete beams with w_c = 4.0 mm and β = 8.0.*

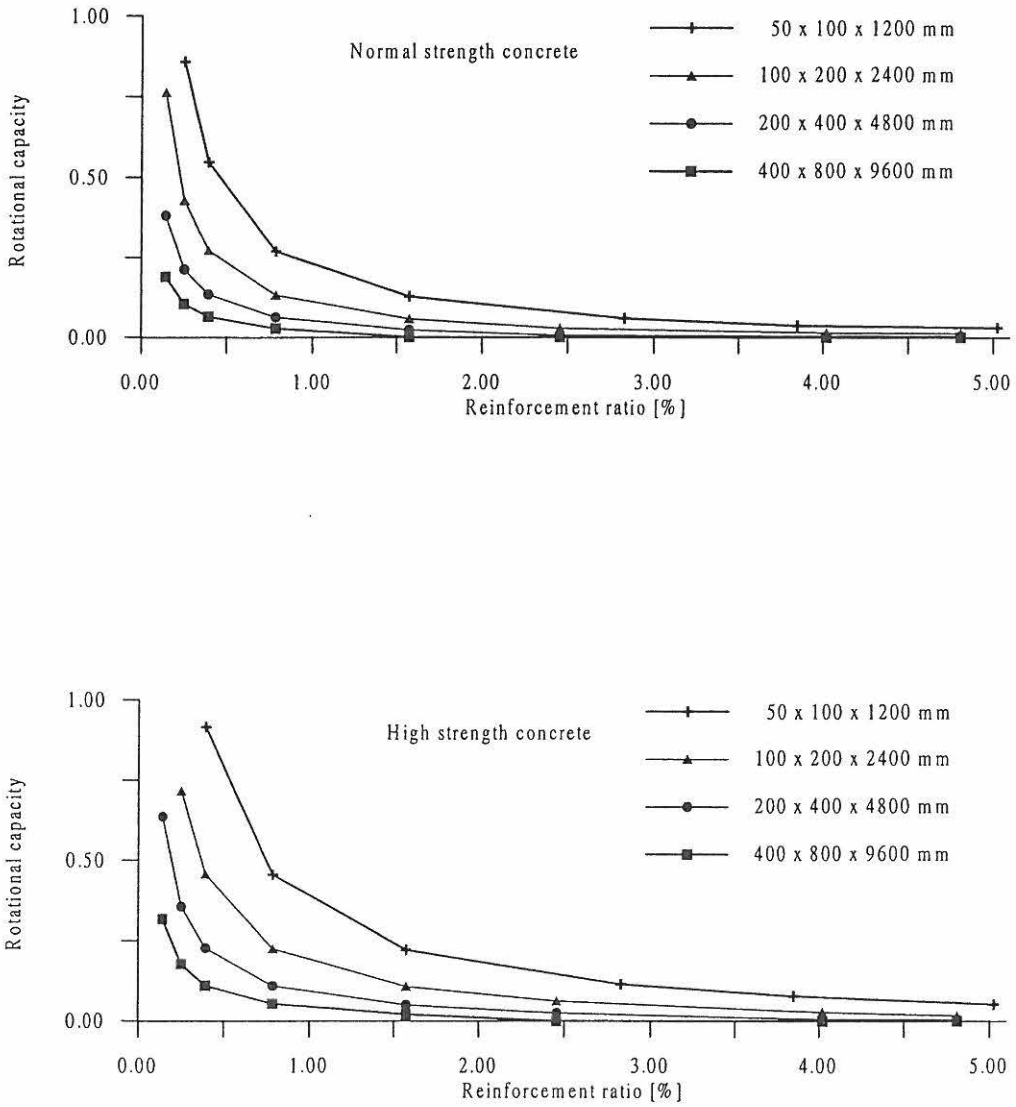

Figure 3.21: *Rotational capacity in the heavily reinforced regime. Top: Normal strength concrete. Bottom: High strength concrete.*

Chapter 4

Experimental Study on the Scale and Strength Dependency on the Ductility of Reinforced Concrete Beams

In this chapter a summary is given of experimental results from tests of reinforced concrete beams in three-point bending carried out in the Structural Research Laboratory at the Department of Building Technology and Structural Engineering, Aalborg University.

The experiments were performed in the period of August 1994 to October 1995 in connection with a Round Robin on "Scale Effects and Transitional Failure Phenomena of Reinforced Concrete Beams in Flexure" initiated by the European Structural Integrity Society - Technical Committee 9 (*ESIS - TC9*). The Round Robin is also refered to as the *ESIS 1*.

The test programme has been designed according to proposals given by *ESIS - TC9*, se Bosco and Carpinteri (1993). One of the main purposes of the Round Robin investigations was to verify the scale dependency of plastic rotational capacity and minimum reinforcement and the existence of transitional phenomena of failure.

The aims of the experiments performed at Aalborg University have been to determine the full load-deflection curves, the distributions of deflections and curvatures along the beam axis and the mutual rotations of the beams for different sizes, different types of concrete and different amounts and types of reinforcement, and to calculate the plastic rotational capacity for all the beams.

The plastic rotational capacity is here defined as (1) the non-dimensional area under the load-deflection curve, (2) the plastic curvature distributed along the beam multiplied by a measuring length and (3) the plastic mutual rotation measured at the supports of the beam. The results are shown as function of the reinforcement ratio. In Henriksen *et al.* (1996) a more detailed description of the experiments is given.

4.1 Test Programme

The test programme has involved 115 reinforced concrete beams for determination of load-deflection curves and displacement and curvature distributions, 54 plain concrete beams for determination of the fracture energy G_F and 324 concrete cylinders for determination of strength parameters. For the reinforced concrete beams four different parameters were varied. The slenderness ratios were 6, 12 and 18 and the beam depth's were 100 mm, 200 mm and 400 mm giving a total of nine different geometries. It should be noted, that alle experiments were repeated three times.

In order to fulfill the requirements for the Round Robin, 6 reinforcement ratios (the steel area A_s divided by the cross-section b x h of the beam) were chosen between 0.06 % and 1.57 % giving a lightly and more heavily reinforced regime. For the concrete both a normal strength and a high strength concrete were chosen with a compressive strength of approximately 60 MPa and 100 MPa. All experiments were repeated three times and only short time loading has been considered.

The geometry of the beams was chosen in accordance with the requirements, and the different geometries and main reinforcements for all beams are given in Table 4.1.

Type - b x h	l/h	NSC	NSC and HSC			NSC	
$\rho_l = A_s / (b\,h)$		0.06 %	0.14 %	0.25 %	0.39 %	0.78 %	1.57 %
A - 100 x 100	6					4 ø5	8 ø10
B - 100 x 100	12		1 ø4	2 ø4	2 ø5	4 ø5	8 ø10
C - 100 x 100	18					4 ø5	8 ø10
D - 100 x 200	6					2 ø10	4 ø10
E - 100 x 200	12		1 ø6	1 ø8	1 ø10	2 ø10	4 ø10
F - 100 x 200	18					2 ø10	4 ø10
G - 200 x 400	6					2 ø20	4 ø20
H - 200 x 400	12	1 ø8	1 ø12	1 ø16	1 ø20	2 ø20	4 ø20
I - 200 x 400	18					2 ø20	4 ø20
J - 200 x 400 (only NSC)	12			4 ø8			

Table 4.1: *Overview of the specimens and main reinforcement included in the ESIS 1 tests.*

The reinforcement ratios were varying from 0.06 % to 1.57 % for the normal strength concrete

beams and 0.14 % to 0.39 % for the high strength concrete beams. As it appears from Table 4.1 some of the beams were singly reinforced with one reinforcement bar, so in order to observe differences in having one instead of four bars, 3 normal strength concrete beams (type J) of dimension 200 x 400 x 4800 mm and reinforcement ratio 0.25 % (4 ø8) were also cast.

For the beam specimens, the reinforcement ratio ρ equal to minimum reinforcement and balanced reinforcement ratio for rectangular beams according to DS 411 (1997) is given as

$$\rho_{min} = 0.45 \frac{f_t}{f_y} \quad \text{where} \quad f_t = \sqrt{0.1 f_c}$$

$$\rho_{bal} = \omega_{bal} \frac{f_c}{f_y} \quad \text{where} \quad \omega_{bal} = \frac{4}{5} \frac{\varepsilon_{cu}}{\varepsilon_{cu} + \varepsilon_y} \tag{4.1}$$

where ω_{bal} is the balanced mechanical reinforcement ratio, f_t is the uniaxial tensile strength, f_c is the uniaxial compressive strength, f_y is the yield strength, ε_{cu} is the ultimate compressive strain and ε_y is the yield strain.

Using a yield strength of f_y = 550 MPa, the minimum reinforcement ratio for NSC beams is equal to 0.20 % and for HSC beams 0.26 % defining a lightly reinforced regime, where rebar tension failure is dominant. The balanced reinforcement ratio for NSC beams is about 4.9 %, and for HSC beams about 8.2 % using a ultimate concrete strain of ε_{cu} = 0.35 % for both NSC and HSC, and a yield strain of ε_y = 0.28 % for the steel. Thus, with the chosen reinforcement ratios the test programme consists of both under-reinforced (lightly regime) and normal-reinforced (heavily regime) beams. The crack picture of the under-reinforced beams will be discrete cracking and for the normal-reinforced beams multiple cracking.

The reinforcement of the beams was designed so that all beams failed in bending. Some of the highly reinforced beams were reinforced with stirrups to avoid anchorage and shear failure. Furthermore, to avoid influence on the compression failure, a zone around the mid section of the beam at least two times the beam depth was free from stirrups and compressive reinforcement.

The geometry of the cross-sections of the beams is shown in Figure 4.1. The distance from the top of the beam to the middle of the reinforcement bars were in all cases equal to 0.9 h, thus h_{ef} = 0.9 h for all beams giving that the reinforcement bars were placed in one layer. Note that the beams and the size of the reinforcement bars are scaled to preserve geometrical similitude.

Each beam has been identified by a unique name. For instance, F2_078_N is the second beam with the dimensions of geometry F (100 x 200 x 3600 mm) with the reinforcement ratio 0.78 % of normal strength concrete. This name system is applied throughout the chapter.

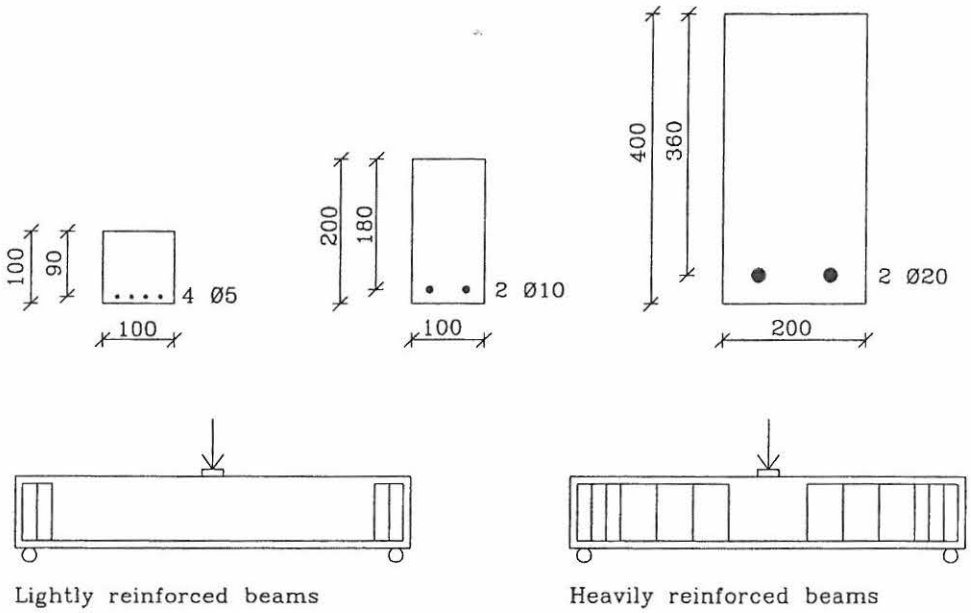

Figure 4.1: *Scaling of cross-section and design of a typical test beam. Units in mm.*

4.2 Materials

The main results of various tests on determining the material parameters of the concrete and reinforcement using national standard tests are listed in this section. The standard tests have been performed at the Structural Research Laboratory and at the Concrete Technology Laboratory. Some compression tests have also been performed at the Department of Structural Engineering and Materials, Technical University of Denmark.

4.2.1 Concrete

Two types of concrete were used for the experiments. The mix of the concrete was prepared in accordance with the requirements and the recipes are listed in Table 4.2. Due to the large amount of concrete for each casting, a commercial manufacturer (ISO 9002 certificate) delivered the concrete. Totally 18 castings have been carried out. The test beams were cast in steel moulds.

The cylinders for splitting tests and the fracture energy beams were all cured in water at 20 °C until the moment of testing. The cylinders for compression test were all cured in water at 20 °C until they were shipped for Copenhagen. The beams from the first three castings were cast outdoors in steel moulds and the beams were stripped after 2 days. Then the beams were covered with wet sheets and wrapped and sealed with plastic. The beams from the other castings were cast indoors and stripped after 2 days. The beams were wrapped with Fibertex sheets and covered and sealed with plastic. All the beams were finally placed inside a room with temperature of 20 °C. Under the plastic, buckets with water were placed to make sure that the relative humidity was

100 % RF. The beams were unwrapped the day before testing.

Contents		Density	Normal Strength Concrete		High Strength Concrete	
Ingredient	Product	[kg/m^3]	[kg/m^3]	[l/m^3]	[kg/m^3]	[l/m^3]
Cement	PC(A/HS/EA/G)	3200	350	111	466	148
Water		1000	160	160	146	146
Microsilica	Elkem - Powder	2200	0	0	36.1	16.4
Plastiziser 1	Conplast 212	1170	3.84	3.20	1.80	1.50
Plastiziser 2	Peramin F	1210	0	0	12.6	10.4
Sand (0-2mm)	Ks. Nr. Halne 0-2/A	2639	898	342	837	318
Gravel (4-8 mm)	Vikan 4-8/A	2760	896	335	899	324
Air		0	0	50	0	35
Density			2307 kg/m^3		2399 kg/m^3	

Table 4.2: *Mix proportions of the two types of concrete.*

The mechanical properties of the concrete were obtained by standard tests. The tensile splitting strength, the compressive strength, the compression softening and the modulus of elasticity were determined on cylinders (diameter 100 mm and depth 200 mm). The bending tensile strength and the bending fracture energy were determined from tests on notched RILEM beams with a span of 800 mm, a thickness of 100 mm and a depth of 100 mm. The material parameters are listed in Table 4.3. A bending experiment for determination of fracture energy and bending tensile strength is shown in Figure 4.2. A detailed describtion of determination of the bending tensile strength and bending fracture energy can be found in Ulfkjær and Brincker (1995).

For both normal strength and high strength concrete experiments on cylinders (100 x 200 mm) to obtain the stress-strain relations in uniaxial compression have been carried out at the Technical University of Denmark by Stang (1996). Typical compression softening curves are shown in Figure 4.2. Note the more brittle behaviour of the high strength concrete.

		Normal Strength Concrete	High Strength Concrete
Compressive Strength	Mean S. Dev	64.0 MPa 6.12 MPa	98.5 MPa 6.60 MPa
Splitting Strength	Mean S. Dev.	4.09 MPa 0.54 MPa	6.06 MPa 0.28 MPa
Modulus of Elasticity	Mean S. Dev.	4.23E4 MPa 0.31E4 MPa	4.55E4 MPa 0.23E4 MPa
Bending Tensile Strength	Mean S. Dev.	5.51 MPa 0.34 MPa	7.16 MPa 0.29 MPa
Specific Bending Fracture Energy	Mean S. Dev.	126 J/m^2 8.30 J/m^2	118 J/m^2 5.24 J/m^2

Table 4.3: *Mechanical proporties of the normal strength and high strength concrete.*

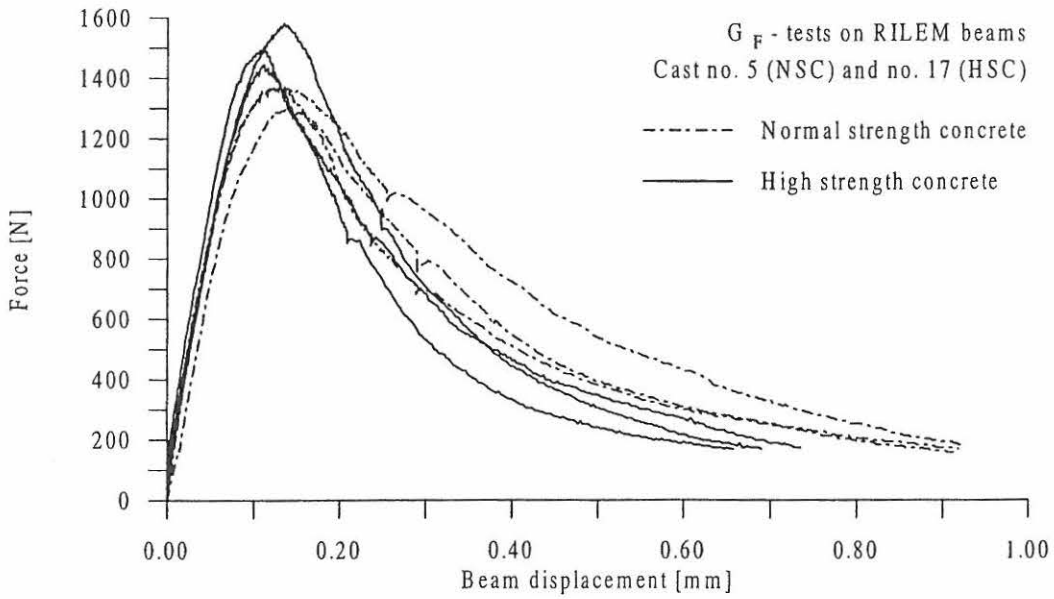

Figure 4.2: *Typical bending experiment for determination of fracture energy and tensile strength in bending for normal strength and high strength concrete.*

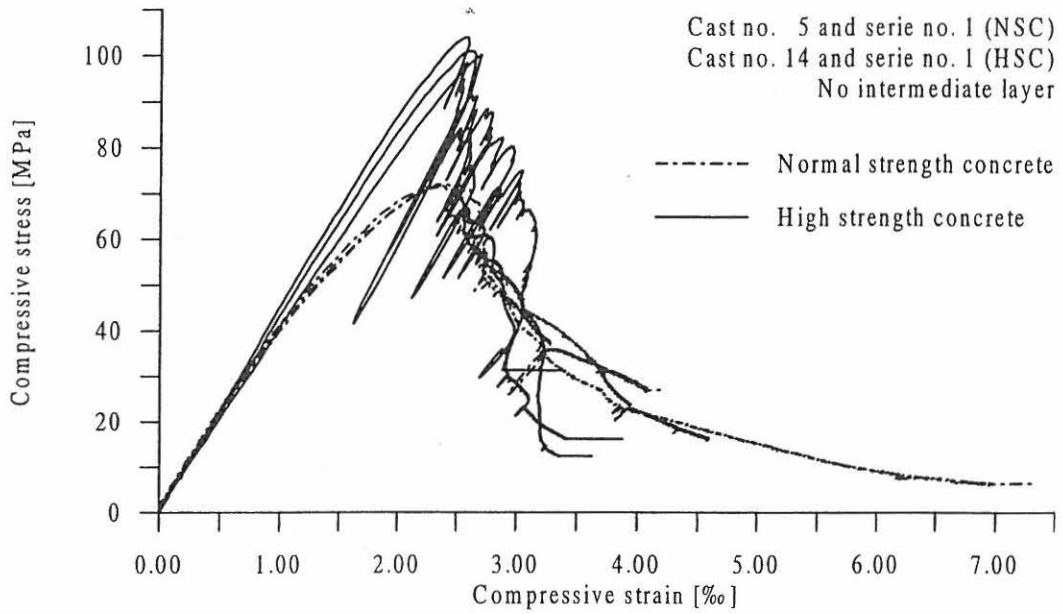

Figure 4.3: *Typical compression tests with softening for normal strength and high strength concrete by Stang (1996). Uniaxial tests on 100 x 200 mm (d x h) cylinders.*

4.2.2 Reinforcement

In order to have six different reinforcement ratios and to reinforce beams of different scale without changing the geometry of the cross-sections it was necessary to use reinforcement with 8 different diameters.

Two types of ribbed reinforcement bars were used with approximately the same type of ribs. The ø4 mm and ø5 mm steel bars were cold deformed and had a relatively small deformation capacity, while the ø6 mm, ø8 mm, ø10 mm, ø12 mm, ø16 mm and ø20 mm steel bars had a large yield capacity and a clear strain hardening.

The mechanical properties of the steel were determined on 500 mm long specimens subjected to uni-axial tension. The tests were divided into two parts. In the first part the modulus of elasticity was determined using two DD1 HBM displacement transducers measuring displacement directly on the specimens. In the second part only the displacements measured using an external LVDT were recorded. Also in the second part the yield strength and the ultimate strength were determined.

The results given as nominal values are summarized in Table 4.4. It is observed from Table 4.4 that the bars with a large yield capacity fulfil the requirements for high ductility reinforcement $f_t/f_y < 1.08$ and $\varepsilon_{su} > 5$ % given by Eurocode 2 (1993). Stress - strain relations from the uniaxial tensile tests of the cold deformed ribbed steel bars are shown in Figure 4.4 steel type A and B, and of the hotrolled ribbed bars in Figure 4.5 steel types C, D and E. Note the difference in the behaviour of the two types of steel.

Steel type	Young's Modulus	Yield strength	Yield plateau	Ultimate strength	Ultimate strain	Ultimate to yield strength ratio
	E_s	f_y	$\Delta\varepsilon_y$	f_u	ε_{su}	f_u / f_y
	[MPa]	[MPa]	[%]	[MPa]	[%]	[-]
ø4	2.01E5	740	0	740	1.41	-
ø5 - ch1	1.94E5	701	0	701	2.20	-
ø5 - ch2	2.01E5	708	0	708	2.94	-
ø6	2.09E5	600	3.44	664	13.1	1.11
ø8	2.05E5	604	2.29	685	10.7	1.13
ø10	2.06E5	611	2.27	681	11.2	1.11
ø12	2.01E5	555	2.56	642	11.5	1.16
ø16	1.96E5	531	1.60	630	11.0	1.19
ø20	1.82E5	531	1.13	624	9.27	1.18

Table 4.4: *Mechanical properties for the ribbed reinforcement bars used for the ESIS 1. For the ø5 mm bar two charges (ch) were used. The yield strain is given by* $\varepsilon_y = f_y / E_s$.

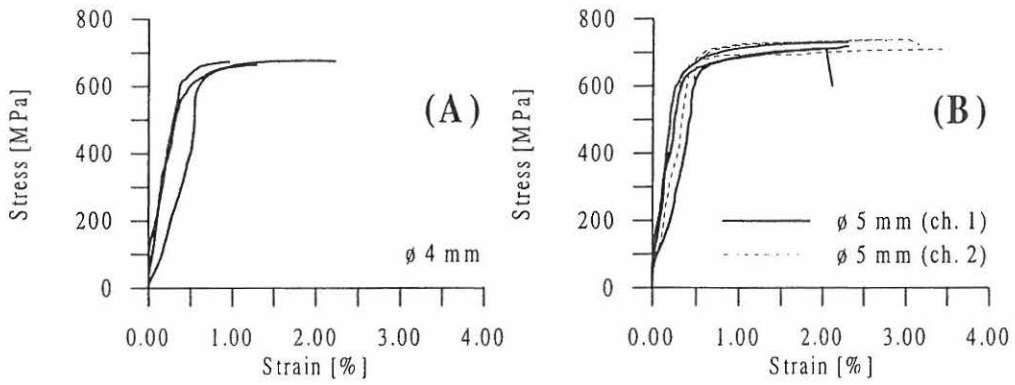

Figure 4.4: *Stress-strain relations for cold deformed ribbed steel bars ø4 (A) and ø5 (B).*

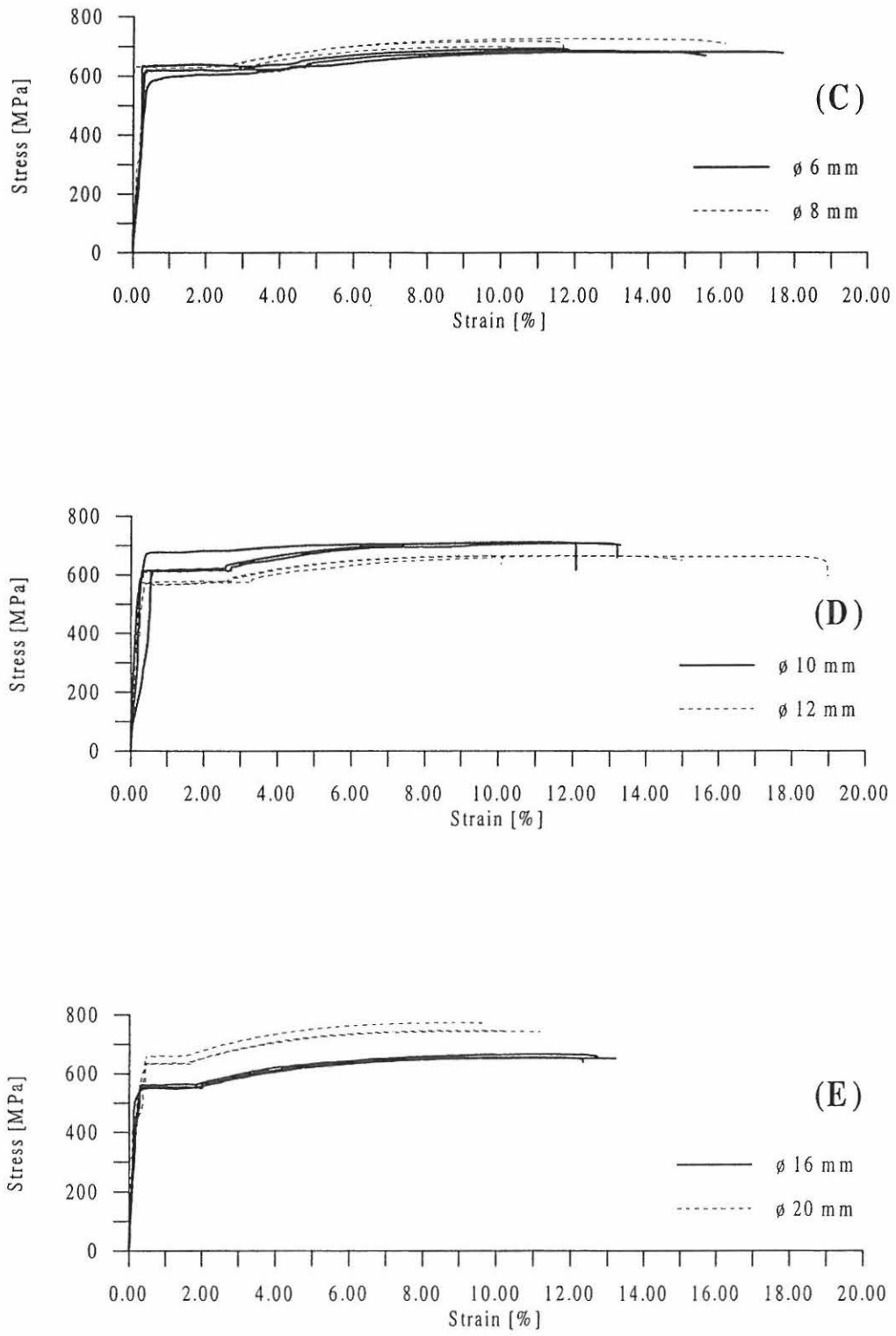

Figure 4.5: *Stress-strain relations for hotrolled normal ribbed bars ø6 and ø8(C) , ø10 and ø12 (D) and ø16 and ø20 (E) subjected to tensile testing.*

4.3 Testing Equiptment and Procedure

The reinforced concrete beams were subjected to three-point bending in a specially designed servo-controlled materials testing system. Due to the many different geometries a flexible test set-up had to be built. A photo of the test set-up for the smallest and the largest beam sizes are shown in Figure 4.6 and 4.7. When changing the beam size the two columns supporting the beam are moved horizontally. The maximum capacity of the Schenk cylinder is a force of 250 kN or a displacement of 100 mm.

4.3.1 Boundary Conditions

At both supports horizontal displacements and rotations were allowed for and, at one support, also rotations around the beam axis were allowed. At the load point rotations were allowed around all three axes. This was done in order to minimize the influence of axial forces and torsion. At both ends a stop was placed at the top of the beam in order to prevent the beam from sliding off the supports.

At the support the size of the supporting steel plate was equal to the thickness of the beam and for a beam depth of 100 mm the width of the steel plate was 50 mm, for he other to beam depths the width of the steel plate was 100 mm. The plate at the loading point was quadratic with sides equal to the beam thickness.

4.3.2 Measurements

The stroke (the piston displacement) was measured using the built-in LVDT (Linear Varible Displacement Transformer). The vertical displacement of the beams was measured at eight points along the beam axis. The base of these LVDT's was 4 mm, 10 mm, 20 mm, 40 mm or 100 mm depending on the size of the beam and the poistion of the LVDT. The rotations of the ends of the beams were measured using two LVDT's at each end.

The mutual rotations of the cross-sections at different points along the beam axis were measured using a number (at least equal to half the slenderness of the beam plus one) of specially designed measuring frames, see Figure 4.8 and 4.9. Dividing these rotations by the distance between the measuring frames gives a direct estimate of the average curvature between the frames. The measuring frames were attached to the beam at three points and with three LVDTs attached to the frames in three of the corners. Thus, the LVDTs were measuring the displacement between two frames at three points. By assuming that plane sections remain plane it is possible to calculate the mean strain in each measuring field for all points in the cross-section. The base of the LVDTs attached to the measuring frames was 2.6 mm, 10 mm, 20 mm, 40 mm depending on the size of the beam and the position of the LVDT. The distance between two frames was equal to the depth of the beam.

The load was measured in a 250 kN load cell or in a 63 kN load cell.

4.3.3 Data Acquistion

All signals and the time t (for the beams with slenderness ratio 18 there were 40 signals) were recorded every three seconds using a data recorder.

4.3.4 Testing Procedure

As mentioned earlier, the tests were servo-controlled. Thus, both a reference signal and a feed-back signal are needed. Here the reference signal was chosen to be linear ramp.

Especially for the lower reinforcement ratios it is necessary to take the formation of tensile crack growth into consideration when controlling the experiment. Therefore the feed-back signal consisted of contributions from both the stroke and from an extra set of measuring frames placed around the midsection of the beam. The distance between the measuring frames was twice the beam depth. By using this distance the critical cracks would always develop between these two extra frames. At the bottom of one of the measuring frames an extra LVDT with a loose core was attached. For simplicity, the signal measured by this LVDT was called the crack opening displacement (COD) even though the signal also includes elastic contributions.

The feed-back signal was then created by analog addition of the COD and the stroke given by

$$\delta_{feedback} = \alpha_1 \delta_{stroke} + \beta_1 \delta_{cod} \tag{4.2}$$

where δ_{stroke} is the signal from the stroke and δ_{cod} is the signal from the COD, α and β are weight factors dependent on the beam size and the reinforcement ratio. Typical values were $\alpha_1 = 0.25$, 0.50 or 1.0 and $\beta_1 = 1.0$, 2.0 or 4.0.

The loading rate was chosen so the cracking load would be reached after 5-15 min. At later stages the displacement rate was increased and a typical experiment would take about 45 min. For some of the beams more than the available stroke was required. An unloading was therefore performed, some extra steel plates were inserted between the beam and the piston and a reloading was then performed. This procedure was repeated until failure of the beam. Experiments with repeated loading could take up to several hours.

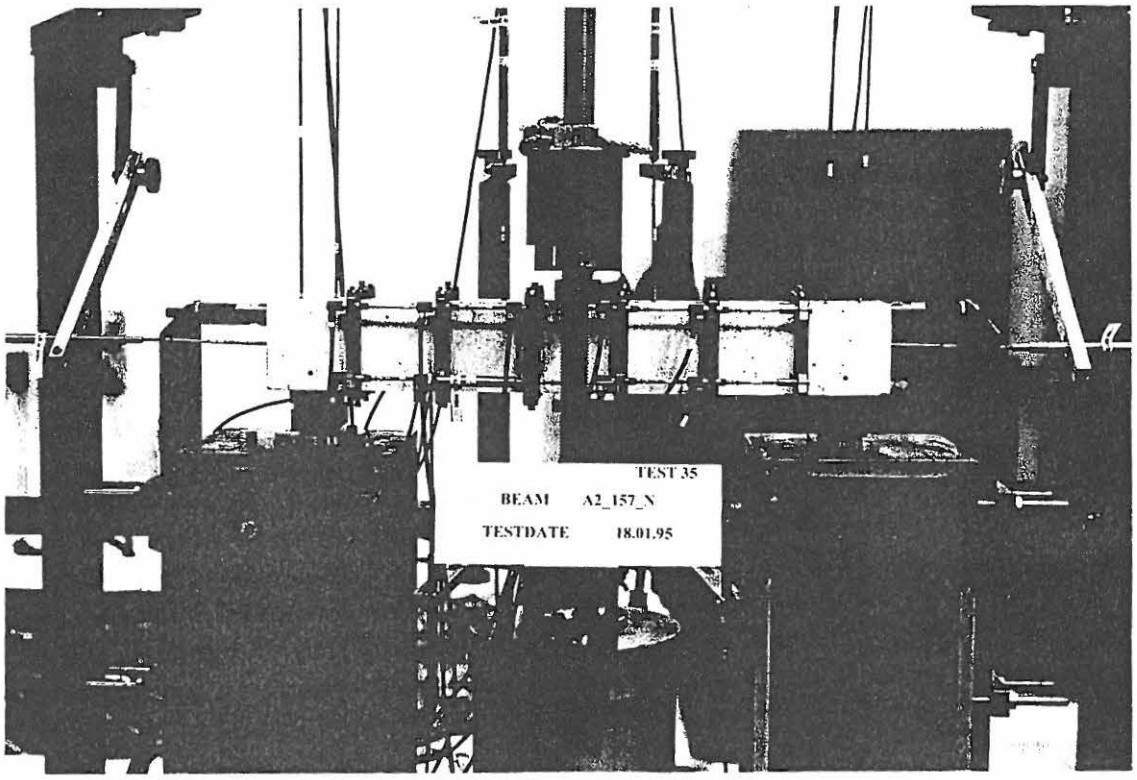

Figure 4.6: *Photo of the test set-up for the smallest beam type.*

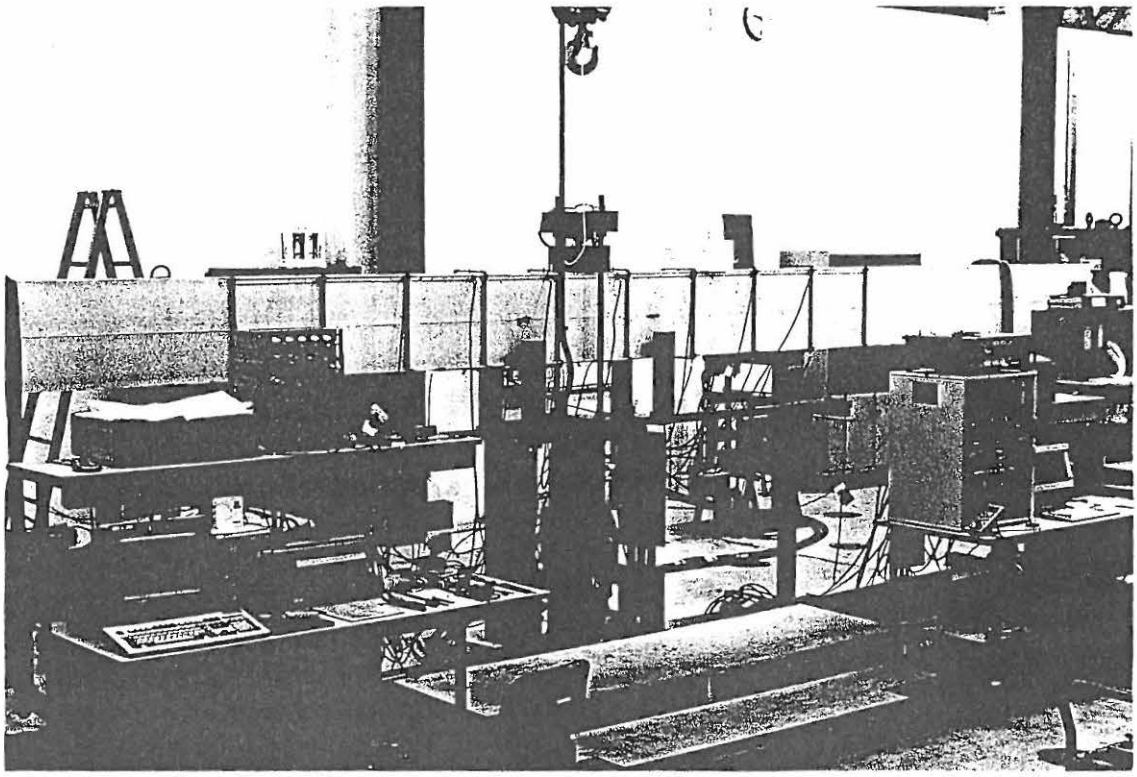

Figure 4.7: *Photo of the test set-up for the largest beam type.*

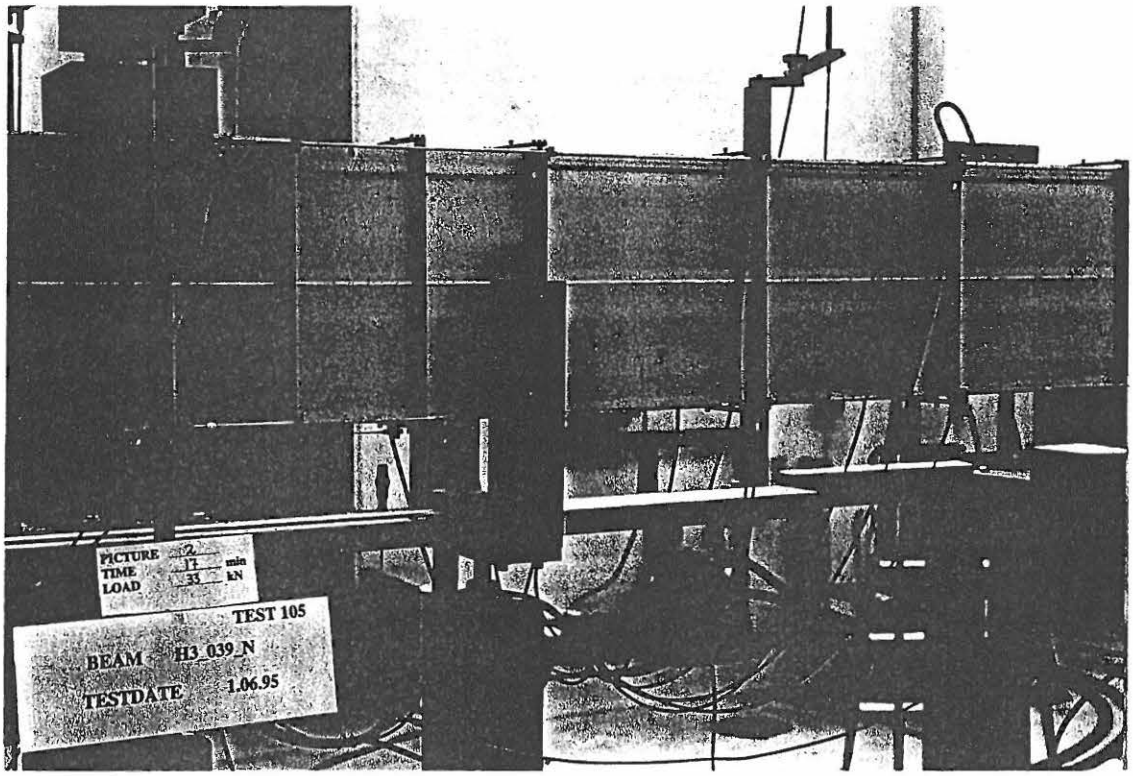

Figure 4.8: *Photo of the measuring frames attached along the beam.*

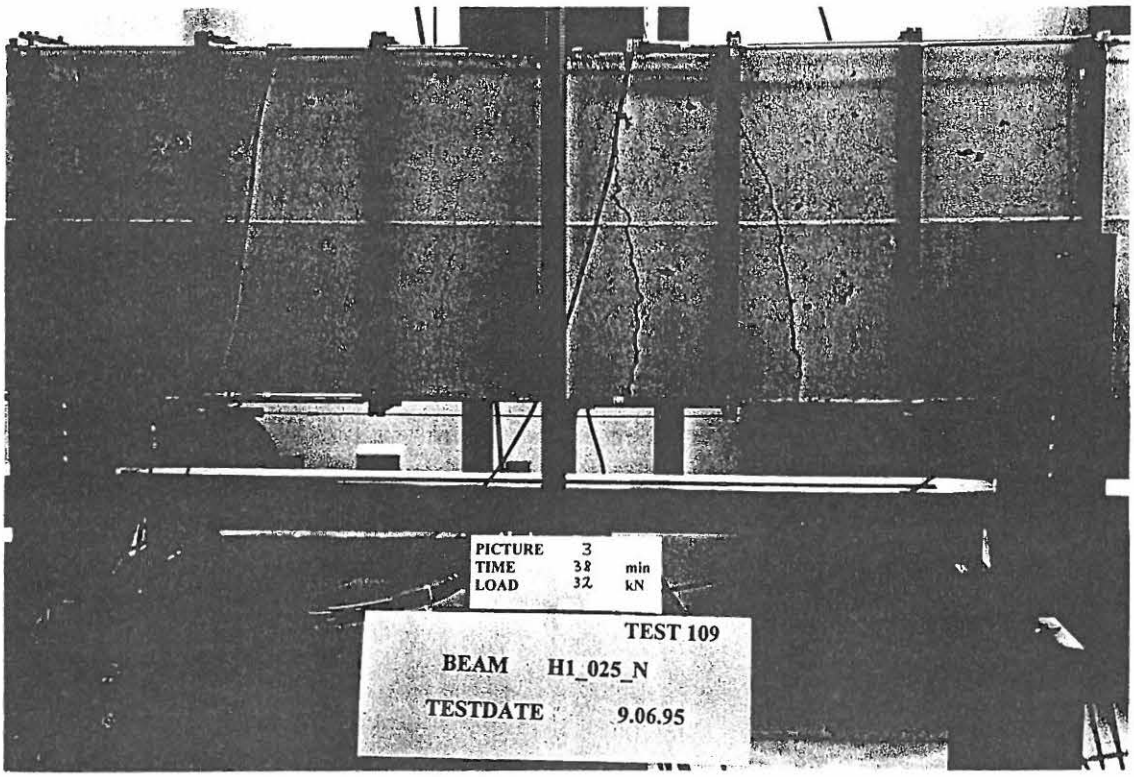

Figure 4.9: *Photo of the measuring frame with the crack opening displacement transducer at the bottom of the midsection of beam.*

4.4 Results and Discussion

In the following some main results and observations will be shown and discussed. Several fracture parameters have been determined from the tests. In appendix A, section A1 results are listed for the measured load-deflection curves, the normalized bending moment-rotation relations and the curvature distributions for the three repetitions of all the beams as well as in section A2 experimental values for the plastic rotational capacities calculated from the measured plastic curvatures, the plastic vertical deflections and the plastic mutual rotations of the beams. Further results are given in Henriksen *et al.* (1996).

4.4.1 Load-Deflection Responses

The main results for the normal strength and high strength concrete beams with slenderness ratio 6, 12 and 18 are shown in Figures 4.10 - 4.14. The results are given as load-deflection curves for the mid point of the beam. It should be noted, that the beam type J is left out of the investigation.

It is clearly seen from Figure 4.11 and 4.12 that it has been possible to measure almost the full range deflection curve for the beams in lightly reinforced regime, because the object of the measuring system is preferable for lightly reinforced beams showing rebar tension failure. However, for the heavily reinforced beams of 0.78 % and 1.57 % showing compression failure, the softening branch has not been captured very well, as the compression failure occurs suddenly and because no control systems were placed in the compression zone. Almost identical curves for the three repetitions have been obtained for most of the low reinforced beams, whereas the scatter of the ultimate deflections for the high reinforced beams are large i most cases. Thus, measurements of the total plastic deformation at midspan taken as the ultimate minus the elastic contribution will then produce a major scatter.

Typical distributions of vertical displacement and of the curvature along the beam axis at different load levels (indicated at the load deflection curve) are shown in Figure 4.15 for a normal strength concrete beam with dimensions 200 x 400 x 4800 mm (b x h x l) reinforced with one ø 20 mm ribbed steel bar corresponding to a total reinforcement ratio of 0.39 %. From knowledge of the measured horizontal displacements between the measuring frames at three points and by assuming that plane sections remain plane the average curvature between the frames can be determined. It is clearly seen, that the rotations are localized in the centre of the beam, see also the total curvature distributions in appendix A.

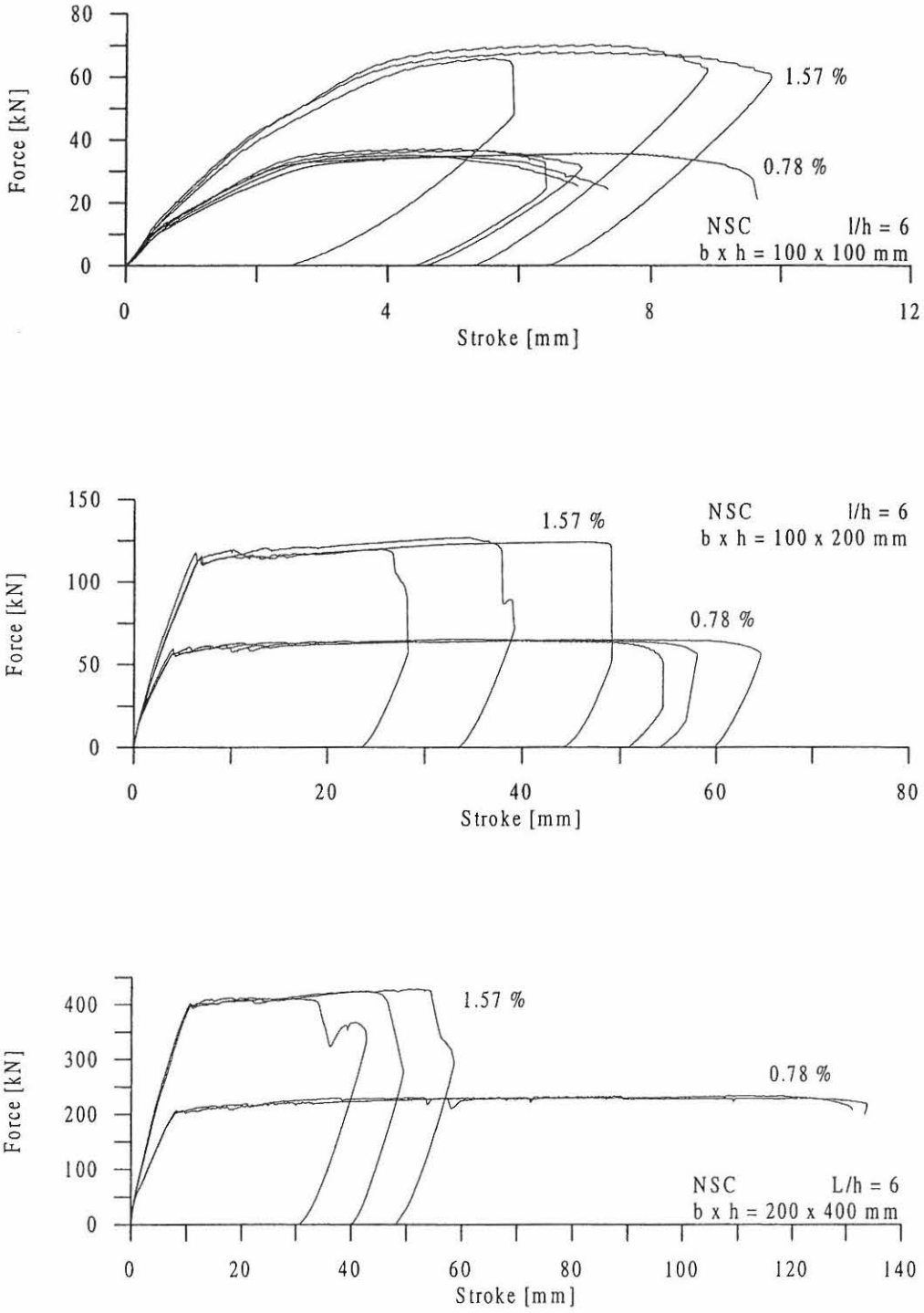

Figure 4.10: *Load-displacements curves for normal strength concrete (NSC) beams with total reinforcement ratios 0.78 % and 1.57 % and slenderness number 6.*

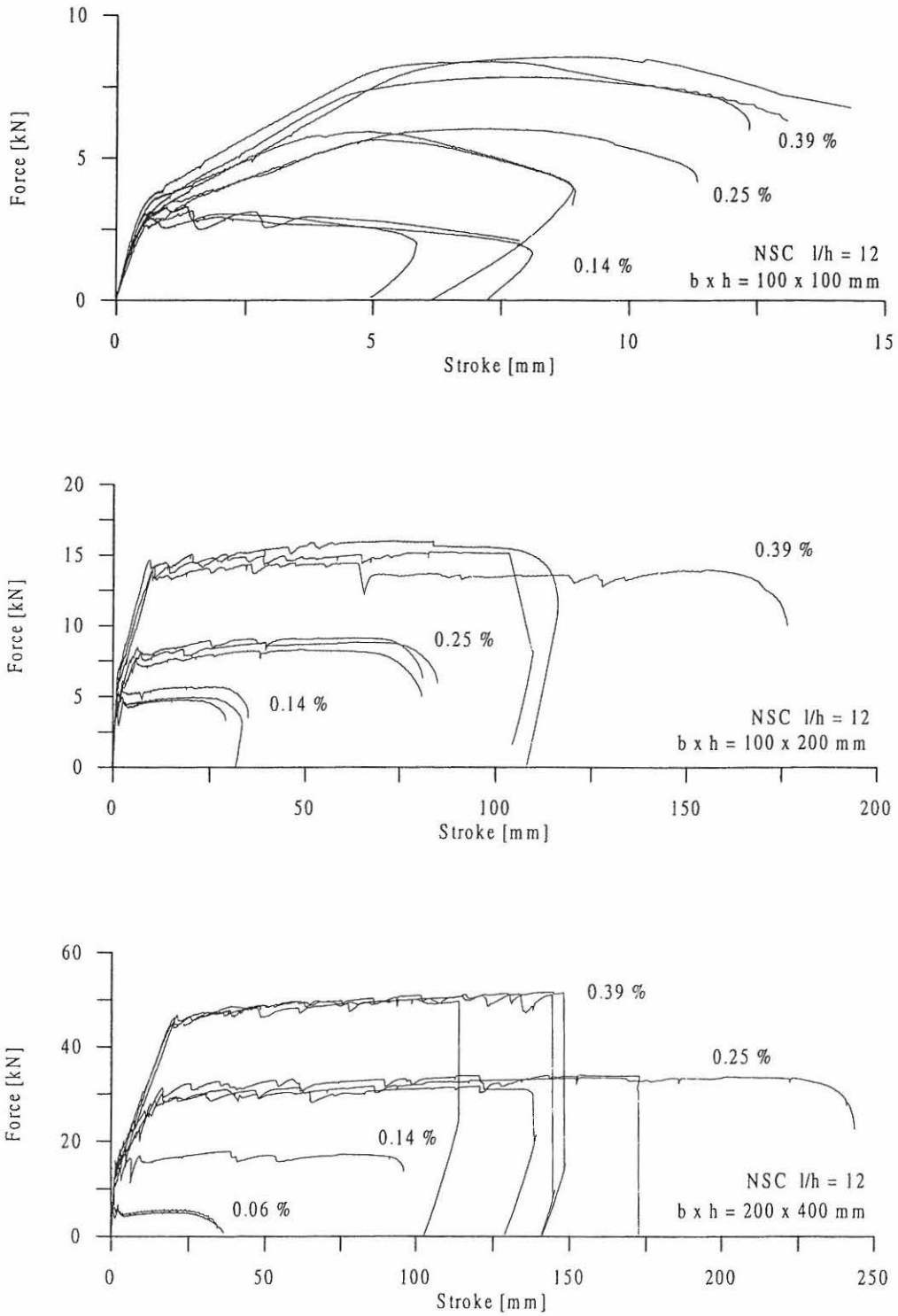

Figure 4.11: *Load-displacements curves for normal strength concrete (NSC) beams with total reinforcement ratios 0.06 %, 0.14 %, 0.25 % and 0.39 % and slenderness number 12.*

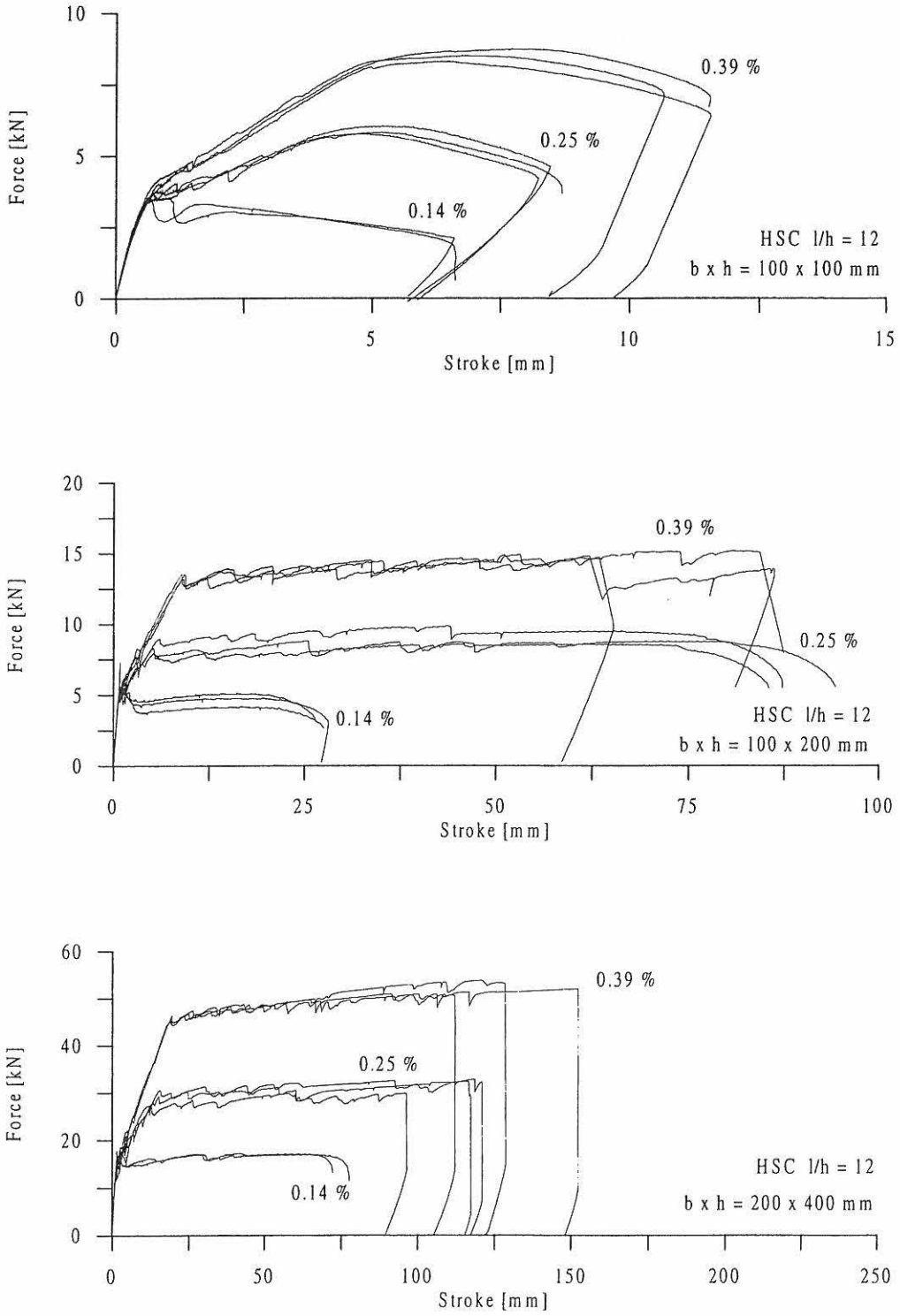

Figure 4.12: *Load-displacements curves for normal strength concrete (HSC) beams with total reinforcement ratios 0.14 %, 0.25 % and 0.39 % and slenderness number 12.*

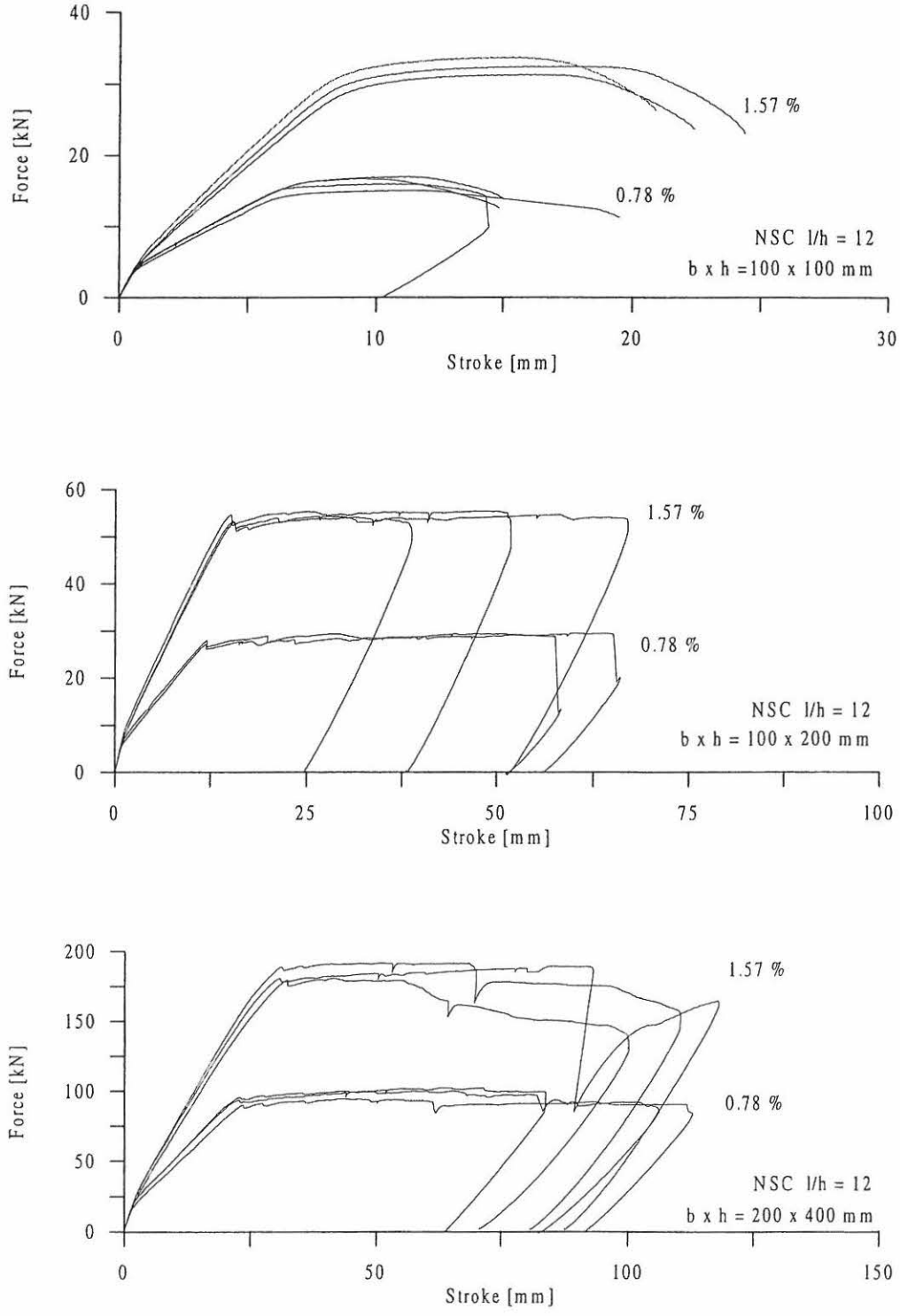

Figure 4.13: *Load-displacements curves for normal strength concrete (NSC) beams with total reinforcement ratios 0.78 % and 1.57 % and slenderness number 12.*

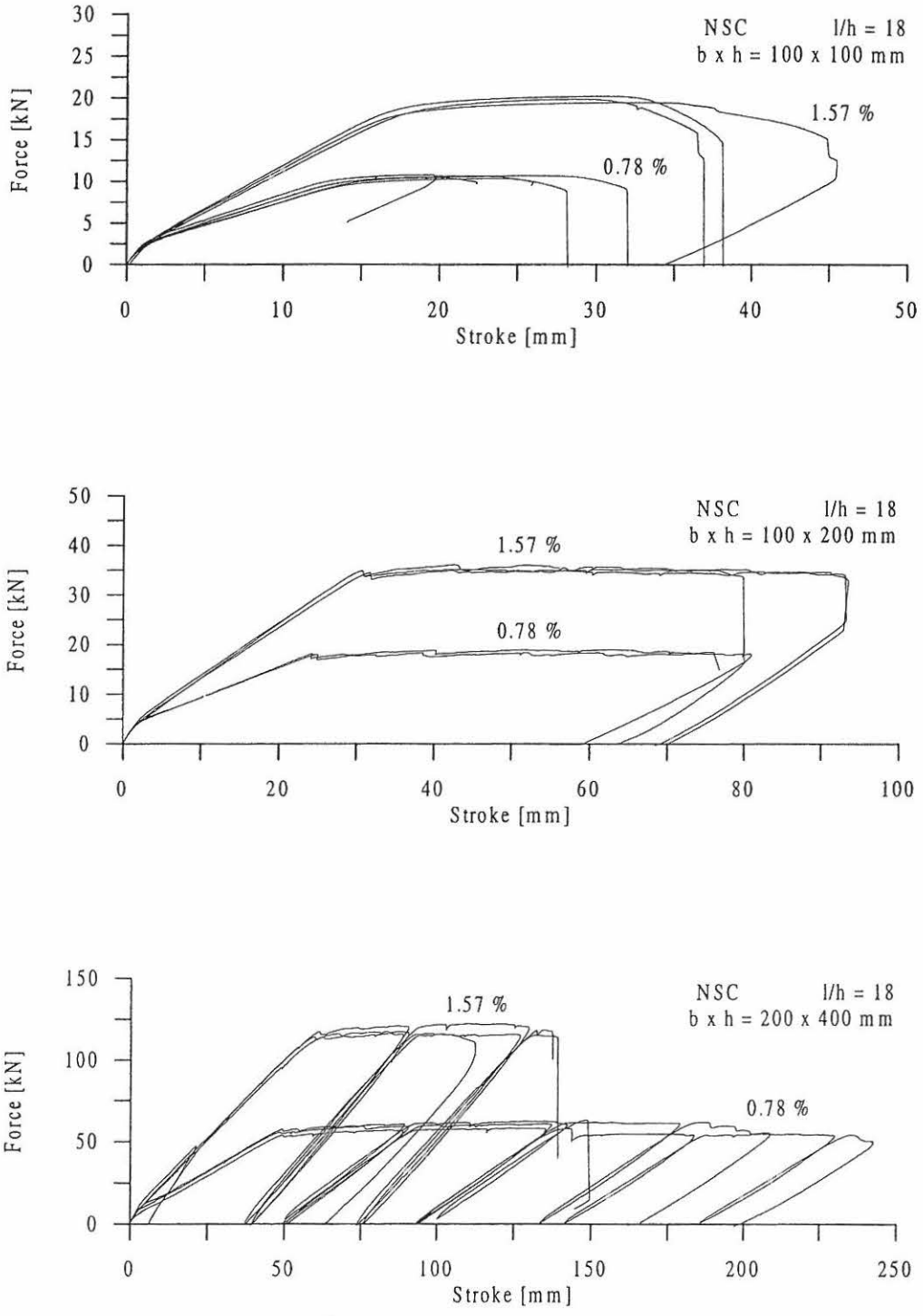

Figure 4.14: *Load-displacements curves for normal strength concrete (NSC) beams with total reinforcement ratios 0.78 % and 1.57 % and slenderness number 18.*

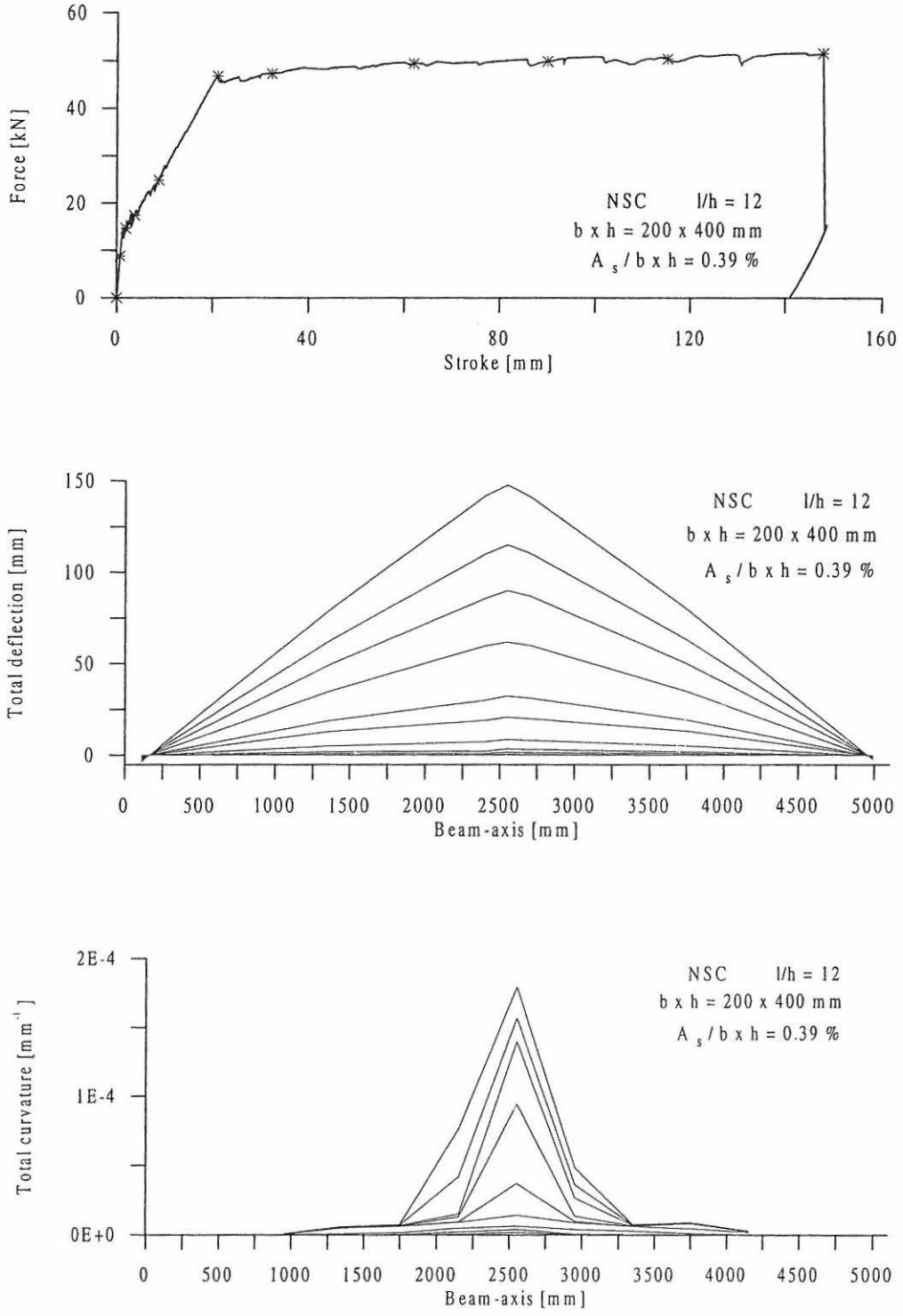

Figure 4.15: *Load-deflection curve (top), vertical distribution (mid) and distribution of curvature (bottom) along the beam axis for a normal strength concrete beam (200 x 400 x 4800 mm) with a total reinforcement ratio of 0.39 %. The load levels are marked with asterisk (top).*

4.4.2 Rotational Capacity

Three different rotational capacities have been determined. The experimental values of the plastic rotational capacities according to the following three models can be found in Appendix A, section A2 for both normal and high strength concrete.

Basic Assumption on Rotational Capacity

Calculation of the plastic rotational capacity depends on the load displacement curve and the way of testing the beam. The forming of a plastic hinge in a concrete beam depends on the testing. In this chapter the experiments are all done in three point bending to be sure of forming a plastic hinge in the centre of the beam.

The size of the plastic rotational capacity is dependent on how the ultimate failure load or ultimate displacement is chosen and how the elastic part is defined. In the litterature there seems to be different ways of doing this, see e.g. CEB Bulletin 242 (1998).

The basic ideas can be shown in Figure 4.16.

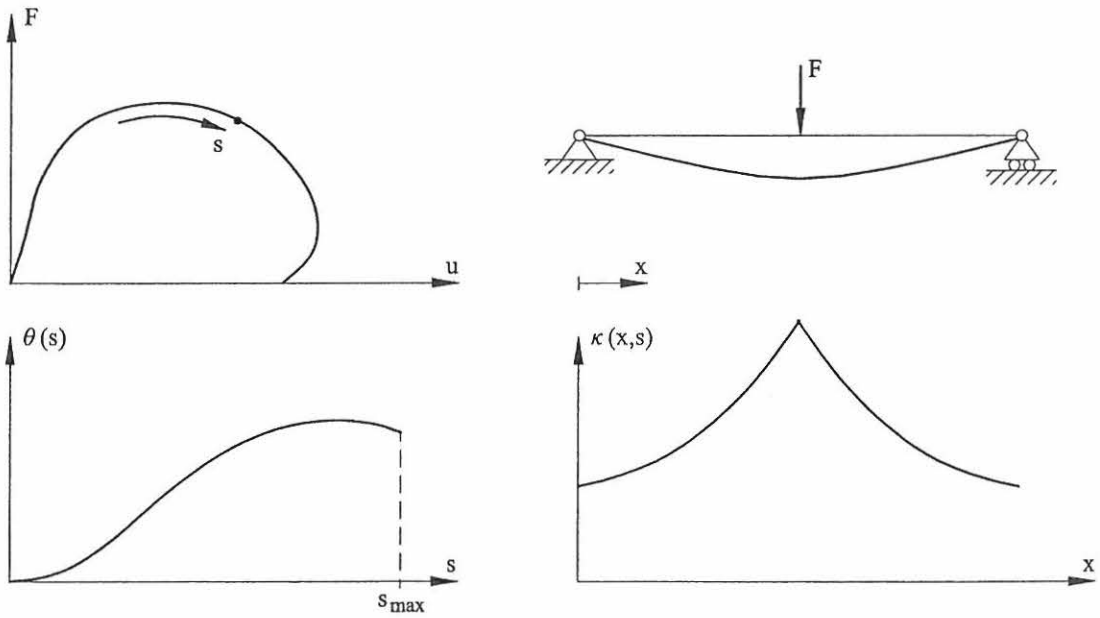

Figure 4.16: *Basic ideas on rotational capacity.*

The point s on the load displacement curve (F - u) and the point x on the beam axis seems to be important factors in calculating the rotational capacity, because the rotational capacity is dependent on the size of s and x.

The curvature is then given as

$$\kappa = \kappa(x,s) \tag{4.3}$$

The rotational capacity can be calculated as

$$\theta(s) = \int_0^l (\kappa(x,s) - \kappa_{el}(x,s))\, dx \tag{4.4}$$

where κ_{el} is the elastic part of the curvature, and l is the span of the beam.

In order to calculate the maximum value of the rotational capacity, the point s on the load displacement curve must be equal to the ultimate displacement u_{max} for an ultimate force F^* corresponding to the value s_u on the curve showing the relation between $\theta(s)$ and s.

Some examples of choosing the point s corresponding to maximum allowed deformation or rotation of a RC beam, could be defined as a decrease in the maximum load or maximum bending moment for the developed plastic hinge at about 0 % to 10 % of the max. F or M, see Figure 4.17.

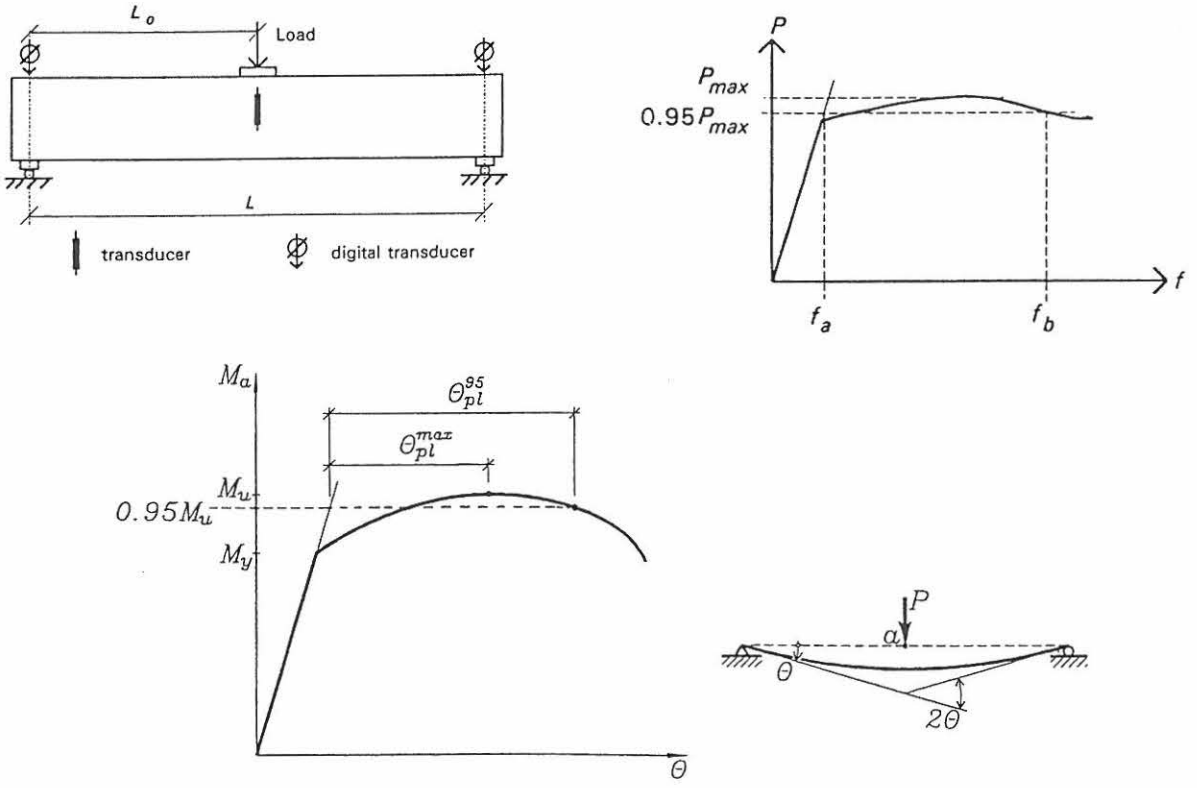

Figure 4.17: *Definition of rotational capacity according to Swedish investigations. Top: Loading arrangement and measurements (left) and defintion of rotational capacity from load-deflection response at midspan according to An and Cederwall (1995). Bottom: Defintion of rotational capacity as the non-elastic rotation* θ_{pl}^{95} *according to Fransson (1997).*

An and Cederwall (1995) have been re-evaluating tests performed at CTH over the years from 1974 until 1994, where a huge amount of experiments on rotational capacity of RC beams have been performed. As a result of the experimental and theoretical investigations, especially by Plem (1977) and Öberg (1977), the ABC formula was developed, see Betonghandbok (1990). An and Cederwall use a definition of the rotational capacity, see Figure 4.17, as an angle of θ_{95} given by

$$\theta_{95} = \frac{(f_a - f_b)}{L_0} \tag{4.5}$$

where f_a and f_b are the deflections at the mid section at a corresponding load of $0.95P_{max}$ and L_0 is a distance between a maximum moment section and a zero moment section.

Fransson (1997) reports an investigation of rotational capacity of reinforced high strength concrete beams, where he uses the non-elastic rotation θ_{pl}^{95} defined as shown in Figure 4.17.

In the following the three calculation models for plastic rotational capacity are presented, where the rotational capacity corresponds to the ultimate failure point given by the maximum midspan deflection as shown in the reponse curves for the test beams, see Figures 4.10-4.14.

Rotational Capacity according to CEB-FIP Model Code 1990

A model for calculating the rotational capacity based on the CEB - FIP Model Code 1990 (1991) is made using the experimental results of measuring the average curvature in each field along the beam axis. The plastic rotational capacity is calculated by integration, along the total length of the measuring fields, of the difference between the ultimate average curvature obtained at the ultimate displacement and the elastic average curvature, thus

$$\theta^{CEB} = \int_{l_{field}} (\kappa_{ult}(x) - \kappa_{el}(x))\, dx \tag{4.6}$$

where κ_{el} is the elastic curvature at F^* obtained at the ultimate displacement, κ_{ult} is the ultimate average curvature at the ultimate displacement and θ^{CEB} is the rotational capacity according to CEB-FIP Model Code. The CEB-FIP rotational capacity is dependent on the definition of the elastic part and on how the load F^* is chosen.

Rotational Capacity according to Plasticity Theory

The area under the load displacement curve is equal to the work done by the external forces during the failure process. If the beam is assumed to be ideal plastic forming a plastic hinge at the mid-section, this work can also be expressed as the yield moment M_y times the total rotation, thus

$$M_y \, \theta^{work} = \int_0^{\delta} F \, du \qquad \Rightarrow \qquad \theta^{work} = \frac{1}{M_y} \int_0^{\delta} F \, du \tag{4.7}$$

where the yield moment and the depth of the compreesion zone are given as

$$M_y = \frac{4}{5} h_c \, b f_c \, (h_{ef} - \frac{2}{5} h_c) \qquad \text{where} \qquad h_c = \frac{5 A_s f_y}{4 b f_c} \tag{4.8}$$

where b is the width of the beam, f_c is the concrete strength and h_{ef} is the effective depth.

Rotational Capacity according to Rotations of the Beam Supports

For the eight vertical measurements performed for all the beams, four of the displacement transducers were placed on each side of the axis around which the beam rotates at the supports. In this way the rotations of the beam supports can be determined. By taking only the plastic part of these rotations, a new rotational capacity is defined as the mutual plastic rotation of the beam assuming rigid body movement

$$\theta^{support} = 2 \, (\alpha_{total} - \alpha_{elastic}) \tag{4.9}$$

where α_{total} is the total rotation of the beam, and $\alpha_{elastic}$ is the rotation from the elastic part calculated from the support rotations.

Results for Rotational Capacity versus Reinforcement Ratio

For each beam the rotational capacity was obtained by three methods e.g. calculating the total plastic work as the area under the load-deflection curve and dividing this work by the maximum yield moment (the maximum moment at the yielding regime for each load-deflection curve). This value is a direct estimate of the total plastic rotation of the beam ends.

Results for the rotational capacity as a function of the reinforcement ratio are given in Figure 4.18 for normal strength concrete and in Figure 4.19 for high strength concrete. The results for slenderness ratios 6 and 18 in Figure 4.18 are too few to indicate any clear size effect. In fact, the small beams have the smallest rotational capacity. This is believed to be due to the low deformation capacity of the reinforcement used for the smallest beams. The results for slenderness ratio 12, however, show a clear size effect for the two larger beam sizes. The smallest beam has a significantly lower rotational capacity, again indicating the large influence from the limited deformation capacity of the cold deformed reinforcement.

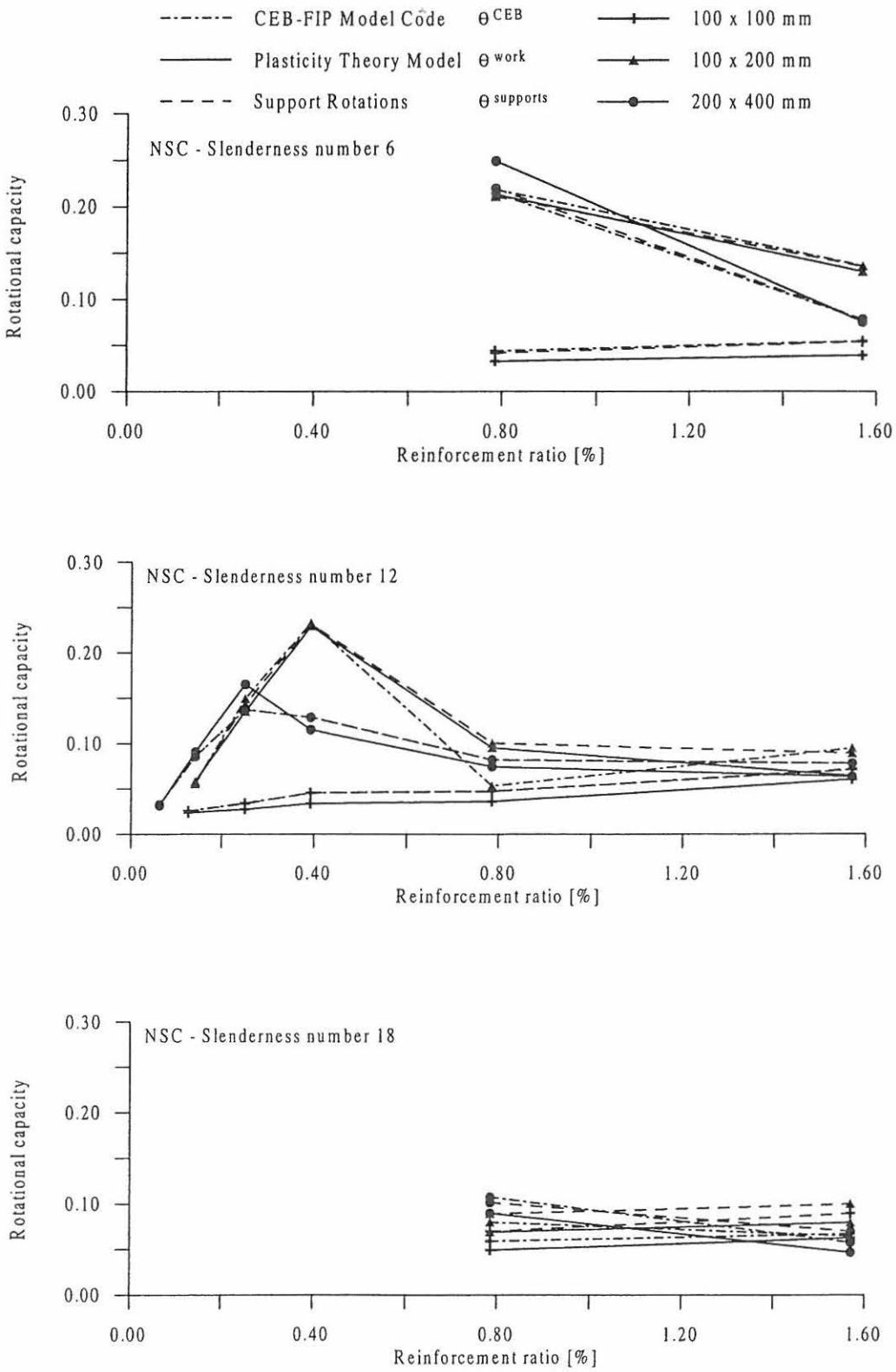

Figure 4.18: *Rotational capacity as a function of reinforcement ratio for normal strength concrete (NSC) beams with slenderness numbers 6, 12 and 18.*

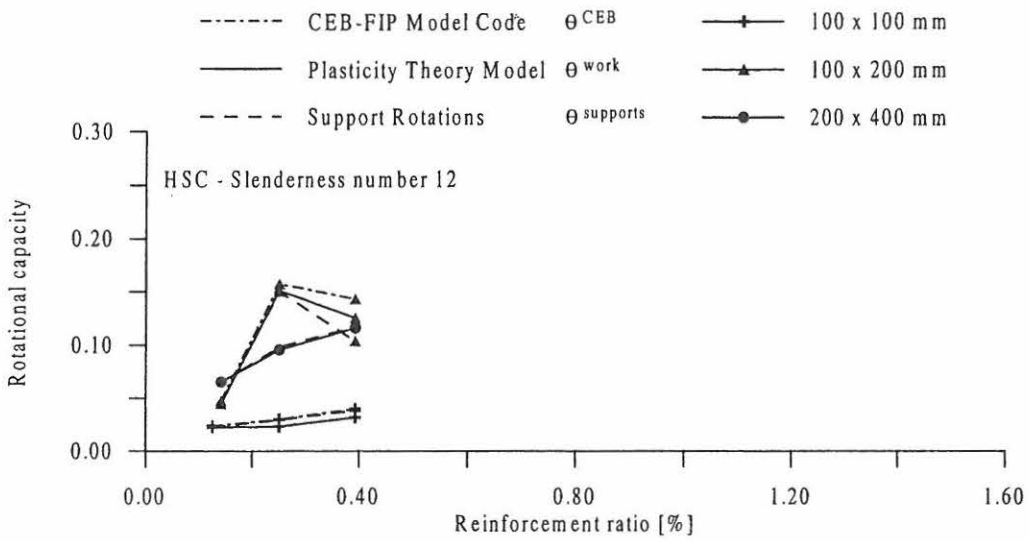

Figure 4.19: *Rotational capacity as a function of reinforcement ratio for high strength concrete (HSC) beams with slenderness number 12.*

The results for high strength concrete in Figure 4.19 are too limited to indicate any clear size effect. Again the limited deformation capacity of the cold deformed reinforcement causes the small beams to have a significantly lower rotational capacity.

4.4.3 Discussion

The rotational capacity of a reinforced concrete beam is dependent on the beam failure mode. For the reinforcement ratios investigated in this chapter the general failure picture of the beams was a tensile failure of the reinforcement for the low reinforcement ratio 0.06 % to 0.14 %, and a bending failure resulting either in a tensile failure of the reinforcement or a compression failure of the concrete for reinforcement ratio 0.25 % to 0.78 %. For the reinforcement ratio 1.57 % all beams failed in compression.

The results for the normal strength concrete beams show, that the rotational capacity for the slenderness number 6 is very low for beam size 100 x 100 mm and reinforcement ratio 0.78 %. This is due to the fact that the reinforcement Ø5 have a very little yield capacity resulting in a tensile failure of the reinforcement. The rotational capacity of beam size 100 x 200 mm and 200 x 400 mm are lower for the reinforcement ratio 1.57 % due to compression failure of the concrete.

For normal strength concrete beams with slenderness number 12 the rotational capacity for the reinforcement ratios from 0.06 % to 0.39 % is increasing due to tensile failure of the reinforcement and development of more and more cracks in the beam. It is observed, that the rotational capacity is decreasing from reinforcement ratio 0.39 % to 0.78 % and is almost the same for 0.78 % to 1.57 % for beam sizes 100 x 200 mm and 200 x 400 mm. For slenderness number 18 (NSC) there seems to be a tendency, that the rotational capacity decreases for beam

size 200 x 400 mm and increases for beam sizes 100 x 100 mm and 100 x 200 mm.

For high strength concrete beams with slenderness number 12 the rotational capacity for the reinforcement ratios from 0.14 % to 0.25 % is increasing due to tensile failure of the reinforcement and development of cracks. There seems to be a tendency, that the rotational capacity is decreasing from reinforcement ratio 0.25 % to 0.39 % for beam size 100 x 200 mm, while it increases for beam sizes 100 x 100 mm and 200 x 400 mm.

It is seen, that for almost all beam sizes the rotational capacity according to CEB-FIP Model Code and according to support rotations are the same, and that the rotational capacity according to the plasticity theory model is lower.

In Figure 4.18 it is also observed, that the rotational capacity according to CEB-FIP Model Code for slenderness number 6 is the largest for beam size 200 x 400 mm and NSC. In general, the rotational capacity is larger for slenderness number 6 for reinforcement ratio 0.78 %. In the Figures 4.10 - 4.14 for the load-displacement curves it is clearly seen, that the rotational capacity for slenderness number 6 is larger than for slenderness number 12 due to the fact, that the displacement and the maximum force are larger for the shorter beam.

The comparison of a normal strength and a high strength concrete beam shows, that the rotational capacity seems to be lower for the HSC beam size 200 x 400 mm, and almost the same for beam sizes 100 x 100 mm and 100 x 200 mm.

Size effects

It should be noticed, that the beams of a beam depth of 100 mm have a totally different reinforcement than the two other beam depth. That is, why the rotational capacity is very small for the beam depth of 100 mm due to small strain capacity of the reinforcement.

The difference in the rotational capacity between a beam depth of 200 mm and 400 mm is small, except for NSC beams with slenderness number 12. Here seems to be a rather large difference for reinforcement ratio 0.39 %. For slenderness number 6 and 18 there seems to be a difference when going from a beam depth of 200 mm to 400 mm.

Chapter 5

Experimental Study on Rotational Capacity of Lightly and Heavily Reinforced Concrete Beams

In this chapter a summary is given of experimental investigations of plastic rotational capacity of lightly reinforced concrete and heavily reinforced concrete beams. The experimental investigations have been carried out in the period of April to June 1998 and is a continuation of the tests described in chapter 4.

Main experimental results and calculations of plastic rotational capacity are presented.

5.1 Introduction

On the basis of the experimental programme and test results described in chapter 4, a new test serie was initiated to perform further investigations on the lightly reinforced and heavily reinforced regime. This chapter deals with rotational capacity of lightly and heavily reinforced concrete beams and are refered to as the second part, *ESIS 2*.

One of the reasons to investigate these two regimes are that for both lightly and heavily reinforced concrete beams there seems to be a lack of deformation capacity due to that only a few cracks will develop in the lightly area giving tensile failure of the reinforcement and that crushing of the concrete for the heavily area is the most important factor. Thus, in the lightly area parameters such as choice of reinforcement type, concrete type and bond-slip behaviour are the most important factors on the failure mode and the load-deflection response. For the heavily area, additional reinforcement such as compressive reinforcement, stirrups spacing, steel fibers and type of main reinforcement are very important for the ductility of the plastic hinge in a beam and therefore also very significant for the failure mode.

The experimental investigations have included lightly reinforced beams with the dimension: 100 x 200 x 2400 mm using two different types of reinforcement and heavily reinforced beams with the dimension: 200 x 400 x 7200 mm with three types of confinement of the compression zone. The reinforcement types in the lightly reinforced regime have been chosen as ribbed and smooth plain rebars with no significant yield capacity and ribbed and smooth plain rebars showing strain hardening effects. The main purpose of chosing different kind of steel types is, that it is possible to investigate both very brittle reinforced and very ductile reinforced beams and thereby estimate different rotational capacities. The results are also compared with lightly reinforced beams from the *ESIS 1*. In the heavily reinforced regime beams of different reinforcement ratios are tested to ultimate failure in order to investigate the plastic rotational capacity. Beams with plain concrete confinement as the beams tested in the *ESIS 1*, steel-fiber confinement and stirrup confinement of the compression zone are investigated.

5.2 Test Programme

The test programme is divided into two parts, one test-serie for the lightly reinforced beams and one test-serie for the heavily reinforced beams. The design of the beams regarding geometry, reinforcement type and concrete comply with the requirements given in the proposals by Bosco and Carpinteri (1993). All the beams have been tested in three-point bending.

5.2.1 The Test Programme for Heavily Reinforced Beams

The test programme for the heavily reinforced beams consists of a total of 16 beams with similar geometries and one concrete strength. 6 beams of same dimension from the *ESIS 1* have also been included in the programme.

The geometry of the beams is shown in Table 5.1.

Dimension of beam [mm]				Ref. ratio	Confinement types		
Thickness b	Depth h	Span L	Length L_{total}	$A_s / b\,h$	Type 1	Type 2	Type 3
200	400	7200	7500	0.78 %	Plain	Steel-fibers	Stirrups
200	400	7200	7500	1.57 %	Plain	Steel-fibers	Stirrups
200	400	7200	7500	2.45 %	Plain	Steel-fibers	Stirrups
200	400	7200	7500	2.76 %	Plain	Steel-fibers	Stirrups

Table 5.1: *Geometry of test specimens for the heavily reinforced normal strength concrete beams with 3 different confinements of the compression zone.*

The specimens have the slenderness number 18 and the reinforcement ratios are given as the steel area A_s divided by the cross-sectional area $b\,h$. All the beams are of normal strength concrete with the same recipe as used in the *ESIS 1*. Only one beam of each confinement type and reinforcement ratio have been prepared, except for the beams of 0.78 % and 1.57 % and confinement type 1 (plain), where there have been three repetitions of each beam.

The confinement types consist of a plain concrete, a steel-fiber reinforced concrete and a concrete with several stirrups. These types of concrete have been placed in the compression zone of the middle of the beam at an area of half the beam depth and half the span, which is the same as 25 % of the beam, see Figure 5.1.

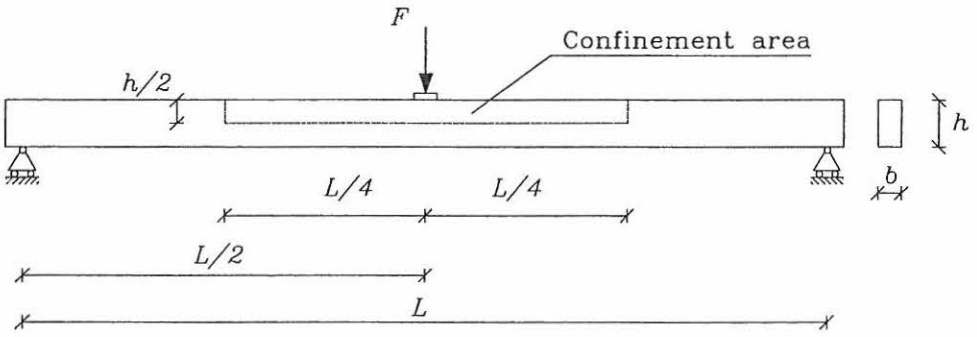

Figure 5.1: *Design and confinement area of the heavily reinforced beams.*

The confinement type 1 is a plain normal strength concrete. The steel-fibers used for the confinement type 2 is of the type Dramiz ZP 30/0.50. The length of the steel-fiber is 30 mm and the diameter is 0.50 mm, and the fiber has hooked ends. The amount of steel-fibers added to the concrete is 80 kg per 1 m^3 concrete giving a volumen procent of 1.0 %. The confinement type 3 is also a plain concrete, but confined with several stirrups placed with a distance of 70 mm.

The main reinforcement is placed with an effective depth of 0.90 h. The types of main reinforcement and reinforcement for stirrups are Rippentor Steel of quality BST 500S (IVS) after DIN 488 with nominal diametres of Ø20 and Ø25. To acheive an over-reinforced state for the failure mode of the beams with reinforcement ratio 2.76 %, it has been necessary to use high ductile Dywidag threadbar steel, type no. 26D with a nominal diameter of Ø26.5 and steel grade (f_y / f_u) 1080/1230.

To avoid anchorage failure and shear failure, stirrups have been placed in all the beams. The reinforcement type for the stirrups has been designed to BST 500S and diameter Ø12. For fixing of the stirrups in the upper zone of the beam plain rebars of steel quality st. 37 and diameter Ø12 have been used for beams with confinement types 1 and 2 demanding, that no stirrups and fixing reinforcement must be placed in a zone of 280 mm from each side of the center of the beam. To

increase ductility of the cross-section several stirrups have been placed in the beams of confinement type 3. The stirrups are here fixed with a small plain compressed steel rebar of diameter Ø3 in the upper zone of the beam. A small rebar has been chosen in order to avoid effects on the rotational capacity.

5.2.2 The Test Programme for Lightly Reinforced Beams

The test programme for the lightly reinforced beams consists of a total amount of 20 beams, where 6 beams are included from *ESIS 1*. The geometry of the test beams is given in Table 5.2.

Dimension of beam [mm]		Ref. ratio	Concrete	Reinforcement type	
b x h x L	Length L_{total}	$A_s / b\,h$	Strength	Brittle	Ductile
100 x 200 x 2400	2600	0.14 %	NSC / HSC	RIB CD	
100 x 200 x 2400	2600	0.14 %	HSC		RIB CD ANN
100 x 200 x 2400	2600	0.14 %	NSC / HSC	SMO CD	
100 x 200 x 2400	2600	0.14 %	NSC / HSC		SMO CD ANN
100 x 200 x 2400	2600	0.14 %	NSC / HSC		RIB HOT ROL

Table 5.2: *Geometry of test specimens for the lightly reinforced normal strength (NSC) and high strength (HSC) concrete beams with hotrolled (HOT ROL), colddrawned (CD) and annealed (ANN) rebars with a smooth (SMO) and ribbed (RIB) profile.*

The specimens have the slenderness number 12 and the reinforcement ratio 0.14 %. The concrete are both a normal strength and high strength concrete prepared from the recipes used in the *ESIS 1*. For each concrete strength and reinforcement type two identically beams are prepared, except for the beams from *ESIS 1*, where three identically beams have been prepared.

The beams are reinforced only by one single rebar placed with an effective depth of 0.90 h. To make very lightly reinforced beams and also an under-reinforced state, that is the reinforcement ratio is below the minimum reinforcement ratio, the diameter of the bar is chosen to Ø6 and the steel quality is RS 550 (BST 500 KR). This small size of diameter is also available at the market. No stirrups and additional reinforcement have been placed in the beams. The reinforcement types are a smooth, plain bar (SMO) and a ribbed bar (RIB). For each of the two types a cold-drawned (CD) and a colddrawned, annealed bar (CD ANN) have been produced.

The annealed reinforcement is made by heating up the cold-drawned bar to a temperature of 400 - 500 °C. Doing so, the 0.2 % - strength of the cold-drawned bar will decrease with about 15 %,

but hereby the reinforcement becomes more ductile and the annealing of the bar is continued, until the 92 % rule is reached. The 92 % rule is a ductility requirement for ductile reinforcement given in DS 411 (1997), which describes, that the relation between the yield strength and the ultimate strength has to be less than 0.92. The annealing procedure is performed and controlled by the factory. From *ESIS 1* also a very ductile ribbed and hot-rolled bar (HOT ROL) is included. This reinforcement bar is of the steel-type BST 500 S.

5.2.3 Identification of Beams

Each beam is identified by a unique name defined for the heavily reinforced beams as in *ESIS 1*. This means, that the beams are given names according to the size of beam, the reinforcement ratio and the concrete strength. For example, the beam with the name In_245_N is a beam of dimension 200 x 400 x 7500 mm given by I, reinforcement ratio 2.45 % given by 245 and confinement type 1, plain concrete given by N. The number of the beam is given by n. If only one beam is cast the number is n. The confinement type 2 and 3 are given by F for steel-fibers and S for stirrups, for example such as In_245_F and In_245_S.

The lightly reinforced beams are identified by the reinforcement and the concrete strength. For instance, a beam called G1_6KT_H is the first beam reinforced with a smooth (G), plain and cold-drawned (KT) bar with the diameter Ø6 given by 6. The concrete is high strength concrete given by H. The annealed bar is identified by (AN) as for example G1_6AN_H and a ribbed bar is identified by R as for example R1_6AN_H. The lightly reinforced beams included from *ESIS 1* are identified as for the heavily reinforced beams.

5.3 Materials

Main results of various tests on determining the mechanical properties of the concrete and the reinforcement are presented. The tests are performed in accordance with current codes for determining mechanical properties, e.g. national codes of DS 423 on concrete properties and DS 13080 on reinforcement properties. The tensile fracture energy of the concrete is determined according to the RILEM.

5.3.1 Concrete

Three types of concrete have been used to cast the specimens. For the heavily reinforced beams a normal strength concrete and a steel-fiber reinforced concrete have been used, and for the lightly reinforced beams a normal strength and a high strength concrete have been used. The compressive strengths for the concrete types are at about 50 MPa for the normal strength concrete (NSC), 35 MPa for steel-fiber reinforced concrete (SFRC) and 100 MPa for the high strength concrete (HSC).

In Table 5.3 the mix proportions of the three types of concrete are listed. The mix proportions are

adjusted to comply with the requirements given Bosco and Carpinteri (1993). The largest aggregate size has been chosen to 8 mm and the concrete slump to 80 mm for the NSC and SFRC and 110 mm for the HSC.

Contents		Density	Normal Strength Concrete		High Strength Concrete	
Ingredient	Product	[kg/m^3]	[kg/m^3]	[*l*/m^3]	[kg/m^3]	[*l*/m^3]
Cement	PC(A/HS/EA/G)	3200	352	110	464	145
Water		1000	150	150	147	147
Microsilica	Elkem - Powder	2200	0	0	37.3	17.0
Plastiziser 1	Peramin F	1210	0	0	12.6	10.4
Plastiziser 2	Conplast 212	1170	3.83	3.27	1.79	1.53
Sand (0-2mm)	Ks. Nr. Halne 0-2/A	2639	957	363	836	317
Gravel (4-8mm)	Vikan 4-8/A	2760	895	324	900	326
Air		0	0	50	0	35
Density			2358 kg/m^3		2399 kg/m^3	
Steel-Fiber Reinforced Concrete						
Steel-fiber	Dramix ZP 30/0.50	7800	78.8	10.1	0	0
Density			2437 kg/m^3		2399 kg/m^3	

Table 5.3: *Mix proportions of the normal strength (NSC), high strength (HSC) and steel-fiber reinforced (SFRC) concrete.*

For each casting 3 fracture energy beams and about 12 - 18 control cylinders were cast, and for the lightly reinforced beams also 3 bond-slip specimens were cast. To cast the beams two steel moulds from *ESIS 1* have been used.

5 castings and 1 pilot casting have been prepared for the heavily reinforced beams. The pilot casting was a SFRC type, and has only been performed to check on the workabilty of the steel-fibers. The 5 castings consisted of 3 NSC and 2 SFRC and NSC castings. The concrete has been delivered from an outside manufactor. The SFRC for 25 % of a beam has been prepared of 150 *l* NSC and 12 kg Dramix ZP fibres mixed in a concrete mixer for 2 min at the place of the casting. This was done twice to gain at about 300 *l* SFRC. For the lightly reinforced beams the castings were performed at the Concrete Technology Laboratory in a concrete mixer with a max. capacity of 200 *l*. 7 castings have been prepared consisting of 4 HSC and 3 NSC castings. The sand and

gravel material were placed outside the laboratory covered with plastic sheets and as the microsilica was added as a slurry, the amount of water in the sand, gravel and the slurry have been subtracted.

Control cylinders, bond-slip specimens and fracture energy beams were stripped after 1 day and then they were all cured in water at 20 °C, until the moment of testing. As bond-slip specimens and fracture energy beams had to be prepared, they were taken out of the water one or two days before testing.

In August 1997 cylinders and fracture energy beams for the heavily reinforced beams were taken out of the water vessel, and wrapped with fibertex sheets, they were placed in a tent with buckets of water to ensure that the relative humidity was 100 % RF, until the day of testing. The beams were cast indoors and stripped after two days at the Concrete Technology Laboratory. The beams were then wrapped with fibertex sheets and covered and sealed with plastic. The beams were stored at the Structural Research Laboratory in a room with a temperature of 20 °C. The tightness of the plastic made it possible to pour water around the beams, so the beams were always kept wet, until one or two days before testing. Information on the maturity days for all the beams can be found in Henriksen *et al.* (1998).

The properties of the concrete were determined using standard tests at the Concrete Technology Laboratory and The Structural Research Laboratory. To analyze the experimental results of the beam tests, it has been important to determine compressive strength f_c, splitting tensile strength and bending tensile strength f_s and f_{bend} and bending tensile fracture energy G_F.

Knowing the full-range compressive softening stress-strain curve for example from the tests performed in *ESIS 1*, ductility parameters such as the compressive fracture energy G_c, Youngs modulus E_c, compressive strength f_c and peak and ultimate strain ε_{co} and ε_{cu} are estimated. The compression strength and the tensile splitting strength have been determined on 100 mm x 200 mm cylinders using a 3000 kN load-controlled testing set-up, Tonipact 3000. The cylinders for compression tests have not been plane-grinded at the end surfaces. The compression strength is determined according to DS 423.23, and the splitting tensile strength is determined according to DS 423.34.

The bending tensile strength and the bending tensile fracture energy were determined on beams with the dimensions: length 840 mm, span 800 mm, depth 100 mm and thickness 100 mm. Shortly before testing, a notch of half the beam depth was diamond saw-cut in the beams. A detailed description of the determination of the bending tensile fracture energy and the bending tensile strength can be found in Ulfkjær and Brincker (1995).

Typical bending experiments for determination of bending tensile fracture energy and bending tensile strength are shown in Figure 5.3 and Figure 5.4. The main results for the mechanical properties of the concrete used for the heavily reinforced beams and the lightly reinforced beams are listed in Table 5.4 and Table 5.5 respectively.

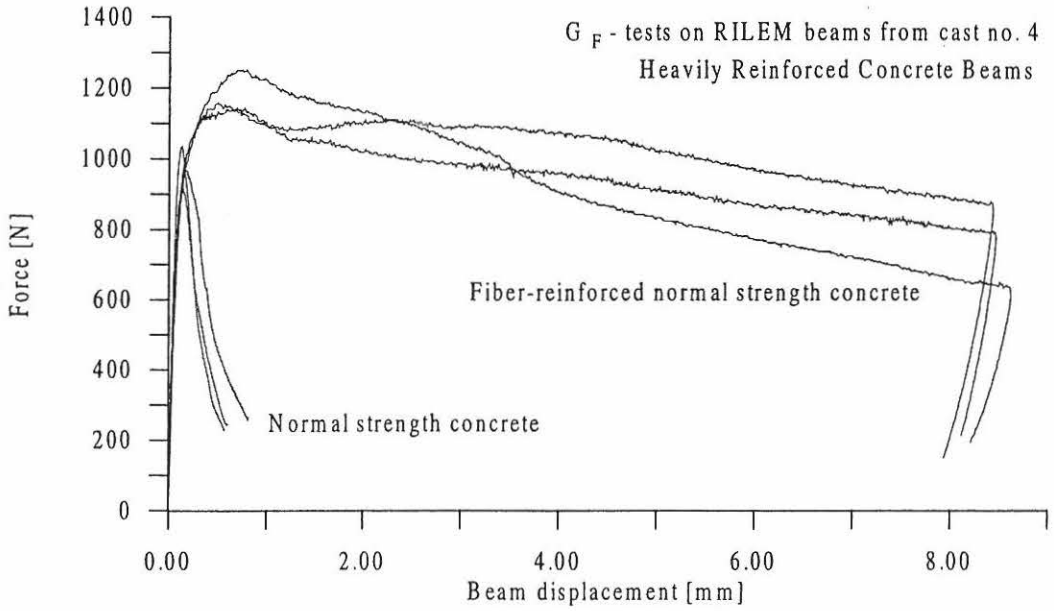

Figure 5.3: *Typical bending experiments for determination of fracture energy and tensile strength in bending for the heavily reinforced beams.*

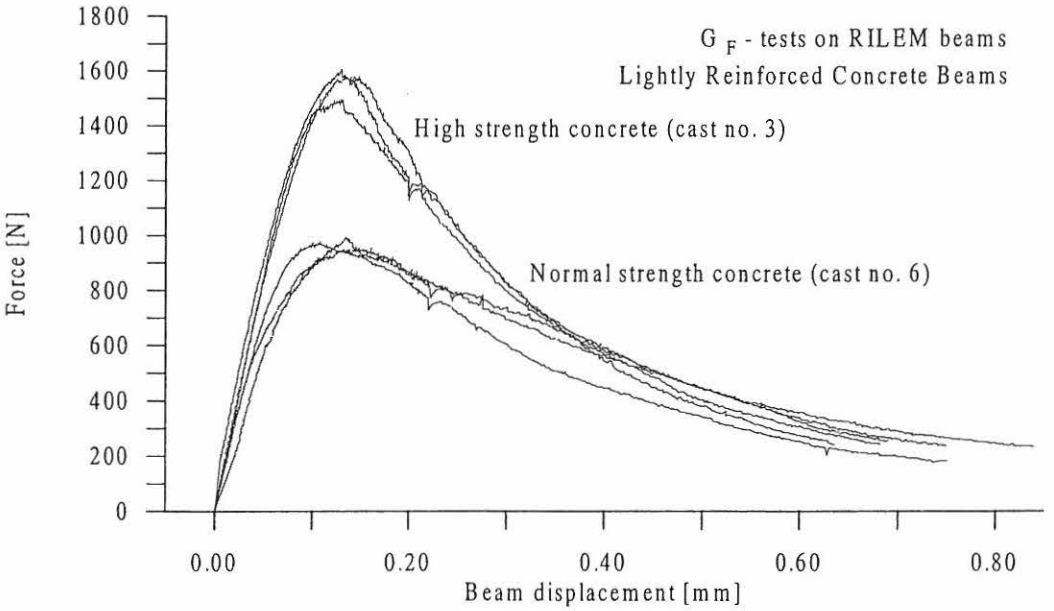

Figure 5.4: *Typical bending experiments for determination of fracture energy and tensile strength in bending for the lightly reinforced beams.*

		Normal Strength Concrete	Steel-Fiber Reinforced Concrete
Compressive Strength	Mean S. Dev	55.0 MPa 3.45 MPa	34.9 MPa 2.86 MPa
Splitting Strength	Mean S. Dev.	4.09 MPa 0.32 MPa	- -
Bending Tensile Strength	Mean S. Dev.	4.75 MPa 0.36 MPa	5.30 MPa 0.34 MPa
Specific Bending Fracture Energy	Mean S. Dev.	108.3 J/m^2 3.88 J/m^2	1873 J/m^2 130 J/m^2

Table 5.4: *Mechanical properties of the normal strength concrete and steel-fiber reinforced concrete for heavily reinforced beams.*

		Normal Strength Concrete	High Strength Concrete
Compressive Strength	Mean S. Dev	60.4 MPa 7.85 MPa	96.6 MPa 5.05 MPa
Splitting Strength	Mean S. Dev.	4.19 MPa 0.15 MPa	6.36 MPa 0.45 MPa
Bending Tensile Strength	Mean S. Dev.	4.47 MPa 0.26 MPa	7.04 MPa 0.32 MPa
Specific Bending Fracture Energy	Mean S. Dev.	119.7 J/m^2 6.08 J/m^2	149.3 J/m^2 16.3 J/m^2

Table 5.5: *Mechanical properties of the normal strength concrete and high strength concrete for lightly reinforced beams.*

5.3.2 Reinforcement

The chosen reinforcement for the test beams consists of steel bars with a quaranteed yield strength of 550 N/mm^2. As the test programme includes very low and very high reinforcement ratios both small diameters and large diameters had to be used, because the reinforcement is only placed in one layer of the beams with an effective depth of 0.90 h.

The reinforcement used for the lightly reinforced beams is both a ribbed steel bar and a smooth, plain steel bar. The behaviour of the rebars is both very ductile and very brittle. The brittle behaviour of the rebars is achevied by chosing cold-drawned bars, while the ductile behaviour

has been acomplished by heating up or annealing of the rebars. The steel quality has been chosen to RS 550 (BST 500 KR) and the diameter of the rebars is Ø6 mm. From *ESIS 1* a very ductile, hot-rolled and ribbed rebar with the diameter Ø6 is also included.

The reinforcement for the heavily reinforced beams consists of ribbed bars with diameters of Ø20 mm, Ø25 mm and Ø26.5 mm. The steel quality is BST 500 S for Ø20 and Ø25, while the steel quality for the Ø26.5 is Dywidag steel. Also, the ribbed steel bars with a diameter of Ø20 from *ESIS 1* have been included.

The mechanical properties of the steel have been determined on 500 mm long specimens subjected to uni-axial tension according to DS 13080-1 and DS 10110. These standard tests were conducted and performed by the staff at the Structural Research Laboratory. The Dywidag steel has not been tested, but material parameters have been received from the steel supplier. The Dywidag steel in the beams will be in an overreinforced state, so only information on the elastic behaviour is necessary.

The tests were divided into two parts. In the first part the modulus of elasticity was determined using two DD1 HBM displacement transducers measurering displacement directly on the specimens. In the second part only the displacements measured using an external LVDT were recorded. Also in the second part the yield strength and and the ultimate strength were determined. Important is to measure the whole stress-strain curve for the reinforcement, so it is necessary to note the length between the two fixing jaws before testing and the length of the bar before and after testing. The strain is also determined as the stroke divided by the length between the two fixing jaws. The rebars were tested in a Mohr-Federhaff testing machine with a capacity of 500 kN and a max. stroke of 100 mm.

The results of the uni-axial tensile tests of the steel-bars are summarized in Table 5.6 and Table 5.7, where also the material parameters of the Ø26.5 Dywidag are mentioned. In Figure 5.5 and Figure 5.6 curves from the tensile tests of the 4 types of steel-bars used for lightly reinforced beams and the ribbed bars used for the heavily reinforced beams are shown. In Table 5.6 and Table 5.7 it should be noted, that the ultimate strength is the strength according to maximum tensile force, and that the ultimate strain is the strain corresponding to ultimate strength. Thus, the softening parameters of the reinforcement is not considered, well-knowing that the fracture energy of the softening zone is of great importance in determining the maximum strain. This zone could be measured in the right test set-up.

The expected results for the cold-drawned and annealed ribbed rebars were, that the behaviour should be more ductile with a larger yield capacity showing strain-hardening effects just as for the cold-drawned and annealed smooth bar, but as observed from the load displacement curve, this behaviour is not achieved, therefore the ribbed ductile rebars from *ESIS 1* was included in the analysis. Conducting and performing of the annealing process of the cold-drawned ribbed and smooth, plain rebars have been carried out by the steel-supplier.

Steel type	Young's Modulus	Yield strength	Yield plateau	Ultimate strength	Ultimate strain	Ultimate to yield strength ratio
	E_s	f_y	$\Delta\varepsilon_y$	f_u	ε_{su}	f_u / f_y
	[MPa]	[MPa]	[%]	[MPa]	[%]	[-]
Cold-drawned reinforcement (CD)						
Ø6 RIB	2.02E5	726	0	726	2.99	1.00
Ø6 SMO	1.96E5	644	0	644	1.78	1.00
Cold-drawned and annealed reinforcement (CD ANN)						
Ø6 RIB	2.07E5	766	0	766	3.98	1.00
Ø6 SMO	1.98E5	586	2.30	624	7.54	1.06
Hot-rolled reinforcement (HOT ROL) from ESIS 1						
Ø6 RIB	2.09E5	600	3.44	664	13.1	1.11

Table 5.6: *Mechanical properties for the reinforcement bars used for lightly reinforced beams. The signatures RIB is ribbed bar and SMO is smooth plain bar.*

Steel type	Young's Modulus	Yield strength	Yield plateau	Ultimate strength	Ultimate strain	Ultimate to yield strength ratio
	E_s	f_y	$\Delta\varepsilon_y$	f_u	ε_{su}	f_u / f_y
	[MPa]	[MPa]	[%]	[MPa]	[%]	[-]
Ø 20	2.02E5	558	1.60	662	10.6	1.19
Ø 25	1.91E5	561	1.13	659	16.2	1.17
Ø 26.5	2.00E5	1080	0.50	1230	3.50	1.14
Reinforcement from the ESIS 1						
Ø 20	1.82E5	531	1.13	624	9.27	1.18

Table 5.7: *Mechanical properties for the ribbed reinforcement bars used for heavily reinforced beams. The Ø26.5 is DYWIDAG steel.*

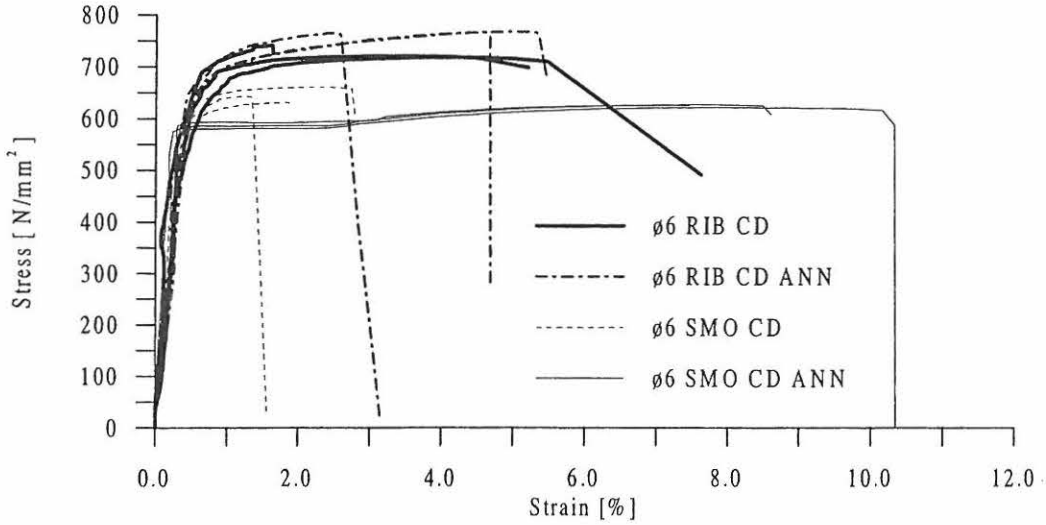

Figure 5.5: *Stress strain relations for reinforcement used for lightly reinforced beams.*

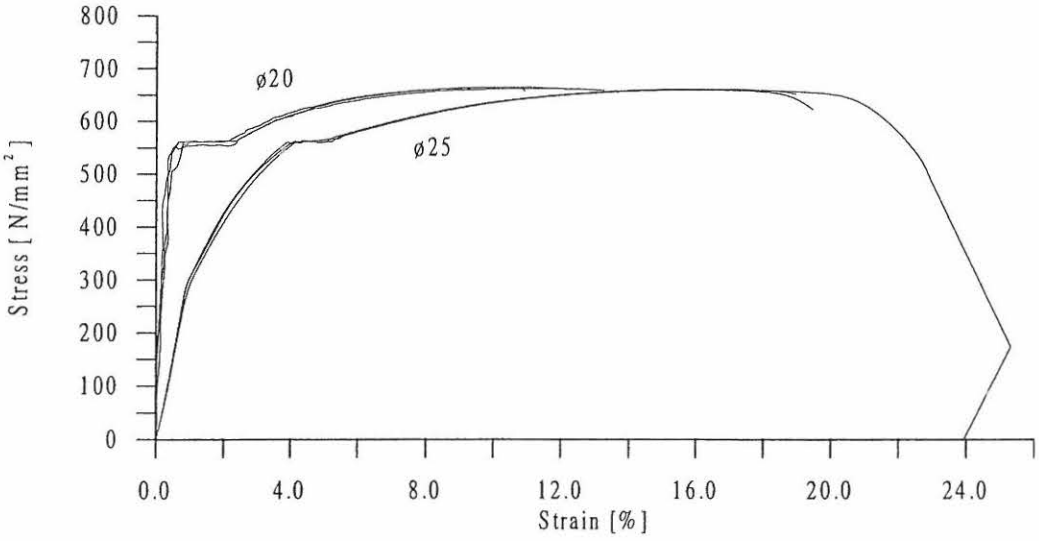

Figure 5.6: *Stress strain relations for reinforcement used for heavily reinforced beams.*

5.3.3 Bond-Slip between Reinforcement and Concrete

The bond-slip plays an important role for the load-deflection behaviour of lightly reinforced beams, until the point where the reinforcement starts to yield. To describe this prepeak behaviour bond-slip curves describing the pull-out of the reinforcement from the concrete have been determined for the lightly reinforced beams.

For calculation of the bond shear strength two shear bond models have been performed. The shear bond model 1 is a pure friction model, while the shear bond model 2 is a model, which assumes, that a cone is pulled out by the experiment. It is assumed for the models, that the slope of the bond-slip curve estimates a value for the bond shear strength. Thus, having identified by experiments the bond-slip curve, a second order best fit curve is made to calculate the slope and the coefficients of the second order best fit.

The second-order best fits for the shear bond model 1 and 2 are given by

$$u_s = a_{12} F_s^2 \tag{5.1}$$

$$u_s = a_{21} F_s^2 + a_{22} F_s \tag{5.2}$$

where u_s is the bond-slip, F_s the pull-out force and a_{12}, a_{21} and a_{22} the coefficients of the best fits.

The bond shear strength τ_{c1} for model 1 and τ_{c2} for model 2 and the cone length l_{cone} are calculated as

$$\tau_{c1} = (2 \pi A_s E_s d a_{12})^{-1} \tag{5.3}$$

$$\tau_{c2} = (2 \pi A_s E_s d a_{21})^{-1} \tag{5.4}$$

$$l_{cone} = A_s E_s a_{22} \tag{5.5}$$

where A_s is the area of the rebar, E_s Youngs Modulus and d the diameter of the rebar.

The pull-out curves are determined on specimens of dimension: depth 100 mm, thickness 100 mm and length 480 mm all reinforced with a Ø6 mm steel rebar. 3 specimens from each casting giving a total of 21 specimens have been tested.

The experiment was performed in a specially designed set-up, see Figure 5.7. Three identical specimens from the same casting after testing are shown in Figure 5.8.

The pull-out of the reinforcement has been carried out in small steps with a load cell with a max. capacity of 200 kN. The loading of the experiment has been performed manual with a LUKAS hand pump. The pull-out of the reinforcement was measured with two DD1 HBM displacement transducers with a base of 5 mm at each end of the specimen. The measuring point of the DD1's was 17.5 mm from the end surface. To measure the horizontal displacements of the specimens due to cracking on the surfaces two LVDT's with a base of 10 mm, which were placed on the top and bottom of the specimen, have been used. Two frames for fixing the DD1 transducers were placed on the specimen with a distance of 40 mm from both ends. An experiment would take 5-7 min dependent on the steel type. The test was continued until either tensile failure of the rebar or measuring of a slip beyond the max. base of the DD1 transducer. To start the experiment a load of about 1 kN was applied to tighten the system, and then all transducers were zero-balanced and next the pull-out loading was applied by the hand pump. It should be noted that the load to tighten the system is not included in the results as it is assumed that it has a very small effect on the slope of the pull-out curve.

From the pull-out curves a second-order best fits were performed to calculate the shear bond strength and the size of the pull-out cone of the concrete. The results of the calculations using the bond models 1 and 2 are summarized in Table 5.8.

Typical experimental curves and best fits are shown in Figure 5.8 and Figure 5.9. In Henriksen *et al.* (1998) all the results from the tests are listed such as the total pull-out curve and the first part of the pull-out curve for determination of the shear bond strength and the fitted curves for the specimens from cast 1. The measurements of the horizontal displacements of the specimen are not listed, as the values are very small due to the fact that no cracks occured on most the specimens.

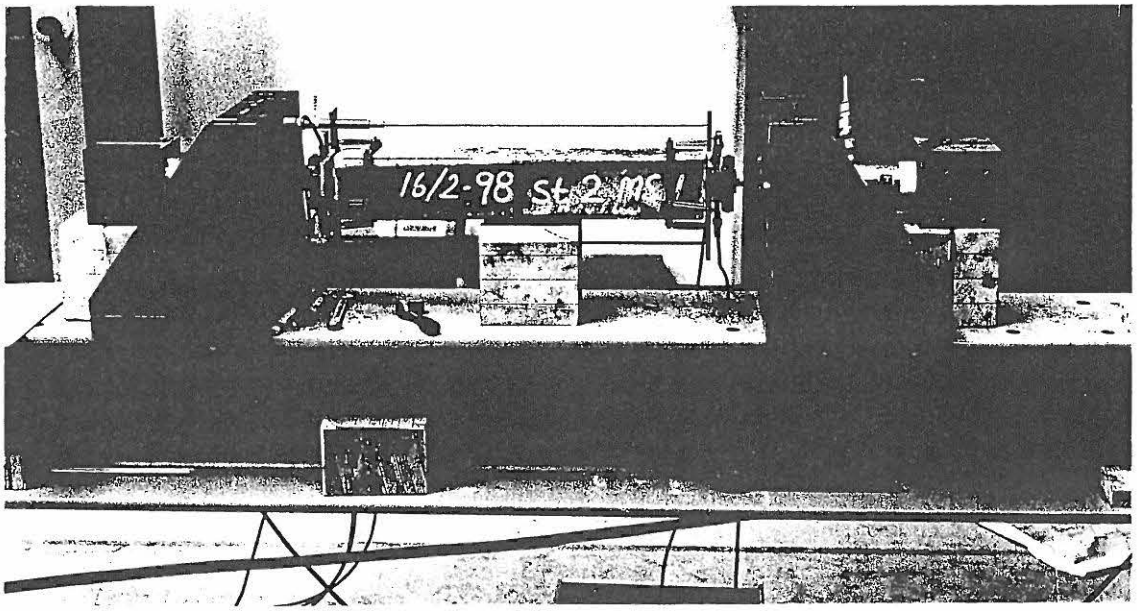

Figure 5.7: *Photo of the test set-up for pull-out tests used for lightly reinforced beams.*

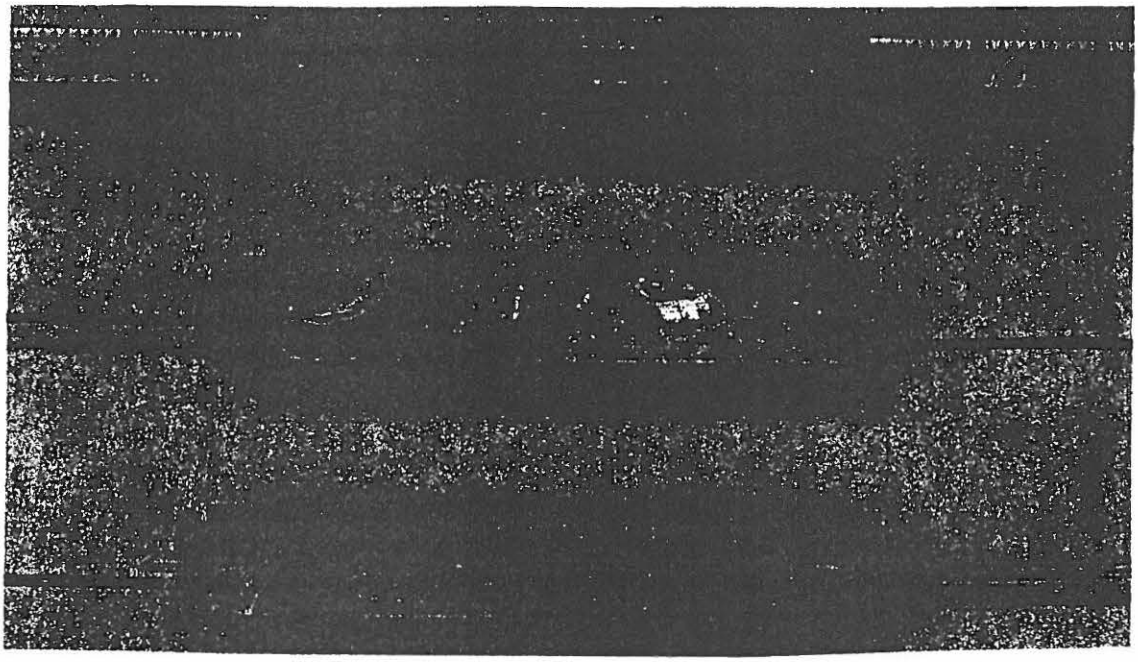

Figure 5.8: *Pull-out specimens ST5_NO1, ST5_NO2 and ST5_NO3 after testing from cast no. 5, normal strength concrete. Note, the RIB CD bars are subjected to tensile failure. One crack in the middle develops.*

Cast / strength	Steel type	Bond model 1		Bond model 2			
		$\tau_{c1,mean}$	(s.dev)	$\tau_{c2,mean}$	(s.dev)	$l_{cone,mean}$	(s.dev)
		[N/mm^2]		[N/mm^2]		[mm]	
1 / HSC	RIB CD	11.4	(0.37)	16.2	(1.37)	8.26	(1.99)
2 / HSC	RIB CD ANN	12.9	(0.16)	18.8	(2.77)	7.76	(2.68)
3 / HSC	SMO CD	1.06	(0.36)	1.13	(0.39)	4.44	(3.47)
4 / HSC	SMO CD ANN	2.80	(0.66)	3.30	(0.96)	5.09	(2.63)
5 / NSC	RIB CD	7.24	(0.99)	9.97	(0.74)	13.4	(4.49)
6 / NSC	SMO CD	1.34	(0.17)	1.38	(0.20)	1.55	(1.18)
7 / NSC	SMO CD ANN	2.88	(0.38)	3.08	(0.51)	2.81	(1.25)
Beams taken from ESIS - 1							
7-8 / NSC	RIB HOT ROL	5.00	(-)	7.00	(-)	(-)	(-)
17-18 / HSC	RIB HOT ROL	8.00	(-)	11.0	(-)	(-)	(-)

Table 5.8: *Mean values for calculated bond shear strengths and pull-out cones of the concrete used for lightly reinforced beams (reinforcement Ø6). The values given for the ESIS-1 beams are taken from the literature. (s.dev) symbolizes the standard deviation.*

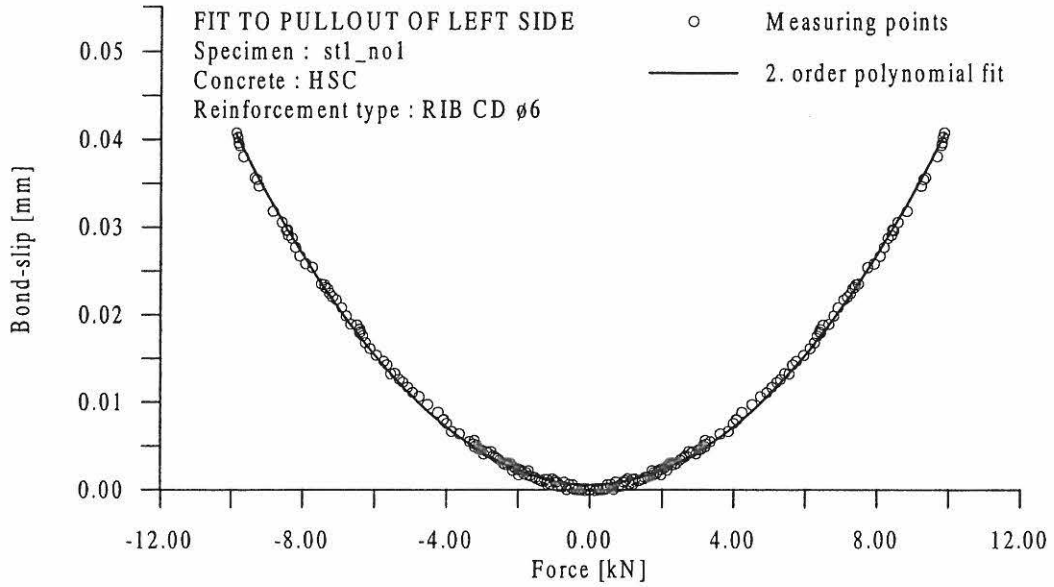

Figure 5.9: *Fit to pull-out of specimen st1_no1 from cast no. 1 using shear bond model 1. Measures are from the pull-out of the left side of the specimen.*

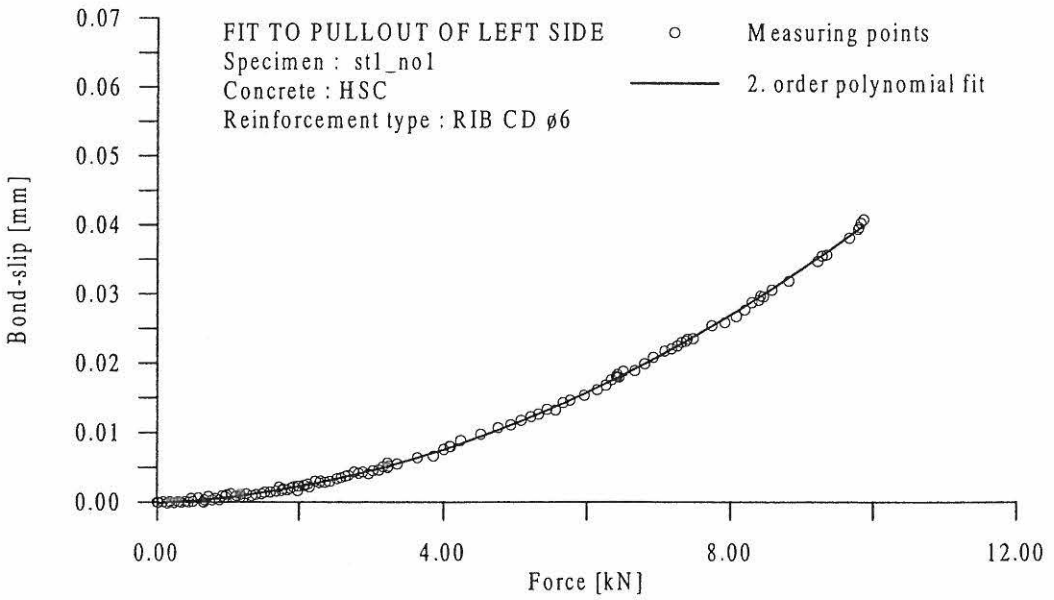

Figure 5.10: *Fit to pull-out of specimen st1_no1 from cast no. 1 using shear bond model 2. Measures are from the pull-out of the left side of the specimen.*

5.4 Experiments

The testing of the heavily and lightly reinforced beams were performed at the Structural Research Laboratory. The main purpose of the testing has been to determine the plastic rotational capacity and the load-deformation behaviour. From measuring of support rotations and load-midspan deflection it is possible to calculate the rotational capacity. A purpose has also been to observe the dependency of different ductilities of the compression zone and different main reinforcement types on the rotational capacity. In *ESIS 1* a test set-up of a max capacity of 250 kN had been built, and this test set-up was applied for testing of the lightly reinforced beams especially as the controlling system was a deformation servo-controlled testing system. It was not possible to use the test set-up for the heavily reinforced beams, because the calculated max. forces of the beams were in the range of 200 - 300 kN. So it was decided to built a new test set-up with the same servo-controlled system. Before the actual testing of the heavily reinforced beams, a pilot test was performed to check on the servo-controlling.

5.4.1 Preparation and Test Series

Before the experiments took place, the beams were placed in a storage room beside the laboratory, and a day before or on the same day of the testing, the beams were unwrapped from the wet sheets and plastic. The beams were then painted white in order to observe cracks and failure modes more clearly. Marking of points for placing of transducers, support plates, loading plates and steel frames for the controlling transducers were made. Finally the whole cross-section of the beam was measured in both ends and at the center of the beam. Testing of the beams has been carried out according to Table 5.9 and Table 5.10.

5.4.2 Test Set-up for Heavily Reinforced Beams

The heavily reinforced beams were subjected to three-point bending in a traditionally test set-up using a servo-controlled materials testing system. The supports of the beam were placed on steel profiles, which were fixed to the laboratory floor. The distance from the bottom of the beam to the floor was about 700 mm. A photo of the test set-up is shown in Figure 5.11. The maximum capacity of the load cylinder was a force of 1000 kN and a displacement of 200 mm measured by an external transducer.

At both supports horizontal displacements and rotations were allowed for and, at the right support also rotations around the beam axis were allowed. Both for security reasons the conditions of the right support was changed after test 3 skipping the rotations around the beam-axis. At the load point no displacements and rotations were allowed. Using the laboratory crane it was possible to place the beam on the supports and also to secure the beam under the actual testing. At the supports the size of the supporting steel plate was equal to the thickness of the beam and the width of the steel plate was 100 mm. The plate at the loading point was quadratic with sides equal to the the beam thickness. At the point of the load cell also some plates of dimension 100 x 200 mm were used, but the steel plate on the beam was always of dimension 200 x 200 mm.

Test No.	Beam name	Cast No.	Cast date	Test date	No. of reloadings
1	In_157_F	4	29-11-96	20/22-04-98	2
2	In_078_F	4	29-11-96	21-04-98	3
3	In_078_S	2	15-11-96	23-04-98	5
4	In_157_S	2	15-11-96	24-04-98	4
5	In_245_S	1	12-11-96	29-04-98	2
6	In_245_N	1	12-11-96	30-04-98	1
7	In_276_S	3	20-11-96	30-04-98	3
	In_276_N	3	20-11-96	04-05-98	1
9	In_245_F	5	04-12-96	04-05-98	2
10	In_276_F	5	04-12-96	05-05-98	1

Table 5.9: *Test Serie for the heavily reinforced concrete beams.*

Test No.	Beam name	Cast No.	Cast date	Test date	No. of reloadings
1	R1_6AN_H	2	16-02-98	26-05-98	1
2	R2_6AN_H	2	16-02-98	26-05-98	0
3	R2_6KT_H	1	11-02-98	26-05-98	0
4	G1_6KT_H	3	19-02-98	26-05-98	1
5	G1_6KT_N	6	11-03-98	27-05-98	1
6	R1_6KT_H	1	11-02-98	27-05-98	0
7	R2_6KT_N	5	05-03-98	27-05-98	0
8	G2_6AN_H	4	02-03-98	28-05-98	1
9	G2_6KT_H	3	19-02-98	28-05-98	1
10	G2_6AN_N	7	13-03-98	28-05-98	1
11	G1_6AN_N	7	13-03-98	02-06-98	1
12	G1_6AN_H	4	02-03-98	02-06-98	1
13	G2_6KT_N	6	11-03-98	02-06-98	1
14	R1_6KT_N	5	05-03-98	02-06-98	0

Table 5.10: *Test Serie for the lightly reinforced concrete beams.*

The vertical deflections of the beam was measured in eight points, and in both ends also horizontal displacements were measured. The midspan deflection was measured from the stroke of the load cylinder. Here was used an external transducer with a loose core, which was fixed on the load cell, and the capacity of the transducer was a base of ± 200 mm.

A measuring of the total stiffness of the loading arrangement, which was fixed in steel profiles connected to steel columns, turned out, that for a force of 100 kN subjected to a beam, a deformation of the steel frame system was measured to 0.7 mm. So, hereby it was assumed, that the system had a sufficiently stiffness and also that the stroke was an accurate measure for the midspan deflection.

The vertical and horizontal displacements of the beams were measured using 10 LVDT transducers of the type HBM (Linear Variable Displacement Transformer). The bases of these LVDT's were ± 5 mm, ± 10 mm, ± 20 mm and ± 50 mm. The placing of the transducers at the beams is shown on Figure 5.12. The placing of the transducers was designed in a way to provide information on the rotations of the beam, especially on the rotation of the supports. The transducers were mounted on a rigid steel-frame system fixed to the floor with no connection to the beam at all.

In order to make a servo-controlled testing system using the signal from the stroke and the deformation of the compression zone, it was necessary to place two specially designed frames attached to the beam in two drilled points on half of the beam depth and attached in two points to the bottom of the beam, see Figure 5.18. The compression deformation of the upper fibre of the beam was measured by two MTS transducers with a base of ± 3.75 mm placed on each side of the loading plate. The total measuring length of the frames was 800 mm. The load subjected to the beams was measured with a 1000 kN load cell.

All signals and the time t (for the beams there were 14 signals) were recorded every three seconds using a data recorder HBM UGR 60. Two different configuration files for the UGR 60 was used. The amount of recordings for each test was limited to 4000 cycles. Before starting the recording of measurements, an initial force in the range of 0 - 1 kN was subjected to compress the loading steel plates. Then all the transducers were zero-balanced on the UGR 60 and at least 5 zero-measurements were taken, before the loading started. It has to be mentioned, that the initial forces have not been taken into consideration as the values are very low compared with the max. forces.

In the MOOG amplifier used for servo-controlling also the time, force, stroke and compression deformation were recorded.

5.4.3 Test Set-up for Lightly Reinforced Beams

The beams were subjected to three-point bending in a specially designed servo-controlled materials testing system also used for the testing of beams in *ESIS 1*. The supports of the beams were placed on rigid steel columns made by steel profiles. A photo of the test set-up is shown in Figure 5.13. The maximum capacity of the Schenck cylinder was a force of 250 kN and a displacement of ± 50 mm.

At both supports horizontal displacements and rotations were allowed for and, at one support, also rotations around the beam axis were allowed. At the load point rotations were allowed around all three axes. This was done in order to minimize the influence of axial forces and torsion. At both ends a stop was placed at the top of the beam in order to prevent the beam from sliding off the supports. At the support the size of the supporting steel plate was equal to the thickness of the beam and for a beam depth of 200 mm the width of the steel plate was 100 mm. The plate at the loading point was quadratic with sides equal to the beam thickness.

The stroke (the displacement of the piston of the hydraulic actuator) was measured using the built-in LVDT (Linear Variable Displacement Transformer). The vertical and horizontal displacement of the beams were measured at eight points using LVDT's with a base of ± 5 mm, ± 20 mm and ± 50 mm. The placing of the transducers is shown in Figure 5.14. Two frames were attached to the beam at a distance of 100 mm (200 mm for test 1-3) from the center of the beam in order to place a COD at the bottom of the beam, see Figure 5.17. The COD used here was a clip-gauge with a base of ± 2 mm. The load was measured in a 63 kN load cell.

All signals and the time t (for the beams there were 14 signals) were recorded every seconds using a data recorder HBM UGR 60. Two different configuration files for the UGR 60 was used. The amount of recordings for each test was limited to 4000 cycles. Before starting the recording of measurements, an initial force in the range of 0 - 0.5 kN was subjected to compress the loading steel plates. Then all the transducers were zero-balanced on the UGR 60 and at least 5 zero-measurements were taken, before the loading started. It has to be mentioned, that the initial forces have not been taken into consideration as the values are very low compared with the max. forces.

In the MOOG amplifier used for servo-controlling also the time, force, stroke and COD were recorded.

5.4.4 Testing Procedure

As mentioned earlier, the tests were servo-controlled. Thus, both a reference signal and a feed-back signal are needed. Here the reference signal was chosen to be a linear ramp.

Especially for the lightly reinforced beams it is necessary to take the formation of tensile crack growth into consideration when controlling the experiment. Therefore the feed-back signal consisted of contributions from both the stroke and the COD. The distance between the measuring frames was equal to the beam depth, and by using this distance the critical cracks would always develop between these two extra frames, which was also seen in *ESIS 1*. At the bottom of one of the measuring frames a clipgauge was attached. For simplicity, the signal measured by this clipgauge was called the crack opening displacement (COD) even though the signal also includes elastic contributions.

For the heavily reinforced beams the feed-back signal consisted of contributions from the stroke and the mean value of the measure from the MTS compression transducers. The distance between the measuring frames was here 800 mm, because the compression failure could occur both under the loading plate or on one of the sides of the loading plate.

The feed-back signal, δ was then created by analog addition of the COD or the MTS transducer and the stroke, see also Figure 5.15 and Figure 5.16

$$\delta = \alpha_1 \delta_{stroke} + \beta_1 \delta_{cod} \tag{5.6}$$

where δ_{stroke} is the signal from the stroke and δ_{cod} is the signal from the COD or the MTS transducer, $\alpha_1$and β_1 are weight factors dependent on the beam size and the reinforcement ratio. The values for the lightly reinforced beams were $\alpha_1 = 0.50$ and $\beta_1 = 0{,}20$, and for the heavily reinforced beams $\alpha_1 = 1.0$ and $\beta_1 = 1{,}0$. When the feed-back signal reaches a value of 10 volt an unloading has to take place. For the ligthly reinforced beams the following values were applied: 10 volt = 50 mm measured stroke, 10 volt = 2.0 mm measured COD and 10 volt = 63.04 kN measured load, and for the heavily reinforced beams: 10 volt = 200 mm measured stroke, 10 volt = 3.75 mm measured MTS deformation and 10 volt = 1000 kN measured load.

In order to make the testing free of vibrations and steady and to make the reference signal as a linear ramp, adjustments of the MOOG amplifier had to take place. The adjustments for the heavily reinforced beams had following values: gain fine = 6.0 and gain coarse = 10.0, and for the lightly reinforced beams the values: gain fine = 9.0 and gain coarse = 3.0. To provide a steady system also adjustments of the amplitude and the frequency of the reference signal and the offset value had to be performed.

For the lightly reinforced beams the loading rate was 0.001 volt/s, 0.005 volt/s and 0.025 volt/s. Typical for all experiments with the lightly reinforced beams were, that the loading rate was 0.001 volt/s up to the cracking load and down to a value of half the cracking load, where the rate was increased to 0.005 volt/s, which continued to the point where the pull-out of the reinforcement started. Then just after that, the rate was increased to 0.025 volt/s. The COD clipgauge was connected from the start of the test, and at the point, where the pull-out started and the cracking of the concrete was fully developed, the COD was disconnected. Unloading and reloading were performed with a rate of 0.025 volt/s.

For the heavily reinforced beams the loading rate was typical 0.01 volt/s up to 2/3 of the maximum calculated force, where the MTS transducers were connected. Then the loading rate was increased to 0.03 volt/s, which continued until an unloading took place with the same rate. A reloading was performed with a rate of 0.01 volt/s until the connecting of the MTS transducers and then again the rate was changed to 0.03 volt/s.

Typically for the experiments were that, the loading rate was chosen so the cracking load would be reached after 1-5 min. At later stages the displacement rate was increased and a typical experiment would take 45 min. For some of the beams more than the available stroke was required. An unloading was therefore performed, some steel plates were inserted between the beam and the piston and a reloading was then performed. This procedure was repeated until failure of the beam. Experiments with repeated loading could take up to several hours. During the test load-midspan and load-COD or MTS deformation were plotted on a x-y recorder to control the stability of the test.

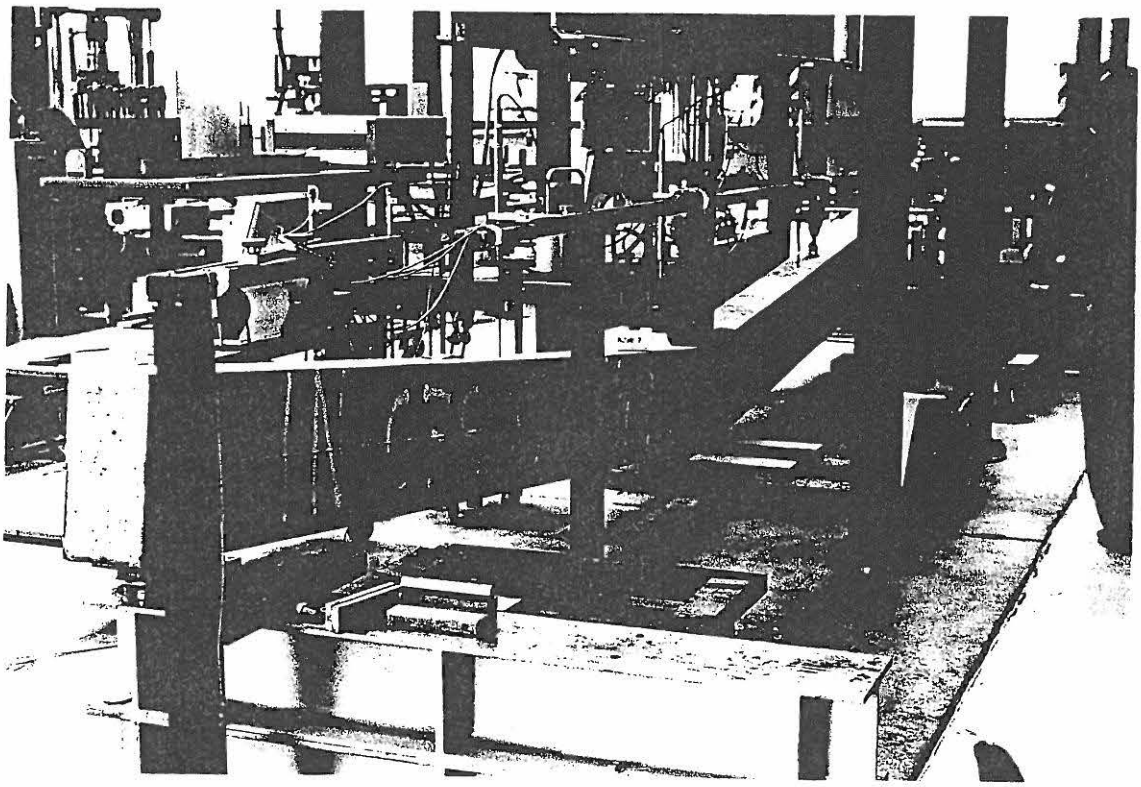

Figure 5.11: *Photo of the test set-up for the heavily reinforced beams. The photo shows the testing of the beam In_078_S.*

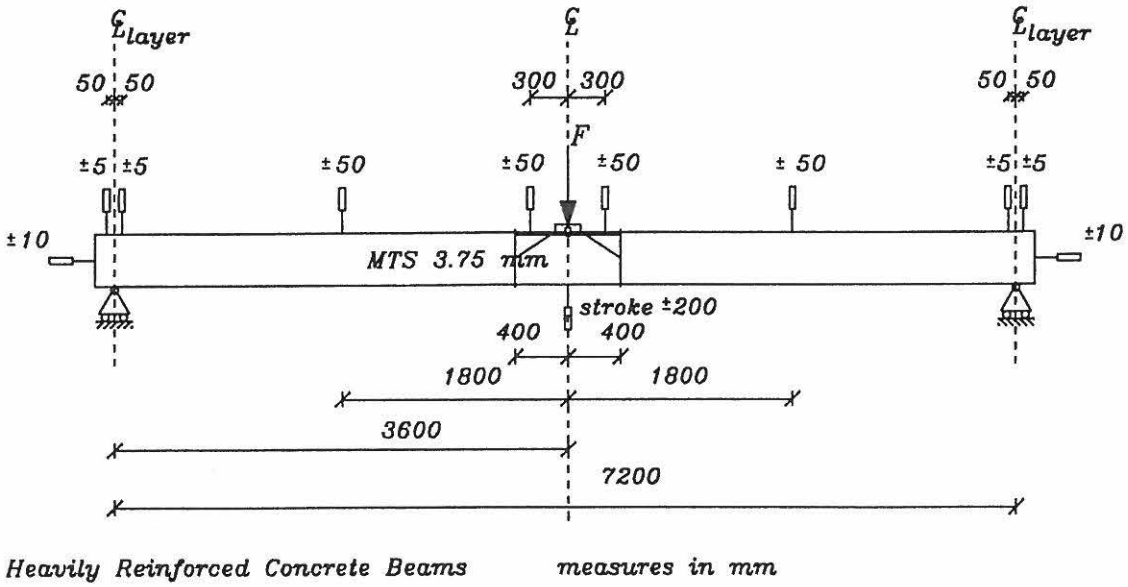

Figure 5.12: *Placing of transducers for the heavily reinforced beams.*

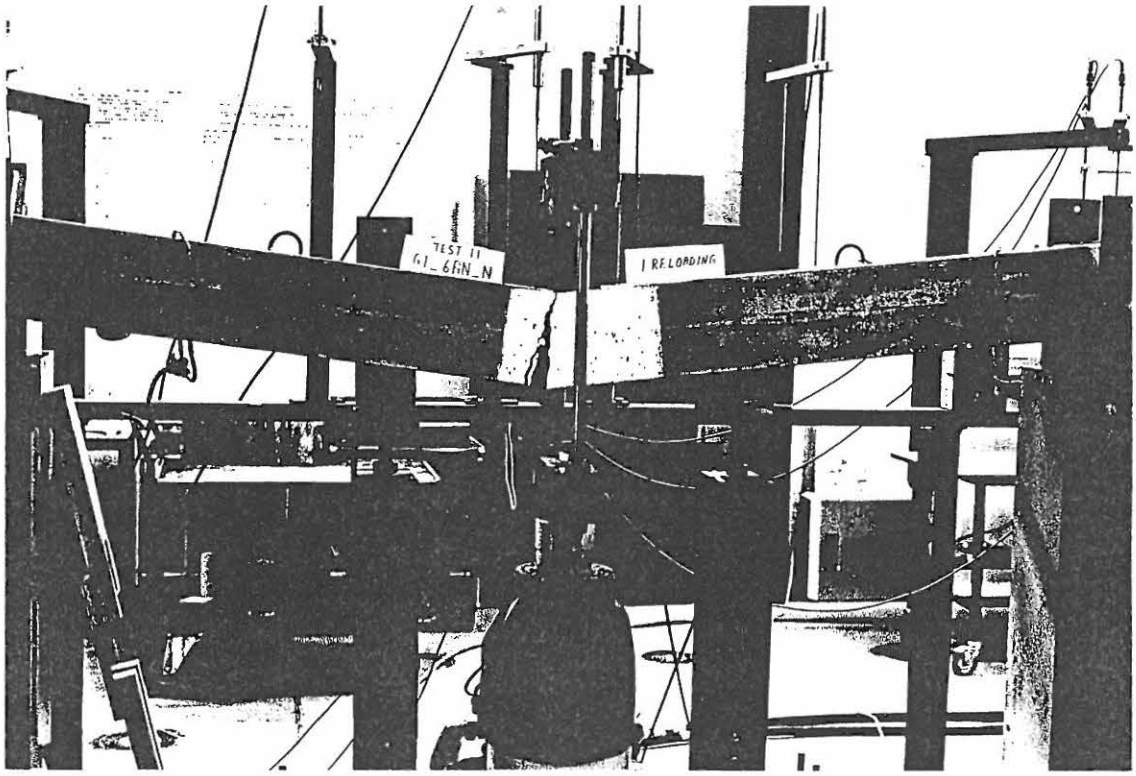

Figure 5.13: *Photo of the test set-up for the lightly reinforced beams. The photo shows the testing of the beam G1_6AN_N.*

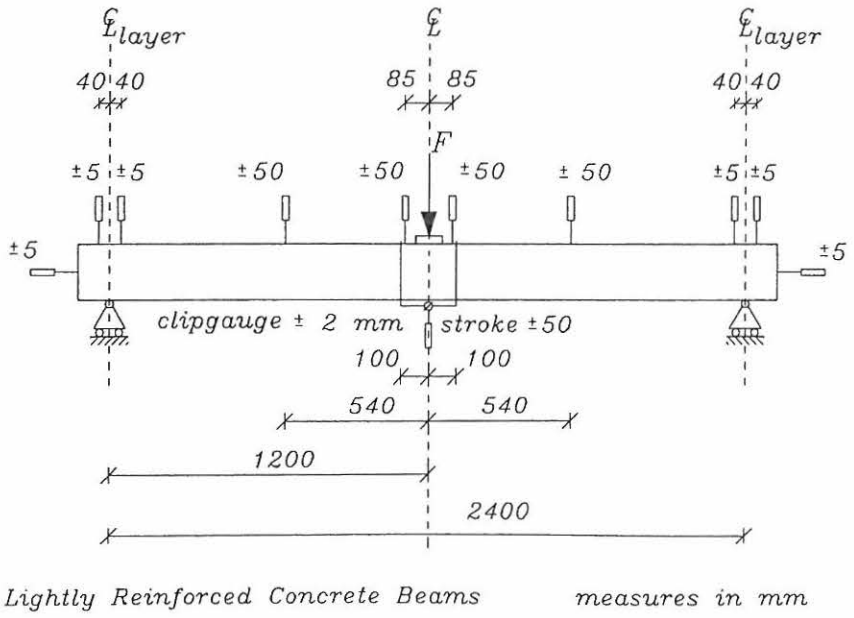

Figure 5.14: *Placing of transducers for the lightly reinforced beams.*

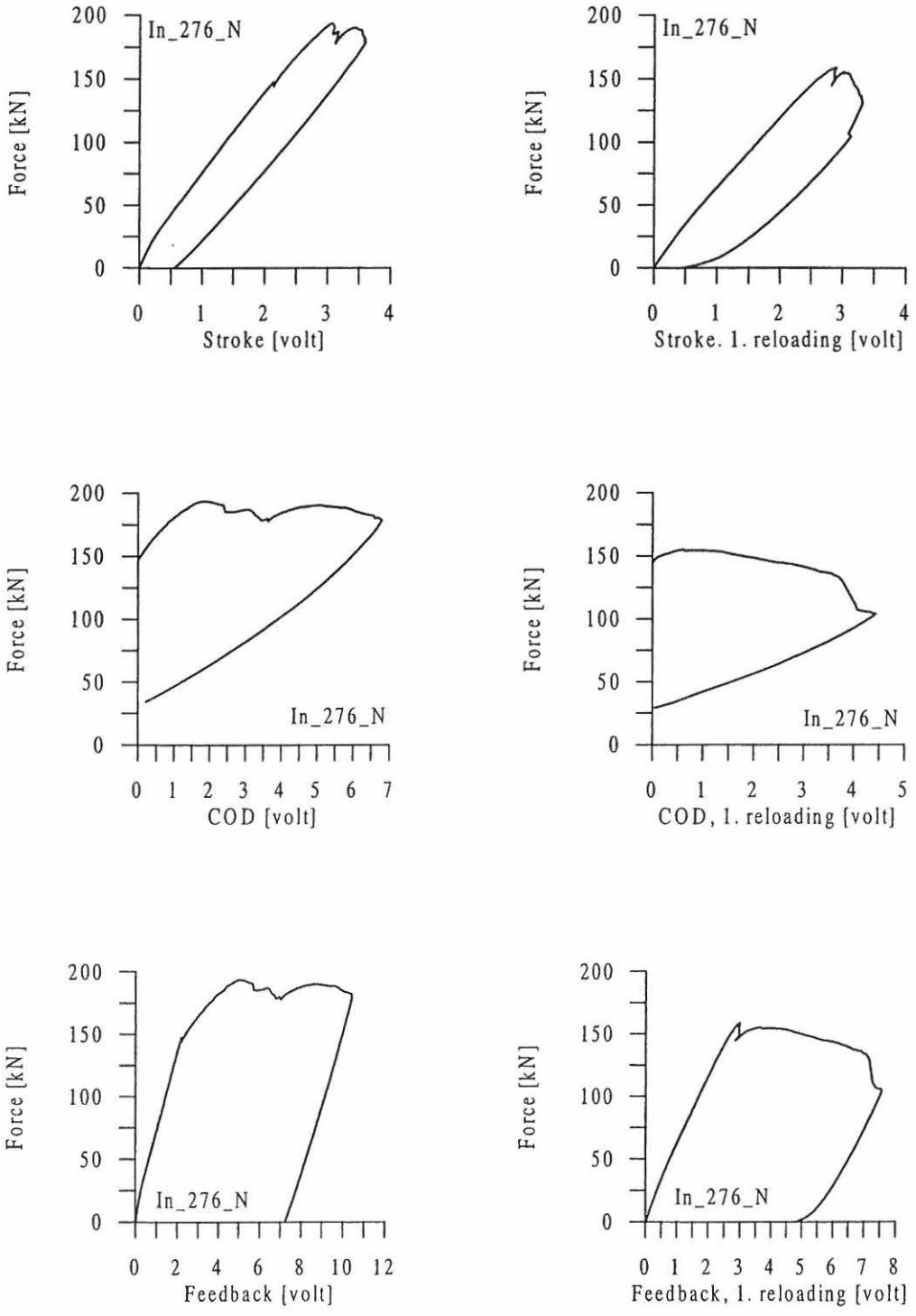

Figure 5.15: *Measured feed-back signal from testing of the heavily reinforced beam In_276_N. Top: the measured stroke, middle: the measured cod and bottom: the feed-back signal.*

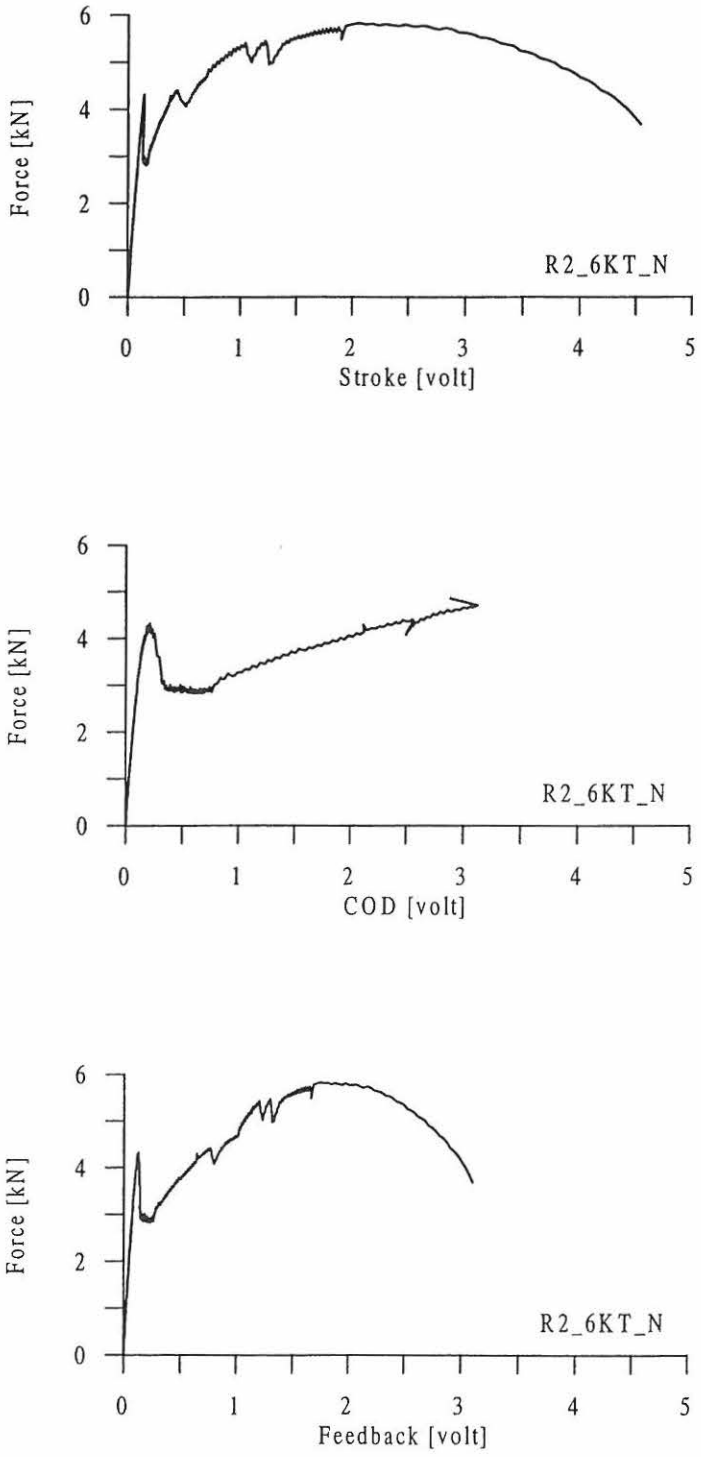

Figure 5.16: *Measured feed-back signal from testing of the lightly reinforced beam R2_6KT_N. Top: the measured stroke, middle: the measured cod and bottom: the feed-back signal.*

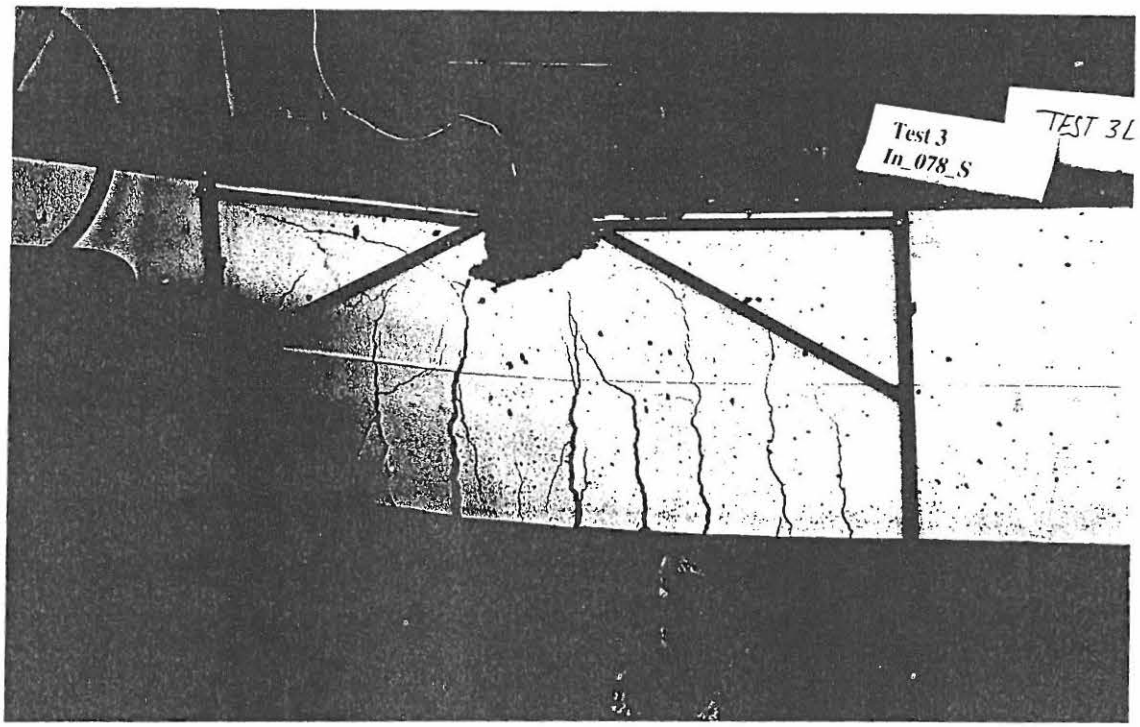

Figure 5.17: *Photo of the measuring frame with the crack opening displacement transducer, clipgauge used for the lightly reinforced beams.*

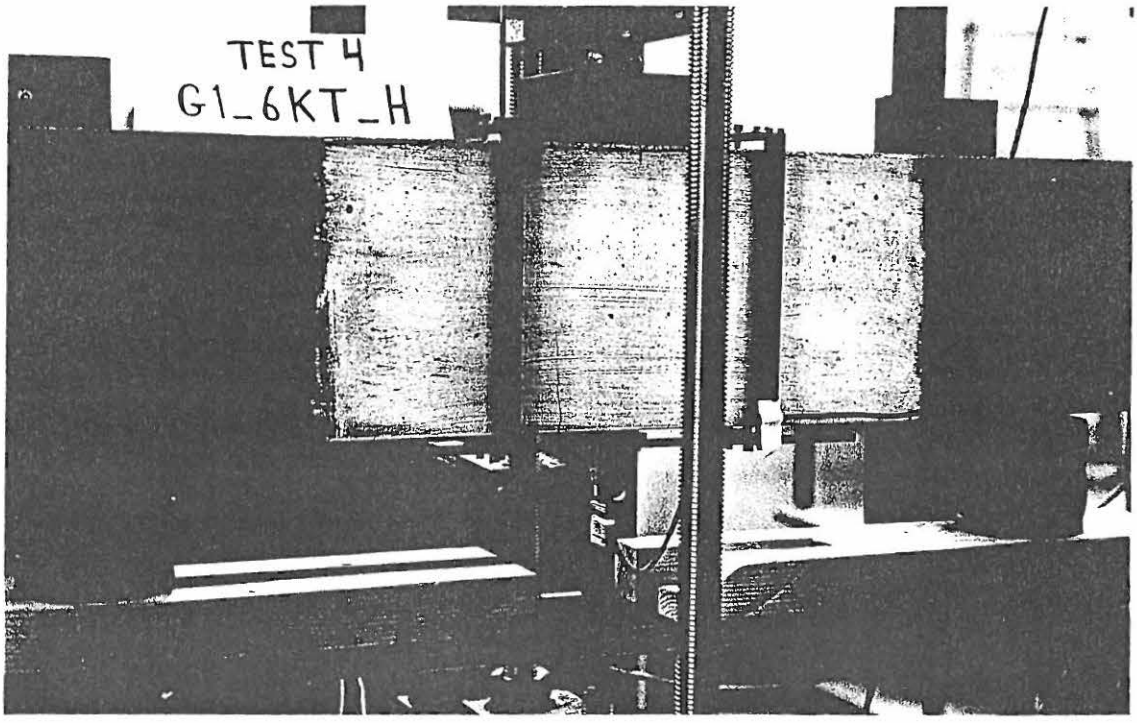

Figure 5.18: *Photo of the measuring frame with the compression deformation transducer, MTS used for the lightly reinforced beams.*

5.5 Experimental Results

The main purpose of the tests is to determine the plastic rotational capacity. The main focus will therefore be on the measurings of the plastic rotational capacity.

In the tests of the reinforced concrete beams the vertical displacement fields have been measured with transducers placed on the beams. The stability of the test is provided by servo-controlling, so it is possible to measure the post-peak behaviour of the beams and hereby determine the ultimate state of failure. From these measurings it is then possible to calculate the plastic rotational capacity.

Values for the plastic rotational capacity are obtained by three different methods. The measurings of the rotation of the beam at the supports and at the midspan makes it possible to calculate the plastic rotational capacity as the mutual rotation of the beam. Using the principle of virtual work a measure of the rotational capacity is achived from the area under the load-displacement curve of the midspan of the beam divided by the yield moment.

5.5.1 Load-Displacement Responses for the Test Beams

The load displacement curves for the heavily reinforced beams for the three different confinement types are shown in Figure 5.19, and the load displacement curves for the lightly reinforced beams are shown in Figure 5.20. The load displacement behaviour up to a max. stroke of 5 mm is shown for selected lightly reinforced beams in Figure 5.21. Typical distributions of vertical displacement along the beam axis for the beams are given in Figure 5.22 and Figure 5.23. Results for all the beams are given in Henriksen *et al.* (1998).

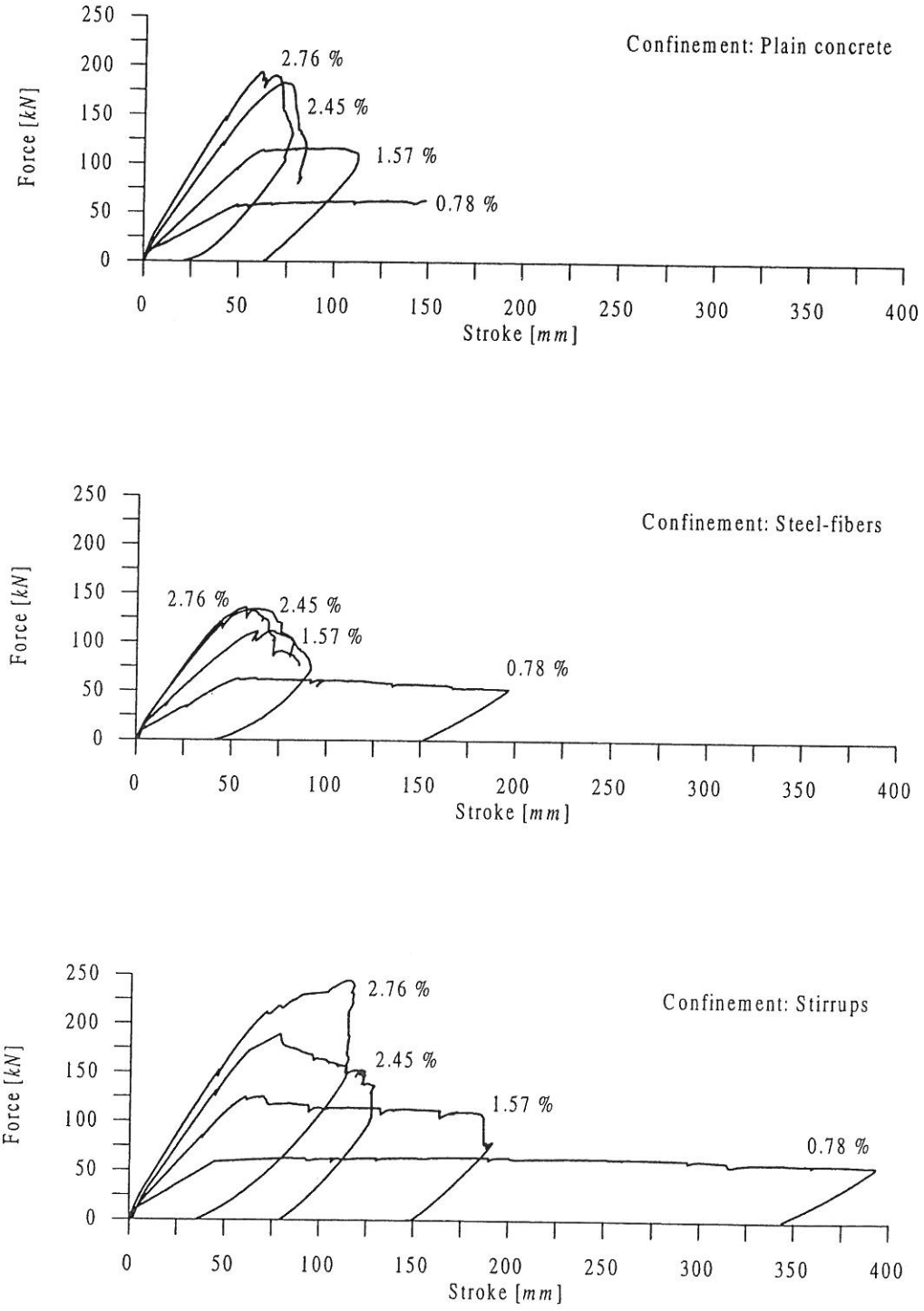

Figure 5.19: *Load displacement curves for the heavily reinforced concrete beams confined in the compression zone with plain concrete (top), steel-fibers (middle) and stirrups (bottom).*

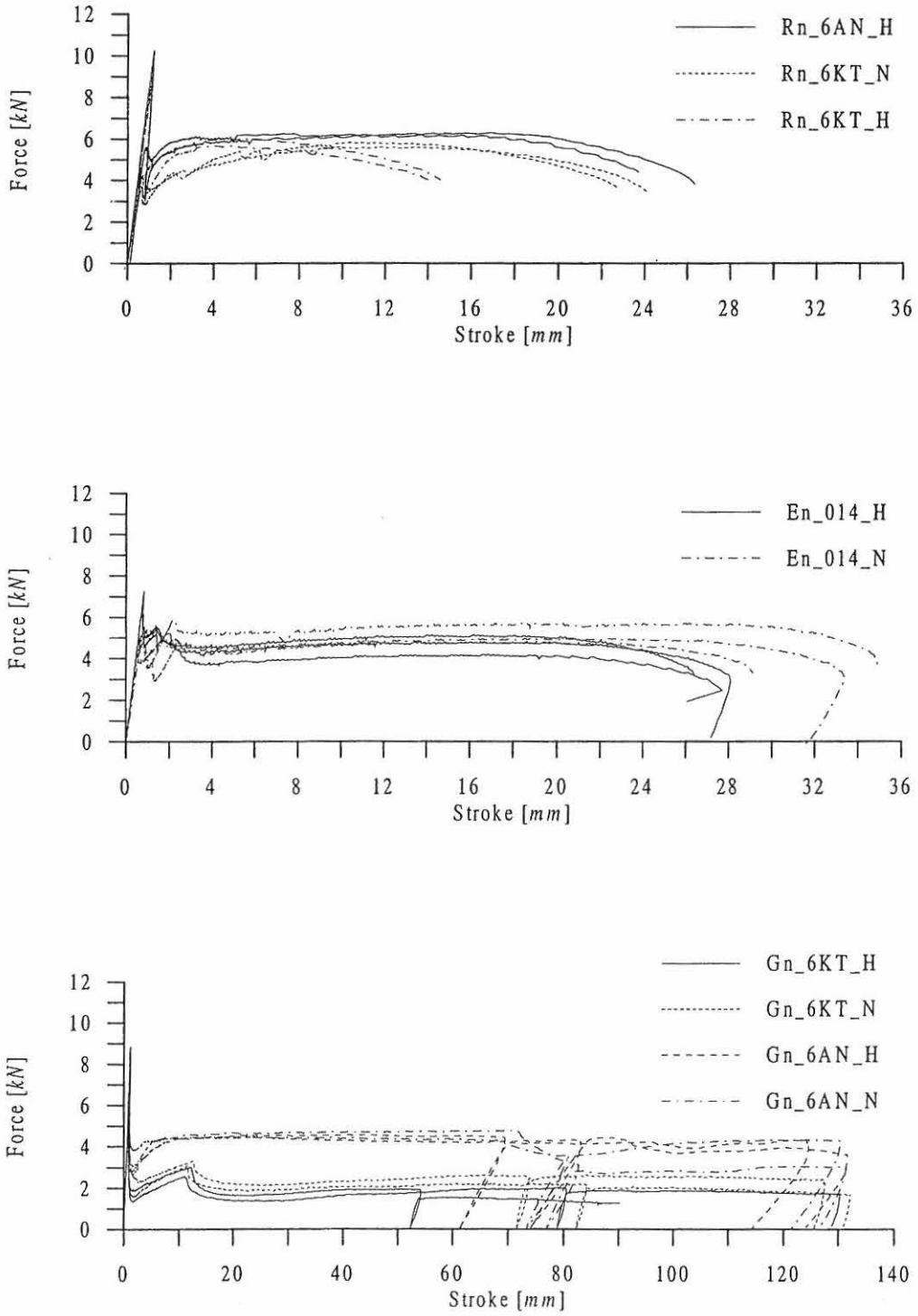

Figure 5.20: *Load displacement curves for lightly reinforced normal strength and high strength concrete beams. (top) Ribbed cold drawned and annealed rebars, (middle) ribbed hot-rolled rebars and (bottom) smooth cold drawned and annealed rebars.*

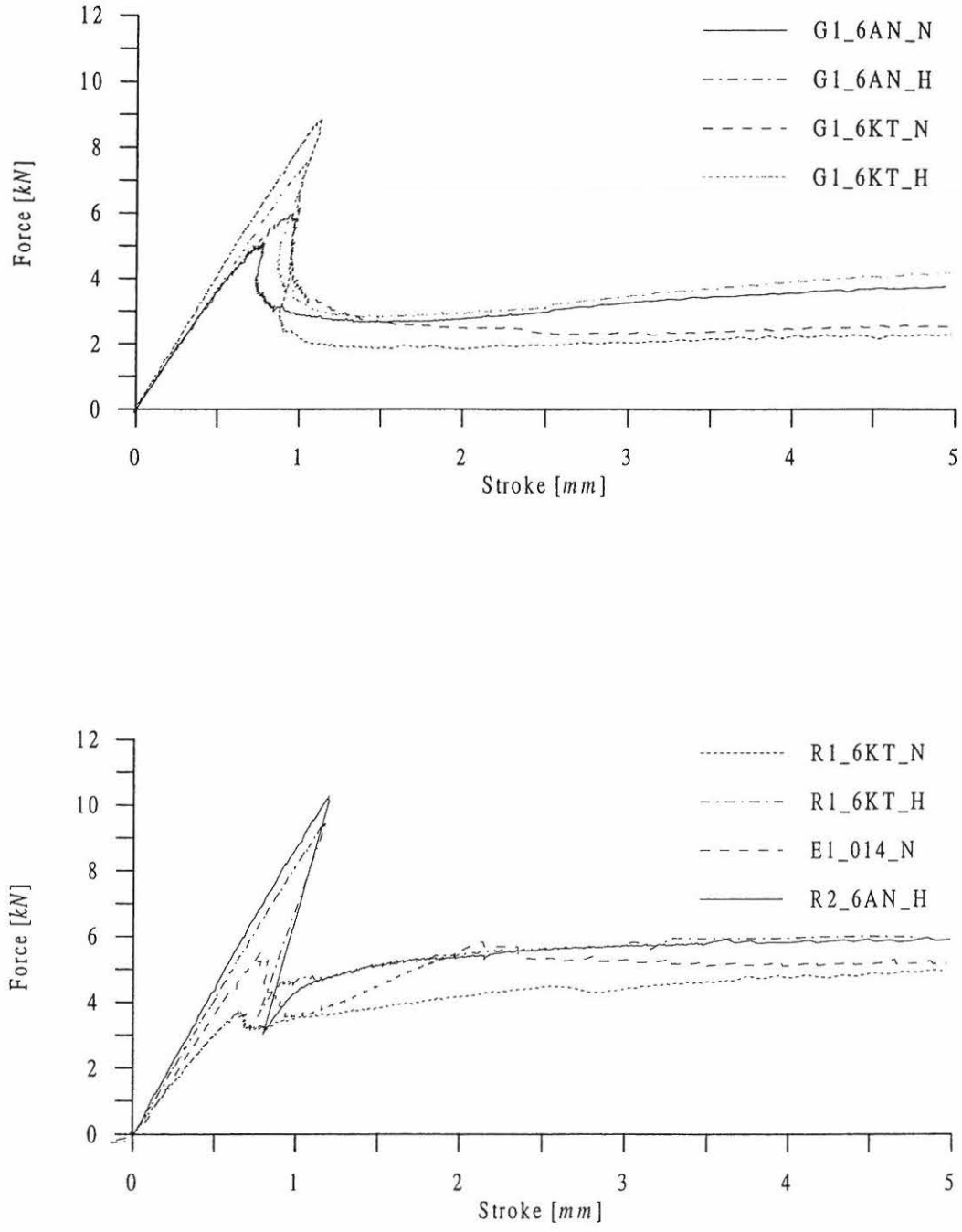

Figure 5.21: *Pre-peak load displacement curves for selected lightly reinforced beams. (top) Ribbed reinforcement and (bottom) smooth reinforcement.*

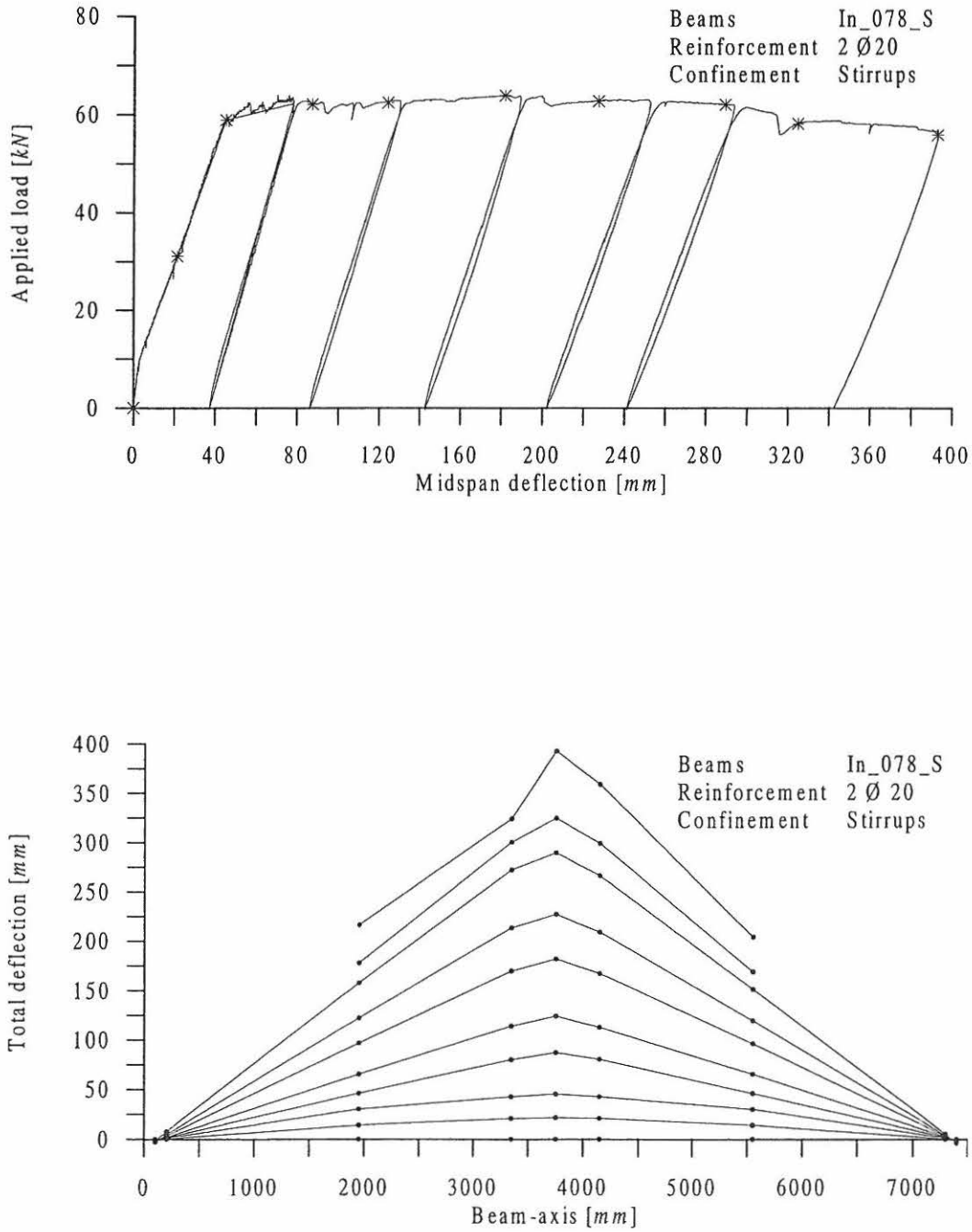

Figure 5.22: *Load-deflection curve (top) and vertical distribution (bottom) for In_078_S. The load levels are marked with asteriks (top).*

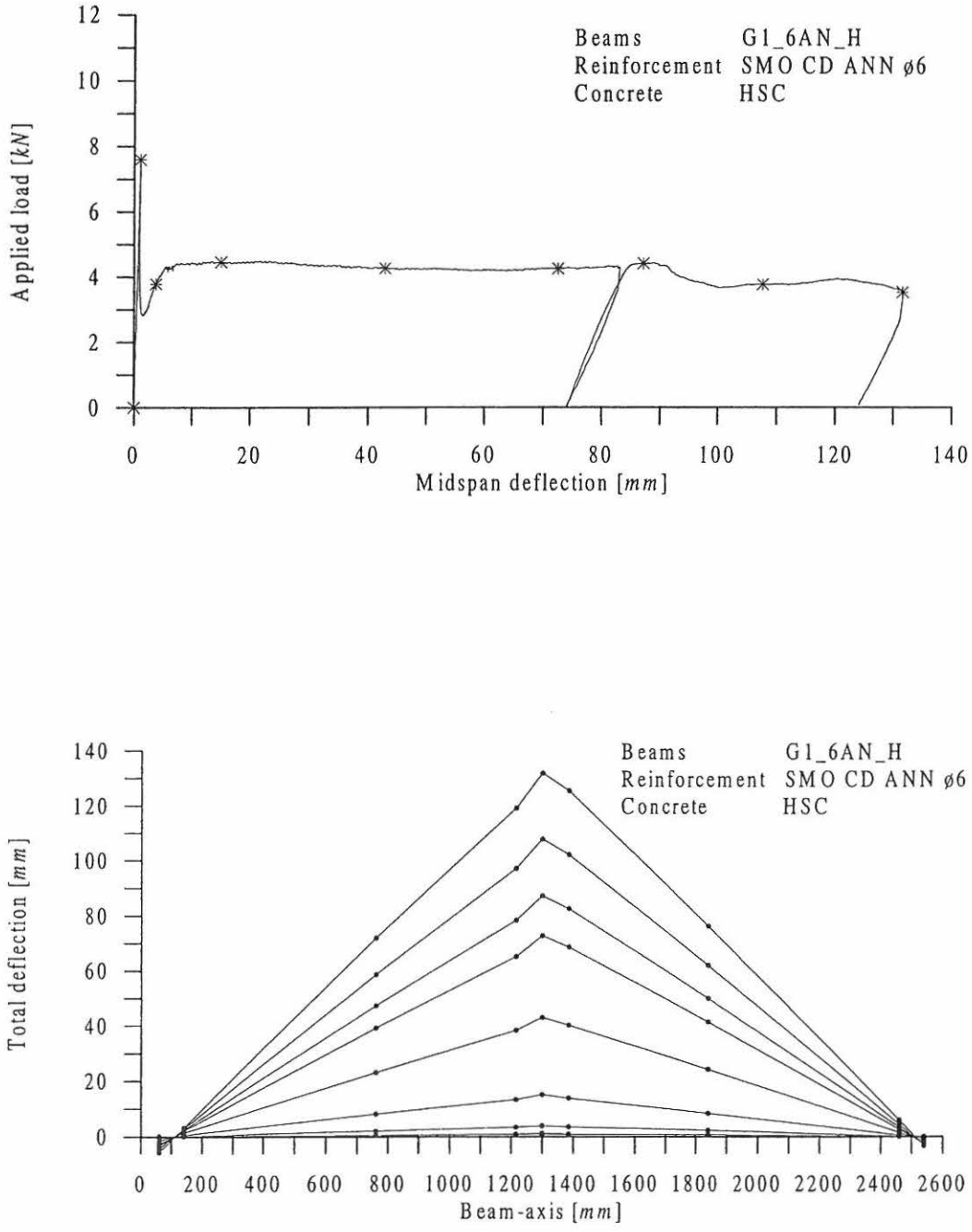

Figure 5.23: *Load-deflection curve (top) and vertical distribution (bottom) for G1_6AN_H. The load levels are marked with asteriks (top).*

5.5.2 Results for Heavily Reinforced Beams

The rotational capacity of a reinforced beam is dependent on the beam failure mode. For the reinforcement ratios investigated in this test programme the general failure picture of the heavily reinforced beams were a bending failure resulting in a compression failure of the concrete. The point of the ultimate compression failure occurs differently for the three types of confinement of the compression zone.

From the load displacement curves shown in Figure 5.19 the effect of the different confinement types on the ductility of the beams are clearly seen. It is obvious that adding of several stirrups at the place of hinge will increase the ductility of the beam and thereby change the point of failure. The failure mode for the reinforcement ratios 2.45 % and 2.76 % will change from a very brittle compression failure for plain concrete confinement to a more ductile failure.

It was observed, that the beams with stirrups confinement after reaching maximum load crushing of the top cover layer of the concrete on both sides of loading plate occured, while the compression zone within the stirrups were uncracked. Further loading resulted in spalling of the concrete layer of the stirrups in the compression zone and finally the beam had failed. These observations are also observed for concrete columns confined with stirrups.

As the uniaxial compressive strength of the steel-fiber reinforced concrete turned out to be 34.9 MPa, whereas the compressive strength of the normal strength concrete was 55.0 MPa, the maximum loads of the beams with steel-fiber confinement were lower than the maximum loads of the beams with plain concrete and stirrups confinement. One way of improving the type of steel-fiber reinforced concrete used for the beams could be to add superplasticisers and microsilica to the concrete to make the concrete more dense resulting in a better bond between the fibers and the concrete. This type of concrete is also called high strength concrete.

From the softening of the load displacement curves it is seen that the beam In_157_F has failed almost at the point of maximum load. The beam In_157_F was actually tested once again resulting in a diagonal crack running from the compression failure zone to the main reinforcement and then running along the main rebars to the support. A result of the steel-fiber confinement seems to be that the slope of the softening load displacement curve is higher than the slope of the plain concrete confinement.

5.5.3 Results for Lightly Reinforced Beams

The failure mode of the lightly reinforced beams consisted of a tensile failure of the reinforcement for the beams with ribbed bars. The beams with smooth plain rebars were not tested to ultimate failure but the tests were stopped when the midspan deflection reached a limit value of about 130 mm. As the bond shear strength between the smooth plain reinforcement and the concrete was very low, it was not possible to obtain a tensile failure of this kind of reinforcement.

From the load displacement curves giving the full range behaviour of the lightly reinforced beams shown in Figure 5.20 the failure modes are clearly observed. Almost all experiments showed

discrete cracking, that is only one crack occured inside the measuring area of the clipgauge.

A general picture for the beams reinforced with ribbed cold-drawned bars and hot-rolled bars is that the ultimate deflections seem to be higher for the NSC beams than for the HSC beams. This could be due to the fact that the bond shear strength is higher for the HSC resulting in a lower slip zone. This means that the HSC beams have a lower rotational capacity. It is also observed, that the HSC beams reinforced with cold-drawned and annealed ribbed bars have higher ultimate deflections resulting in a higher rotational capacity.

For the beams reinforced with smooth plain bars a difference in the yielding load is observed. For the smooth cold-drawned and annealed reinforcement the yielding load reaches about 4 kN (f_y = 586 N/mm^2 for SMO CD ANN), while the smooth cold-drawned reinforcement only reaches about 2 kN (f_y = 644 *N/mm*^{2} for SMO CD). This could be due to the Weibull effect, that the smooth cold-drawned reinforcement reaches the lowest value in the yielding zone around the crack.

In Figure 5.21 the load deflection behaviour for a stroke of 0 - 5 mm is shown for some of the beams. It is clearly seen, that the cracking load of the HSC beams are higher than for the NSC beams.

5.5.4 Measured Rotations of the Test Beams

The rotations of the beams are measured both at the supports by two transducer placed on each side of the center line of the layer and at the midspan of the beam using the stroke.

Typical curves showing the rotations of a few selected beams In_245_S, In_276_S and Gn_6kt_H are given in Figure 5.24. In Henriksen *et al.* (1998) curves showing the rotations as a function of the load and values of the measured rotations for all the experiments are listed.

For the heavily reinforced beams it is observed, that the rotations at the supports are higher than the rotations at the midspan due to the more curved distributions of the vertical displacements as shown in Figure 5.22. For the two last load levels the transducers at the supports were removed of security reasons. The ultimate beam rotations were then calculated from the two transducer on each side of the loading plate. For the lightly reinforced beams there seems to be a good agreement between the two ways of calculating the beam rotations. From Figure 5.23 it is observed, that the lightly reinforced beam acts more like a rigid body during loading. When only one crack occur, the beam-parts act like rigid bodies.

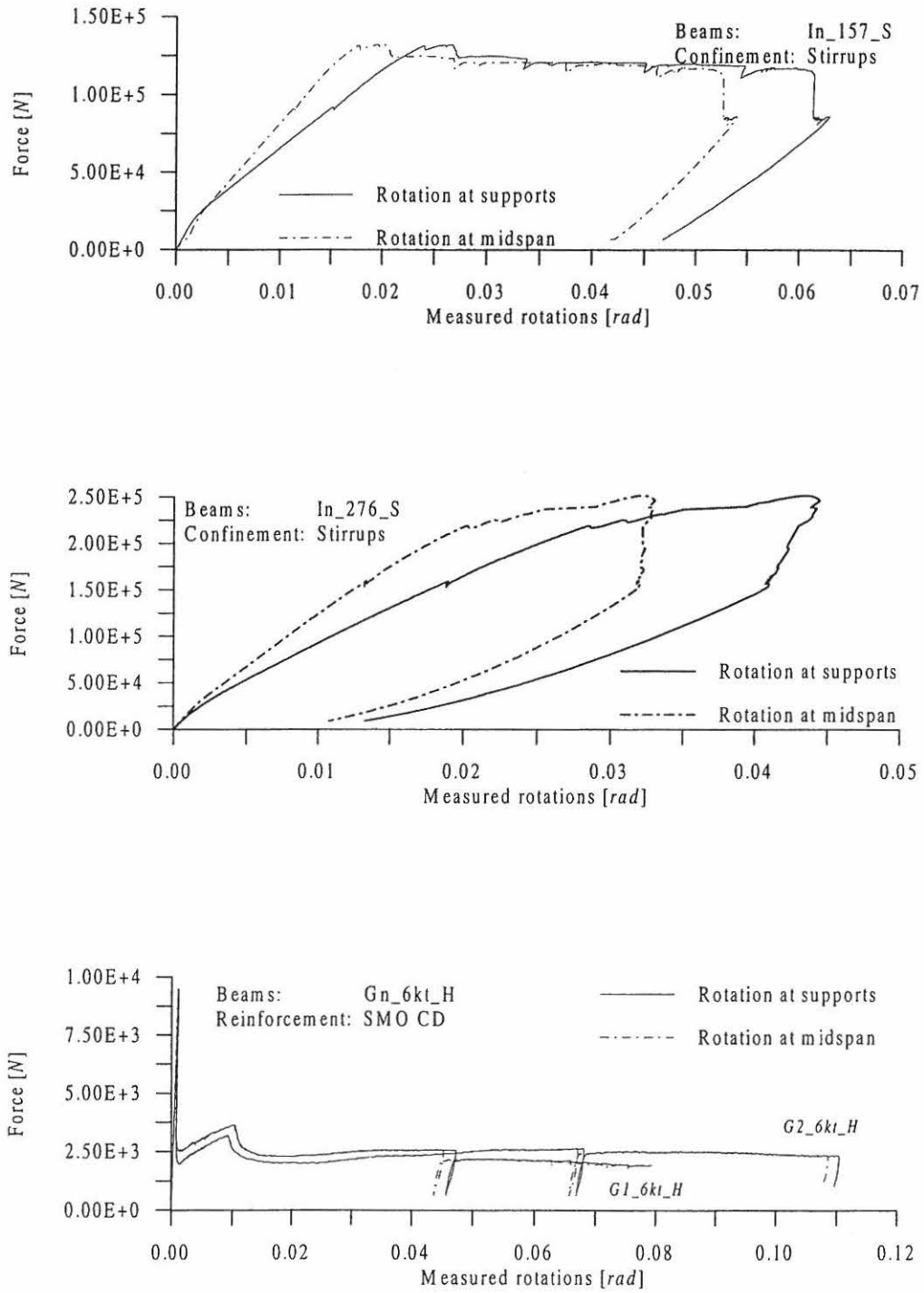

Figure 5.24: *Measured rotations as a function of the applied load for the heavily reinforced beams In_157_S (top) and In_276_S (middle) and the lightly reinforced high strength concrete beams G1_6kt_H and G2_6kt_H (bottom).*

5.6 Rotational Capacity of the Test Beams

The rotational capacity is determined by three different methods. Main results for the rotational capacities according to the following three models are presented both for heavily and lightly reinforced concrete beams. More detailed results are listed in Henriksen *et al.* (1998).

5.6.1 Basic Assumption on Rotational Capacity

Calculation of the plastic rotational capacity depends on the load displacement curve and the way of testing the beam. The forming of a plastic hinge in a concrete beam depends on the testing. In this report the experiments are all done in three point bending to be sure of forming a plastic hinge in the centre of the beam.

The size of the plastic rotational capacity is dependent on how the ultimate failure load or ultimate displacement is chosen and how the elastic part is defined. In the literature there seems to be different ways of doing this.

The basic ideas can be shown in Figure 5.25.

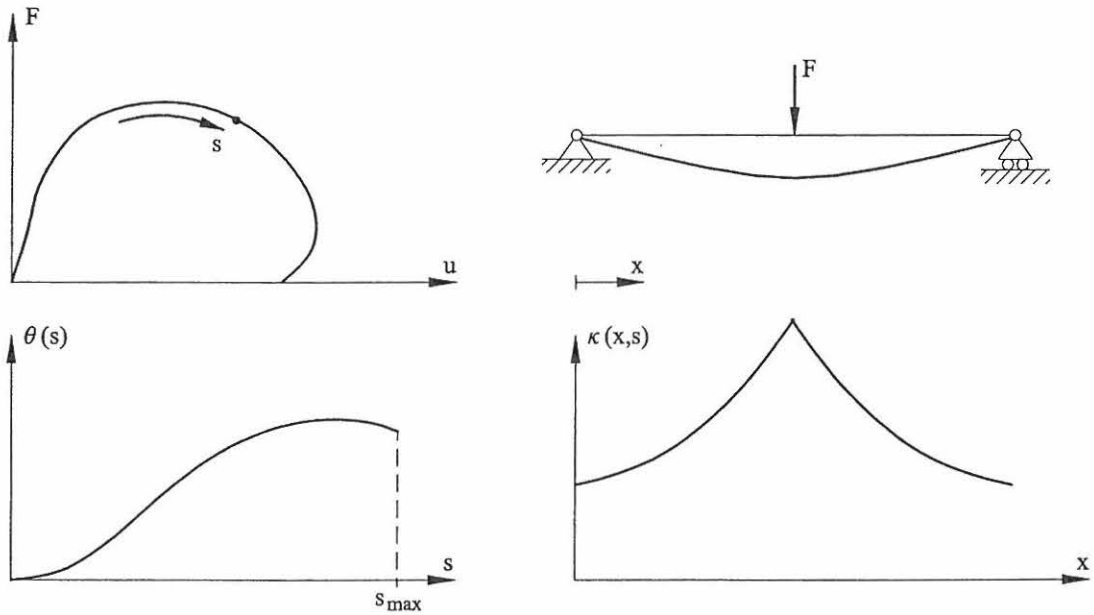

Figure 5.25: *Basic assumptions on rotational capacity.*

The point s on the load displacement curve and the point x on the beam axis seems to be important factors in calculating the rotational capacity, because the rotational capacity is dependent on the size of s and x.

The curvature is then given as

$$\kappa = \kappa(x, s) \tag{5.7}$$

The rotational capacity can be calculated as

$$\theta(s) = \int_0^L (\kappa(x,s) - \kappa_{el}(x,s))dx \tag{5.8}$$

where κ_{el} is the elastic part of the curvature.

In order to calculate the maximum value of the rotational capacity, the point s on the load displacement curve must be equal to the ultimate displacement u_{max} corresponding to the value s_u on the curve showing the relation between $\theta(s)$ and s.

5.6.2 Rotational Capacity according to Plasticity Theory

The area under the load displacement curve is equal to the work done by the external forces during the failure process. If the beam is assumed to be ideal plastic forming a plastic hinge at the mid-section, this work can also be expressed as the yield moment M_y times the total rotation, thus

$$M_y \, \theta_{plast,1} = \int_0^{\delta} F \, du \qquad \Rightarrow \tag{5.9}$$

$$\theta_{plast,1} = \frac{1}{M_y} \int_0^{\delta} F \, du \tag{5.10}$$

The yield moment of the cross-section, M_y is given as

$$M_y = 0.8 \, h_c \, b \, f_c \, (h_{ef} - 0.4 \, h_c) \tag{5.11}$$

where b is the thickness of the beam, f_c is the concrete strength and h_{ef} is the effective depth of the cross-section.

The depth of the compression zone, h_c is given as

$$h_c = \frac{A_s f_y}{0.8\, b f_c} \tag{5.12}$$

where A_s is the steel area and f_y is the yield strength.

5.6.3 Rotational Capacity according to Rotations of the Beam Supports

For the eight vertical measurements performed for all the beams, four of the displacement transducers were placed on each side of the axis around which the beam rotates at the supports. In this way the rotations of the beam supports can be determined.

By taking only the plastic part of these rotations and multiplying by 2 to achieve the mutual plastic rotations, a new rotational capacity is defined as

$$\theta_{plast,2} = (\alpha_{sup,total} - \alpha_{sup,elastic})\, 2 \tag{5.13}$$

where $\alpha_{sup,total}$ is the total rotation of the beam and $\alpha_{sup,elastic}$ is the rotation from the elastic part calculated from the support rotations.

5.6.4 Rotational Capacity according to Rotations of the Midspan

Assuming that the beam deforms as a rigid body after forming a plastic hinge at the center of the beam, the plastic rotations can be found from the measurements of the midspan deflection using the stroke subtracting the settlements of the beam supports.

The rotational capacity is hereby given as the mutual rotation of the beam and defined as

$$\begin{aligned} \theta_{plast,3} &= 4\, \frac{(\delta_{ult} - \delta_{elast1})}{L} \\ \theta_{plast,3} &= 2\, \frac{(\delta_{ult} - \delta_{elast1})}{L_0} \\ \theta_{plast,3} &= (\alpha_{stroke,total} - \alpha_{stroke,elastic})\, 2 \end{aligned} \tag{5.14}$$

where δ_{ult} and δ_{elast1} are the ultimate and elastic deflections, $\alpha_{stroke,total}$ and $\alpha_{stroke,elastic}$ are the total and elastic rotations of the midspan, L is the span and L_0 is the distance between the cross-section of maximum moment and zero moment (in this case $L_0 = ½\, L$).

5.6.5 Plastic Rotational Capacity of the Test Beams

The average plastic rotational capacity of the test beams using the three models are given in Table 5.11 and Table 5.12. Further results on the rotational capacity of the test beams are listed in Henriksen *et al.* (1998).

The plastic rotational capacity as a function of the reinforcement ratio for the three different ductilities of the compression zone of the heavily reinforced beams are shown in Figure 5.26. It is clearly seen, that the beams with stirrup confinement have the largest plastic rotational capacity.

In Figure 5.27 is shown the plastic rotational capacity calculated from the support rotations versus the reinforcement ratio. It is observed, that there is a remarkable difference in the rotational capacity for the low reinforcement ratios, 0.78 % and 1.57 %, and that the values are almost the same for the high reinforcement ratios, 2.45 % and 2.76 %. This is due to the failure modes for the beams. The beams reinforced with 0.78 % and 1.57 % have a normal reinforced cross-section, thus the failure load depends on both the yielding of the reinforcement and the ductilty of the concrete compression zone, while the beams reinforced with 2.45 % and 2.76 % have a over-reinforced cross-section, where the failure load only depends on the ductility of the concrete compression zone.

In Figure 5.28 the plastic rotational capacity is plotted as a function of the neutral axis depth given by $h_{c,y} / h_{ef}$, where the depth of compression zone is calculated according to Equation (5.12), and the values obtained are clearly higher than the allowable plastic rotation according to Eurocode 2 (1993), see Figure 5.29.

In Figure 5.30 the average values of the plastic rotational capacity of the lightly reinforced beams are plotted for the different steel types. It is clearly seen, that smooth reinforcement bars give very high rotational capacities bcause of the low bond shear strength. The ribbed reinforcement bars have high bond shear strengths and thereby the size of the rotational capacity will be dependent on the tensile properties of the steel as tensile failure will occur.

Beam	Plasticity model	Rotation at supports	Rotation at midspan
θ_{plast} in [10^{-2} *rad*]	$\theta_{plast,1}$	$\theta_{plast,2}$	$\theta_{plast,3}$
In_078_N	9.69	10.1	10.3
In_078_F	9.14	11.9	10.1
In_078_S	2.06	21.3	20.8
In_157_N	5.02	6.96	5.64
In_157_F	2.26	3.94	3.12
In_157_S	8.22	10.8	9.10
In_245_N	2.31	5.46	2.93
In_245_F	2.39	4.88	4.03
In_245_S	4.30	5.84	5.11
In_276_N	1.29	3.47	2.85
In_276_F	1.19	4.40	3.66
In_276_S	2.06	4.77	3.48

Table 5.11: *Test results for plastic rotational capacity in radians of the heavily reinforced concrete beams with plain concrete (N), steel-fibers (F) and stirrups (S) confinement.*

Beam	Plasticity model	Rotation at supports	Rotation at midspan
θ_{plast} in [10^{-2} *rad*]	$\theta_{plast,1}$	$\theta_{plast,2}$	$\theta_{plast,3}$
Rn_6kt_N	3.49	3.92	3.76
Rn_6kt_H	2.20	2.31	2.26
En_014_N	5.84	5.63	5.33
En_014_H	4.51	4.71	4.47
Rn_6an_H	4.07	4.13	4.05
Gn_6kt_N	11.6	20.8	21.6
Gn_6kt_H	8.13	19.0	18.4
Gn_6an_N	20.5	22.3	21.7
Gn_6an_H	21.0	21.6	21.3

Table 5.12: *Test results for plastic rotational capacity in radians of the lightly reinforced concrete beams with ribbed (R), hotrolled (E) and smooth (G) reinforcement.*

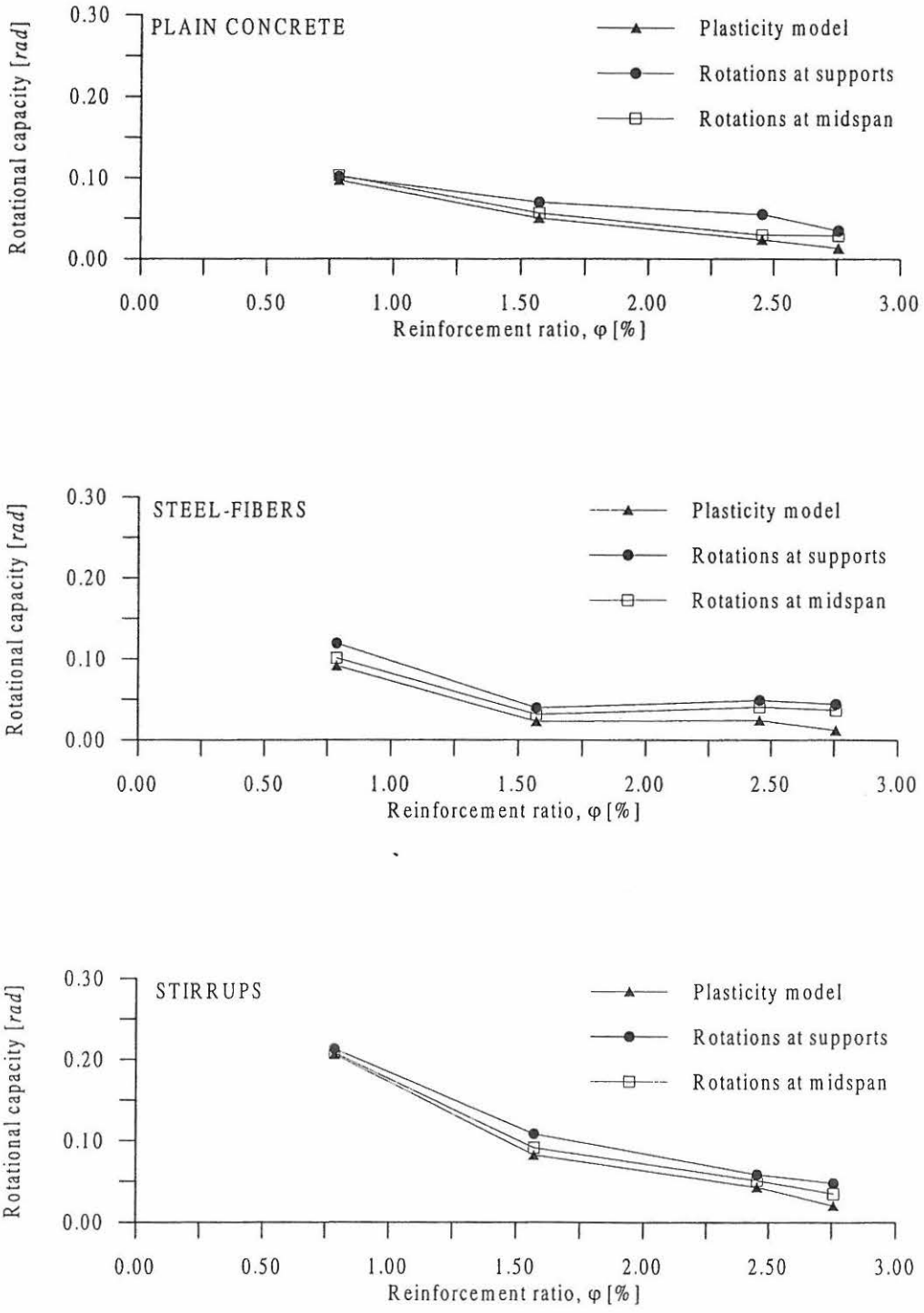

Figure 5.26: *The plastic rotational capacity as a function of the reinforcement ratios for the heavily reinforced concrete beams with plain concrete (top), steel-fibers (middle) and stirrups (bottom) confinement.*

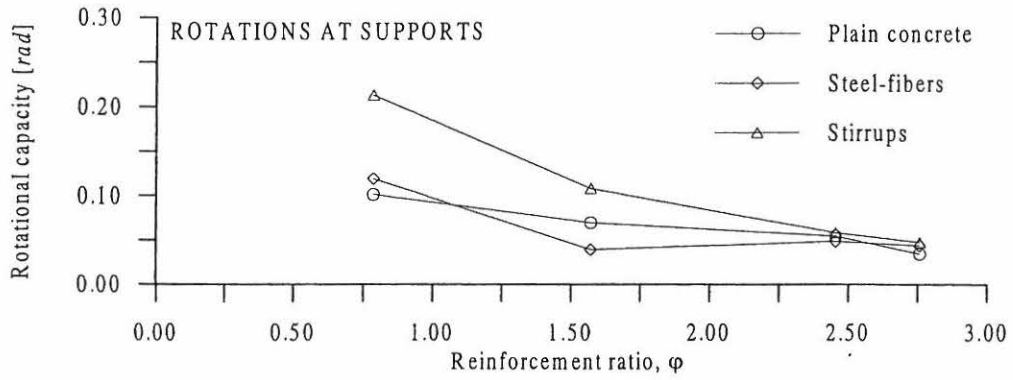

Figure 5.27: *Plastic rotational capacity from support rotations as a function of the reinforcement ratio for the heavily reinforced beams.*

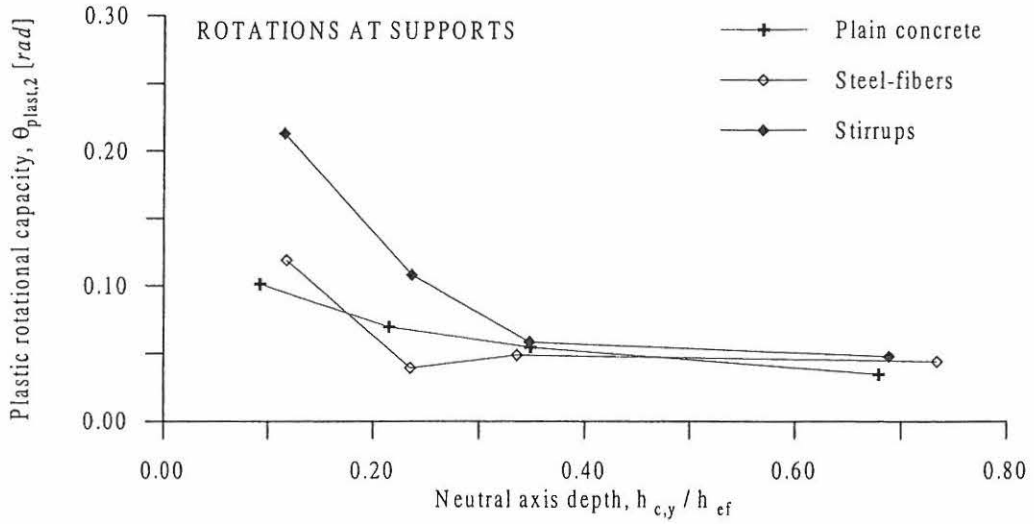

Figure 5.28: *Plastic rotational capacity from support rotations as a function of the neutal axis depth for the heavily reinforced beams.*

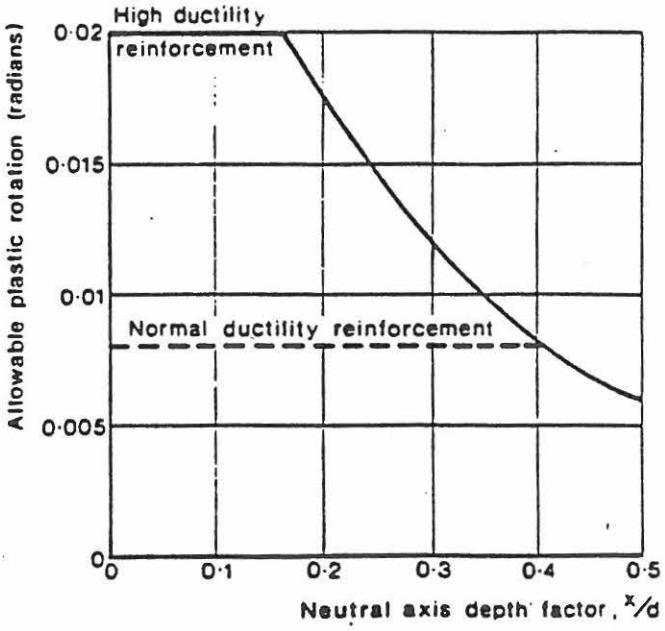

Figure 5.29: *Allowable plastic rotation of reinforced concrete sections according to Eurocode 2 (1993). The symbols are given as depth of compression zone* $x = h_c$ *and effective depth of xross-section* $d = h_{ef}$.

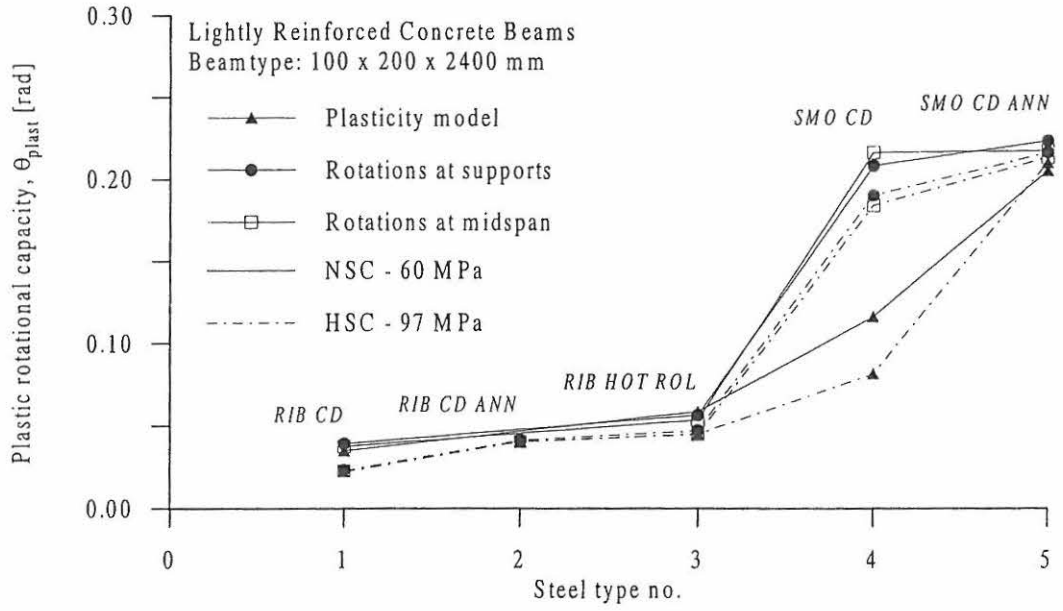

Figure 5.30: *Plastic rotational capacity for the different steel types of the lightly reinforced normal strength and high strength concrete beams.*

Chapter 6

Comparison of Analytical and Experimental Methods

In this chapter main results of modelling the test beams are presented. The modelling of the beams is limited to modelling of the load displacement curve for the heavily reinforced beams and modelling the pre-peak behaviour of the lightly reinforced beams. The pre-peak behaviour is here defined as the load displacement response for 0 - 5 mm stroke.

Besides, comparison of analytical and experimental results for the plastic rotational capacity of the beams of different scale and strength described in chapter 4 and the heavily and lightly reinforced beams described in chapter 5 are also presented. Model results for the plastic rotational capacity of the normal and high strength concrete beams calculated from the load displacement curve as the plastic work divided by the yield moment are presented.

Modelling of the test beams are performed in accordance with the models described in chapter 2 and 3. For the lightly reinforced beams presented in chapter 5 showing discrete cracking, further analysis of the prepeak behaviour has been performed in accordance with a Direct Subtructure Model, which is described in Brincker *et al.* (1999). The DSM model is a model for single crack extension in lightly reinforced beams.

Model results for all the heavily and lightly reinforced test beams from *ESIS 2* are listed in Henriksen *et al.* (1998), and some results from *ESIS 1* are presented in Brincker *et al.* (1999).

6.1 Modelling of Heavily Reinforced Beams

The main results of the modelling carried out in Henriksen *et al.* (1998) are presented as load displacement curves predicting the full range behaviour and estimates of the plastic rotational capacity calculated as the plastic work divided by the cross-sectional yield moment.

6.1.1 Model Results of Plastic Rotational Capacity

In Henriksen *et al.* (1998) analytical results of the plastic rotational capacity given by three models are listed. Model 1 predicts the rotational capacity, $\theta_{cal,1}$ as the total plastic curvature from the yielding of the reinforcement and the crushing of the concrete multiplied by the yielding length of the hinge. Model 2 gives the rotational capacity, $\theta_{cal,2}$ as the plastic work from the load displacement curve divided by the yield moment of the cross-section. Finally, model 3 estimates the plastic rotational capacity, $\theta_{cal,3}$ as the plastic mutual rotations of the midspan.

In Henriksen *et al.* (1998) comparisons of model and experimental load displacement curves are presented for all experiments for different values of the key parameters: the characteristic length parameter β and the critical softening deformation w_c. As the ultimate uniaxial compressive strain ε_{cu} is defined as w_c / l_{ch}, where the size of the compression fracture zone $l_{ch} = \beta h_c$ giving $\varepsilon_{cu} = w_c / (\beta h_c)$ it is clear, that the key parameters play an important role on the softening of the concrete.

In chapter 3 the influence of the key parameters on the model plastic rotational capacity of the reinforced beams corresponding to the beams from *ESIS 1* are presented. The values of the rotational capacity estimated by the calculation model taking into account the plastic work are shown in Figures 6.1 - 6.3 as a function of the reinforcement ratio, and compared with experimental results from chapter 4 for normal strength concrete beams with a cross-section of 100 x 100 mm, 100 x 200 mm and 200 x 400 mm and slenderness numbers 12. As it appears from these investigations the following values of the key parameters $\beta = 8.0$ and $w_c = 4.0$ mm give the best agreement.

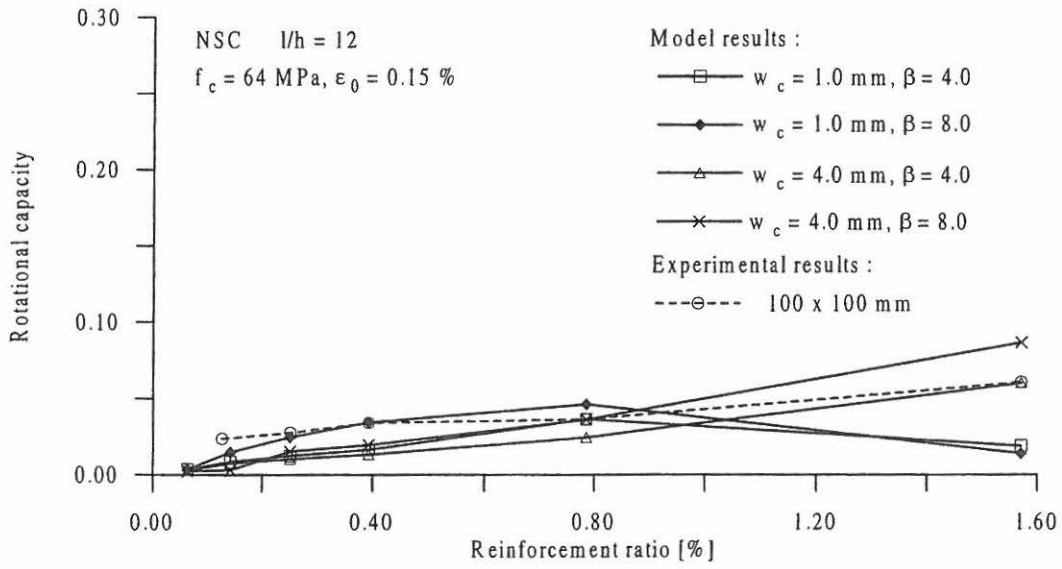

Figure 6.1: *Model Results compared with experimental results for 100 x 100 x 1200 mm normal strength concrete beams varying the key parameters wc = 1.0 - 4.0 mm and β = 4.0 - 8.0.*

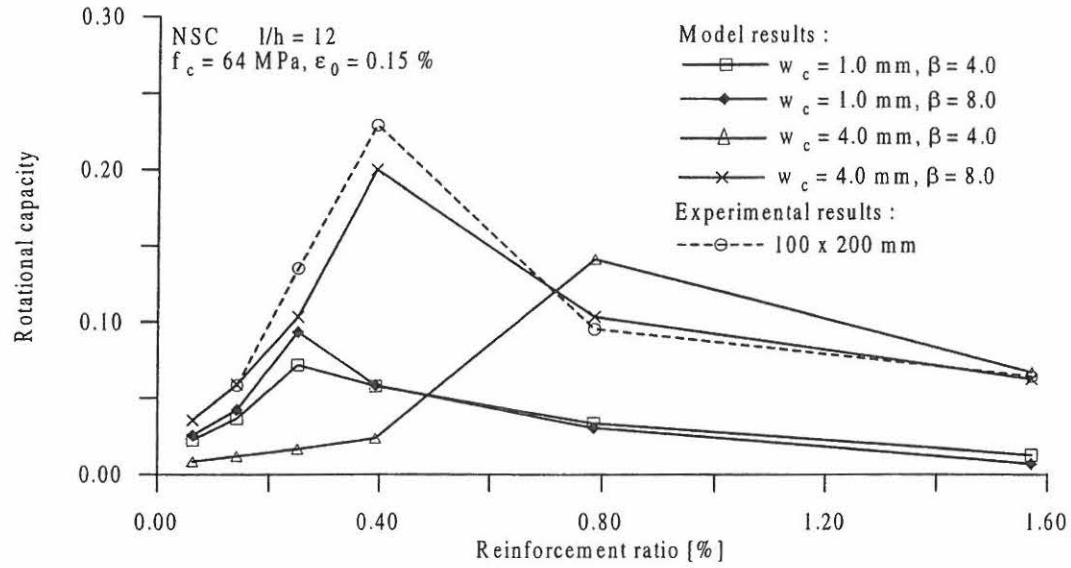

Figure 6.2: *Model Results compared with experimental results for 100 x 200 x 2400 mm normal strength concrete beams varying the key parameters wc = 1.0 - 4.0 mm and β = 4.0 - 8.0.*

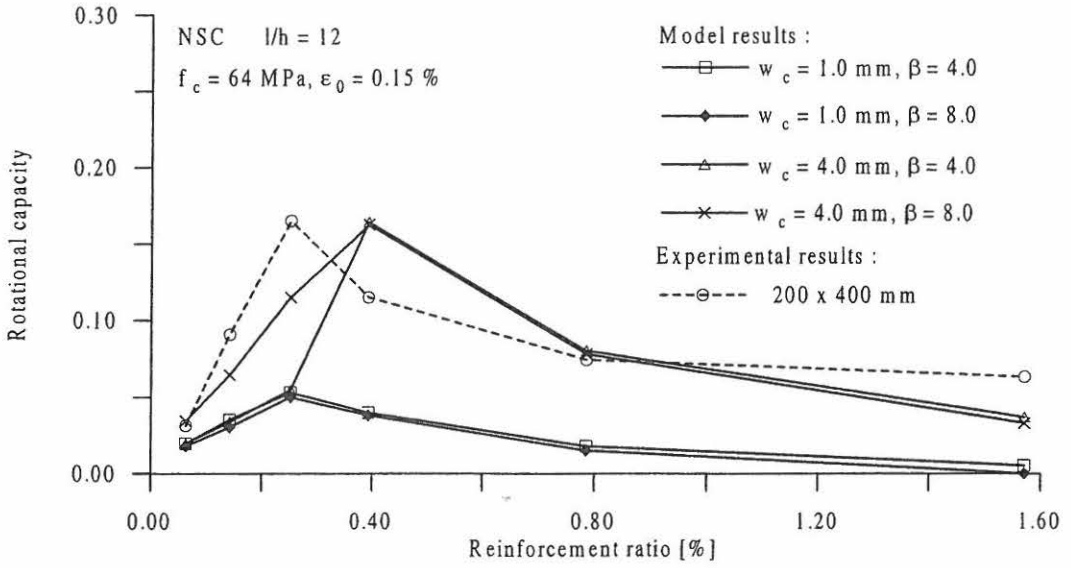

Figure 6.3: *Model Results compared with experimental results for 200 x 400 x 4800 mm normal strength concrete beams varying the key parameters wc = 1.0 - 4.0 mm and β = 4.0 - 8.0.*

Figure 6.4 shows, that using the values $w_c \cong 4$ mm and $\beta \cong 8$, the rotational capacity estimated by the model compares reasonable well with experimental results for all the three beam sizes.

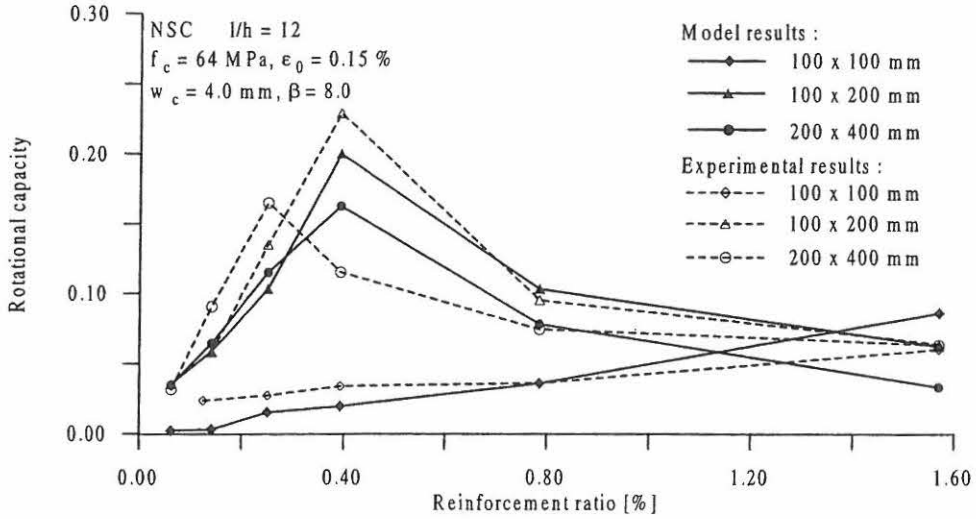

Figure 6.4: *Model Results compared with experimental results for 200 x 400 x 4800 mm normal strength concrete beams with key parameters wc = 4.0 mm and* $\beta = 8.0$.

It should however be noted, that the influence of the loading arrangement for the tests, where the loading plate used for distribution of the concentrated load might act as confinement, which could cause the rather high values of β and w_c . The loading plate is not taken into account in the calculation model.

For the heavily reinforced beams in *ESIS 2* described in chapter 5, the modelled plastic rotational capacity, $\theta_{cal,2}$ are shown as a function of the reinforcement ratio for the key parameters: $\beta = 8.0$ and $w_c = 4.0$ mm in Figure 6.5. It is observed, that the major differences in the model and experimental values are largest for the beams confined with stirrups. For the reinforcement ratios 2.45 % and 2.76 % it seems to be a good agreement between the values.

In Figure 6.6 the best estimates of the load displacement curves are shown. The key parameters used for the model are listed in Table 6.1 together with the plastic rotational capacity. It is observed, that the value of the critical compression deformation w_c differs from 4.0 mm for the beams with steel-fibers and stirrups. It is also observed, that the modelled load-displacements curves fit well for the reinforcement ratios of 0.78 % and 1.57 % especially for the plain concrete and stirrups confinement. The model will try to estimate the area under the load deflection curve and compare it with the experimental result. That is why for steel-fiber confinement the values seem to fit very well, see Table 6.1, even though the peak load for reinforcement ratios 2.45 % and 2.76 % are over-estimated, and there also seems to be a feedback in the compression stress-strain curve for the softening response.

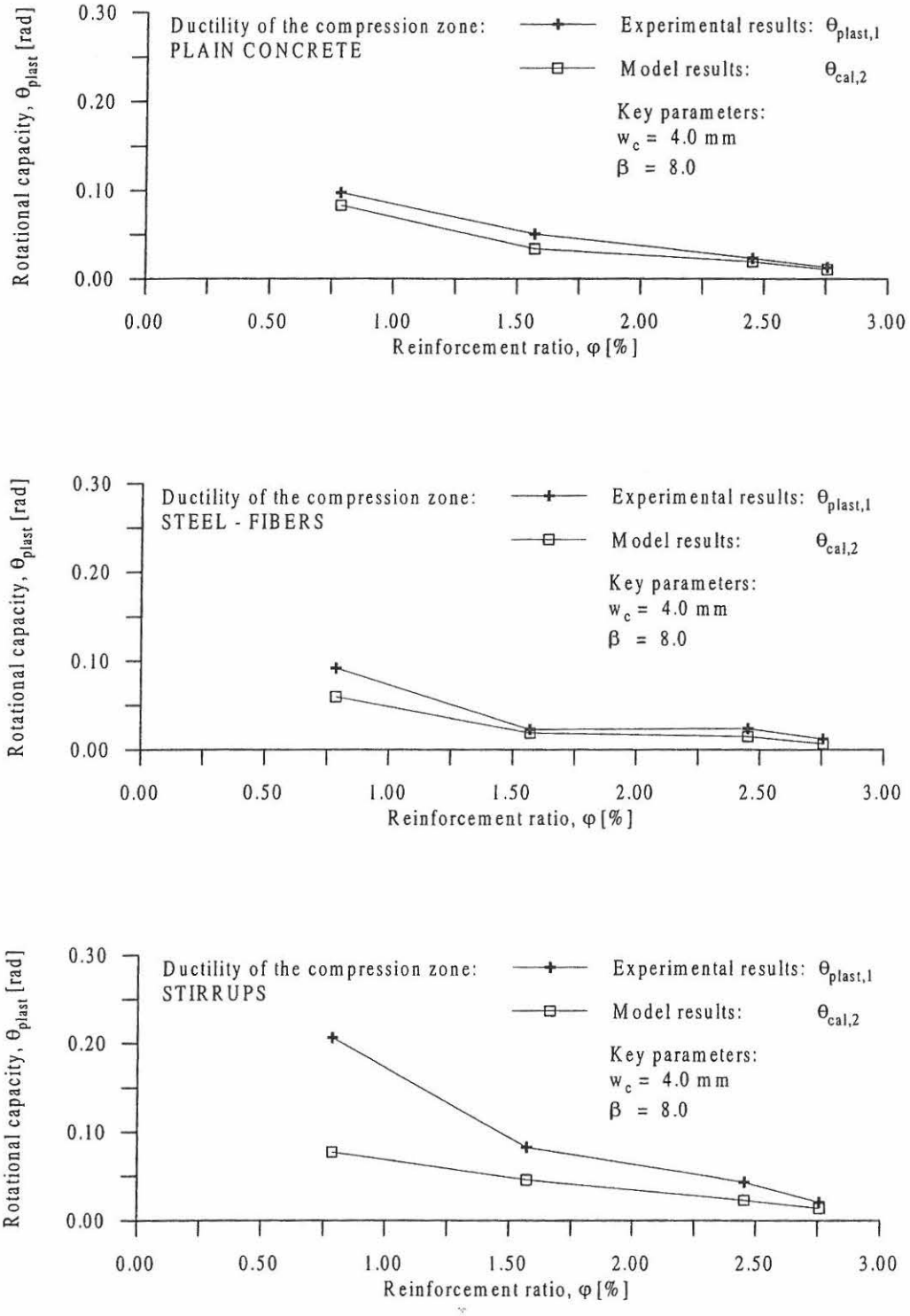

Figure 6.5: *Modelled and experimental plastic rotational capacity obtained from the plastic work under the load-deflection curve as a function of the reinforcement ratio for the heavily reinforced beams from ESIS 2 with confinement types for the mid section of the beam: plain concrete (top), steel-fibers (middle) and stirrups (bottom).*

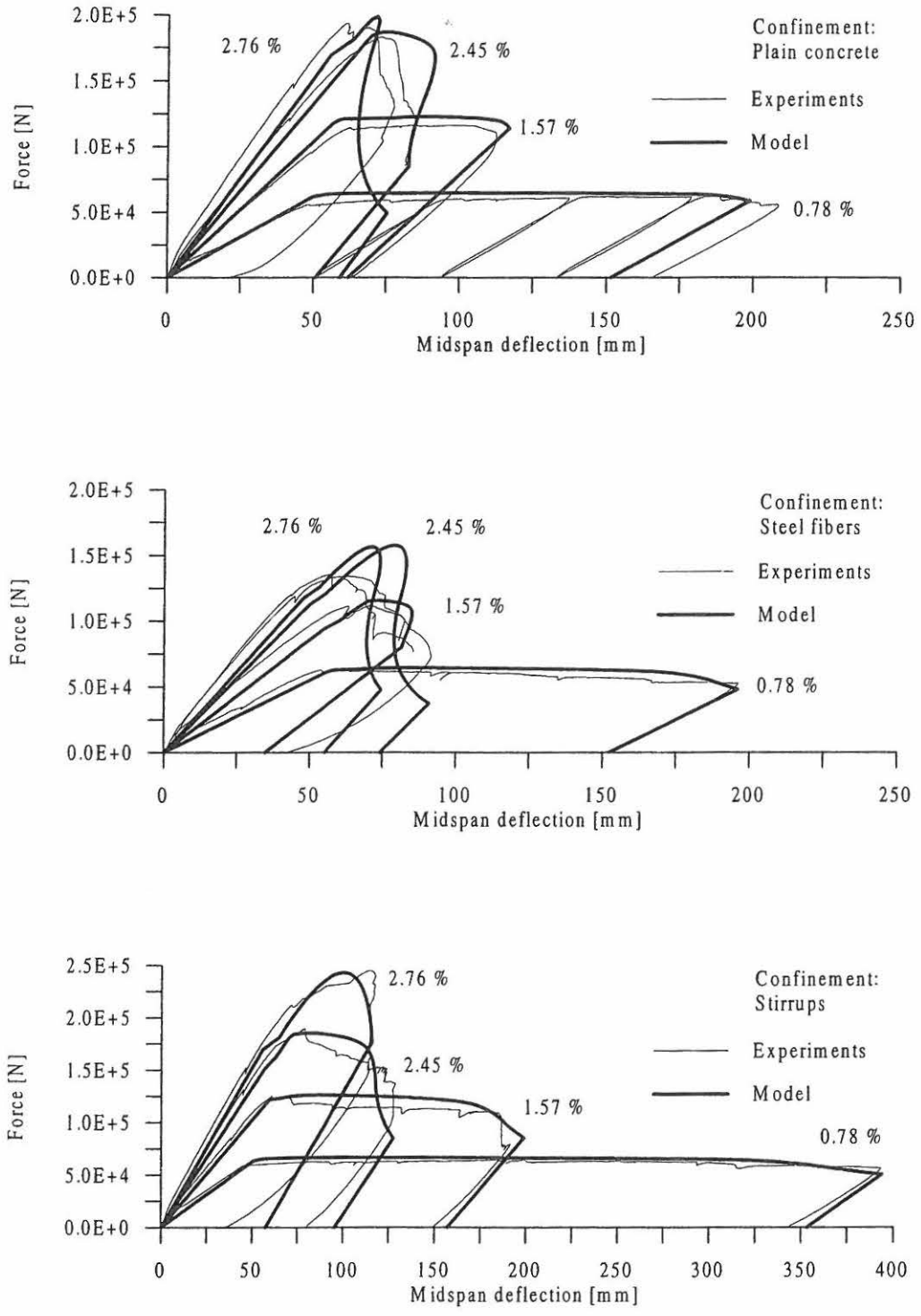

Figure 6.6: *Modelled best fits compared with the experimental load-displacements curves for the heavily reinforced concrete beams from ESIS 2 with confinement types in the mid section of the beam: plain concrete (top), steel-fibers (middle) and stirrups (bottom).*

Beam	Key Parameters		Model	Experiment
	β	w_c	$\theta_{cal,2}$	$\theta_{plast,1}$
	[-]	[mm]	[10^{-2} rad]	[10^{-2} rad]
Plain concrete confinement				
In_078_N	8.0	4.0	8.28	9.69
In_157_N	8.0	4.0	3.36	5.02
In_245_N	1.0	4.0	2.32	2.31
In_276_N	6.0	4.0	1.11	1.29
Steel-fibers confinement				
In_078_F	4.0	8.0	8.03	9.14
In_157_F	4.0	5.0	1.71	2.26
In_245_F	4.0	7.0	2.30	2.39
In_276_F	4.0	6.0	1.22	1.19
Stirrups confinement				
In_078_S	4.0	11.0	18.8	20.6
In_157_S	4.0	10.0	8.08	8.22
In_245_S	4.0	8.0	4.30	4.30
In_276_S	7.0	12.0	2.01	2.06

Table 6.1: *Best fits and model results for the plastic rotational capacity using the plastic work under the load-deflection curve of the heavily reinforced concrete beams from ESIS 2 assuming failure reponses and ultimate failure points corresponding to the modelled load-displacements curves shown in Figure 6.6.*

6.2 Modelling of Lightly Reinforced Beams

Some results of modelling the lightly reinforced concrete beams are given in this section using the tools of chapter 2 for *ESIS 1* beams, and a model taken into account the tensile failure process of the concrete and the debonding between concrete and reinforcement using a direct subtructure method for *ESIS 2* beams. The model is suitable for discrete cracking showing a single crack failure, and predicts the prepeak load deflection behaviour, see Brincker *et al.* (1999). It is also possible to incorporate a yield plateau for the steel in order to predict the ultimate failure point, but this is left out of the investigation herein.

Using the model described in chapter 2, it is shown from Figure 6.7 and 6.8 how the model compares with the experimental results for the rotational capacity. In Figure 6.7 the case of normal strength concrete is shown.

In case of reinforcement ratios of 0.14 % and 0.25 % the model results fit the experiments well, whereas in some cases of 0.39 % reinforcement ratio the experiments show, that the reinforcement tensile failure is no longer the dominating failure mode and therefore the model over-estimates the rotational capacity. The experimental results show, as the model, that the rotational capacity is higher in the case of normal strength concrete.

Some results of modelling of the pre-peak behaviour of the lightly reinforced beams from *ESIS 2* are shown in Figure 6.9 and 6.10. In Figure 6.9 estimates on the load displacement response for the high strength concrete beams reinforced with smooth plain rebars Gn_6AN_H are given for the bond shear models. In Figure 6.10 estimates are given for the high strength concrete beams reinforced with ribbed bars En_014_H are given. Further estimates and explanations of the DSM modelling of the experiments are listed in Henriksen *et al.* (1998).

It is observed from the model results for the *ESIS 2* beams, that the stiffness of the modelled curves are higher than the experimental curves. This could be due to the fact, that the deflection of the midspan is plotted as the measured stroke, which could contain contributions from the loading arrangement and steel-axes frame. The input value for the elasticity of the concrete are here defined as 40000 N/mm^2, which are the experimental value from the *ESIS 1*. The influence of changing this value in the range of 30000 - 45000 N/mm^2 has been left out of the analyses.

Using two bond models it is observed, that the yielding of the reinforcement starts at an earlier point for the high bond shear strengths of bond model 2 than for the lower values of bond model 1. The pull-out of the reinforcement seems to take place at higher load for the bond model 2.

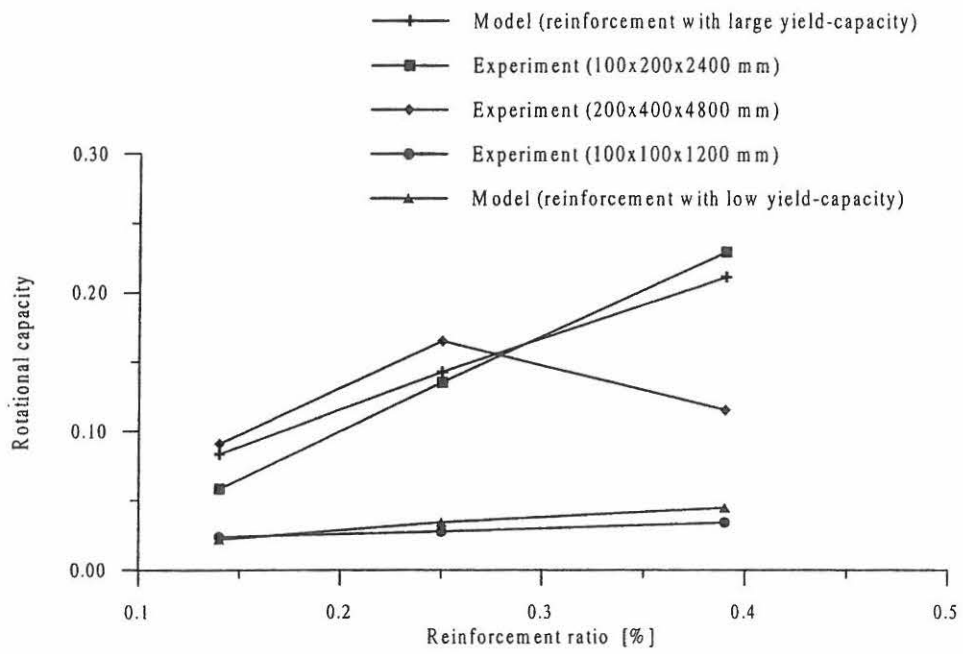

Figure 6.7: *Comparison between rotational capacities obtained from model and experiments (normal strength concrete).*

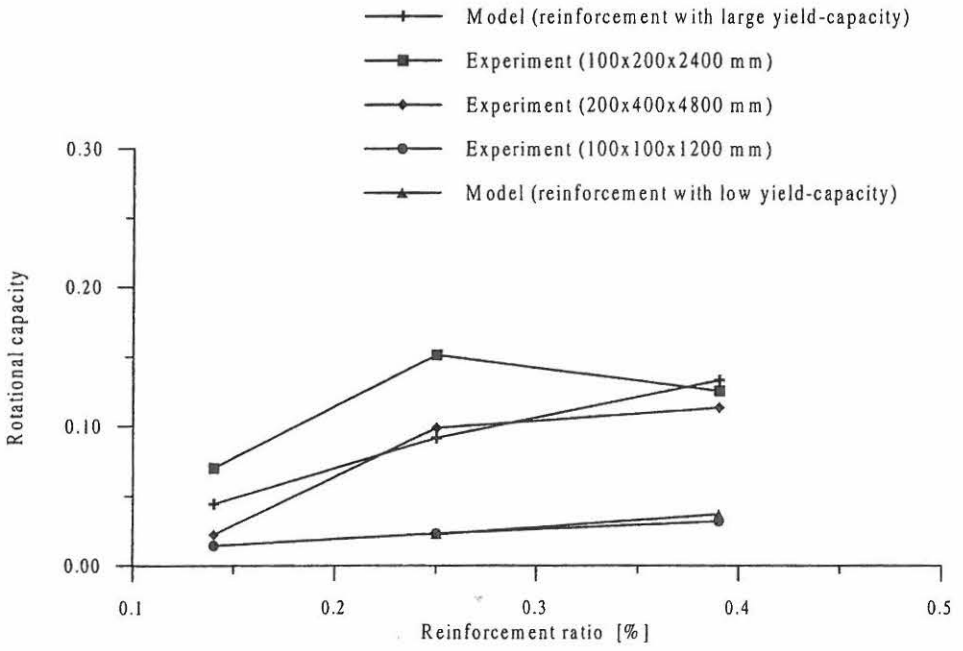

Figure 6.8: *Comparison between rotational capacities obtained from model and experiments (high strength concrete).*

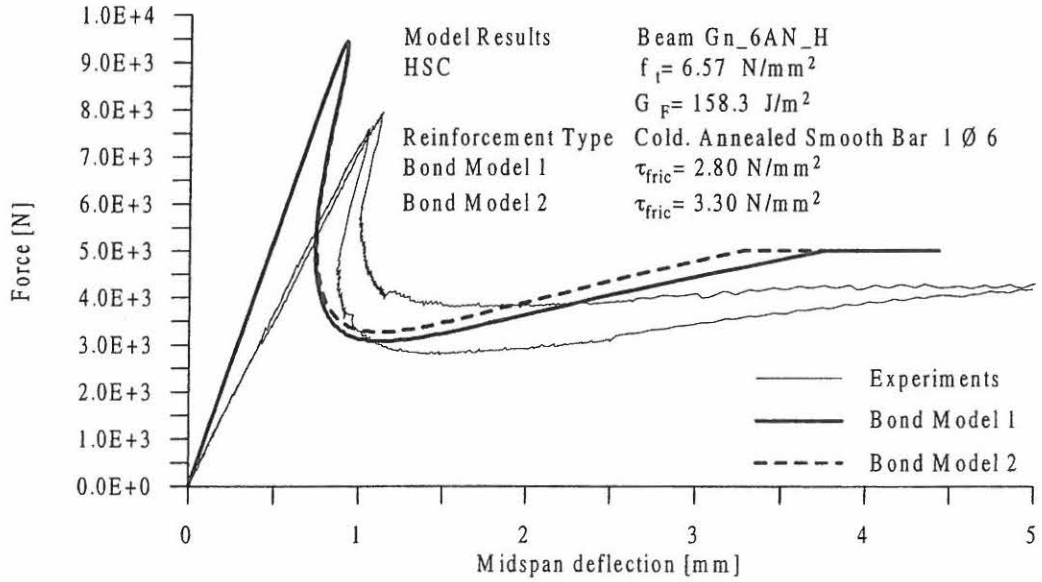

Figure 6.9: *Modelled load deflection curves with two different bond models compared with experiments for Gn_6AN_H.*

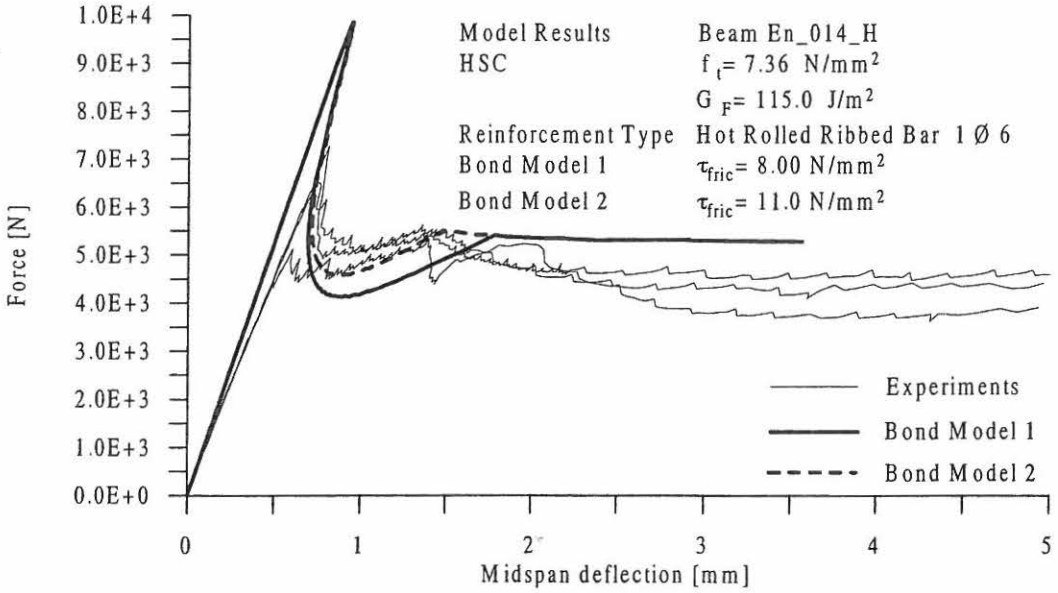

Figure 6.10: *Modelled load deflection curves with two different bond models compared with experiments for En_014_H.*

Chapter 7

Conclusion and Summary

In this chapter the outline of the thesis is summarized and conclusions are given. Some suggestions to further research are described.

This thesis contains experimental results for normal strength and high strength concrete beams with reinforcement ratios ranging from very low to very high ratios. All kinds of reinforced states have been investigated by analytical and experimental methods. Two research projects *ESIS 1* and *ESIS 2* have been established in order to examine plastic rotational capacity of both normal strength concrete at concrete grade C50 and high strength concrete at concrete grade C90.

A large test programme has been performed in connection with a Round Robin on " Scale Effects and Transitional Failure Phenomena of Reinforced Concrete Beams in Flexure " in cooperation with the European Structural Integrity Society. At Aalborg University approximately 120 beams have been tested. The main results have been presented as load displacements curves, and three different models for calculating the rotational capacity have been applied.

Investigations of measured curvature distributions for test beams have shown, that for low reinforcement ratios the curvature is very concentrated around one or a few cracks, which develop in these types of beams. However, when increasing the reinforcement ratio the cracks develop all over the beam, and therefore the curvature will not be so concentrated resulting in a larger plastic rotational capacity.

Estimates of the experimental plastic rotational capacity was performed using models based on CEB-FIP Model Code 1990, on plasticity theory and on measuring the rotations of the beam supports. The results have shown, that the rotational capacity according to the CEB-FIP Model Code and to rotations of beam supports are almost the same in most cases. The rotational capacity is observed to be lower for a beam size of 100 x 100 mm than for the two other beam sizes investigated. This could be due to the lack of yield capacity of the ø4 and ø5 cold-deformed reinforcement. Also it has been observed, that the mechanical properties of the reinforcement are very important for achieving sufficient rotational capacity of beams at very low reinforcement

ratios, because here the failure mode is tensile failure of the steel bars. For beams with reinforcement ratios 0.25 %, 0.39 % and 0.78 % bending failure occurs resulting in either compression failure of the concrete or tensile failure of the reinforcement. Taking into account the scatter in the results, it has been difficult to conclude on any major size effects for the experiments.

A continuation and extension of the large test programme on "Scale Effects and Transitional Failure Phenomena of Reinforced Concrete Beams in Flexure" was established for the very low and very high reinforcement ratios in order to incorporate also very brittle and very ductile behaviour of beams subjected to ultimate failure. At the Structural Research Laboratory, Aalborg University 10 heavily reinforced concrete beams and 14 lightly reinforced concrete beams was tested to ultimate failure in a three point bending servo controlled testing materials set-up under *ESIS 2*.

Results of these investigations of the ductility of the beams have been presented as curves showing the plastic rotational capacity as a function of the reinforcement ratio. The experimental results of the plastic rotational capacity have shown, that heavily reinforced beams with several stirrups placed in the hinge of the beam predict a very high ductility compared with beams confined with plain concrete and steel-fibers without stirrups in the hinge of the beam. The plastic rotational capacity of the lightly reinforced concrete beams are very dependent on the type of reinforcement. The results show, that smooth reinforcement bars give a very high ductility compared with beams reinforced with ribbed steel rebars. The bond shear strength between the rebar and the concrete plays a major role in the ductility of lightly reinforced concrete beams.

Some methods have been adopted in modelling of the load displacements curves for the test beams. For the heavily reinforced regime a model taking into account the softening of the concrete in compression and taking into account, that the ultimate compressive uniaxial strain could depend on the size of the structure has been presented. The failure modes of the heavily reinforced beams have been analyzed using different values of the key parameters for the model. The key parameters have been defined as a compression softening deformation, w_c and a characteristic length parameter, β dependent on the length of the failure zone. It has turned out, that to achieve reasonable model load displacements curves, the key parameters had to be of the values $w_c = 4.0\ mm$ and $\beta = 8.0$ for the beams with plain concrete and steel-fiber confinement. For the beams confined with several stirrups, the values turned out to be somewhat higher giving $w_c = 4.0 - 7.0\ mm$ and $\beta = 8.0 - 12.0$. The effect of the extra confinement from the loading plate could be a reason to the high values of the key parameters. The contributions from the loading plate were not incorporated in the model.

For the lightly reinforced beams analyses of the load displacement behaviour of the midspan of the beam to a maximum stroke of 5 *mm* have been presented. A model based on the Direct Substructure Method (DSM) has been presented and the input parameters were given as the bond shear strength between the reinforcement and the concrete together with the material parameters of the reinforcement and the concrete. Only a few simulations have been performed to model the first part of the load displacements curves, and there seems to be a reasonable agreement between the modelled and experimental curves. A parametric study of the influence and changing of the key parameters found by the experiments on the first part of the load displacement response was

left out of the investigations.

In the past 5 to 10 years a lot of research have been focused on the softening behaviour of the stress-strain relation in uniaxial and multiaxial compression, and a lot of research are being performed on the subject of finding and explaning size effects in the compression softening relation. Until now, not that many researchers are examined reinforced concrete structures using a size effect law for the compression zone in a structure. But, Round Robin on strain softening in compression and ductility of reinforced concrete structures are being performed of CEB FIP and RILEM task groups, so further research in this area are needed.

Also, research on the practical use of high strength concrete beyond C50 for concrete structures are needed, e.g. investigations on serviceability limit states focusing on the cracking response and possibilities of adding steel-fibers and on ultimate limit states focusing on the new rules for sufficient ductility.

Chapter 8

References

An, L. and Cederwall, K. (1995): *Rotational Capacity of Concrete Beams, - summary of Re-evaluation of Test Results*, Chalmers University of Technology, Division of Concrete Structures, Göteborg, Sweden, Report 95:1, May 1995, 19 pp.

Betonghandbok (1990): *Betonghandbok, Konstruktion*, utgåva 2, AB Svensk Byggtjänst. Redigerad av K. Cederwall (CTH), M. Lorentsen (KTH), L. Östlund. In Swedish.

Bosco, C. and Carpinteri, A. (1993): *Proposal for a Round Robin on Scale Effects and Transitional Failure Phenomena of Reinforced Concrete Beams in Flexure*, July 1993. European Structural Integrity Society, Technical Commitee 9 on Concrete.

Brincker, R., M. S. Henriksen, F. A. Christensen and G. Heshe (1999): *Size Effects on the Bending Behaviour of Reinforced Concrete Beams*. In: Minimum Reinforcement in Concrete Members. ESIS Publication 24. Edited by A. Carpinteri.

CEB Bulletin 228 (1995): *High Performance Concrete*, Comité Euro-International du Beton, CEB Bulletin d'Information N° 228, July 1995.

CEB Bulletin 242 (1998): *Ductility of Reinforced Concrete Structures*, Comité Euro-International du Beton, CEB Bulletin d'Information N° 242, May 1998.

CEB-FIP Model Code 1990 (1991): *CEB - FIP Model Code 1990 - Final Draft*, The Euro-International Commitee for Concrete and the International Federation for Prestressing, Bulletin d'Information N° 203, July 1991.

DS 411 (1997): *Code of Practice for the Structural Use of Concrete*, Draft for new code proposal, July 1997.

Eurocode 2 (1993): *Design of Concrete Structures*, Part 1-1: General rules and rules for buildings, 2. edition, March 1993.

Fransson, H. (1997) *Rotation Capacity of Reinforced High Strength Concrete Beams*, Licentiate Thesis, Royal Institute of Technology, Department of Structural Engineering, Stockholm, Sweden, Bulletin 32, 1997.

Henriksen, M. S., J. P. Ulfkjær and R. Brincker (1996): *Scale Effects and Transitional Failure Phenomena of Reinforced Concrete Beams in Flexure. Part 1,* Fracture & Dynamics Paper No. 81. Department of Building Technology and Structural Engineering, Aalborg University, Denmark.

Henriksen, M. S., R. Brincker and G. Heshe (1998): *Rotational Capacity of Heavily and Lightly Reinforced Concrete Beams*, Scale Effects and Transitional Failure Phenomena of Reinforced Concrete Beams in Flexure, Part 2. Final report to the Danish Technical Research Council, STVF. Structural Research Laboratory, Department of Building Technology and Structural Engineering, Aalborg University, Denmark. October 1998.

Hillerborg, A. (1988): *Rotational Capacity of Reinforced Concrete Beams*, in Nordic Concrete Research, no. 7, pp. 121-134.

Hillerborg, A. (1990): *Fracture Mechanics Concepts Applied to Moment Capacity and Rotational Capacity of Reinforced Concrete Beams*, Engineering Fracture Mechanics, vol. 35, No. 1/2/3, pp. 233-240. 1990.

Hillerborg, A. (1991): *Size Dependency of the Stress-Strain Curve in Compression*, in Analysis of Concrete Structures by Fracture Mechanics, Rilem Report 6, eds. L. Elfgren & S. P.Shah, Chapman & Hall, London, pp. 171-178.

Jansen, D.C. and S.F. Shah (1997): *Effect of Length on Compressive Strain Softening of Concrete*, in Journal of Engineering Mechanics, vol. 123, No. 1, pp. 25-35.

Markeset, G. (1995): *A Compressive Softening Model for Concrete*. In: Fracture Mechanics of Concrete Structures, Proceedings FRAMCOS-2, edited by Folker H. Wittmann.

Meyer, J. (1997): Deformation Capacity of the Concrete Compression Zone - Stress-Strain Curves for Non-Linear Calculation. In: Leipzig Annual Civil Engineering Report (LACER), no. 2, 1997, pp. 87-102.

Mihashi, H. (1998): *FRAMCOS-3*, Proceedings of the Third International Conference on Fracture Mechanics of Concrete Structures, Gifu, Japan, vol. 2, October 1998.

Plem, E. (1977): *Rotationskapacitet hos flytleder i armerade betongbalkar - en teoretisk studie*. Rapport 50:1977. Statens råd för byggnadsforskning, Stockholm, 1977. In Swedish.

Stang, H. (1996) *Compression Tests carried out at the Technical University of Denmark for the ESIS - TC9 Project.* Report not published yet.

Ulfkjær, J. P., van Mier J. G. M and Stang H. (1997): *Invitation to Competition on Modelling of Over-reinforced Concrete Beams*, pp. 1 -33. RILEM TC 148 SSC.

Ulfkjær, J. P. and Brincker, R. (1995): *Fracture Energy of Normal Strength Concrete, High Strength Concrete and Ultra High Strength Ultra Ductile Steel Fibre Reinforced Concrete*, in Fracture Mechanics of Concrete Structures, Vol. 1., pp. 31 - 44, 1995.

van Mier, J. G. M *et al.* (1997): *Strain Softening of Concrete in Uniaxial Compression*, Report of Round Robin Test by RILEM TC 148-SSC, in Materials and Structures, vol. 30, pp. 195-209, May 1997.

van Vliet, M. R. A. and van Mier, J. G. M. (1995): *Strain Softening Behaviour of Concrete in Uniaxial Compression*, Delft University of Technology, Department of Civil Engineering, Report no. 25.5-95-9, May 1995. 87 pp.

van Mier, J.G.M. (1986): *Multi-axial Strain-Softening of Concrete*, in Materials and Structures vol. 19, No. 111, Rilem, pp. 179-200.

Vonk, R. A. (1993). *A Micromechanical Investigation of Softening of Concrete loaded in Compression*, in Heron, vol. 38, No. 3.

Wittmann, F. H. (1995): *FRAMCOS-2*, Proceedings of the Second International Conference on Fracture Mechanics of Concrete Structures, ETH, Zurich, Switzerland, vol. I, July 1995.

Öberg, S (1977): *Flytledsteori för armerade betongbalkar på oeftergivliga stöd. Analys av försögsresultat.* Rapport 77:11. Inst för Betongbyggnad, CTH, december 1977.

Chapter 9

Summary in Danish

Titlen på denne afhandling er *Deformationskapacitet og Revner i Armerede Beton Bjælker*, og som titlen antyder, drejer det sig om beton bjælkers evne til at deformere sig og dannelse af revner i bjælker.

Afhandlingen har omfattet to forsøgsprogrammer, hvor hovedformålet har været at bestemme beton bjælkers rotationskapacitet her angivet som en deformationskapacitet, som er et udtryk for bjælkers evne til at optage plastiske deformationer, som kommer fra flydning i armeringsstålet og brud t betonens trykkede zone.

Forsøgsprogrammerne har været en del af en større projekt i samarbejde med andre forskningsinstitutioner, som har udført fælles forsøg ud fra det samme oplæg.

Instituttet har udført i samarbejde med 7 udenlandske universiteter forskningsprojektet "Størrelseseffekter af armerede betonbjælker - rotationskapacitet og minimumsarmering". Målet med projektet har været at udføre en forsøgsrække, der har skullet afklare, hvorledes rotationskapaciteten afhænger af dimensionen, armeringsgraden samt konstruktionens slankhed for både højstyrke- og normalstyrkebeton. Derudover er der undersøgt, hvorledes bæreevnen og sejheden af svagtarmerede betonbjælker er afhængig af de samme variable. Der er i 1994 støbt 159 bjælker, hvor størrelsen af bjælkerne varierer imellem 0,6 m og 7.2 m.

Der blev i tilknytning til projektet opbygget en ny meget fleksibel forsøgsopstilling, hvor hovedparten af bjælkerne er testet. Forsøgsprojektet er fulgt op af analytiske beregninger, hvor nye materialmodeller er blevet afprøvet. Projektet er støttet af STVF.

Appendix A

Test Results for Reinforced Concrete Beams of different Scale and Strength

In this appendix results for the load-deflection curve at the midspan of the beam, the normalized bending moment as a function of the measured rotation at the supports and the curvature distribution along the beam axis are listed for the beam included in *ESIS 1* investigations described in Chapter 4.

In the last section the values for the plastic rotational capacity calculated using the three methods described in Chapter 4 are given.

A1 Flexural Response Curves and Curvature Distribution for Test Beams in ESIS 1

The following curves show the actual load subjected to the test beam as a function of the measured displacement of the mid section.

The mid section displacement is measured as the stroke of the load cylinder.

The dimension of the beams are as follows

Type - b x h x l	Type - b x h x l	Type - b x h x l
A - 100 x 100 x 600 mm	D - 100 x 200 x 1200 mm	G - 200 x 400 x 2400 mm
B - 100 x 100 x 1200 mm	E - 100 x 200 x 2400 mm	H - 200 x 400 x 4800 mm
C - 100 x 100 x 1800 mm	F - 100 x 200 x 3600 mm	I - 200 x 400 x 7200 mm

A1.1 Test Results for Normal Strength Concrete Beams A, D and G with Reinforcement Ratio 0.78 % and Slenderness Number 6.

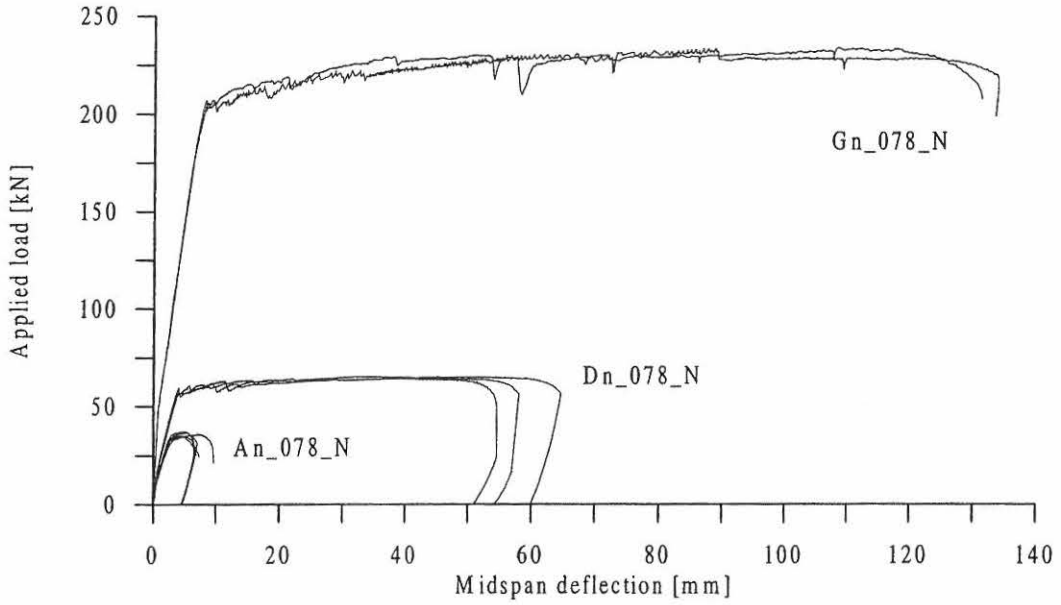

Figure A1.1: *Load-displacement curves for NSC beams A, D and G with reinforcement ratio 0.78 % and slenderness no. 6.*

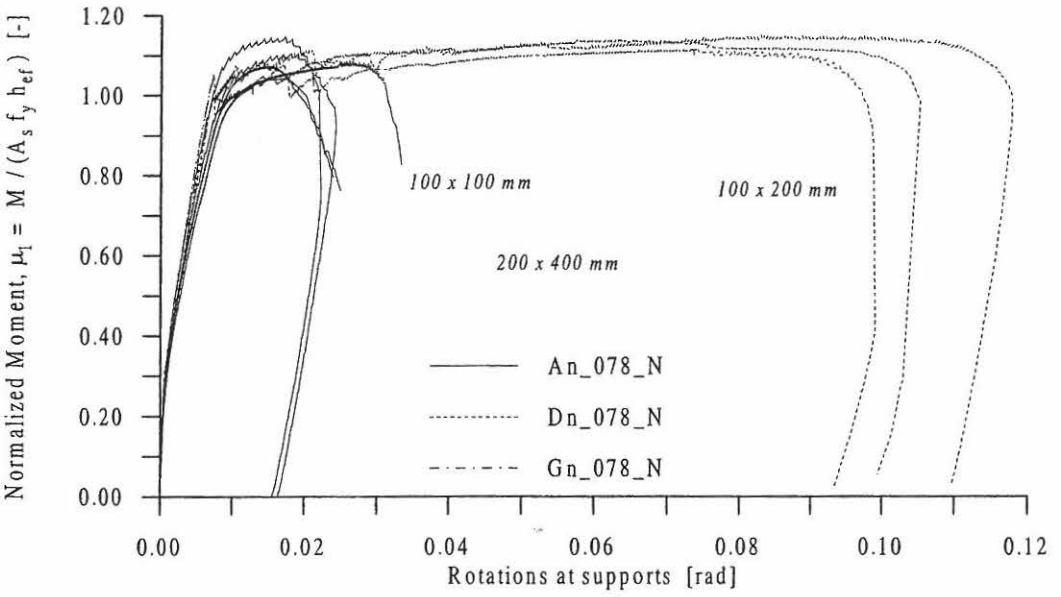

Figure A1.2: *The rotation measured at the supports as a function of the normalized moment, μ_1 for NSC beams A, D and G reinforcement ratio 0.78 % and slenderness no. 6.*

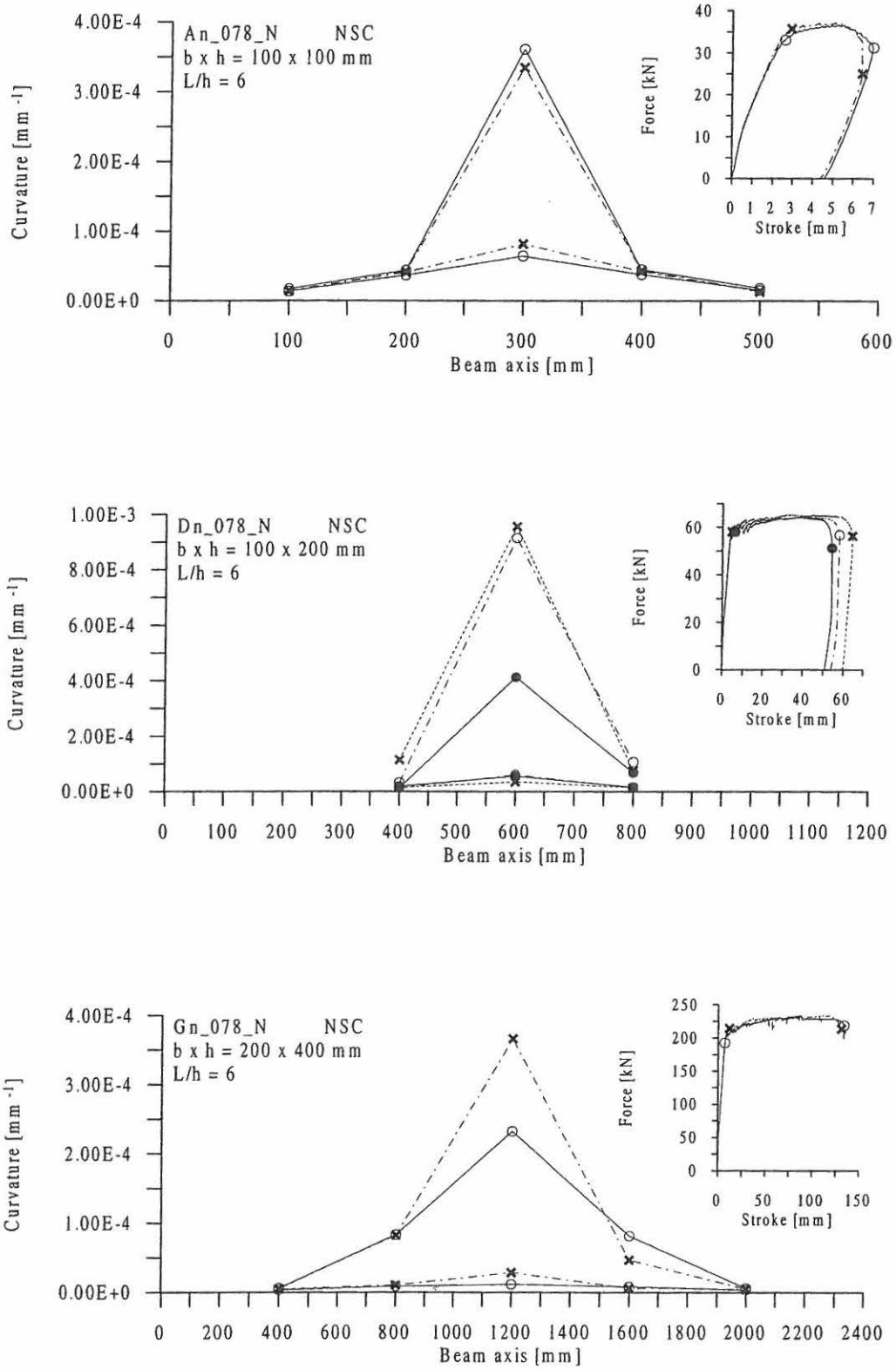

Figure A1.3: *Distribution of curvatures along the beam axis for NSC beams An_078_N (top), Dn_078_N (middle) and Gn_078_N (bottom).*

A1.2 Test Results for Normal Strength Concrete Beams B, E and H with Reinforcement Ratio 0.78 % and Slenderness Number 12.

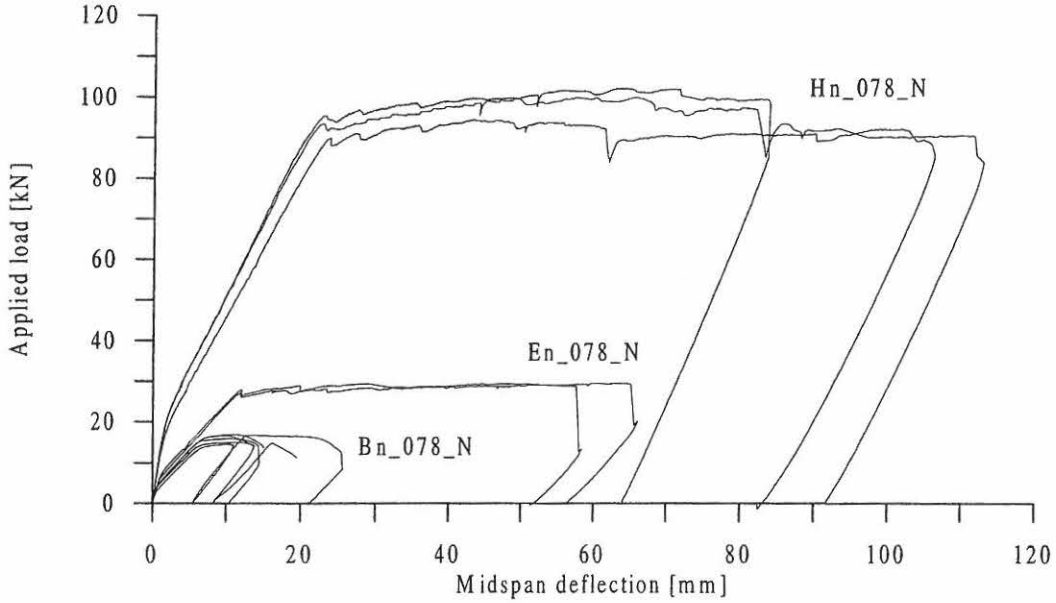

Figure A1.4: *Load-displacement curves for NSC beams B, E and H with reinforcement ratio 0.78 % and slenderness no. 12.*

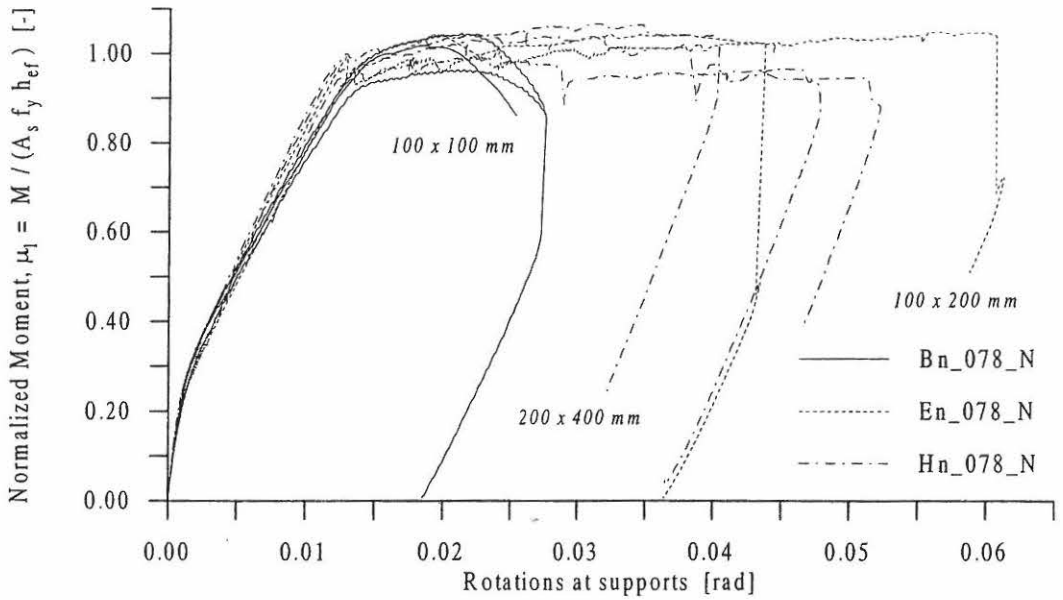

Figure A1.5: *The rotation measured at the supports as a function of the normalized moment, μ_1 for NSC beams B, E and H reinforcement ratio 0.78 % and slenderness no. 12.*

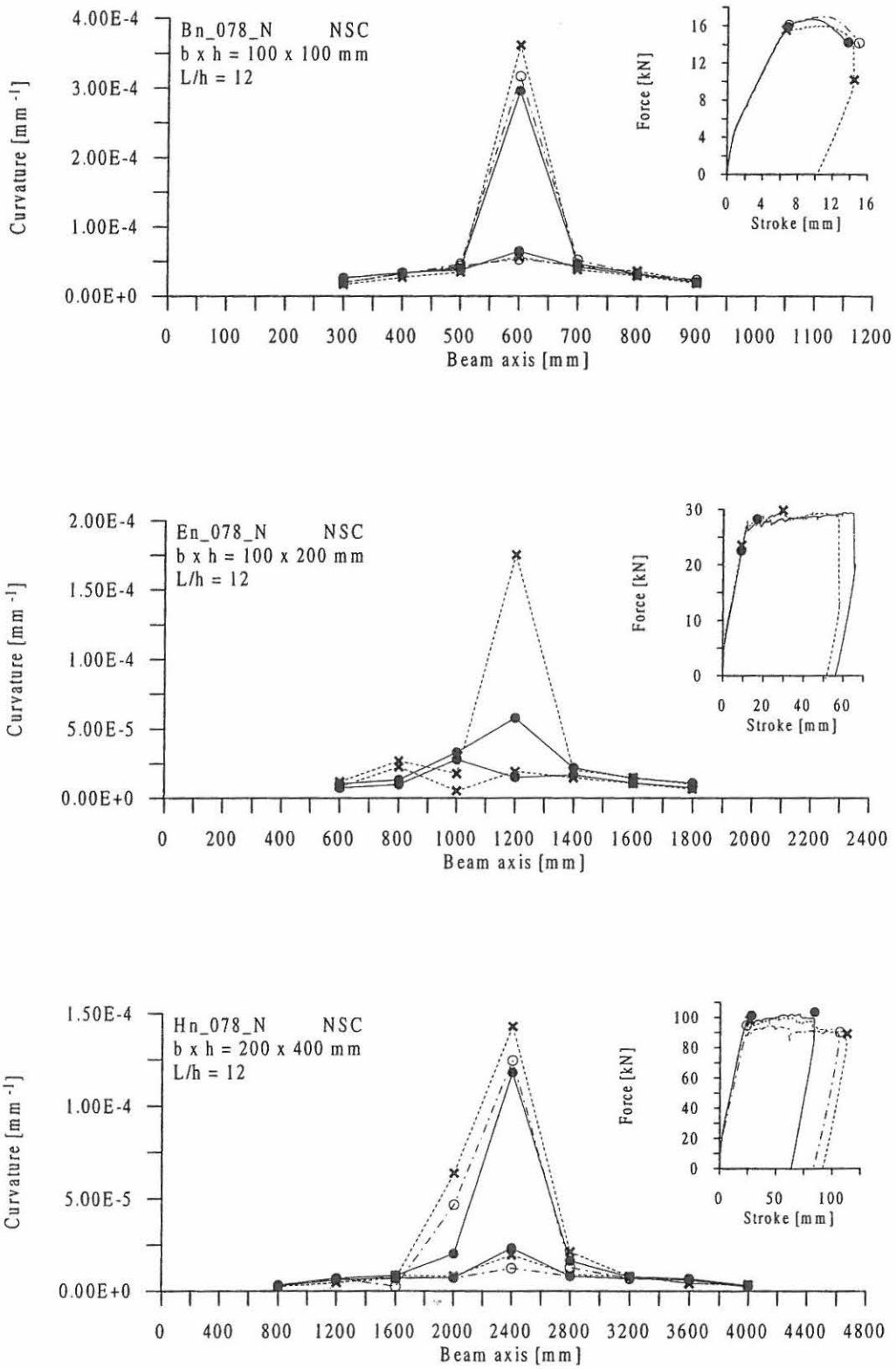

Figure A1.6: *Distribution of curvatures along the beam axis for NSC beams Bn_078_N (top), En_078_N (middle) and Hn_078_N (bottom).*

A1.3 Test Results for Normal Strength Concrete Beams C, F and I with Reinforcement Ratio 0.78 % and Slenderness Number 18.

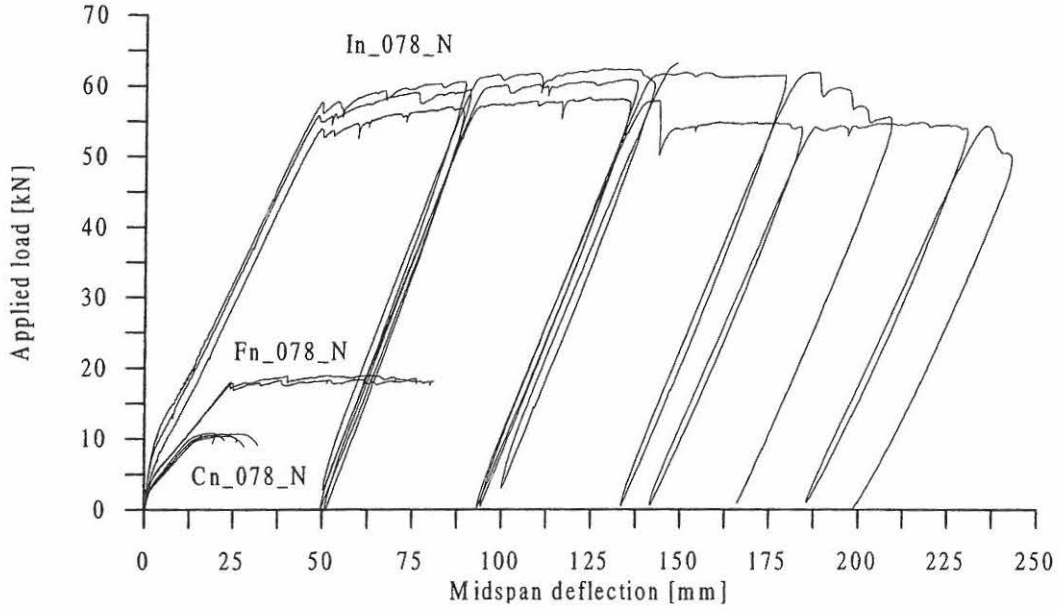

Figure A1.7: *Load-displacement curves for NSC beams C, F and I with reinforcement ratio 0.78 % and slenderness no. 18.*

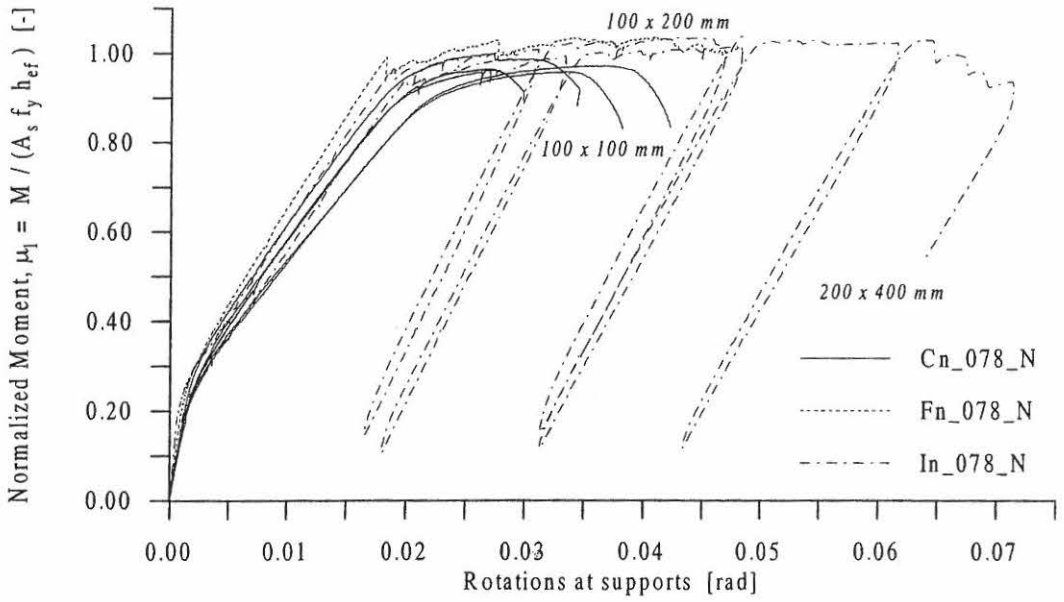

Figure A1.8: *The rotation measured at the supports as a function of the normalized moment, μ_1 for NSC beams C, F and I reinforcement ratio 0.78 % and slenderness no. 18.*

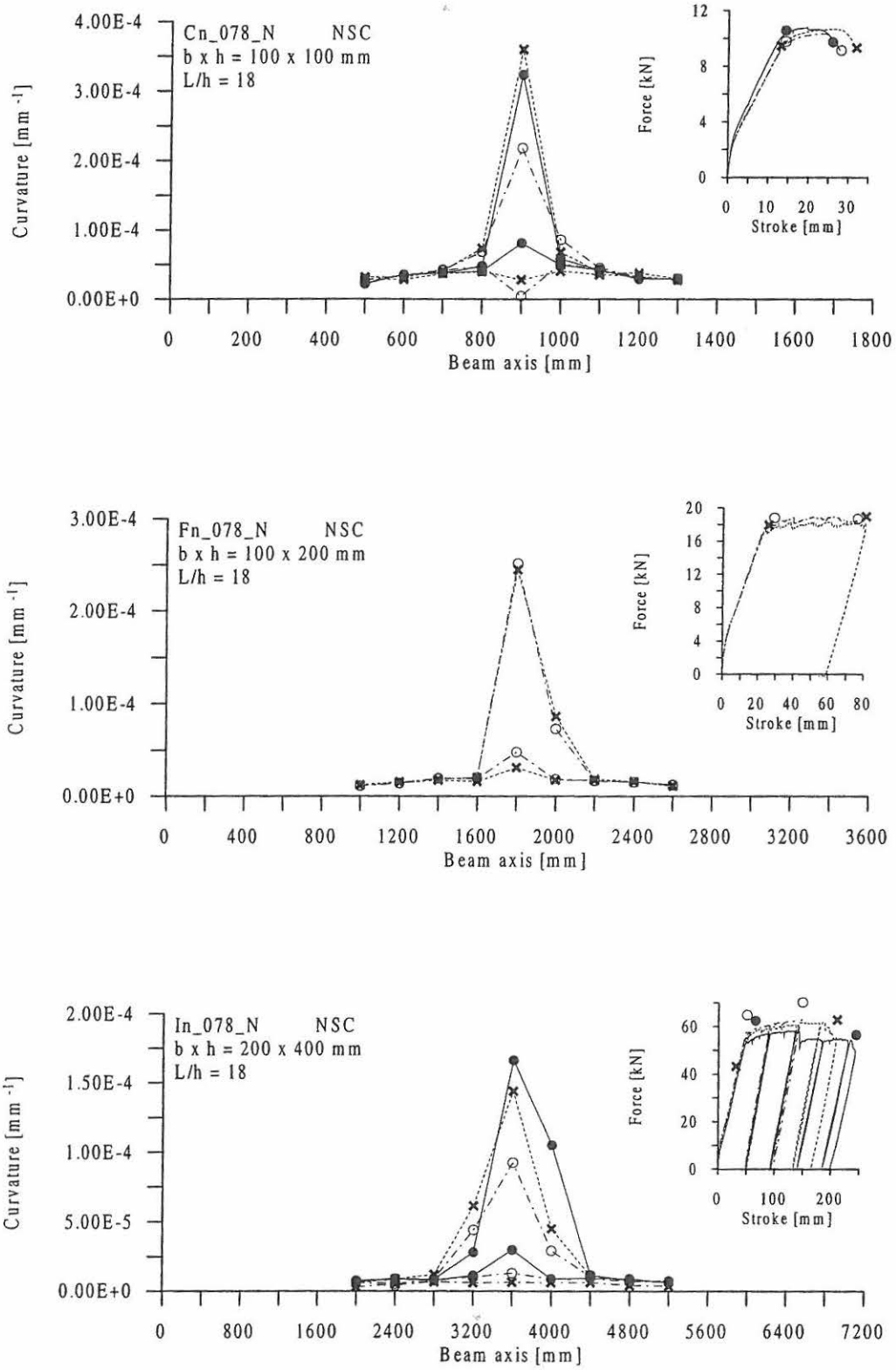

Figure A1.9: *Distribution of curvatures along the beam axis for NSC beams Cn_078_N (top), Fn_078_N (middle) and In_078_N (bottom).*

A1.4 Test Results for Normal Strength Concrete Beams A, D and G with Reinforcement Ratio 1.57 % and Slenderness Number 6.

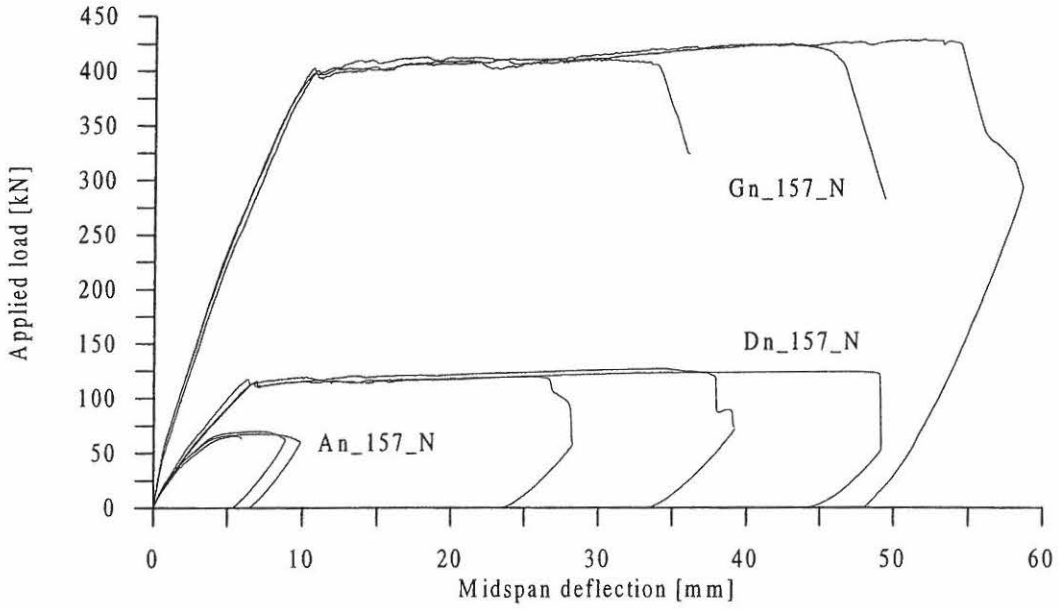

Figure A1.10: *Load-displacement curves for NSC beams A, D and G with reinforcement ratio 1.57 % and slenderness no. 6.*

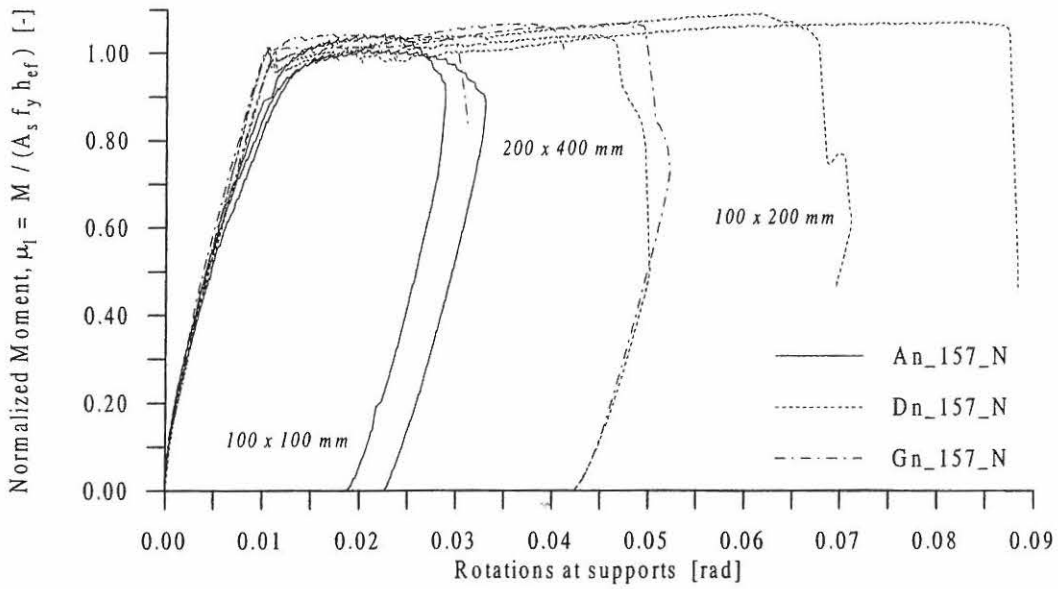

Figure A1.11: *The rotation measured at the supports as a function of the normalized moment, μ_1 for NSC beams A, D and G reinforcement ratio 1.57 % and slenderness no. 6.*

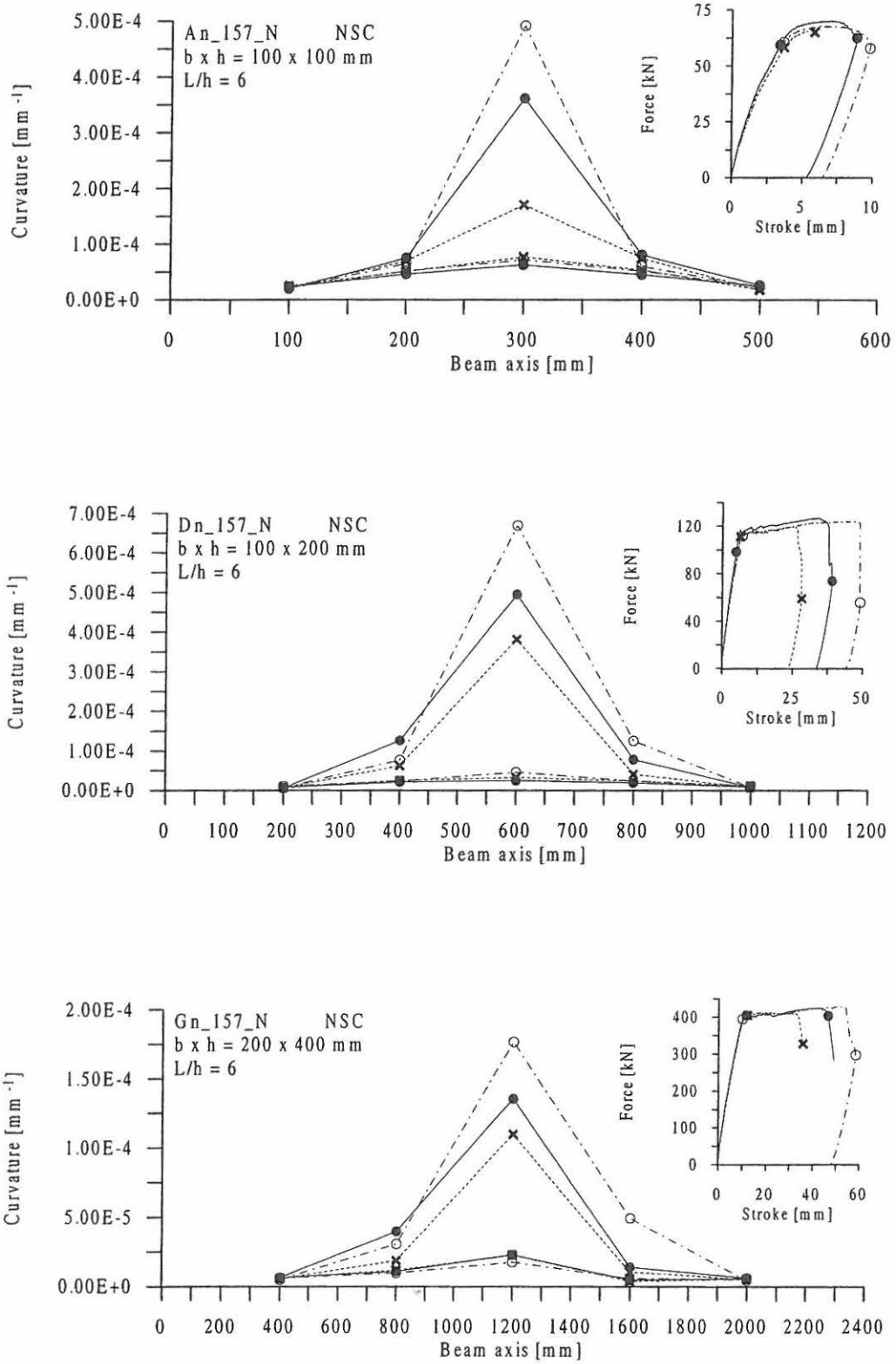

Figure A1.12: *Distribution of curvatures along the beam axis for NSC beams An_157_N (top), Dn_157_N (middle) and Gn_157_N (bottom).*

A1.5 Test Results for Normal Strength Concrete Beams B, E and H with Reinforcement Ratio 1.57 % and Slenderness Number 12.

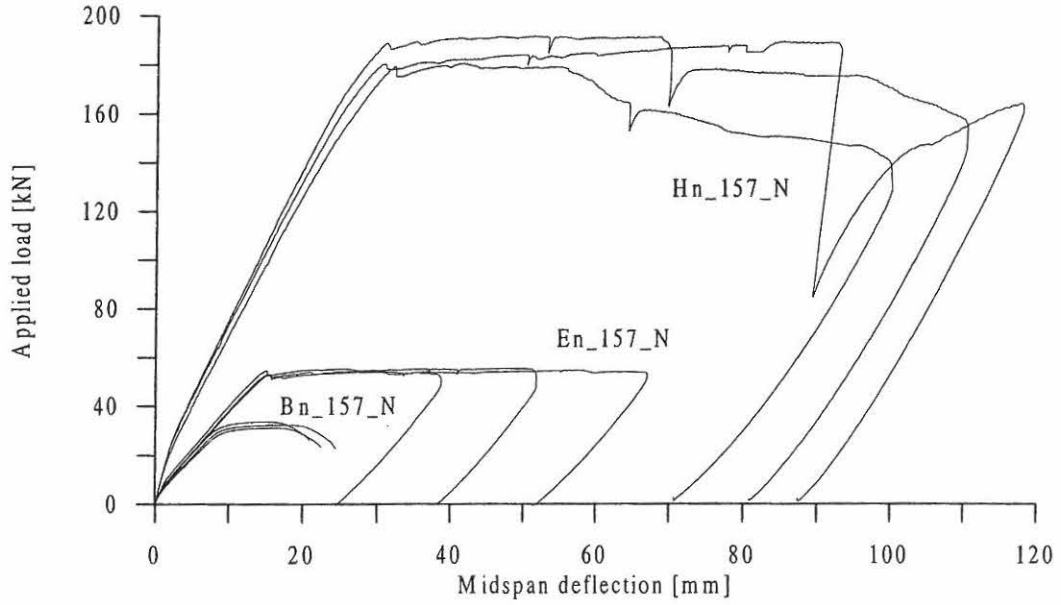

Figure A1.13: *Load-displacement curves for NSC beams B, E and H with reinforcement ratio 1.57 % and slenderness no. 12.*

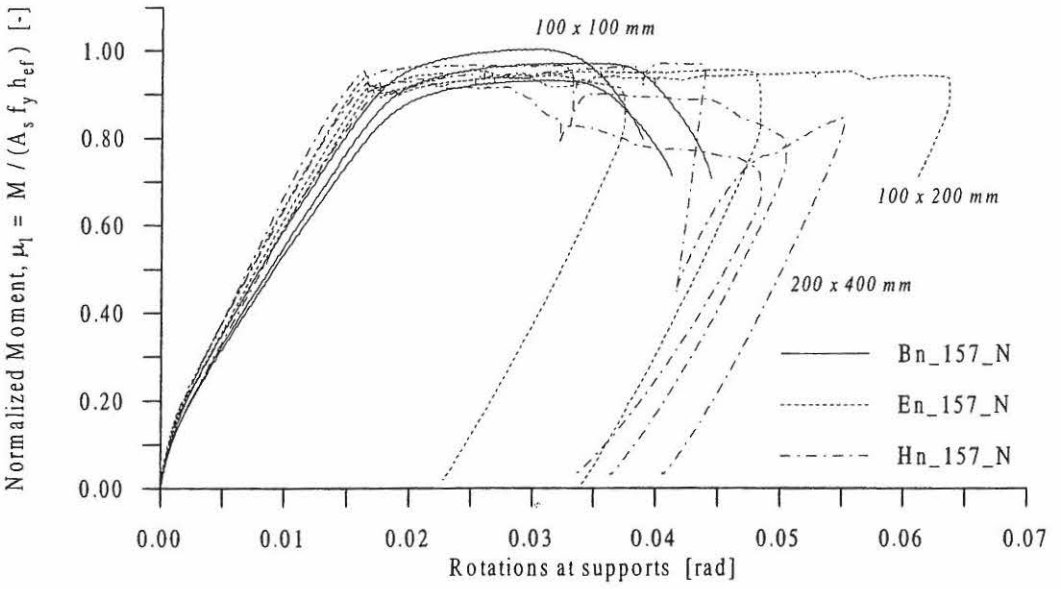

Figure A1.14: *The rotation measured at the supports as a function of the normalized moment, μ_1 for NSC beams B, E and H reinforcement ratio 1.57 % and slenderness no. 12.*

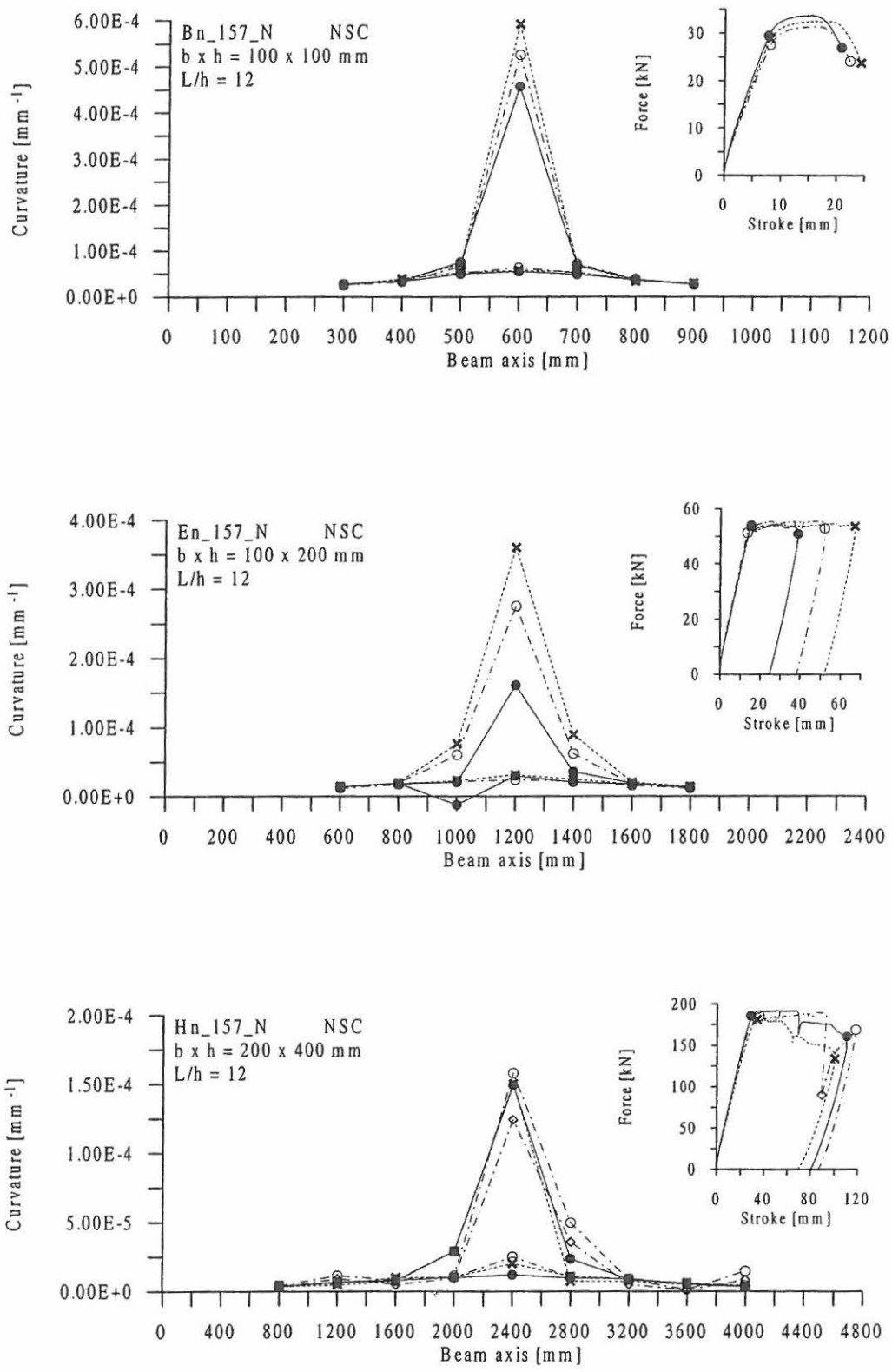

Figure A1.15: *Distribution of curvatures along the beam axis for NSC beams Bn_157_N (top), En_157_N (middle) and Hn_157_N (bottom).*

A1.6 Test Results for Normal Strength Concrete Beams C, F and I with Reinforcement Ratio 1.57 % and Slenderness Number 18.

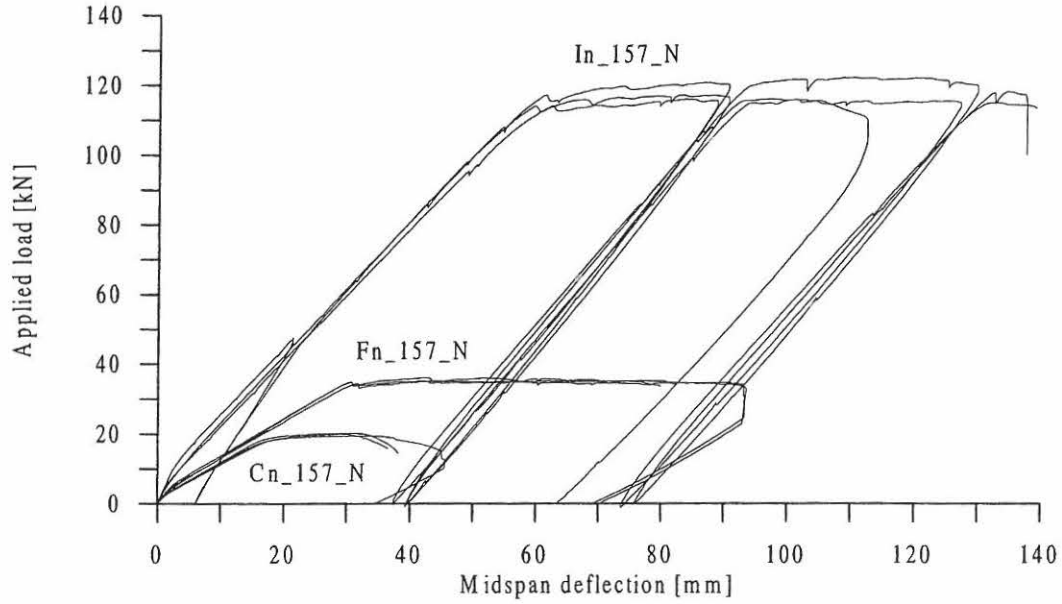

Figure A1.16: *Load-displacement curves for NSC beams C, F and I with reinforcement ratio 1.57 % and slenderness no. 18.*

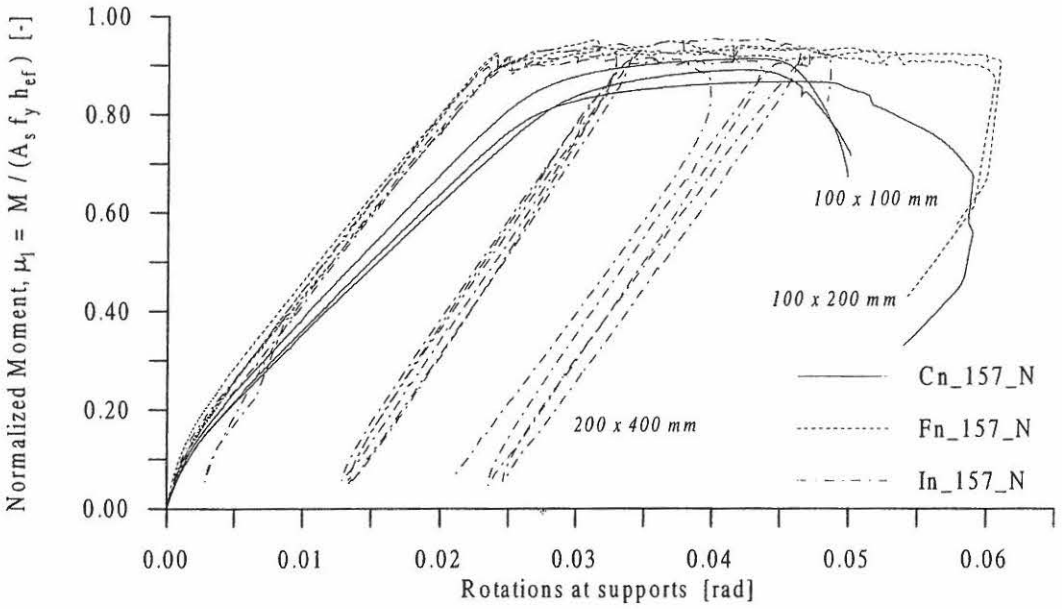

Figure A1.17: *The rotation measured at the supports as a function of the normalized moment, μ_1 for NSC beams C, F and I reinforcement ratio 1.57 % and slenderness no. 18.*

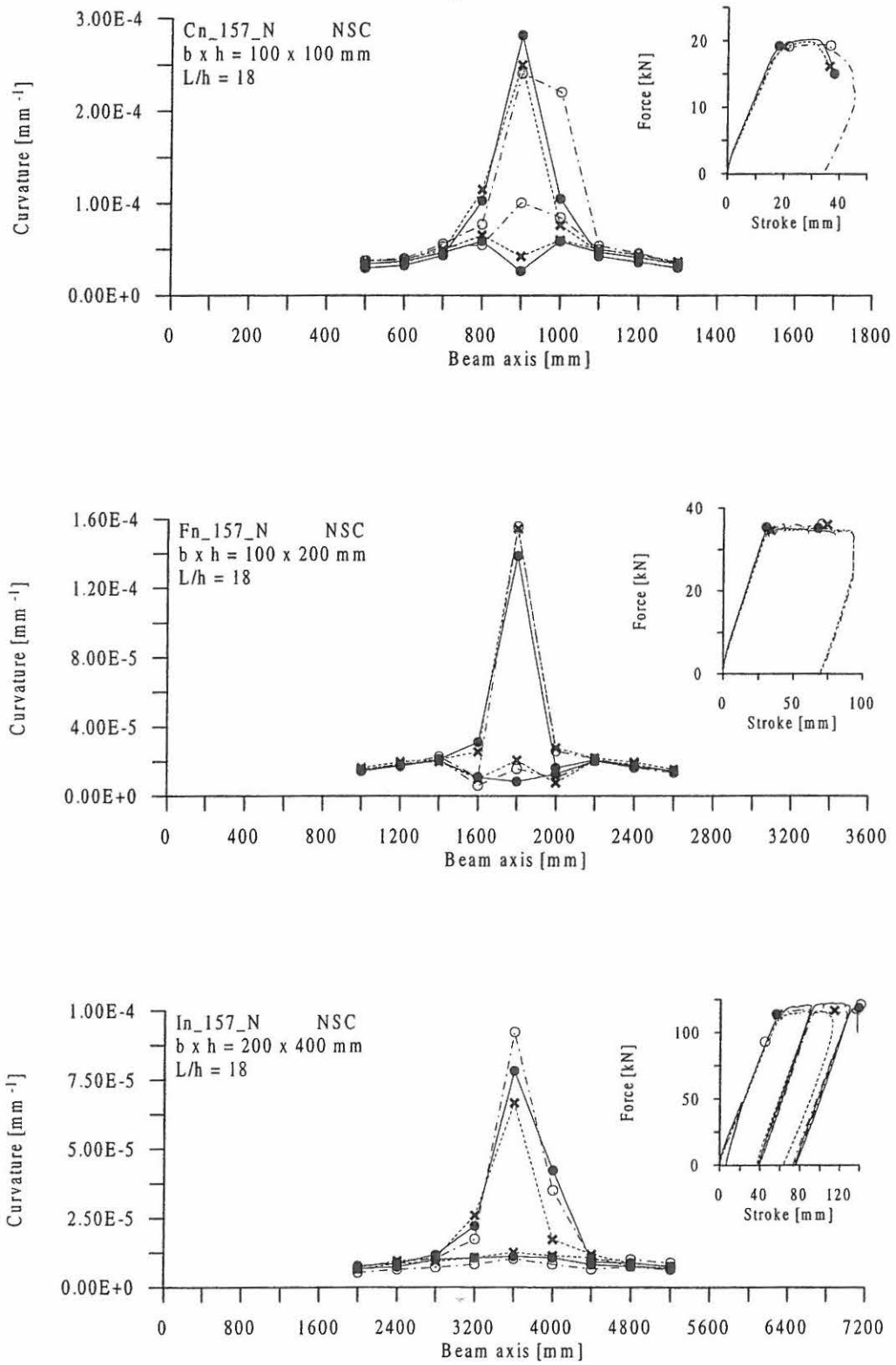

Figure A1.18: *Distribution of curvatures along the beam axis for NSC beams Cn_157_N (top), Fn_157_N (middle) and In_157_N (bottom).*

A1.7 Test Results for Normal Strength Concrete Beams B, E and H with Reinforcement Ratio 0.14 % and Slenderness Number 12.

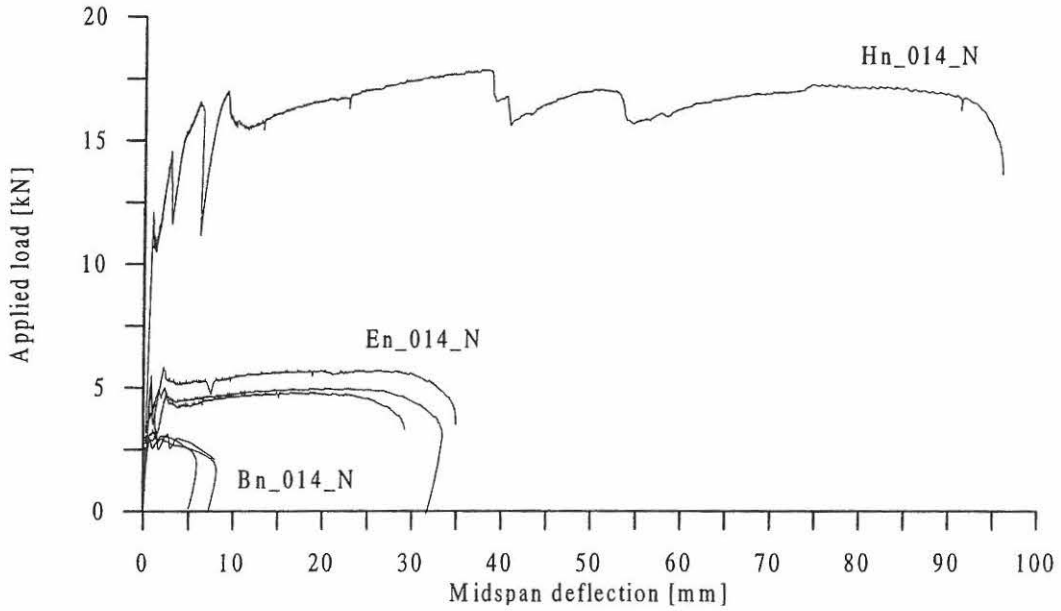

Figure A1.19 *Load-displacement curves for NSC beams B, E and H with reinforcement ratio 0.14 % and slenderness no. 12.*

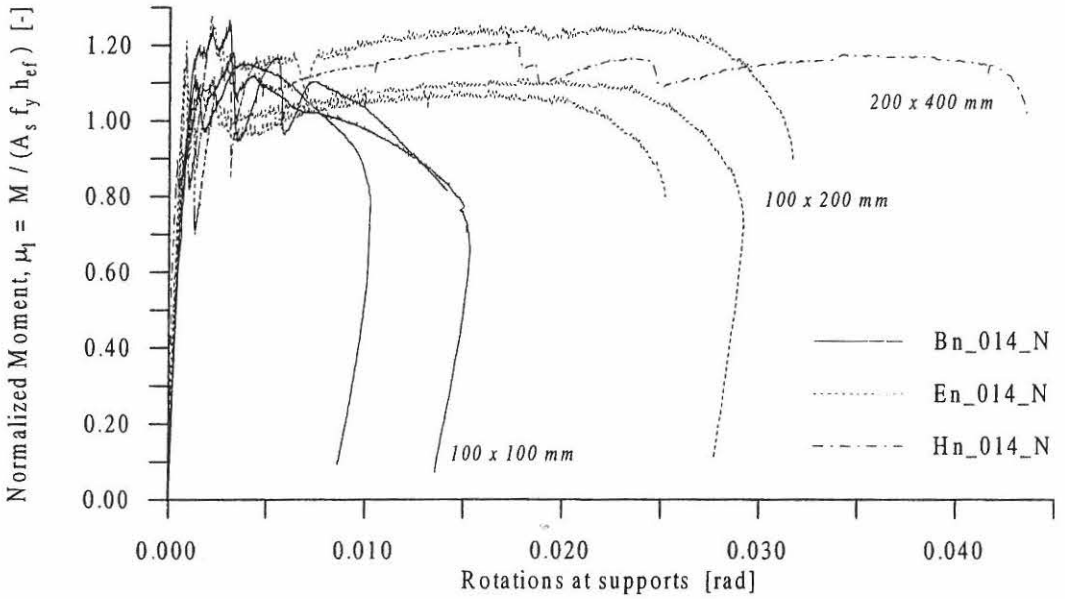

Figure A1.20: *The rotation measured at the supports as a function of the normalized moment, μ_1 for NSC beams B, E and H reinforcement ratio 0.14 % and slenderness no. 12.*

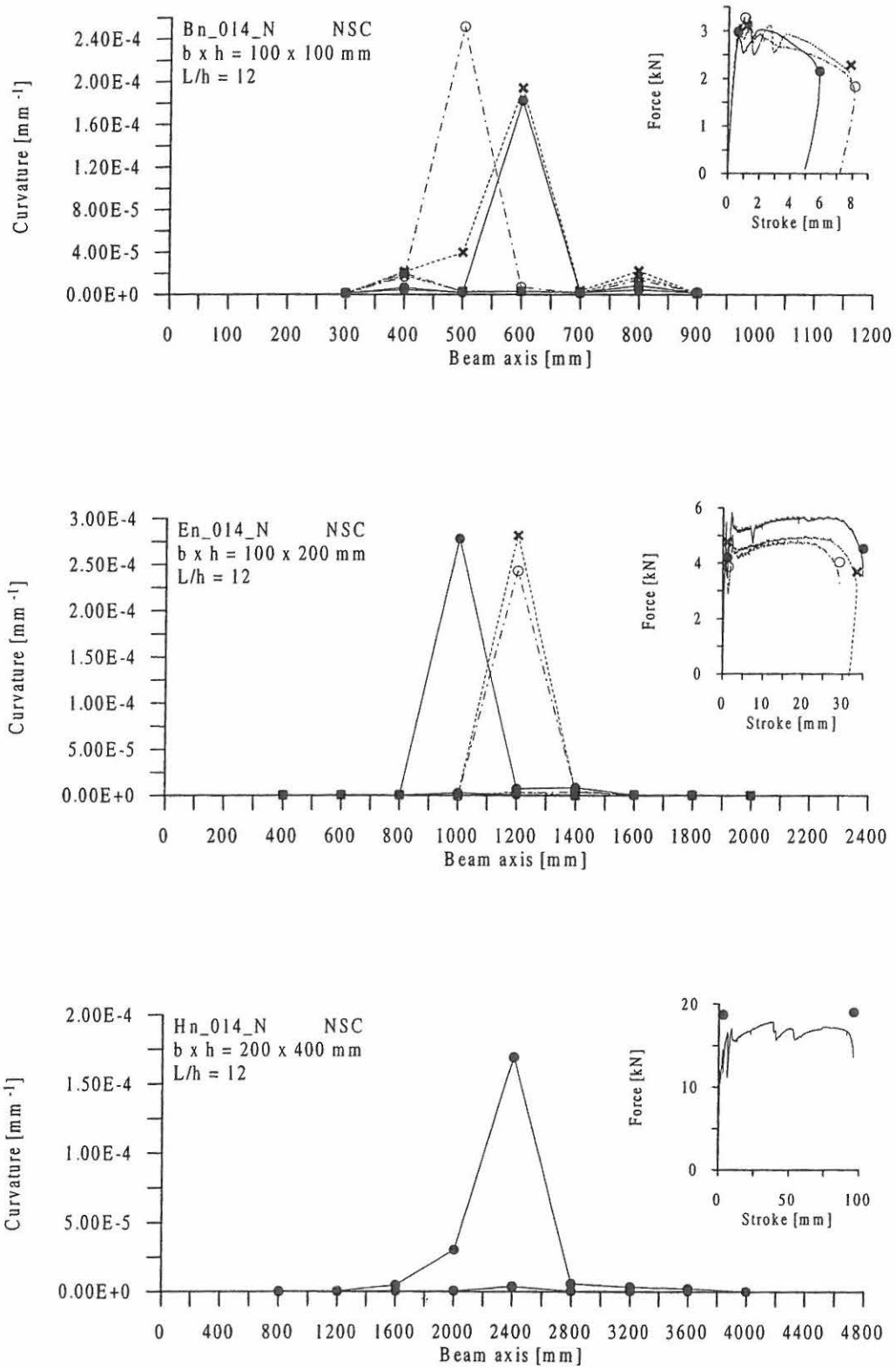

Figure A1.21: *Distribution of curvatures along the beam axis for NSC beams Bn_014_N (top), En_014_N (middle) and Hn_014_N (bottom).*

A1.8 Test Results for Normal Strength Concrete Beams B, E and H with Reinforcement Ratio 0.25 % and Slenderness Number 12.

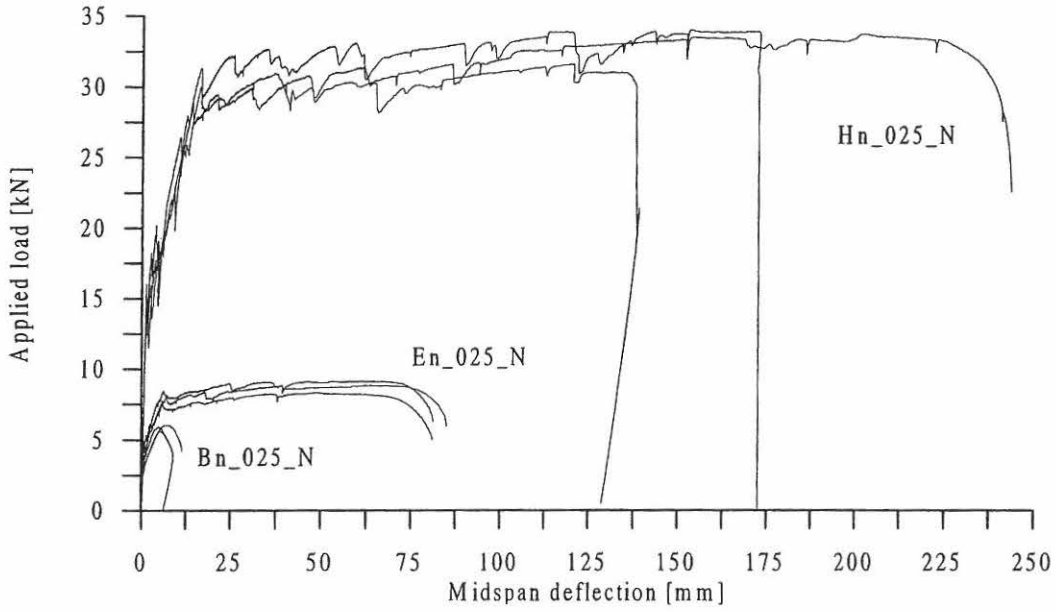

Figure A1.22: *Load-displacement curves for NSC beams B, E and H with reinforcement ratio 0.25 % and slenderness no. 12.*

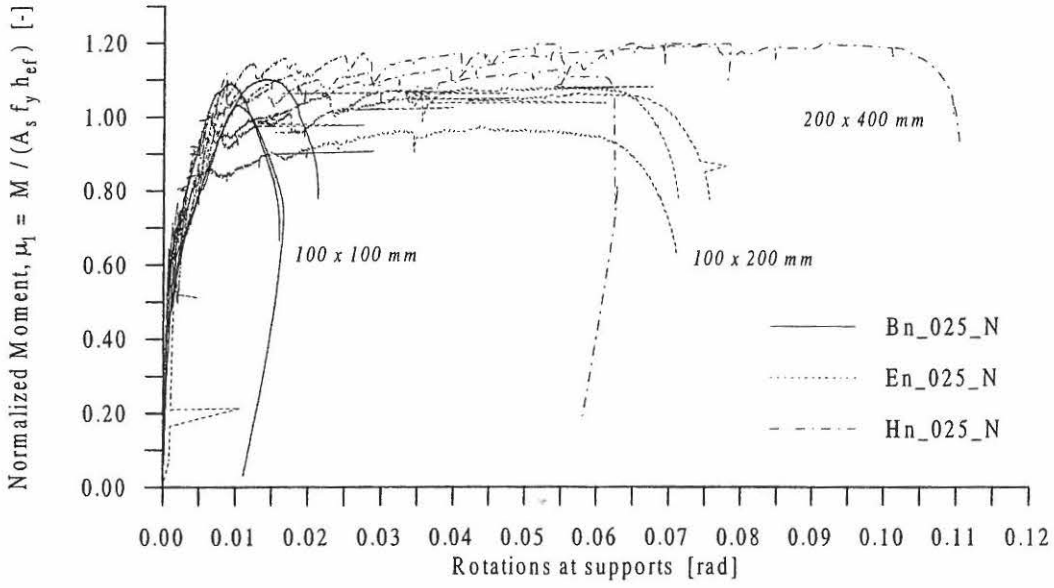

Figure A1.23: *The rotation measured at the supports as a function of the normalized moment, μ_1 for NSC beams B, E and H reinforcement ratio 0.25 % and slenderness no. 12.*

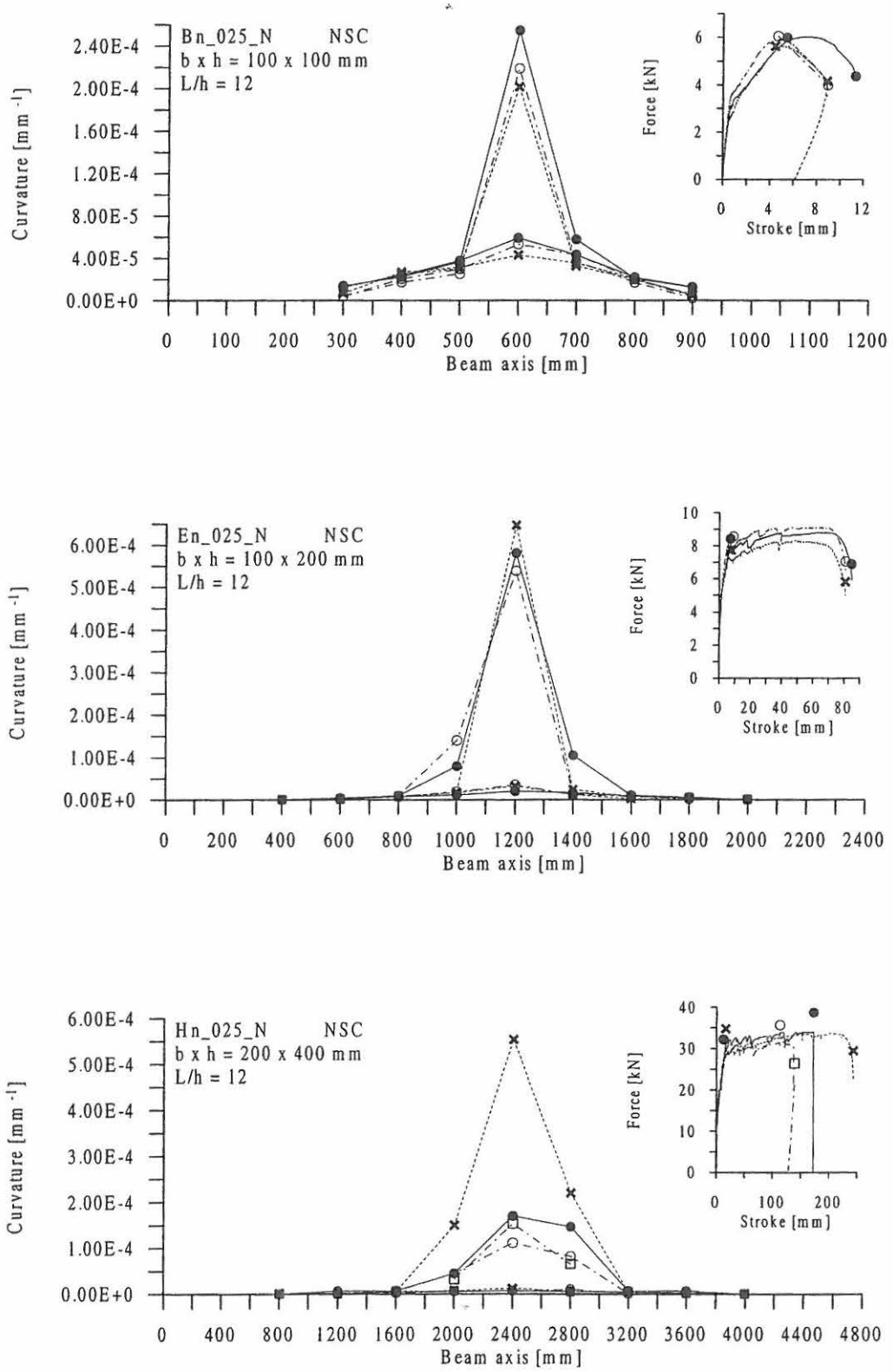

Figure A1.24: *Distribution of curvatures along the beam axis for NSC beams Bn_025_N (top), En_025_N (middle) and Hn_025_N (bottom).*

A1.9 Test Results for Normal Strength Concrete Beams B, E and H with Reinforcement Ratio 0.39 % and Slenderness Number 12.

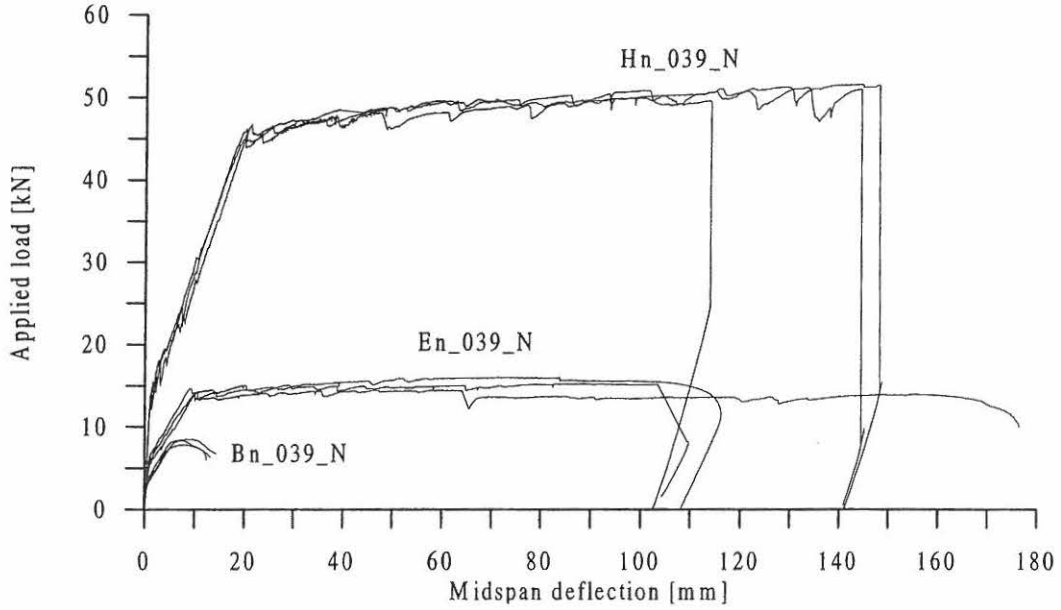

Figure A1.25: *Load-displacement curves for NSC beams B, E and H with reinforcement ratio 0.39 % and slenderness no. 12.*

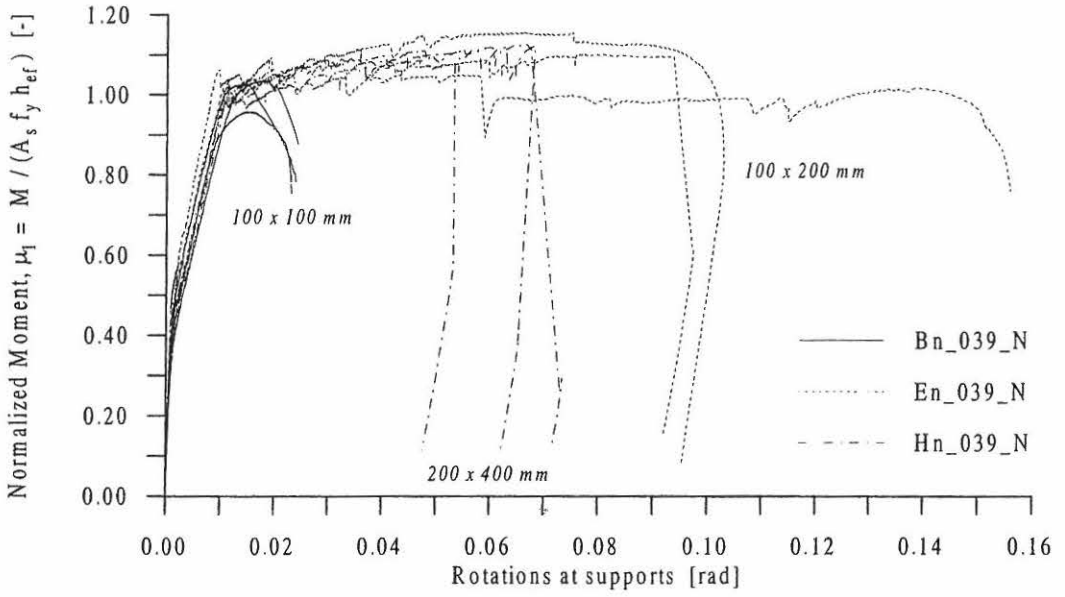

Figure A1.26: *The rotation measured at the supports as a function of the normalized moment, μ_1 for NSC beams B, E and H reinforcement ratio 0.39 % and slenderness no. 12.*

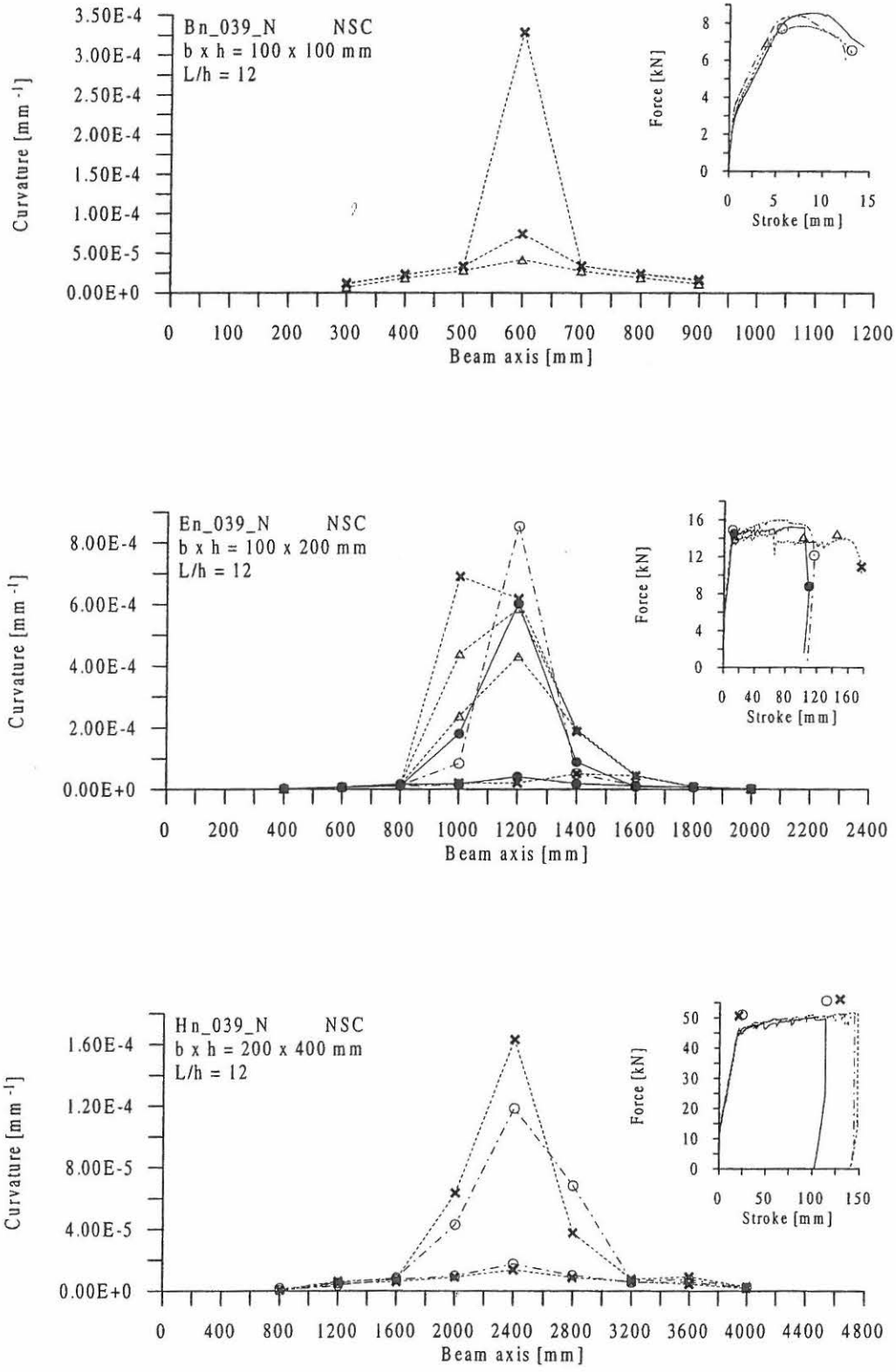

Figure A1.27: *Distribution of curvatures along the beam axis for NSC beams Bn_039_N (top), En_039_N (middle) and Hn_039_N (bottom).*

A1.10 Test Results for High Strength Concrete Beams B, E and H with Reinforcement Ratio 0.14 % and Slenderness Number 12.

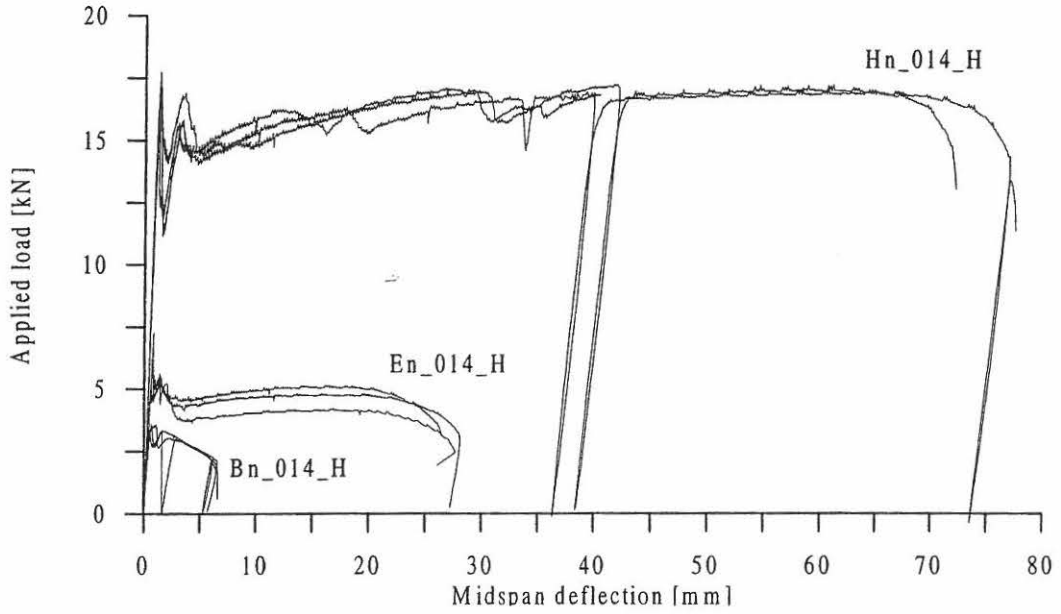

Figure A1.28: *Load-displacement curves for HSC beams B, E and H with reinforcement ratio 0.14 % and slenderness no. 12.*

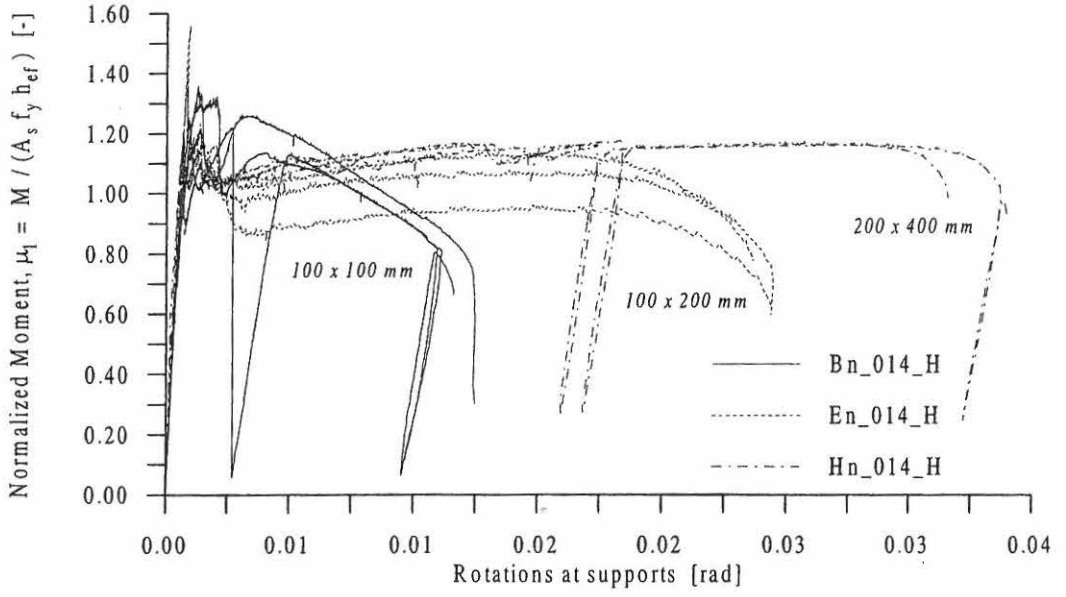

Figure A1.29: *The rotation measured at the supports as a function of the normalized moment, μ_1 for HSC beams B, E and H reinforcement ratio 0.14 % and slenderness no. 12.*

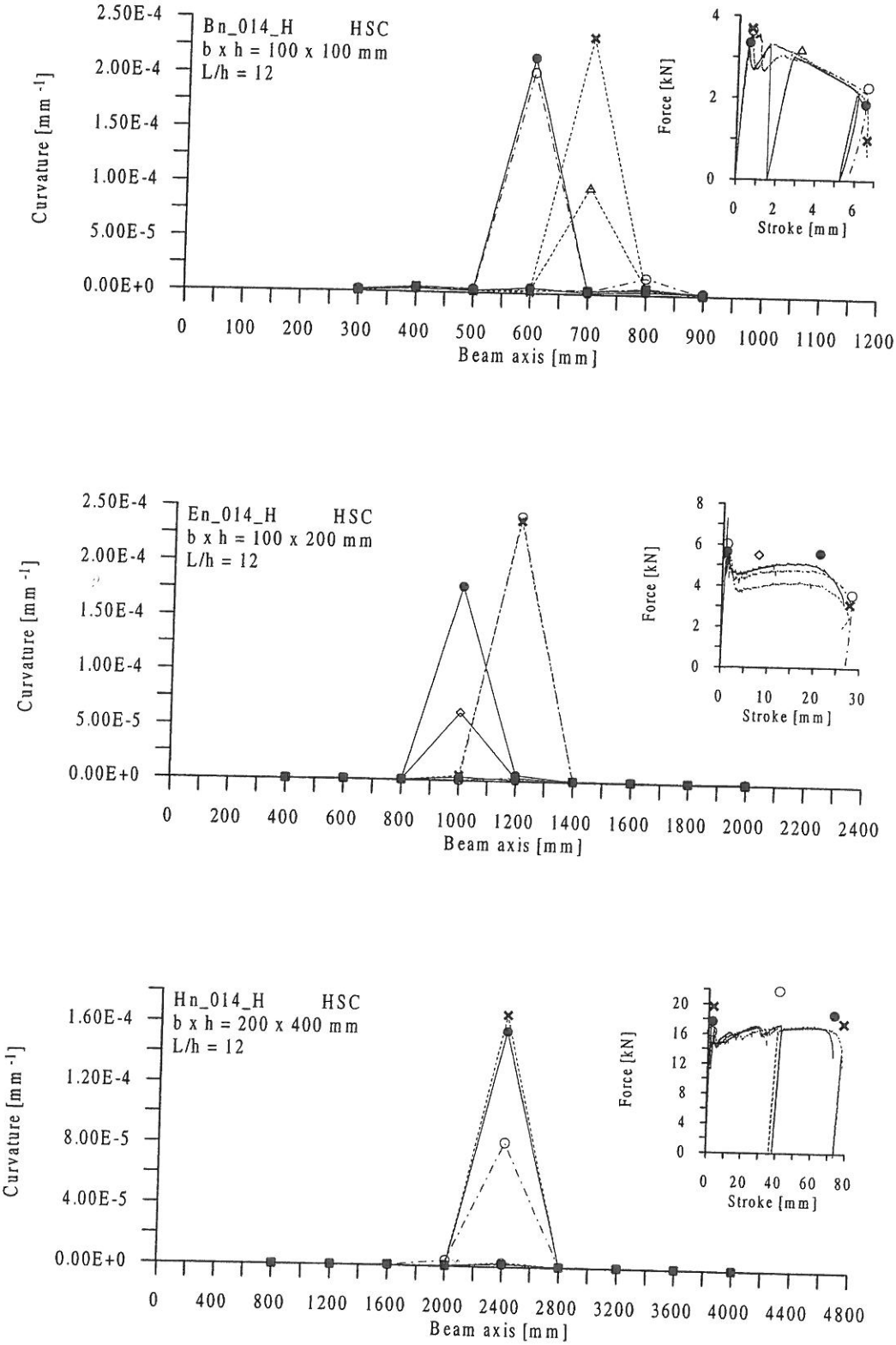

Figure A1.30: *Distribution of curvatures along the beam axis for HSC beams Bn_014_H (top), En_014_H (middle) and Hn_014_H (bottom).*

A1.11 Test Results for High Strength Concrete Beams B, E and H with Reinforcement Ratio 0.25 % and Slenderness Number 12.

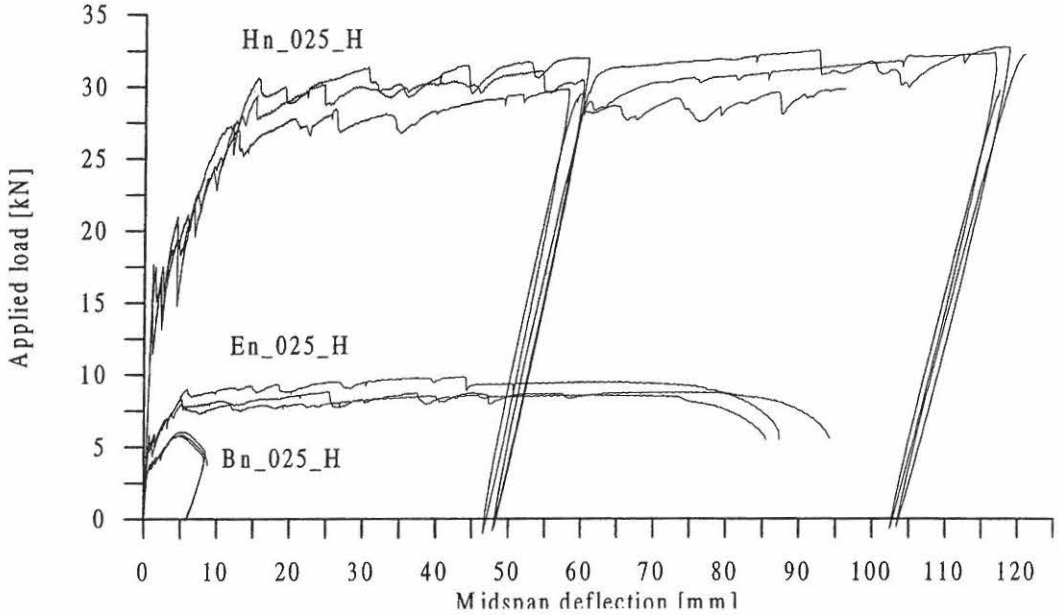

Figure A1.31: *Load-displacement curves for HSC beams B, E and H with reinforcement ratio 0.25 % and slenderness no. 12.*

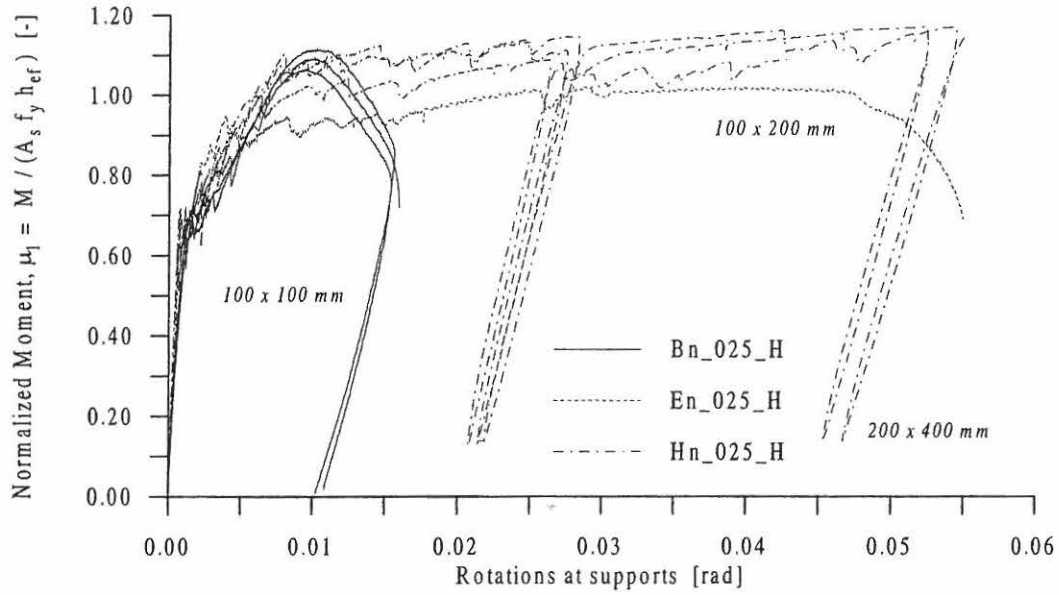

Figure A1.32: *The rotation measured at the supports as a function of the normalized moment, μ_1 for HSC beams B, E and H reinforcement ratio 0.25 % and slenderness no. 12.*

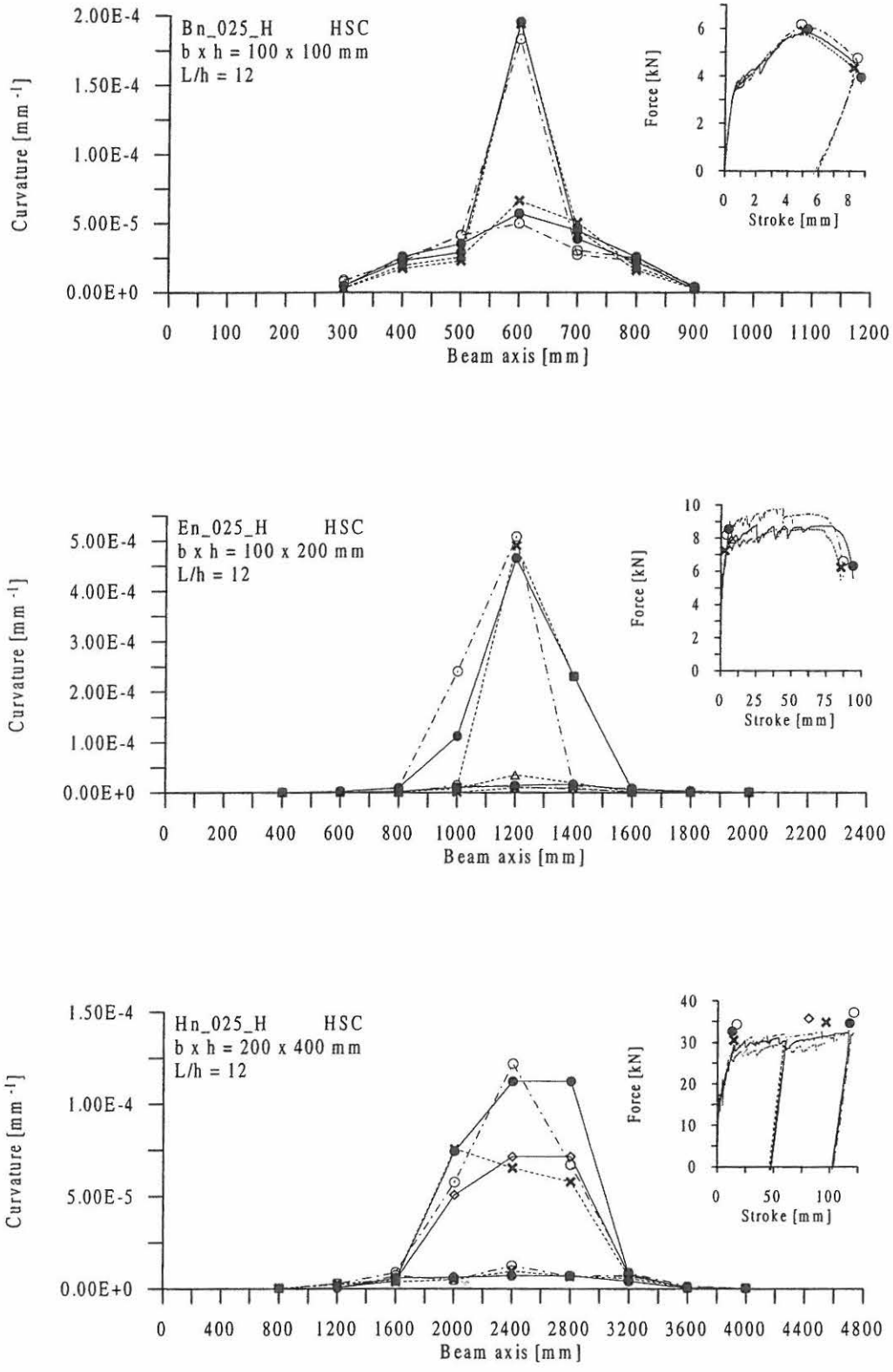

Figure A1.33: *Distribution of curvatures along the beam axis for HSC beams Bn_025_H (top), En_025_H (middle) and Hn_025_H (bottom).*

A1.12 Test Results for High Strength Concrete Beams B, E and H with Reinforcement Ratio 0.39 % and Slenderness Number 12.

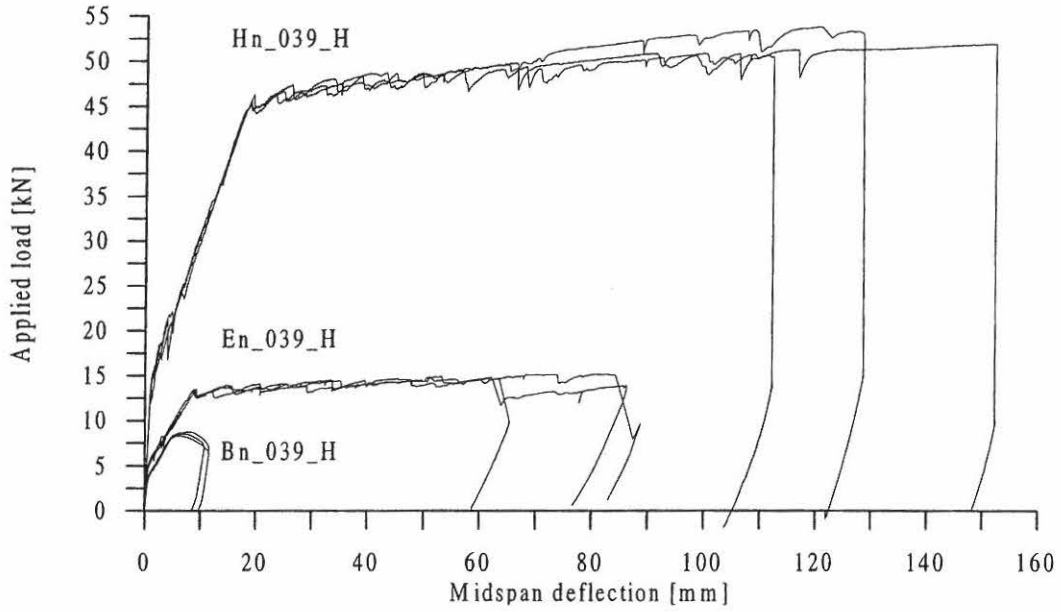

Figure A1.34: *Load-displacement curves for HSC beams B, E and H with reinforcement ratio 0.39 % and slenderness no. 12.*

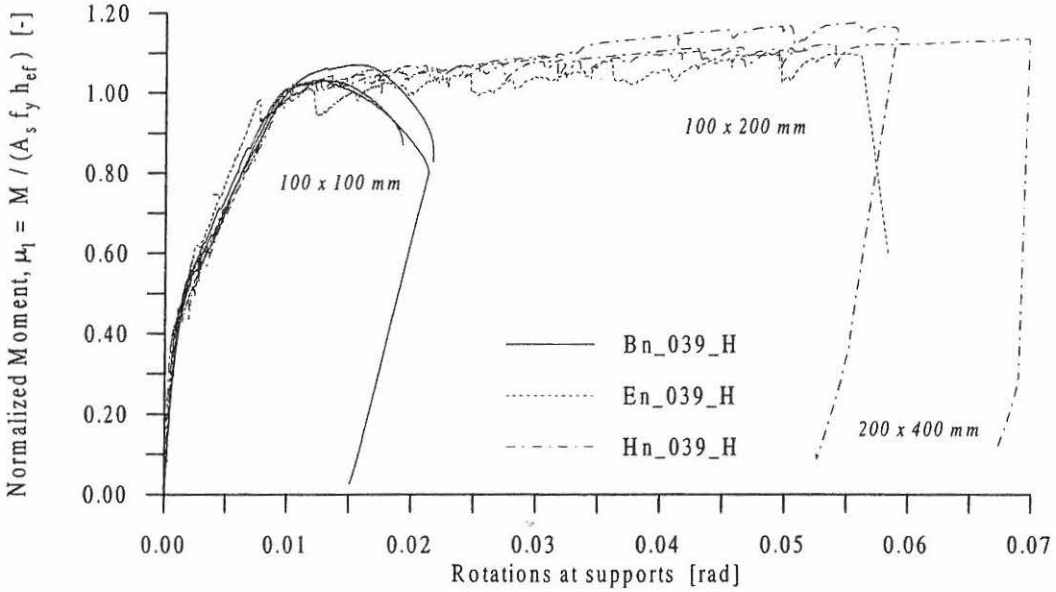

Figure A1.35: *The rotation measured at the supports as a function of the normalized moment, μ_1 for HSC beams B, E and H reinforcement ratio 0.39 % and slenderness no. 12.*

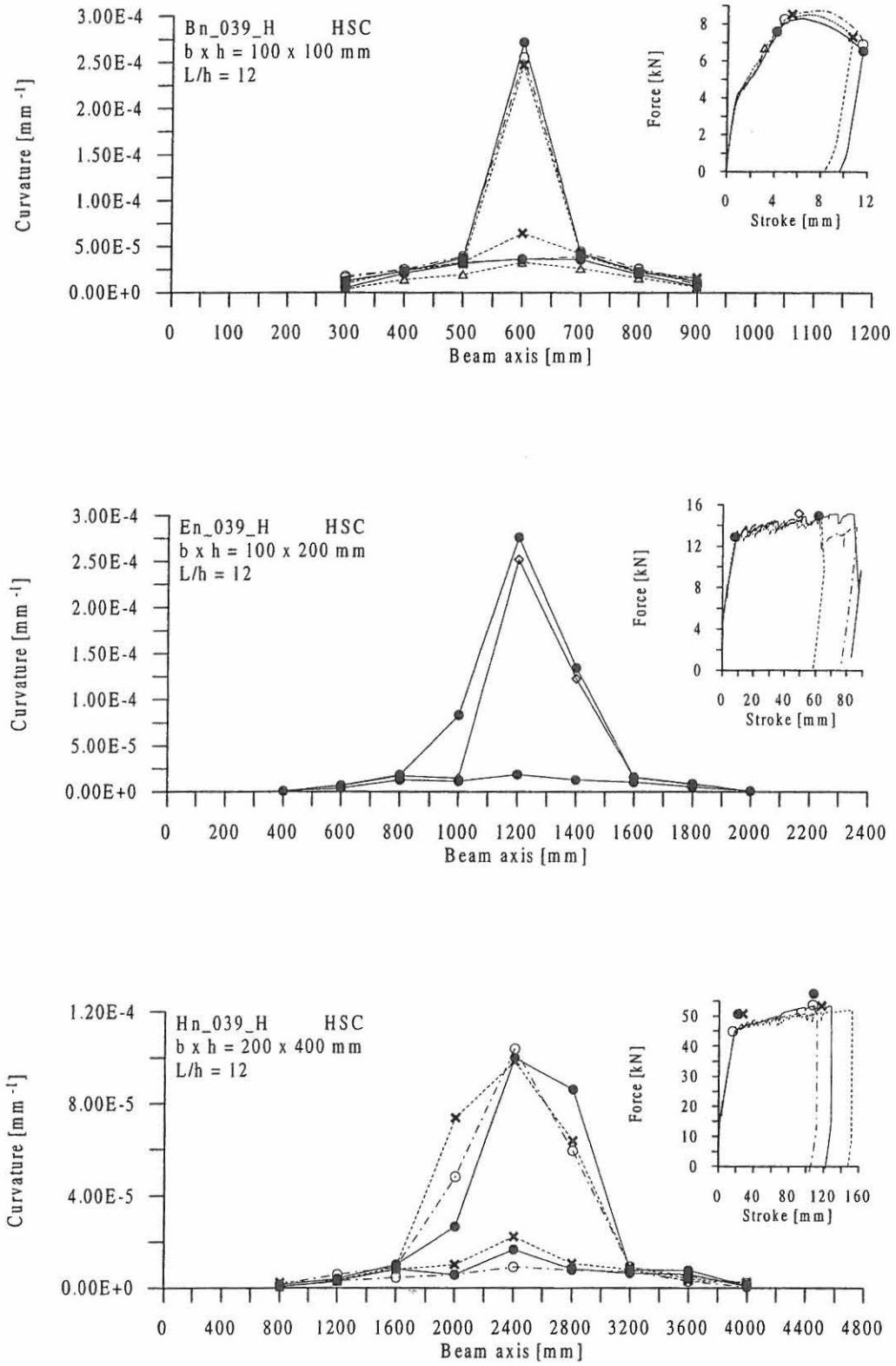

Figure A1.36: *Distribution of curvatures along the beam axis for HSC beams Bn_039_H (top), En_039_H (middle) and Hn_039_H (bottom).*

A2 Rotational Capacity of Reinforced Normal Strength and High Concrete Beams

In this section values of the rotational capacity according to CEB FIP Model Code, a plasticity theory model and support rotations are listed for the test beams of normal strength and high strength concrete.

Beam type	No. of tests	CEB - FIP Model Code		Plasticity theory model		Rotation at supports	
		Mean	Coef. of Var.	Mean	Coef. of Var.	Mean	Coef. of Var.
		[-]	[%]	[-]	[%]	[-]	[%]
A_078_N	2	0.0440	4.44	0.0329	3.10	0.0432	4.61
A_157_N	2	0.0548	11.3	0.0394	10.7	0.0543	12.1
B_014_N	3	0.0255	19.4	0.0235	18.5	0.0254	20.9
B_025_N	3	0.0341	14.7	0.0273	24.6	0.0338	16.6
B_039_N	2	0.0453	0.00	0.0338	8.91	0.0455	2.78
B_078_N	3	0.0473	6.17	0.0360	10.1	0.0472	6.20
B_157_N	3	0.0711	10.3	0.0603	10.6	0.0717	8.00
C_078_N	2	0.0591	17.2	0.0491	11.6	0.0698	7.82
C_157_N	3	0.0672	13.5	0.0626	13.8	0.0894	10.3
D_078_N	3	0.218[1]	6.39	0.213	9.40	0.211	9.17
D_157_N	3	0.136	28.9	0.130	30.8	0.136	28.5
E_014_N	3	0.0553	8.98	0.0581	16.8	0.0563	11.4
E_025_N	3	0.149	9.16	0.135	7.83	0.143	3.19
E_039_N	3	0.233	28.9	0.229	25.6	0.231	29.5
E_078_N	2	0.0531[2]	-	0.100[1]	7.27	0.101[1]	23.5
E_157_N	3	0.0947[1]	19.6	0.0641	37.8	0.0891	30.1
F_078_N	2	0.0798	0.493	0.0689	10.1	0.0890	2.37
F_157_N	3	0.0645	7.67	0.0795	10.6	0.0995	5.71
G_078_N	2	0.214	9.78	0.249	0.216	0.219	2.00
G_157_N	3	0.0781	29.9	0.0756	23.9	0.0784	26.2
H_006_N	2	0.0323	5.67	0.0314	1.44	0.0321	5.07
H_014_N	1	0.0854	-	0.0907	-	0.0865	-

Beam type	No. of tests	CEB - FIP Model Code		Plasticity theory model		Rotation at supports	
		Mean	Coef. of Var.	Mean	Coef. of Var.	Mean	Coef. of Var.
		[-]	[%]	[-]	[%]	[-]	[%]
H_025_N	3	0.137[1]	17.4	0.165	27.0	0.164	29.6
H_039_N	3	0.128[1]	1.86	0.115	16.1	0.121	13.6
H_078_N	3	0.0819	18.3	0.0744	15.4	0.0864	15.8
H_157_N	3	0.0779	9.07	0.0633	9.48	0.0834	10.2
I_078_N	3	0.107	25.2	0.0897	19.4	0.101	24.3
I_157_N	3	0.0574	15.8	0.0466	36.9	0.0696	19.5

Beam type	No. of tests	CEB - FIP Model Code		Plasticity theory model		Rotation at supports	
		Mean	Coef. of Var.	Mean	Coef. of Var.	Mean	Coef. of Var.
		[-]	[%]	[-]	[%]	[-]	[%]
B_014_H	2	0.0236	7.22	0.0222	5.94	0.0228	9.08
B_025_H	3	0.0298	2.29	0.0229	11.1	0.0293	2.56
B_039_H	3	0.0395	4.44	0.0316	5.50	0.0382	6.55
E_014_H	3	0.0475	5.37	0.0442	7.68	0.0468	4.84
E_025_H	3	0.157	4.52	0.151	5.77	0.150	23.2
E_039_H	3	0.143	11.5	0.125	15.7	0.104	19.0
H_014_H	2	0.0650[1]	4.81	0.0700[1]	5.09	0.0646[1]	5.20
H_025_H	3	0.0955[1]	16.3	0.0985	15.9	0.0982	13.2
H_039_H	3	0.116	15.3	0.113	16.8	0.117	15.5

[1] refers to that only two tests are included.

[2] refers to that only one test is included.